



A University of Sussex DPhil thesis

Available online via Sussex Research Online:

<http://eprints.sussex.ac.uk/>

This thesis is protected by copyright which belongs to the author.

This thesis cannot be reproduced or quoted extensively from without first obtaining permission in writing from the Author

The content must not be changed in any way or sold commercially in any format or medium without the formal permission of the Author

When referring to this work, full bibliographic details including the author, title, awarding institution and date of the thesis must be given

Please visit Sussex Research Online for more information and further details

EHD PHENOMENA IN
GREASE LUBRICATED CONTACTS

- by -

Yuichiro Nagata

A Thesis Submitted for the Degree of
DOCTOR OF PHILOSOPHY
of the University of Sussex

January 2011

PREFACE

This thesis is a description of the work carried out in the Department of Mechanical Engineering, Brunel University and University of Sussex, under the supervision of Dr. Romeo Glovnea. Except where acknowledged and Section 8.4, the material presented is the original work of the author. Section 8.4 is the part of the joint work with Kyushu University and conducted under their facilities. Also, the thesis incorporates the extent indicated in the next page, materials already submitted as a part of required course field and/or for the degree of Doctor of Philosophy.

SELECTED PRESENTATIONS AND PUBLISHED WORK

Nagata, Y., Furtuna, M., Bell, C. and Glovnea, R., 2008. "Evaluation of Electric Permittivity of Lubricating Oils in EHD Conditions", *Proc. of 2nd International Conference on Advanced Tribology*, December 2008, Singapore

Nagata, Y., Sugimura, J., and Glovnea, R.P., 2009, "The effect of working parameters upon the dielectric permittivity of grease lubricants in EHD contacts", *Proc. World Tribology Congress*, Kyoto, Japan, 6-11 Sept. 2009

Glovnea, R.P., and Nagata, Y., "Dielectric spectroscopy studies of grease lubricants", *Invited talk Imperial College London Symposium*, March 2010

Otsu, T., Nagata, Y., Sugimura, J., and Glovnea, R.P., "Cavitation phenomena in pure-sliding grease EHL films", *Proc. ASME/STLE 2010 Intern. Trib. Conf.*, San Francisco, USA, 17-20 Oct. 2010

Otsu, T., Nagata, Y., Sugimura, J., and Glovnea, R.P., "Observation of cavitation in EHL films", *Invited Lecture, Proc. ROTRIB'10, Int. Conf.*, 3-5 Nov. 2010, Iasi, Romania, pp. 39-48 also Submitted to "*The Bulletin of the Polytechnic Institute of Iasi*"

Nagata, Y., and Glovnea, R.P., 2010, "Dielectric properties of grease lubricants", *Acta Tribologica*, Vol. 18, pp. 34-41, ISSN 1220 - 8434

Glovnea, R.P., Furtuna, M.D., Nagata, Y., and Sugimura, J., 2010, "Electrical methods for the study of elastohydrodynamic films", *Tribology Online*, (Journal of the Japanese Society of Tribologists), accepted for publication

Otsu, T., Nagata, Y., Sugimura, J., and Glovnea, R.P., 2010, "Study of cavitation in grease EHL films", submitted to *ASME Transactions, J. of Tribology*

DECLARATION

I hereby declare that this thesis has not been and will not be, submitted in whole or in part to another University for the award of any other degree.

Signature:

ABSTRACT

This thesis examines the rheological behaviour and film formation of greases and oils under elastohydrodynamic (EHD) conditions. It approaches the lubrication of non-conforming contacts from tribological as well as from dielectric point of view.

The experimental work was carried out on a point contact formed between a ball and the flat of a disc, which was either transparent, for optical interferometry study or steel in order to evaluate the conditions in real-life machine components. In the second case electrical capacitance method has been employed to study film formation. The experimental equipment has also been adapted to study the starvation behaviour of grease lubricants in point EHD contacts under vibrations.

Dielectric properties of lubricants have been studied in static conditions and correlated to their performance in EHD conditions. The dielectric constant of greases indicates in general higher value than corresponding base oils and the dielectric relaxation time of greases is proved to be shorter. It has been found that in EHD conditions higher-polar greases show higher shear stress, while the dielectric constant of the lubricating film decreases with increasing contact pressure.

The effect of three parameters upon grease EHD films was evaluated: operating speed, load and vibration of the contact. The results showed that greases possess an intrinsic time to starvation related to the operating speed but independent of the exerted load. The results also showed that a high speed was not necessarily associated with the high likelihood of occurrence of starvation. The vibration tests revealed that the lateral motion perpendicular to the rotating direction helped maintain the inlet region flooded and, under oscillations, starvation of the contact seems to never occur. This would suggest that machine elements such as rolling element bearings could operate under the fully flooded conditions as vibrations are almost inevitable in any machinery.

Finally, the cavitation phenomenon was also investigated and found that the rheological model of greases could be predicted from the observation of the cavity pattern.

ACKNOWLEDGEMENTS

Special thanks go to Dr. Romeo Glovnea, for the opportunity, as well as guidance and support.

I would like to thank Kyodo Yushi Co., Ltd. for cooperating with the research project and to Dr. Toshiaki Endo and Dr. Shinya Kondo for their consistent support and assistance with materials and resources.

I would like to thank Prof. Joichi Sugimura for the enthusiastic discussions and guidance, Hiroyoshi Tanaka and Kazuyuki Yagi, both is an associate professor at Kyushu University, for their interest, guidance and support. Thanks also to Takefumi Ohtsu for his research advice and assistance especially in my stay in Japan and for experimental works using facilities of Kyushu University. Special thanks go to Howard Mead at Shell Global Solutions for supplying some of the lubricants. Also thanks to Prof. Shigeka Yoshimoto and Prof. Yuji Nakasone at Tokyo University of Science, Konstantinos Kalogiannis, Marian Fortuna, Colin Bell, Karolina Jablonka, Yutaka Makida and other members for making the Tribology Section a fun place to be.

A huge vote of thanks goes to the following people at Daihatsu Motor Company: Mr Toyoda, Mr Sato, Miss Okada, Mr Miyazaki and other members at General Affairs and Personal Department for appreciating my work.

Finally I am enormously grateful to my family for their patience, support and understanding.

TABLE OF CONTENTS

| | |
|---|----|
| PREFACE | 2 |
| SELECTED PRESENTATIONS AND PUBLISHED WORK | 3 |
| DECLARATION | 4 |
| ABSTRACT | 5 |
| ACKNOWLEDGEMENTS | 6 |
| TABLE OF CONTENTS | 7 |
| LIST OF FIGURES | 14 |
| LIST OF TABLES | 22 |
| NOMENCLATURE | 23 |
| Chapter 1 Introduction | 30 |
| 1.1 General Introduction | 30 |
| 1.2 Aims of the Study | 31 |
| 1.3 Structure of the Thesis | 32 |
| Chapter 2 Background on Elastohydrodynamic Lubrication | 34 |
| 2.1 Contact of Elastic Smooth Bodies. Hertz Theory | 35 |
| 2.2 Reynolds Equation | 39 |
| 2.3 Viscosity Variation with Pressure and Temperature | 44 |
| 2.4 Regimes of Lubrication | 45 |
| 2.5 Elastohydrodynamic Lubrication Regime | 47 |
| 2.5.1 Mechanisms of elastohydrodynamic lubrication | 47 |

| | | |
|-----------|---|----|
| 2.5.2 | Accurate formula for EHL film thickness | 49 |
| 2.5.3 | Characteristics of EHL films | 51 |
| 2.5.4 | Starved lubrication | 53 |
| 2.6 | EHD Friction and Rheology | 55 |
| 2.6.1 | EHD friction behaviour | 55 |
| 2.6.2 | Rheological models | 57 |
| 2.6.3 | Rheology of EHD films | 61 |
| Chapter 3 | Lubricants | 65 |
| 3.1 | Lubricating Oils | 66 |
| 3.2 | Lubricating Greases | 68 |
| 3.2.1 | Structure of greases | 68 |
| 3.2.2 | Rheological models of greases | 69 |
| 3.2.3 | Lubricating behaviour of greases | 71 |
| Chapter 4 | Electrical Methods in EHD Lubrication and Dielectric Applications | 77 |
| 4.1 | Electrical Methods in EHL | 77 |
| 4.1.1 | Film thickness measurements | 78 |
| 4.1.2 | Detection of asperity contact in mixed regime | 79 |
| 4.1.3 | Effect of the electric field upon lubrication phenomena | 81 |
| 4.2 | Studies on Lubricants as Dielectrics | 81 |
| 4.2.1 | Basics of dielectrics | 82 |
| 4.2.2 | Dielectric studies on materials | 85 |

| | | |
|-----------|---|-----|
| 4.2.3 | Dielectric relaxation versus mechanical relaxation | 93 |
| Chapter 5 | Experimental Methodology | 95 |
| 5.1 | General Introduction | 95 |
| 5.2 | Static Conditions | 97 |
| 5.2.1 | Description of the micrometre based measurements | 97 |
| 5.2.2 | Description of the EHD rig modified for dielectric measurements | 98 |
| 5.3 | EHD Measurements | 101 |
| 5.3.1 | Film thickness measurements | 101 |
| 5.3.1.1 | Optical interferometry | 101 |
| 5.3.1.2 | RGB value | 104 |
| 5.3.1.3 | Hue value | 106 |
| 5.3.2 | Starvation measurements | 110 |
| 5.3.3 | Traction measurements | 113 |
| 5.3.4 | Vibration measurements | 116 |
| 5.3.5 | Camera equipment | 117 |
| 5.4 | Test Materials | 117 |
| 5.4.1 | Oil lubricants | 117 |
| 5.4.2 | Grease lubricants | 118 |
| Chapter 6 | Dielectric Properties of Lubricants | 121 |
| 6.1 | Static Conditions | 121 |
| 6.1.1 | Oil lubricants | 122 |

| | |
|---|-----|
| 6.1.1.1 Dielectric constant | 122 |
| 6.1.1.2 Dielectric relaxation behaviour | 124 |
| 6.1.1.3 Conclusions | 125 |
| 6.1.2 Grease lubricants | 126 |
| 6.1.2.1 Dielectric constant | 127 |
| 6.1.2.2 Dielectric relaxation behaviour | 130 |
| 6.1.2.3 Conclusions | 131 |
| 6.2 EHD Conditions | 133 |
| 6.2.1 Dielectric properties under shear conditions | 133 |
| 6.2.2 Dielectric constant under pure rolling EHD conditions | 135 |
| 6.2.3 Dielectric constant under sliding rolling EHD conditions | 142 |
| 6.2.4 Conclusions | 145 |
| Chapter 7 Observation of Rheological Behaviour of Lubricants | 146 |
| 7.1 Traction Curves | 146 |
| 7.1.1 12OH-LiSt greases | 148 |
| 7.1.1.1 Grease and corresponding base oil | 148 |
| 7.1.1.2 Effect of base oil and correlation to dielectric properties | 150 |
| 7.1.2 LiSt greases | 152 |
| 7.1.2.1 Grease and corresponding base oil | 152 |
| 7.1.2.2 Effect of base oil and correlation to dielectric properties | 154 |
| 7.1.3 Urea greases | 155 |

| | |
|---|-----|
| 7.1.3.1 Grease and corresponding base oil | 155 |
| 7.1.3.2 Correlation to dielectric properties | 158 |
| 7.1.4 “Viscosity 68” oils | 159 |
| 7.1.5 Conclusions | 160 |
| 7.2 Eyring Stress | 163 |
| 7.2.1 12OH-LiSt greases | 164 |
| 7.2.2 LiSt greases | 166 |
| 7.2.3 Urea greases | 169 |
| 7.2.4 Conclusions | 171 |
| 7.3 Effective Viscosity | 173 |
| 7.3.1 12OH-LiSt greases | 173 |
| 7.3.2 LiSt greases | 175 |
| 7.3.3 Urea greases | 178 |
| 7.3.4 Conclusions | 180 |
| 7.4 Mechanical Relaxation | 181 |
| 7.4.1 12OH-LiSt greases | 182 |
| 7.4.2 LiSt greases | 184 |
| 7.4.3 Urea greases | 186 |
| 7.4.4 Comparison between mechanical and dielectric relaxation | 189 |
| 7.4.5 Conclusions | 189 |
| Chapter 8 Observation of EHL Film Formation | 192 |

| | |
|--|-----|
| 8.1 Starvation Behaviour by Electrical Method | 192 |
| 8.1.1 Results of RL2 | 194 |
| 8.1.2 Results of RLS2 | 196 |
| 8.1.3 Results of SB-M | 197 |
| 8.1.4 Results of SRL | 199 |
| 8.1.5 Conclusions | 200 |
| 8.2 Effects of Lateral Oscillations on EHD Film Formation | 202 |
| 8.2.1 Grease film thickness decay and recovery | 202 |
| 8.2.2 Grease film thickness changes during the vibration cycle | 208 |
| 8.2.3 Conclusions | 215 |
| 8.3 Film Thickness under Shear Conditions | 216 |
| 8.3.1 Results and discussions | 216 |
| 8.3.2 Conclusions | 219 |
| 8.4 Cavitation Phenomena in Grease EHL Films | 220 |
| 8.4.1 Introduction | 220 |
| 8.4.2 Experimental procedure | 220 |
| 8.4.3 Results and discussions | 222 |
| 8.4.4 Conclusions | 227 |
| Chapter 9 Conclusions and Future Work | 229 |
| 9.1 Test Rig | 229 |
| 9.2 Study of Dielectric Properties of Lubricants | 229 |

| | |
|---|-----|
| 9.3 Dielectric Studies in EHD conditions | 231 |
| 9.4 Traction Measurements | 231 |
| 9.5 Study of the Starvation Behaviour | 234 |
| 9.6 Study of the Cavitation Behaviour | 234 |
| 9.7 Suggestions for Future Work | 235 |
| 9.7.1 Dielectric properties of lubricants | 235 |
| 9.7.2 Starvation behaviour under lateral oscillations | 236 |
| 9.7.3 Study of the cavitation behaviour | 236 |
| References | 238 |
| Appendix 1 Dielectric Properties of Thickeners | 248 |
| A1.1 Dielectric Constant | 250 |
| A1.2 Dielectric Relaxation Process | 251 |
| Appendix 2 Film Thickness Used for Rheological Observation | 252 |
| Appendix 3 Pressure Distribution for the Cavitation Phenomena | 253 |

LIST OF FIGURES

| | | |
|-------------|--|----|
| Figure 2.1 | Contact between a sphere and a flat surface | 36 |
| Figure 2.2 | Hertz contact pressure | 37 |
| Figure 2.3 | Geometry of two elastic bodies with convex surfaces | 38 |
| Figure 2.4 | Two surfaces in relative motion | 39 |
| Figure 2.5 | Flow into an element of a fluid | 42 |
| Figure 2.6 | Map of lubrication regimes for a point contact | 47 |
| Figure 2.7 | Grubin's film geometry | 48 |
| Figure 2.8 | Typical image of the EHD contact | 51 |
| Figure 2.9 | Pressure distribution and shape of the EHL lubricating film | 53 |
| Figure 2.10 | Contact geometry showing required measurements for starvation | 54 |
| Figure 2.11 | Friction and traction force | 56 |
| Figure 2.12 | Typical traction curve | 56 |
| Figure 2.13 | Maxwell model for viscoelastic liquids | 58 |
| Figure 2.14 | Typical traction curves predicted by Equation 2.45 | 59 |
| Figure 2.15 | Effect of contact pressure on traction curves for SR-1 | 62 |
| Figure 2.16 | Effect of temperature on traction curves for WI-1 | 63 |
| Figure 3.1 | Chemical structures of hydrocarbons | 66 |
| Figure 3.2 | Structure of soap fibre in greases | 69 |
| Figure 3.3 | Time and amount dependence of the film thickness of the grease | 72 |

| | | |
|-------------|---|-----|
| Figure 3.4 | Film thickness as a function of speed for the fully flooded and starved regimes | 74 |
| Figure 4.1 | Electrical contact resistance trace for smooth ball and for rough ball | 80 |
| Figure 4.2 | Equivalent circuit of a dielectric | 83 |
| Figure 4.3 | Frequency dependences of the real and imaginary parts of a dielectric constant | 84 |
| Figure 4.4 | Frequency dependence of loss tangent for various solutions | 87 |
| Figure 4.5 | Dielectric properties of solution PVP/1-heptanol | 89 |
| Figure 4.6 | Schematic representations of dipole vectors in polymer | 91 |
| Figure 5.1 | PCS Instruments test rig | 96 |
| Figure 5.2 | Micrometre based measurement | 97 |
| Figure 5.3 | Schematic diagram of the EHD rig for dielectric measurements | 99 |
| Figure 5.4 | Capacitance of the rig for air and full-oil measurements | 100 |
| Figure 5.5 | ULTRA interferometric system | 102 |
| Figure 5.6 | Film thickness versus entrainment speed | 103 |
| Figure 5.7 | Typical images of various film thickness | 105 |
| Figure 5.8 | RGB value function of film thickness | 106 |
| Figure 5.9 | Typical interference image of a static contact | 107 |
| Figure 5.10 | Hue values at the cross section AB in Figure 5.9 | 108 |
| Figure 5.11 | Relationship between Hue values and gap | 109 |
| Figure 5.12 | Film thickness as a function of Hue values | 109 |
| Figure 5.13 | Grease film thickness decay | 112 |

| | | |
|-------------|---|-----|
| Figure 5.14 | Friction force measurement on PCS Instruments test rig | 113 |
| Figure 5.15 | Typical traction curves | 114 |
| Figure 5.16 | Traction curves for calculating Eyring stress and effective viscosity | 115 |
| Figure 5.17 | Schematic diagram of EHL vibration rig | 116 |
| Figure 6.1 | Dielectric constant of “viscosity 68” oils | 122 |
| Figure 6.2 | Dielectric loss of “viscosity 68” oils | 124 |
| Figure 6.3 | Dielectric constant of greases | 128 |
| Figure 6.4 | Relaxation time of greases | 130 |
| Figure 6.5 | Dielectric loss of greases | 131 |
| Figure 6.6 | Dielectric properties of greases | 132 |
| Figure 6.7 | Dielectric constant of the base oil of SRL under sheared condition | 134 |
| Figure 6.8 | Dielectric loss of the base oil of SRL under sheared condition | 134 |
| Figure 6.9 | EHD contact capacitance of the base oil of SRL at 0.3m/s | 136 |
| Figure 6.10 | ULTRA film thickness measurement for base oil of SRL | 137 |
| Figure 6.11 | Dielectric constant of the base oil of SRL in the EHD condition | 138 |
| Figure 6.12 | Schematic diagram of the EHD contact and assumed capacitor | 139 |
| Figure 6.13 | Dielectric constant of the base oil of SRL with error bars | 140 |
| Figure 6.14 | Molecular behaviour inside the EHD contact | 142 |
| Figure 6.15 | EHD contact capacitance of HVI 160S | 143 |
| Figure 6.16 | Dielectric constant of HVI 160S in the EHD condition | 144 |
| Figure 7.1 | Traction curves of SRL at 10N and 20mm/s | 147 |

| | | |
|-------------|--|-----|
| Figure 7.2 | SRL film thickness changes with time at 20mm/s | 147 |
| Figure 7.3 | Traction curves of Grease1 and PAO4 | 148 |
| Figure 7.4 | Traction curves of Grease2 and PAO68 | 149 |
| Figure 7.5 | Traction curves of Grease3 and PAO40 | 149 |
| Figure 7.6 | Traction curves of 12OH-LiSt greases | 151 |
| Figure 7.7 | Traction curves of Grease5 and PAO4 | 152 |
| Figure 7.8 | Traction curves of Grease6 and PAO40 | 153 |
| Figure 7.9 | Traction curves of SRL and its base oil | 153 |
| Figure 7.10 | Traction curves of LiSt greases | 154 |
| Figure 7.11 | Traction curves of Grease4 and PAO4 | 156 |
| Figure 7.12 | Traction curves of RL2 and its base oil | 156 |
| Figure 7.13 | Traction curves of RLS2 and its base oil | 157 |
| Figure 7.14 | Traction curves of SB-M and its base oil | 157 |
| Figure 7.15 | Traction curves of urea greases | 158 |
| Figure 7.16 | Traction curves of “viscosity 68” oils | 160 |
| Figure 7.17 | Traction curves of investigated greases | 161 |
| Figure 7.18 | Structure of soap fibre in greases | 162 |
| Figure 7.19 | Traction curves of SRL | 163 |
| Figure 7.20 | Traction curves of SRL for Eyring stress and effective viscosity | 164 |
| Figure 7.21 | Eyring stress of Grease1 and PAO4 | 165 |
| Figure 7.22 | Eyring stress of Grease2 and PAO68 | 165 |

| | | |
|-------------|---|-----|
| Figure 7.23 | Eyring stress of Grease3 and PAO40 | 166 |
| Figure 7.24 | Eyring stress of Grease5 and PAO4 | 167 |
| Figure 7.25 | Eyring stress of Grease6 and PAO40 | 168 |
| Figure 7.26 | Eyring stress of SRL and its base oil | 168 |
| Figure 7.27 | Eyring stress of Grease4 and PAO4 | 169 |
| Figure 7.28 | Eyring stress of RL2 and its base oil | 170 |
| Figure 7.29 | Eyring stress of RLS2 and its base oil | 170 |
| Figure 7.30 | Eyring stress of SB-M and its base oil | 171 |
| Figure 7.31 | Film thickness measurements of SRL and its base oil at 30°C | 173 |
| Figure 7.32 | Effective viscosity of Grease1 and PAO4 | 174 |
| Figure 7.33 | Effective viscosity of Grease2 and PAO68 | 174 |
| Figure 7.34 | Effective viscosity of Grease3 and PAO40 | 175 |
| Figure 7.35 | Effective viscosity of Grease5 and PAO4 | 176 |
| Figure 7.36 | Effective viscosity of Grease6 and PAO40 | 176 |
| Figure 7.37 | Effective viscosity of SRL and its base oil | 177 |
| Figure 7.38 | Effective viscosity of Grease4 and PAO4 | 178 |
| Figure 7.39 | Effective viscosity of RL2 and its base oil | 179 |
| Figure 7.40 | Effective viscosity of RLS2 and its base oil | 179 |
| Figure 7.41 | Effective viscosity of SB-M and its base oil | 180 |
| Figure 7.42 | Mechanical relaxation time of Grease1 and PAO4 | 182 |
| Figure 7.43 | Mechanical relaxation time of Grease2 and PAO68 | 183 |

| | | |
|-------------|---|-----|
| Figure 7.44 | Mechanical relaxation time of Grease3 and PAO40 | 183 |
| Figure 7.45 | Mechanical relaxation time of Grease5 and PAO4 | 185 |
| Figure 7.46 | Mechanical relaxation time of Grease6 and PAO40 | 185 |
| Figure 7.47 | Mechanical relaxation time of SRL and its base oil | 186 |
| Figure 7.48 | Mechanical relaxation time of Grease4 and PAO4 | 187 |
| Figure 7.49 | Mechanical relaxation time of RL2 and its base oil | 187 |
| Figure 7.50 | Mechanical relaxation time of RLS2 and its base oil | 188 |
| Figure 7.51 | Mechanical relaxation time of SB-M and its base oil | 188 |
| Figure 7.52 | Mechanical relaxation time of greases | 191 |
| Figure 8.1 | Comparison of grease film decay | 193 |
| Figure 8.2 | RL2 time to starvation | 194 |
| Figure 8.3 | RL2 sliding distance to starvation | 195 |
| Figure 8.4 | RLS2 time to starvation | 196 |
| Figure 8.5 | RLS2 sliding distance to starvation | 197 |
| Figure 8.6 | SB-M time to starvation | 198 |
| Figure 8.7 | SB-M sliding distance to starvation | 198 |
| Figure 8.8 | SRL time to starvation | 199 |
| Figure 8.9 | SRL sliding distance to starvation | 200 |
| Figure 8.10 | Grease film thickness decay and recovery under lateral oscillations | 203 |
| Figure 8.11 | Grease2 film thickness decay and recovery | 204 |
| Figure 8.12 | Grease4 film thickness decay and recovery | 204 |

| | | |
|-------------|---|-----|
| Figure 8.13 | Grease6 film thickness decay and recovery | 205 |
| Figure 8.14 | RL2 film thickness decay and recovery | 205 |
| Figure 8.15 | RLS2 film thickness decay and recovery | 206 |
| Figure 8.16 | SB-M film thickness decay and recovery | 206 |
| Figure 8.17 | SRL film thickness decay and recovery | 207 |
| Figure 8.18 | Typical behaviour of an EHD contact in lateral vibrations | 209 |
| Figure 8.19 | SB-M film thickness changes during one lateral cycle at 10Hz | 210 |
| Figure 8.20 | Definition of the S value | 210 |
| Figure 8.21 | SB-M relationship between film thickness and distance S | 211 |
| Figure 8.22 | SB-M measured S values and theoretical values for each film | 212 |
| Figure 8.23 | SB-M EHD contact under lateral vibrations at the point of (a) | 212 |
| Figure 8.24 | SB-M film thickness changes under lateral motion | 214 |
| Figure 8.25 | RL2 film thickness decay under shear | 217 |
| Figure 8.26 | RLS2 film thickness decay under shear | 218 |
| Figure 8.27 | SB-M film thickness decay under shear | 218 |
| Figure 8.28 | SRL film thickness decay under shear | 219 |
| Figure 8.29 | Definition of the cavity length | 221 |
| Figure 8.30 | Changes of cavity length with time | 222 |
| Figure 8.31 | Cavity length as a function of film thickness | 223 |
| Figure 8.32 | Effect of viscosity of the base oil upon the cavity length | 224 |
| Figure 8.33 | Investigating region and the general solution of Equation 8.3 | 226 |

| | | |
|-------------|---|-----|
| Figure 8.34 | Effect of viscosity upon the cavity length in the rheological model | 227 |
| Figure A1.1 | Powder of thickener | 248 |
| Figure A1.2 | Dielectric constant of thickeners | 250 |
| Figure A1.3 | Dielectric loss of thickeners | 251 |
| Figure A3.1 | Exit of conjunction | 254 |

LIST OF TABLES

| | | |
|------------|---|-----|
| Table 4.1 | Dielectric constant of lubricants | 92 |
| Table 5.1 | Physical and chemical properties of oils | 119 |
| Table 5.2 | Physical properties of studied greases | 120 |
| Table A1.1 | Details of thickeners | 249 |
| Table A2.1 | Film thickness at 20mm/s and 20N for all lubricants | 252 |

NOMENCLATURE

| | |
|----------------|--|
| A | area (contact area) |
| a | radius of the contact |
| a_{θ} | shift factor relating to temperature |
| $a_{\theta,p}$ | shift factor relating to both temperature and pressure |
| C | capacitance |
| c | constant |
| C^* | complex capacitance |
| C_0 | capacitance of free space |
| C_1 | constant |
| C_2 | constant |
| C_3 | constant of integration |
| C_{air} | air capacitance |
| C_b | background capacitance |
| C_D | capacitance between unloaded pads |
| C_m | measured capacitance |
| D | Deborah number |
| d | separation |
| E | electric field |

| | |
|------------------|---|
| E' | reduced modulus of elasticity |
| E_A | Young's modulus of body A |
| E_B | Young's modulus of body B |
| F | friction force |
| G | dimensionless material parameter |
| G_e | elastic shear modulus |
| H | dimensionless film thickness parameter |
| h | film thickness |
| h_0 | minimum film thickness (= central film thickness only in literature 16) |
| h_b | film thickness outside the contact (gap between two bodies) |
| h_c | central film thickness |
| h_D^* | separation between the discs at positions just outside the pressurised region |
| h_H | gap between two bodies in Hertzian dry contact |
| h_m | constant of integration |
| \hat{H}_{\min} | dimensionless minimum film thickness parameter |
| i | angle of incident |
| i' | angle of refraction |
| k | ellipticity parameter |
| l | length of the film |
| M' | real part of the dielectric modulus |

| | |
|------------|--|
| M'' | imaginary part of the dielectric modulus |
| m | constant |
| N | integer |
| n | refractive index |
| p | pressure |
| p' | reduced pressure |
| p_r | pressure at reference point |
| p_{\max} | maximum Hertzian pressure |
| q_x | flow per unit width in y direction |
| q_y | flow per unit width in x direction |
| R | resistance |
| R' | reduced radius of curvature |
| R_A | radius of a sphere body A |
| R_{ax} | radius of body A in x direction |
| R_{ay} | radius of body A in y direction |
| R_b | radius of the ball |
| R_{bx} | radius of body B in x direction |
| R_{by} | radius of body B in y direction |
| R_x | reduced radius of curvature parallel to rolling direction (in x direction) |

| | |
|-------------|---|
| R_y | reduced radius of curvature perpendicular to rolling direction (in y direction) |
| S | distance of the region filled with the lubricant from the inlet of the contact |
| s | entropy |
| s_0 | entropy under no electric field |
| SRR | slide-roll ratio (represented by S in literature) |
| T | traction force |
| t | time |
| U | dimensionless speed parameter |
| u | velocity |
| \bar{u} | mean surface velocity (mean velocity in x direction) |
| u_1 | velocity of body (surface) 1 (velocity in x direction at $z = 0$) |
| u_2 | velocity of body (surface) 2 (velocity in x direction at $z = h$) |
| u_s | sum velocity of the velocities of the two surfaces |
| u_x | velocity in x direction |
| u_y | velocity in y direction |
| \bar{u}_y | mean velocity in y direction |
| u_{y1} | velocity in y direction at $z = 0$ |
| u_{y2} | velocity in y direction at $z = h$ |
| u_z | velocity in z direction |

| | |
|-----------------------|---|
| u_{z1} | velocity in z direction at $z = 0$ |
| u_{z2} | velocity in z direction at $z = h$ |
| Δu | sliding speed |
| W | dimensionless load parameter |
| w | normal applied load |
| x_b | distance of the region filled with the lubricant from the centre of the contact |
| Z | impedance |
| α | pressure-viscosity coefficient |
| γ | strain |
| $\dot{\gamma}$ | shear rate |
| γ_e | strain of spring |
| γ_v | strain of dashpot |
| δ_d | tangent loss factor |
| δ_o | optical path difference |
| ε' | real part of the complex permittivity (dielectric constant) |
| ε'' | imaginary part of the complex permittivity |
| ε^* | complex permittivity |
| ε_0 | permittivity of free space |
| ε_∞' | relative permittivity at very high frequency (= square of the refractive index) |

| | |
|---------------|--|
| ϵ_0' | relative permittivity at the zero frequency |
| ϵ_r | relative permittivity (dielectric constant) |
| μ | traction coefficient |
| ϕ | correction factor |
| η | dynamic viscosity of the lubricant |
| η_0 | viscosity of the lubricant at atmospheric pressure |
| η_r | viscosity at the reference point |
| θ | temperature |
| θ_r | reference temperature |
| λ | wavelength of the light |
| ν_A | Poisson's ratio of body A |
| ν_B | Poisson's ratio of body B |
| T_d | dielectric relaxation time |
| T_m | mechanical relaxation time |
| τ | shear stress |
| τ_0 | Eyring stress |
| τ_c | limiting shear stress |
| τ_y | yield stress |
| σ_e | electrical conductivity of the material |

| | |
|------------|--|
| ρ | density of the fluid |
| ρ_0 | density of the fluid at ambient pressure |
| ρ_r | density at reference point |
| ω | angular frequency |
| ω_p | peak angular frequency |

Chapter 1

Introduction

This chapter provides a general introduction to the subject of this experimental study. The aims of this study are outlined and the layout of this thesis is described.

1.1 General Introduction

This study is part of a wider study into the correlation between the rheological properties of lubricants, especially in elastohydrodynamic (EHD) contacts, and their dielectric characteristics, focusing mainly on lubricating greases and corresponding base oils. EHD contacts can be found in many machine elements such as rolling element bearings, gears, constant velocity joints and others, where a thin lubricating film, usually under one micrometer, separates the interacting surfaces and therefore plays an important role in the durability of components by avoiding mechanical failure induced by metallic surfaces contacting each other. Improving the conditions of film forming in EHD lubrication (EHL) regime has the potential to increase the efficiency of devices without major design changes and it is useful in any field because bearings, for example, are necessary for everything from aircrafts to mobile phones. Almost all rolling element bearings, nowadays, are lubricated by greases and operate in conditions which satisfy the industrial standards. It is, however, difficult to establish the lubrication principle of greases and their behaviour is remarkably less known in comparison with the well-established lubrication theory of oils. This is because greases commonly consist of more than two materials and form a semi-solid material which features considerably less fluidity compared to liquids.

Dielectric properties are, on the other hand, particular to substances and any change in their values indicates chemical changes in structure, for example such as those due to oxidation. They are also influenced by temperature and pressure, and the dielectric behaviour can also be correlated to the mechanical loading of the material. Moreover, it is useful to utilise the dielectric properties of lubricants for EHL film thickness measurements in some cases. Dielectric spectroscopy (measurement of dielectric properties, a function of frequency) has been used in this research not only for predicting in-contact rheological properties of lubricants from dielectric properties but also for evaluating directly the condition inside the contact.

1.2 Aims of the Study

The overall aim of this research study is to gain a better understanding of grease lubricated contacts utilised in many applications. A better prediction of the lubrication conditions in the operation of machine elements contributes not only to the improved functioning of devices but also to the reduction of emissions and thereby has impact on the environment. Climate change is a serious problem affecting us all and there is strong evidence that human emissions of CO₂ are changing the world's climate and a significant increase of the emission can be attributed to the inefficiency of various equipments.

There are two main problems to grease lubrication. Firstly, grease behaviour is complicated compared to that of oil due to the dual phases of its structure, namely solid and liquid. Secondly, many experimental studies in the EHD conditions are conducted using unrealistic materials, i.e. one transparent sample, in order to observe the contact behaviour by optical methods. The latter is not only about greases and the investigation from the dielectric point of view provides the opportunity to observe the real contact behaviour such as metal-to-metal contact. Furthermore, it is hoped that the understanding of the combined tribological behaviour and dielectric behaviour would help predicting the lubrication conditions for better operation in any machinery.

The main aims of the study are summarised as follows:

- To investigate materials from the dielectric point of view and assess the correlation between tribological and dielectric properties of lubricants including greases.
- To develop the capacitive method for measuring the film thickness in the steel-to-steel contact and evaluate the intrinsic changes of lubricants inside the real contact.
- To observe the film formation and starvation in the EHD contact in order to explain the behaviour of greases.

1.3 Structure of the Thesis

This thesis is organised in nine chapters preceded by the abstract, acknowledgements, table of contents, list of figures, list of tables and nomenclature. The work presented in the thesis is structured as follows.

Chapter 1 contains a brief introduction and main aims related to the studied field. It also includes a description of the structure of the thesis.

Chapter 2 contains a more comprehensive introduction to the EHD lubrication. It describes the phenomena, main constitutive equations and EHL film equations. Rheology in EHD lubrication is also discussed.

Chapter 3 is a description of lubricants. A brief description of lubricating oils and greases is presented followed by the behaviour of greases in EHD lubrication.

In chapter 4 the history of electrical measurements in lubrication is outlined. Previous studies based on the dielectric spectroscopy are also reviewed.

Chapter 5 describes the test rig and the test methods as well as the indication of the experimental results obtained in this study.

Chapter 6 includes results of dielectric properties of lubricants in both static and dynamic conditions. For greases the effect of thickeners and base oils is discussed, while the effect of the chemical structure is investigated in the case of lubricating oils.

In chapter 7 the results of the EHD conditions are presented in terms of rheological properties such as the effective viscosity and Eyring stress, focusing mainly on greases. Correlation between rheological and dielectric behaviour is discussed.

Chapter 8 contains the effect of lateral oscillations on the starvation behaviour of greases. The grease behaviour based on this vibration study is discussed for explaining the grease behaviour in the real situation. Finally, the cavitation phenomena in grease lubrication were fundamentally investigated.

Chapter 9 is the final chapter in which conclusions of this study are presented and future work is suggested.

Chapter 2

Background on Elastohydrodynamic Lubrication

This chapter provides an introduction to elastohydrodynamic lubrication. It gives a brief description of the phenomena and constitutive equations as well as actual images of elastohydrodynamic lubrication films.

Lubrication is necessary for all kinds of mechanical device. When two surfaces in machine elements move at relative speed to each other in the presence of a lubricant, a continuous lubricant film is formed by viscous drag action to separate the two surfaces with micrometre scale. This helps machine function without premature failure. This principle is called hydrodynamic lubrication. When the pressure generated between the lubricated surfaces becomes much larger, due to non-conformal geometry, relatively large elastic deformations of the surfaces occur. In this regime, the lubrication principle is generally called as the elastohydrodynamic lubrication (EHL). It is likely that, in this case, the fluid no longer obeys Newtonian characteristics due to the exposure to the high pressure. Thus, the changes in viscosity of a lubricant with pressure, as well as the changes in shape of contacting surfaces, play important roles in the EHL regime.

The EHL regime can be found in many machine elements, where contacts between interacting surfaces have dimensions less than 1mm and pressures of up to 3GPa. The film of lubricant formed between surfaces is typically less than one micrometer thick and passes through the conjunction in a time interval of about one thousand of a second. When the two surfaces move relative to each other at the same speed, the relative motion is called pure rolling. When a speed difference occurs, sliding motion becomes present between the two surfaces moving relative to one another. The motion, in the circumstance when one surface moves against a fixed surface such as that experienced between a piston ring and a cylinder liner in an IC engine, is known as pure sliding.

2.1 Contact of Elastic Smooth Bodies. Hertz Theory

In most cases such as rolling element bearings, gears, cams and traction drives, the contacting surfaces are non-conformal and hence the area of contact is very small compared to the dimensions of contacting bodies. In this situation, the stress in the contact becomes very high and the contacting surfaces are deformed either elastically or even plastically depending on the magnitude of the applied pressure and the materials' properties. Studies to determine the analytical formula of contact dimensions under such large pressure are based on the theory of the elastic contact which was developed by Hertz in 1881 [1, 2].

The contact between a sphere and a plane surface can be seen in Figure 2.1. This combination yields the same situation as experiments in this study, where the contact is circular, and the radius of curvature and the Young's modulus of the materials dominate the configuration of the area through the following equations.

Radius of contact:

$$a = \left(\frac{3wR_A}{E'} \right)^{1/3} \quad (2.1)$$

where: w = normal load

R_A = radius of a sphere

E' = reduced Young's modulus

$$\text{where: } \frac{1}{E'} = \frac{1}{2} \left[\left(\frac{1 - \nu_A^2}{E_A} \right) + \left(\frac{1 - \nu_B^2}{E_B} \right) \right] \quad (2.2)$$

E_A = Young's modulus of body A

E_B = Young's modulus of body B

ν_A = Poisson's ratio of body A

ν_B = Poisson's ratio of body B

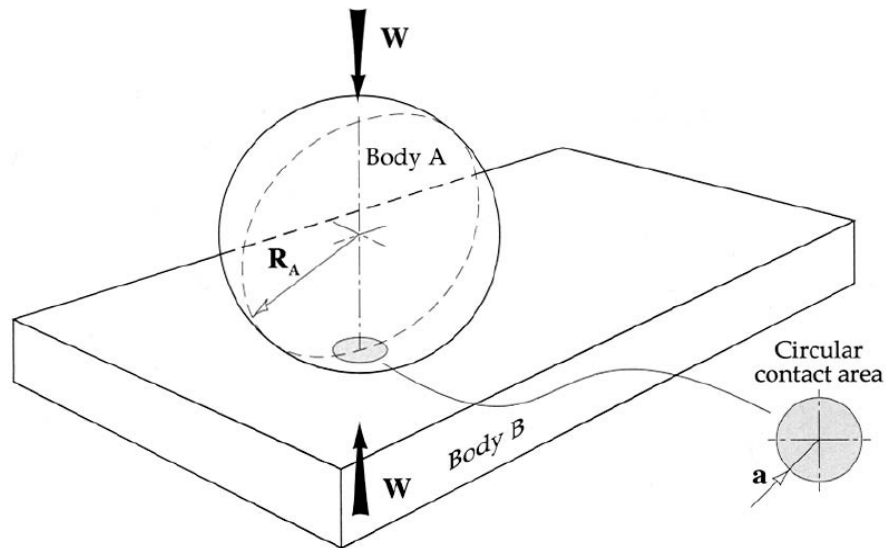


Figure 2.1 Contact between a sphere and a flat surface [2]

Contact pressure

The distribution of the contact pressure is parabolic as it was firstly proposed by Hertz [1] and shown in Figure 2.2. The maximum pressure, also called *Hertzian pressure*, is expressed by Equation 2.3.

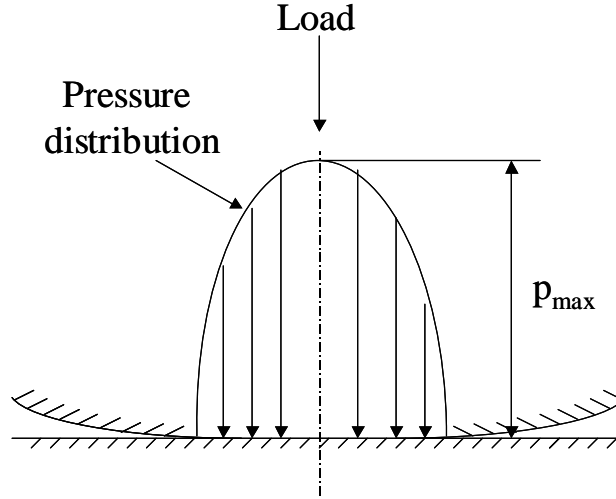


Figure 2.2 Hertz contact pressure

Maximum contact pressure:

$$p_{\max} = \frac{3w}{2\pi a^2} \quad (2.3)$$

where w is applied load and a is the radius of the contact.

Equation of the gap between two bodies

Because the elliptical contact between two ellipsoid bodies is the general case of the point contact (when one body has infinity radius it is considered as flat), from now on, the parameters between those bodies are discussed. The geometry of the elliptical contact is shown in Figure 2.3. The actual gap between two bodies is expressed by Equation 2.4 with the consideration of the elastic deformation [2, 3].

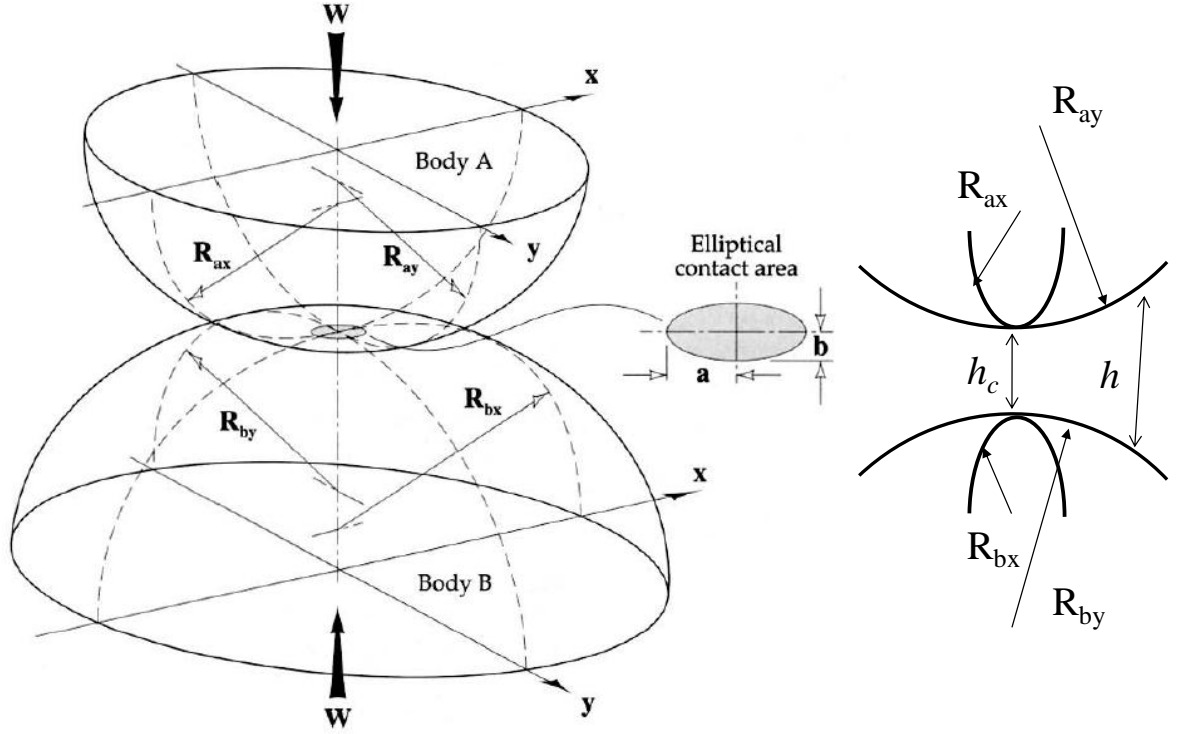


Figure 2.3 Geometry of two elastic bodies with convex surfaces [2]

$$h(x, y, t) = h_c + \frac{x^2}{2R_x} + \frac{y^2}{2R_y} + \frac{2}{\pi E'} \iint \frac{p(x', y', t) dx' dy'}{\sqrt{(x - x')^2 + (y - y')^2}} \quad (2.4)$$

where: t = time

h_c = central film thickness

$$\frac{1}{R_x} = \frac{1}{R_{ax}} + \frac{1}{R_{bx}} \quad (2.5)$$

$$\frac{1}{R_y} = \frac{1}{R_{ay}} + \frac{1}{R_{by}} \quad (2.6)$$

where: R_{ax} = radius of body A in x direction

R_{ay} = radius of body A in y direction

R_{bx} = radius of body B in x direction

R_{by} = radius of body B in y direction

2.2 Reynolds Equation

One of the governing equations of EHD lubrication is the so-called Reynolds equation which is the differential equation of the pressure distribution in fluid film lubrication. This was obtained in 1886 by the British scientist and engineer Osborne Reynolds [4].

General fluid situation between two surfaces is shown in Figure 2.4, where u_x and u_y are the velocities in x direction and y direction, respectively. The surface separation (lubricant film) and fluid dynamic viscosity η vary over x and y .

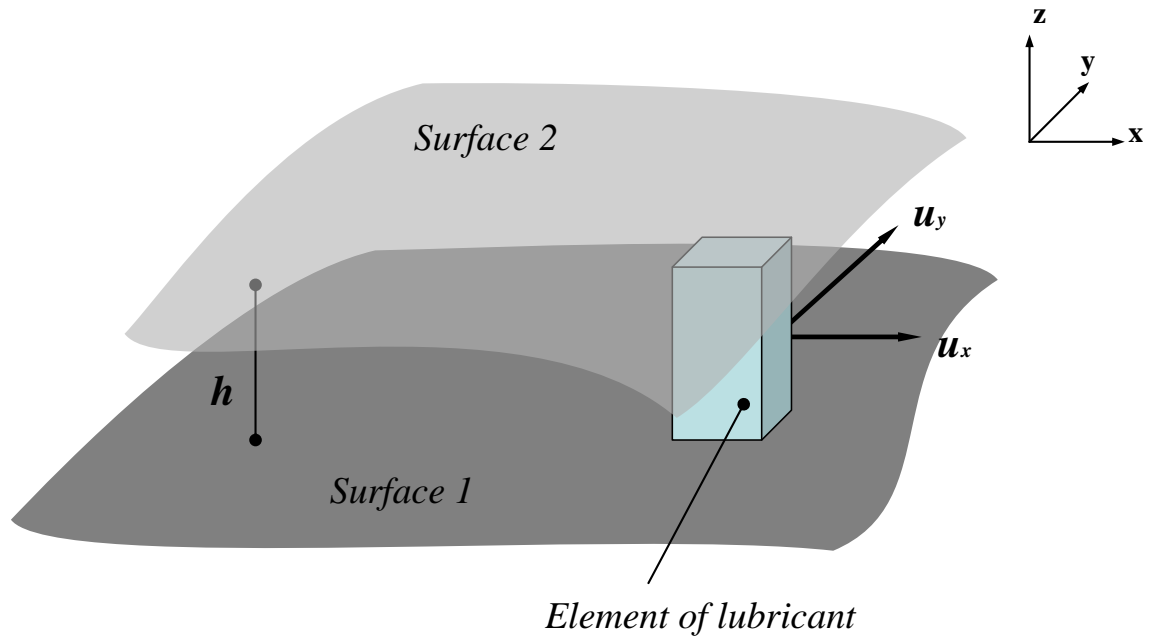


Figure 2.4 Two surfaces in relative motion

Reynolds made a number of simplifying assumptions, which apply to thin-film lubrication. These assumptions are:

- The height (thickness) of the film is very small in comparison to its span
- Pressure is constant through the fluid film
- The flow is laminar
- Body forces (including inertia forces) are negligible
- There is no slip at the boundaries
- Density of fluid constant
- Lubricant is Newtonian
- Viscosity constant of shear rate

With those assumptions, Reynolds equation can be derived by simplifying the Navier-Stokes equations to obtain a relation which correlates the pressure between two surfaces and its geometry [5].

Simplified Navier-Stokes equations are:

$$\begin{aligned}\frac{\partial p}{\partial x} &= \eta \frac{\partial^2 u_x}{\partial z^2} \\ \frac{\partial p}{\partial y} &= \eta \frac{\partial^2 u_y}{\partial z^2} \\ \frac{\partial p}{\partial z} &= 0\end{aligned}\quad (2.7)$$

When the fluid pressure and viscosity are assumed to be constant across the film thickness ($p \neq f(z)$, $\eta \neq f(z)$), integrating Equation 2.7 becomes:

$$\begin{aligned}\eta \frac{\partial u_x}{\partial z} &= \int \frac{\partial p}{\partial x} dz = \frac{\partial p}{\partial x} z + C_1 \\ \eta u &= \int \left(\frac{\partial p}{\partial x} z + C_1 \right) dz = \frac{\partial p}{\partial x} \frac{z^2}{2} + C_1 z + C_2\end{aligned}\quad (2.8)$$

where C_1 and C_2 are constants of integration.

The following boundary conditions, $u_x = u_1$ at $z = 0$ and $u_x = u_2$ at $z = h$, give:

$$\begin{aligned}C_2 &= \eta u_1 \\ C_1 &= (u_2 - u_1) \frac{\eta}{h} - \frac{\partial p}{\partial x} \cdot \frac{h}{2}\end{aligned}\quad (2.9)$$

Consequently, the velocity profile in x direction is obtained.

$$\eta u = \frac{1}{2} \frac{\partial p}{\partial x} z^2 + \eta (u_1 - u_2) \frac{z}{h} - \frac{1}{2} \frac{\partial p}{\partial x} h z + \eta u_1 \quad (2.10)$$

The velocity profile in y direction can be deduced in the same way.

When considering the flow volume, such as the element of a lubricant between two surfaces in Figure 2.4, flow can be obtained by integrating the velocity over the film thickness. Flow per unit width in y direction q_x can be calculated as follows.

$$\begin{aligned}q_x &= \int_0^h u dz \\ &= \left[\frac{1}{2\eta} \frac{\partial p}{\partial x} \left(\frac{z^3}{3} - \frac{h}{2} z^2 \right) + (u_2 - u_1) \frac{z^2}{2h} + z u_1 \right]_0^h \\ &= -\frac{h^3}{12\eta} \frac{\partial p}{\partial x} + (u_2 + u_1) \frac{h}{2}\end{aligned}\quad (2.11)$$

whilst q_y is expressed as:

$$q_y = -\frac{h^3}{12\eta} \frac{\partial p}{\partial x} + (u_{y2} + u_{y1}) \frac{h}{2} \quad (2.12)$$

where u_{y1} and u_{y2} are the velocities in y direction at $z = 0$ and $z = h$, respectively.

When the velocity in z direction is expressed as u_{z1} and u_{z2} at $z = 0$ and $z = h$, respectively, and with the assumption that the fluid density is constant, we obtain (shown in Figure 2.5):

$$q_x dy + q_y dx + u_{z1} dx dy = \left(q_x + \frac{\partial q_x}{\partial x} dx \right) dy + \left(q_y + \frac{\partial q_y}{\partial y} dy \right) dx + u_{z2} dx dy \quad (2.13)$$

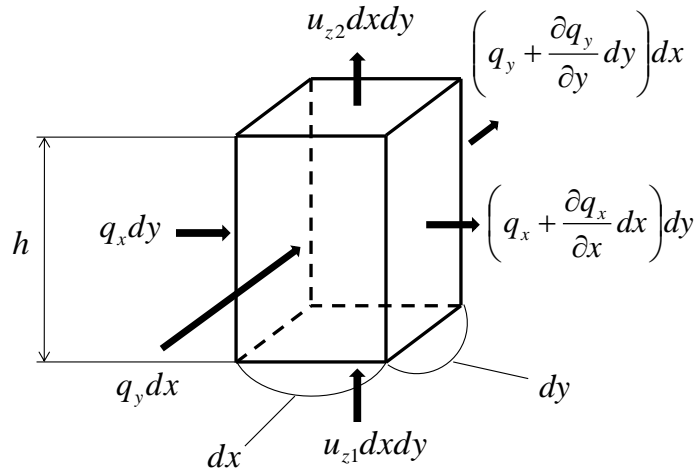


Figure 2.5 Flow into an element of a fluid

Hence

$$\frac{\partial q_x}{\partial x} + \frac{\partial q_y}{\partial y} + (u_{z2} - u_{z1}) = 0 \quad (2.14)$$

Substituting Equation 2.11 and 2.12 into Equation 2.14,

$$\frac{\partial}{\partial x} \left[-\frac{h^3}{12\eta} \frac{\partial p}{\partial x} + (u_2 + u_1) \frac{h}{2} \right] + \frac{\partial}{\partial y} \left[-\frac{h^3}{12\eta} \frac{\partial p}{\partial y} + (u_{y2} + u_{y1}) \frac{h}{2} \right] + (u_{z2} - u_{z1}) = 0 \quad (2.15)$$

Regarding the mean velocities as $\bar{u} = (u_1 + u_2)/2$ and $\bar{u}_y = (u_{y1} + u_{y2})/2$:

$$\frac{\partial}{\partial x} \left(\frac{h^3}{12\eta} \frac{\partial p}{\partial x} \right) + \frac{\partial}{\partial y} \left(\frac{h^3}{12\eta} \frac{\partial p}{\partial y} \right) = \frac{\partial}{\partial x} \bar{u} h + \frac{\partial}{\partial y} \bar{u}_y h + (u_{z2} - u_{z1}) \quad (2.16)$$

Reynolds equation can be obtained by assuming $\bar{u} \neq f(x)$ and $\bar{u}_y \neq f(y)$

$$\frac{\partial}{\partial x} \left(\frac{h^3}{\eta} \frac{\partial p}{\partial x} \right) + \frac{\partial}{\partial y} \left(\frac{h^3}{\eta} \frac{\partial p}{\partial y} \right) = 12 \left[\bar{u} \frac{\partial h}{\partial x} + \bar{u}_y \frac{\partial h}{\partial y} + (u_{z2} - u_{z1}) \right] \quad (2.17)$$

When only the velocities in one direction (x direction) is considered and the film thickness is constant along y direction, Reynolds equation reads:

$$\frac{dp}{dx} = 12\bar{u}\eta \left(\frac{h - h_m}{h^3} \right) \quad (2.18)$$

where h_m is the film thickness at $\frac{dp}{dx} = 0$.

2.3 Viscosity Variation with Pressure and Temperature

Pressure dependence of viscosity

One of the most used pressure-viscosity equations in EHL is known as Barus law described by Equation 2.19 [6].

$$\eta = \eta_0 e^{\alpha p} \quad (2.19)$$

where: η = viscosity of the lubricant

η_0 = viscosity of the lubricant at ambient pressure

α = pressure-viscosity coefficient

p = pressure

Pressure-viscosity coefficient characterises the variation of viscosity with pressure.

Temperature dependence of viscosity

The following equation can be used for the dependence of the viscosity with temperature, although many such formulas are known.

$$\log \log(\eta/\rho + 0.7) = C_1 + C_2 \log \theta \quad (2.20)$$

where C_1 and C_2 are constants for the lubricant and θ is the temperature in Kelvin scale.

ρ is the density of the lubricant.

2.4 Regimes of Lubrication

The lubrication of solid surfaces can be defined according to various criteria. It has been established that the deformation of the contacting surfaces and the variation of the viscosity with pressure play major roles in the type of lubrication characteristic to a certain application. From this point of view Hamrock and Dowson [7] have suggested the following four regimes:

Isoviscous-rigid body (IR regime)

In this regime, both the deformation of the surfaces and the changes in lubricant viscosity are ignored. This is comparable to the classical hydrodynamic case.

Piezoviscous-rigid body (PR regime)

In this regime, the increase in the lubricant viscosity cannot be negligible because of high pressure generated inside the contact whereas the deformation of surfaces can be negligible.

Isoviscous-elastic body (IE regime)

The viscosity of the lubricant does not change when the lubricant flows through the contact in this regime. However, the deformation of contacting surfaces has to be taken into account.

Piezoviscous-elastic body (PE regime)

The EHL is generally considered to take place in this regime, where the contacting surfaces are deformed and the viscosity of the lubricant between them increases due to the large pressure exerted onto the contact.

According to Hamrock and Dowson [7] these regimes can be defined by two parameters given by equations 2.21 and 2.22. A chart locating these regimes with a function of the

values of parameters G_V and G_E is shown in Figure 2.6 accompanied with dimensionless minimum film thickness parameter.

$$G_V = \frac{GW^3}{U^2} \quad (2.21)$$

$$G_E = \frac{W^{8/3}}{U^2} \quad (2.22)$$

$$\hat{H}_{\min} = \left(\frac{W}{U} \right)^2 H \quad (2.23)$$

The dimensionless parameters U , G , W and H are expressed as:

$$\text{Dimensionless speed parameter } U = \frac{\bar{u} \eta_0}{E'R'} \quad (2.24)$$

$$\text{Dimensionless material parameter } G = \alpha E' \quad (2.25)$$

$$\text{Dimensionless load parameter } W = \frac{w}{E'R'^2} \quad (2.26)$$

$$\text{Dimensionless film thickness parameter } H = \frac{h_0}{R'} \quad (2.27)$$

where R' = reduced radius of curvature expressed by

$$\frac{1}{R'} = \frac{1}{R_x} + \frac{1}{R_y} \quad (2.28)$$

and

\bar{u} = mean surface velocity

η_0 = viscosity of the lubricant at atmospheric pressure

α = pressure-viscosity coefficient

h_0 = minimum film thickness

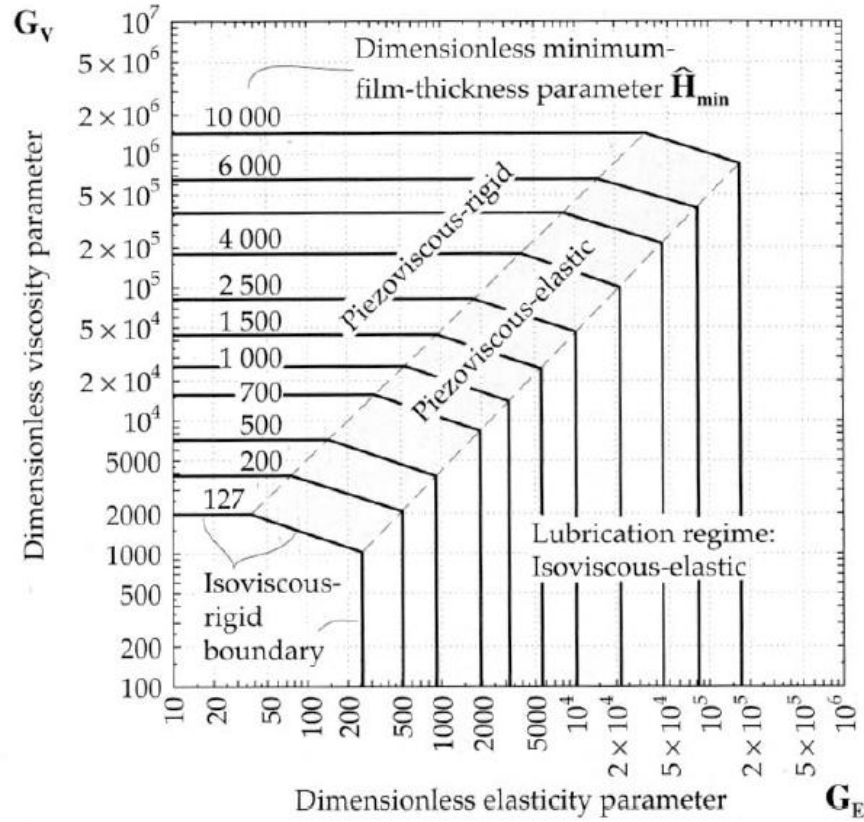


Figure 2.6 Map of lubrication regimes for a point contact [2]

2.5 Elastohydrodynamic Lubrication Regime

2.5.1 Mechanisms of elastohydrodynamic lubrication

The first insight into the mechanics of the EHD contact was obtained by Grubin *et al* [8, 9].

The main assumptions of their semi-analytical solution are:

- The geometry of the deformed bodies obey Hertz's theory
- The film thickness is constant throughout the contact
- The viscosity of the lubricant varies with pressure according to Barus's law

Their analysis started from Reynolds equation in form of Equation 2.18. At a first step, they substituted Equation 2.19 into Equation 2.18.

$$e^{-\alpha p} \frac{dp}{dx} = 12U\eta_0 \left(\frac{h - \bar{h}}{h^3} \right) \quad (2.29)$$

They assumed the deformed surface was separated by the film forming a constant film thickness, h_0 , and Hertz theory was used for the contact shape as shown in Figure 2.7.

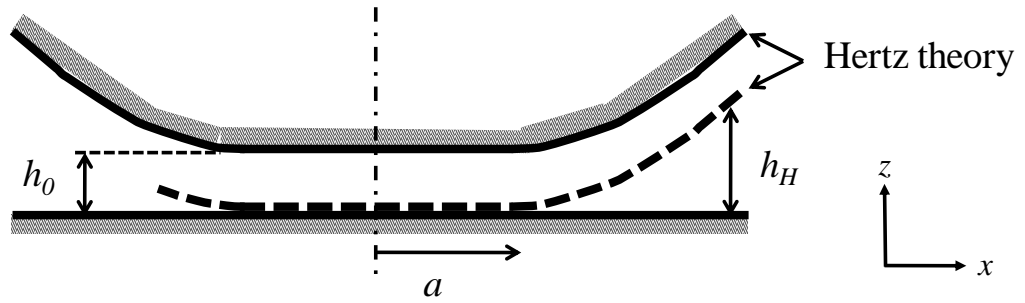


Figure 2.7 Grubin's film geometry

The gap between the two bodies outside the contact h_H was taken as:

$$h_H = \frac{a}{2R'} \left[\frac{x}{a} \sqrt{\frac{x^2}{a^2} - 1} - \ln \left(\frac{x}{a} + \sqrt{\frac{x^2}{a^2} - 1} \right) \right] \quad (2.30)$$

where R' is the reduced radius of curvature, a is the contact radius and x is the distance from the centre of the contact in flow direction.

Consequently, they regarded the film thickness in the inlet as

$$h(x) = h_0 + \frac{a}{2R'} \left[\frac{x}{a} \sqrt{\frac{x^2}{a^2} - 1} - \ln \left(\frac{x}{a} + \sqrt{\frac{x^2}{a^2} - 1} \right) \right] \quad (2.31)$$

They also defined a reduced pressure p' by:

$$p' = \frac{1 - e^{-\alpha p}}{\alpha} \quad (2.32)$$

By substituting Equation 2.31 and 2.32 into Equation 2.29, they firstly estimate the pressure profile in the EHD contact, which was given by:

$$\frac{h_0}{R'} = 1.93(U)^{3/4} (G)^{3/4} (W)^{-1/8} \quad (2.33)$$

where U , G and W have been defined in a previous section.

Thanks to the development of computer nowadays and more sophisticated experiments, several valuable formulae for the EHD contact have been proposed.

2.5.2 Accurate formula for EHL film thickness

Hamrock and Dowson [7] derived the EHL film thickness formula by solving Reynolds equation with the pressure-viscosity relationship and the pressure-density relationship in a lubricant as well as the elastic deformation, details of which have been described above.

$$\frac{h_c}{R'} = 2.69U^{0.67} G^{0.53} W^{-0.067} (1 - 0.61e^{-0.73k}) \quad (2.34)$$

where:

$$\text{Dimensionless speed parameter } U = \frac{\bar{u} \eta_0}{E' R'}$$

$$\text{Dimensionless material parameter } G = \alpha E'$$

$$\text{Dimensionless load parameter } W = \frac{w}{E' R'^2}$$

$$\text{Ellipticity parameter } k = 1.03 \left(\frac{R_y}{R_x} \right)^{0.636} \quad (2.35)$$

$$\text{Reduced Young's modulus } \frac{1}{E'} = \frac{1}{2} \left[\left(\frac{1 - \nu_A^2}{E_A} \right) + \left(\frac{1 - \nu_B^2}{E_B} \right) \right]$$

where:

E_A = Young's modulus of body A

E_B = Young's modulus of body B

R' = reduced radius of curvature

R_x = reduced radius of curvature parallel to rolling direction

R_y = reduced radius of curvature perpendicular to rolling direction

\bar{u} = mean surface velocity

w = normal applied load

α = pressure-viscosity coefficient

η_0 = viscosity of the lubricant at atmospheric pressure

ν_A = Poisson's ratio of body A

ν_B = Poisson's ratio of body B

For a line contact the ellipticity parameter is $k = \infty$, while it takes the value of one for a point contact. Equation 2.34 can be used to calculate the EHL film of any contact geometry by varying the value of k . Finally, the EHL film thickness is strongly influenced by the speed and the lubricant viscosity and weakly influenced by the load.

While the formulae derived by Dowson and Higginson [6] concentrated on the film thickness of a line contact such as between two cylinders, Hamrock-Dowson formula is valid for any contact geometry and offers a good agreement with new experimental results obtained by using the optical interferometry technique. Thus, in the later part of this thesis, this formula detailed above will be used for the calculation of the central film thickness h_c .

2.5.3 Characteristics of EHL films

The most versatile tool for the study of EHL films is based on optical interferometry phenomenon and uses a contact formed between a ball and a transparent flat body. The arrangement, established by Cameron and Gohar [10], simulates well the condition occurring in a rolling bearing, thus this technique has been adopted and developed by many researchers [11-15] as the usual way to study the EHL phenomena. The typical EHD contact taken by this method is presented in Figure 2.8.

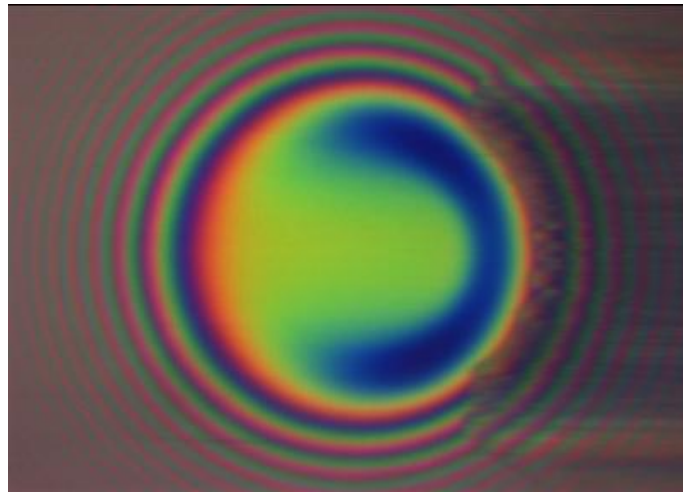


Figure 2.8 Typical image of the EHD contact

The distinct features in EHL films can be described as follows, which is the consensus established from not only the theoretical but also the experimental point of view.

- (1) The flat region, in terms of the film thickness, accounts for most of the contact area.
- (2) Constricted regions can be found at the sides and in the exit region of the contact, giving the EHL contact a distinctive horse-shoe shape.
- (3) The film constriction is accompanied by a sharp increase in pressure.
- (4) The film thickness is affected considerably by the lubricant viscosity and can be calculated by using lubricant properties in the inlet region.
- (5) The effect of the load on the film thickness is weak.

EHL contact pressure

As seen above, Grubin *et al* [8] considered that the film thickness was constant over the deformed contact area and the pressure distribution was found to be close to the Hertzian pressure corresponding to the static contact. Later on, Archard [16] found that the pressure distribution inside the contact and the shape of the surfaces were largely shifted from the Hertzian theory especially in the outlet region. The pressure spike in the exit region and the squeezed shape of the film thickness, or of the surface in other words, were proved by experimental work [10].

Today, there is consensus regarding the contact shape and the pressure distribution, although under very heavy load there is minor inconsistency with the general film shape and the pressure distribution described in Figure 2.9.

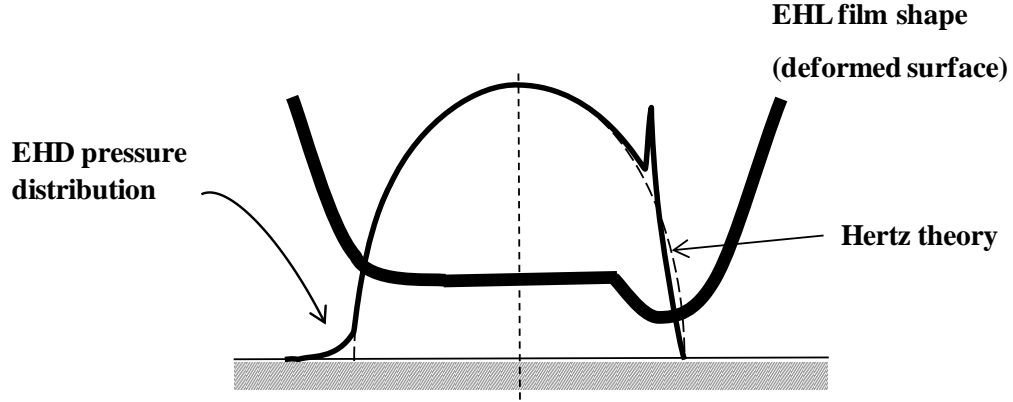


Figure 2.9 Pressure distribution and shape of the EHL lubricating film

2.5.4 Starved lubrication

The lubricant starvation can be caused when there is not enough amount of lubricant available in the inlet zone. This phenomenon can be evaluated by the following parameters, which are also shown in Figure 2.10 [17].

$$\frac{h_b}{h_0} = \frac{h_0 + h_H}{h_0} \quad (2.36)$$

$$S = x_b - a \quad (2.37)$$

where h_b is the film thickness outside the contact and h_0 is the central film thickness while h_H is the distance between two bodies in Hertzian dry contact theory and expressed as Equation 2.38.

$$h_H = \frac{ap_{\max}}{E'} \left[3.81 \left(\frac{x_b}{a} - 1 \right)^{1.5} \right] \quad (2.38)$$

where p_{\max} is the maximum contact pressure and E' is the reduced elastic modulus defined in the previous section.

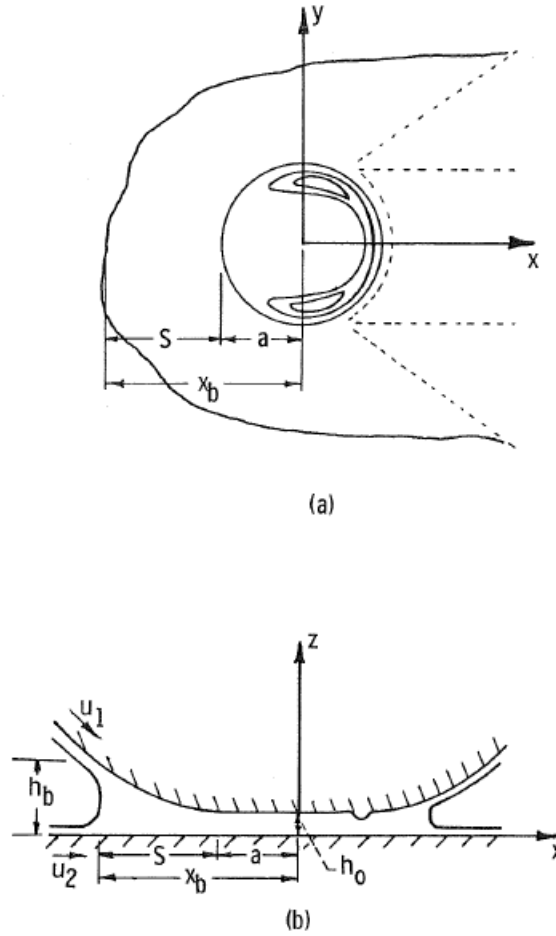


Figure 2.10 Contact geometry showing required measurements for starvation;

(a) plain view, (b) cross-sectional view along centreline [17]

Wedeven *et al* [17] based on experimental results, stated that there was no concern about the occurrence of the oil starvation when the region limited by parameter S (at which point $h_b/h_0 = 9$) was filled with oil.

2.6 EHD Friction and Rheology

2.6.1 EHD friction behaviour

The friction force F is defined as the resistance generated between two contacting bodies with relative motion. The direction of this force is opposite to that of the relative motion (shown in Figure 2.11). When the difference in rotating speeds between two surfaces occurs the tangential force generated on the surface moving at lower speed will have the same direction as the rotating speed while the direction of the force on the higher speed surface remains opposite to the body.

These two forces T are called *traction force* and are used to derive the traction coefficient μ by dividing it by the perpendicular loading force w .

$$\mu = \frac{T}{w} \quad (2.39)$$

The shear stress τ is expressed by dividing the traction force by the area A where the traction force is applied.

$$\tau = \frac{T}{A} \quad (2.40)$$

When the two speeds of the contacting surfaces are u_1 and u_2 , the slide-roll ratio is defined as the ratio between the sliding speed, Δu , and the rolling speed.

$$SRR = \frac{u_1 - u_2}{\left(\frac{u_1 + u_2}{2} \right)} = \frac{2\Delta u}{u_1 + u_2} \quad (2.41)$$

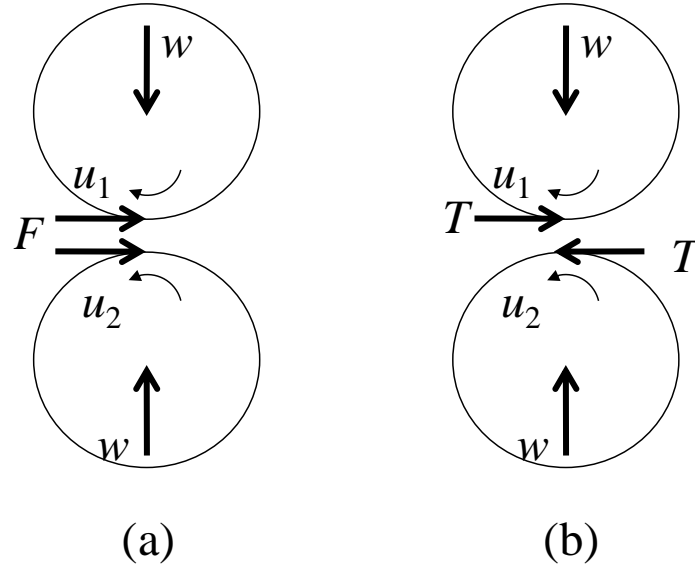


Figure 2.11 Friction and traction force; (a) $u_1 = u_2$, (b) $u_1 > u_2$

The traction behaviour of EHL oil films was well described by Johnson and Tevaarwerk [18] and the typical behaviour is shown in Figure 2.12.

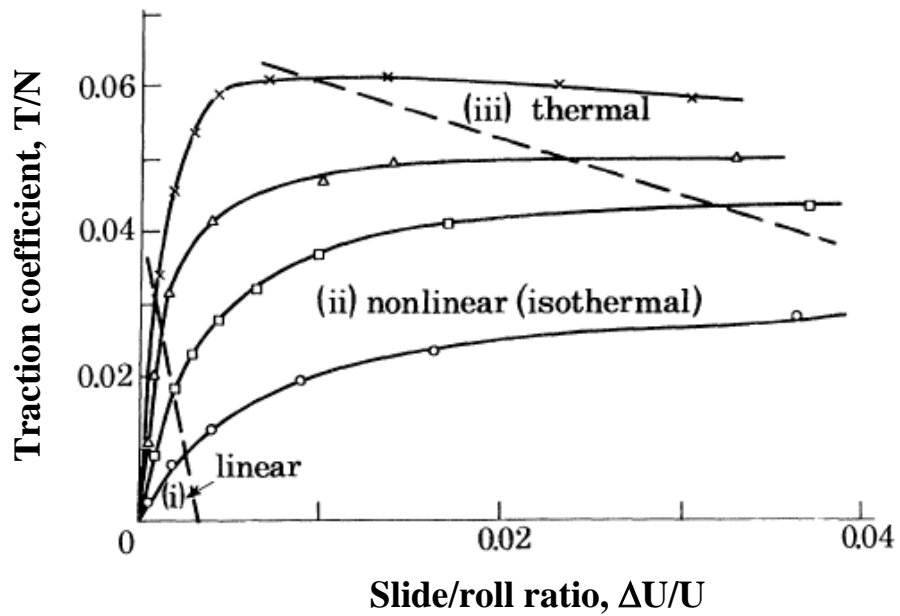


Figure 2.12 Typical traction curve [18]

Once a speed difference, often used as slide-roll ratio or shear rate, between two surfaces a traction force is generated in the lubricant film inside a contact. The traction coefficient increases linearly in the small slide-roll ratio region (linear region) and then increases gently with slide-roll ratio until a certain value of the slide-roll ratio (non-linear region). After the traction coefficient reaches the maximum value, it decreases slightly because the temperature rise due to the sliding causes the decrease of the lubricant viscosity in the contact. This is called thermal region. The traction coefficient shows steeper slope in the linear region and larger maximum values at increased pressure in the contact.

2.6.2 Rheological models

“Rheology is the study of the deformation and flow of matter.” This description has become used since the classical idea that elasticity and fluid dynamics cannot deal with the behaviour of fluids especially between elastically deformed walls. The term rheology is usually adopted to describe Non-Newtonian flow such as a grease’s behaviour. Meanwhile, tribology replaced words of lubrication, friction and wear since the 1960s [19].

Maxwell model

In general the traction behaviour in EHL films is explained by using the Maxwell visco-elastic model shown in Figure 2.13. In the Maxwell model, the relationship between a stress τ and a strain γ is expressed as follows.

$$\begin{aligned}\tau &= G_e \gamma_e = \eta \dot{\gamma}_v \\ \dot{\gamma} &= \dot{\gamma}_e + \dot{\gamma}_v = \frac{\dot{\tau}}{G_e} + \frac{\tau}{\eta}\end{aligned}\tag{2.42}$$

where G_e is the elastic shear modulus while the strains of the spring and the dashpot are γ_e and γ_v respectively. Newtonian law is assumed in a dashpot.

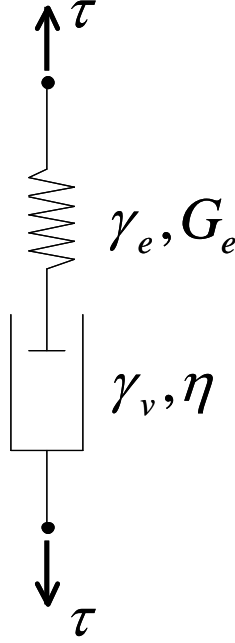


Figure 2.13 Maxwell model for viscoelastic liquids

The stress will decrease gradually according to Equation 2.43 when the strain is remains constant for time $t > 0$.

$$\tau = \tau^* \exp\left\{-t/(\eta/G_e)\right\} \quad (2.43)$$

where τ^* is the shear stress at $t = 0$. This relaxation process is called mechanical relaxation and η/G_e , i.e. the time for the initial value to decrease to $1/e$, is called mechanical relaxation time.

Johnson and Tevaarwerk model

Investigations into the elastohydrodynamic lubrication have also used the Eyring viscous model, described as Equation 2.44.

$$\dot{\gamma} = \frac{\tau_0}{\eta} \sinh\left(\frac{\tau}{\tau_0}\right) \quad (2.44)$$

where τ_0 is a representative stress called Eyring stress, which is a function of temperature and pressure. It indicates that a liquid obeys Newtonian law for $\tau \leq \tau_0$.

In EHL traction tests the shear rate $\dot{\gamma}$ and the shear stress play important roles. The former is given by $\Delta u/h$, where Δu is the sliding speed and h is the film thickness, and the latter is given by T/A , where A is considered the area of the contact.

Johnson and Tevaarwerk [18] substituted Eyring viscous model for Maxwell model and derived following equation.

$$\dot{\gamma} = \frac{\dot{\tau}}{G_e} + \frac{\tau_0}{\eta} \sinh\left(\frac{\tau}{\tau_0}\right) \quad (2.45)$$

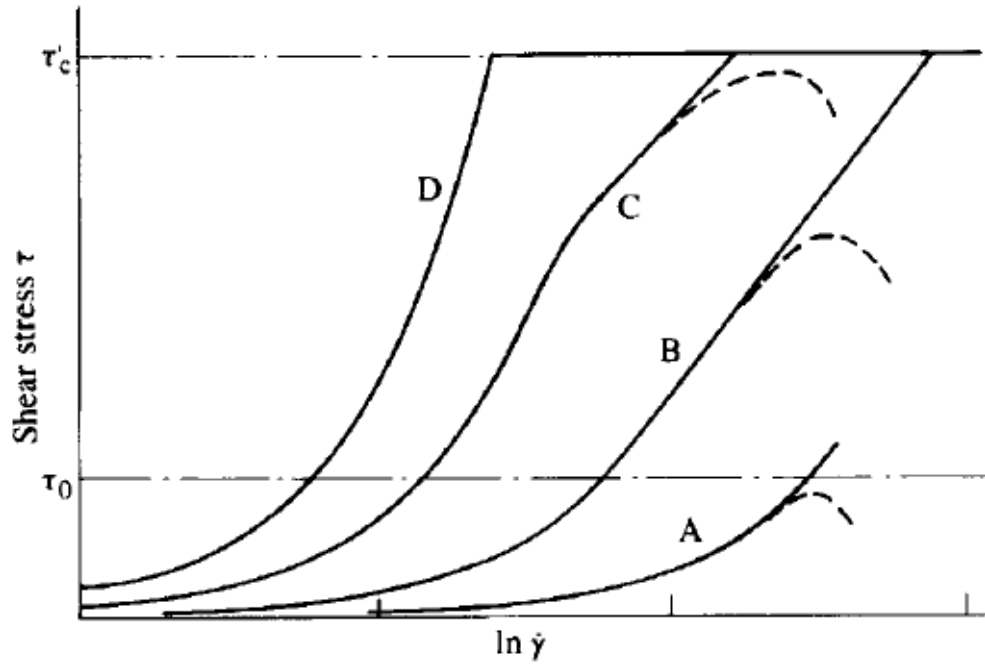


Figure 2.14 Typical traction curves predicted by Equation 2.45 [20]

Evans and Johnson model

Evans and Johnson [20] used the Deborah number D and showed the change of the traction behaviour predicted by Equation 2.45 with this parameter (Figure 2.14). Deborah number is expressed as the ratio between the relaxation time and the time of passage through the EHD contact: $\bar{\eta}u/G_e l$, where \bar{u} was the rolling speed, and l was the length of the film in the rolling direction and the traction behaviour was classified into four regimes. Curve A follows the Newtonian fluid and the Deborah number is much less than unity. As D increases, typical traction curve changes its shape from B to D.

To calculate the viscosity from the linear relationship in traction curves, Evans and Johnson transformed Equation 2.45 to Equation 2.46

$$\tau \cong \tau_0 \ln \dot{\gamma} + \tau_0 \ln \left(\frac{2\eta}{\tau_0} \right) \quad (2.46)$$

Consequently, they were able to successfully predict the viscosity of lubricants at high pressure by using the EHL equipment as a rheometer.

Hirst and Moore model

Hirst and Moore [21] have showed, based on extensive experimental traction results, that the EHD films behave elastically at low shear rates but lose elastic properties at higher rates of shear. They proposed a traction coefficient of the form as

$$\frac{T}{w} = \alpha \tau_0 - \frac{\tau_0}{p} \ln \left(\frac{\tau_0}{2\eta_0 \dot{\gamma}} \right) \quad (2.47)$$

where α is the pressure-viscosity coefficient and η_0 is the viscosity at ambient pressure.

Lee and Hamrock model

Lee and Hamrock model was developed relatively recently and it is expressed as follow [22, 23].

$$\dot{\gamma} = \frac{1}{\eta} \left[1 - (\tau/\tau_0)^2 \right]^{-1/2} \quad (2.48)$$

2.6.3 Rheology of EHD films

The observation of lubricants inside the elastohydrodynamic (EHD) contact is widely conducted with an arrangement featuring a transparent disc and a steel ball, and the film thickness measurements based on the optical interferometry is proved well in accordance with the theory. The film thickness is influenced mainly by the entrainment speed and the viscosity of the lubricant forming the film. Hence, for accurate prediction of the film thickness, it is essential to know the viscosity of lubricants as well as the rolling speed and temperature. For traction prediction, on the other hand, knowledge of the viscosity at high pressure is required. However it is difficult to predict the behaviour of oils at high pressure because oils beyond a certain point no longer obey the Newtonian, linear law between shear stress and shear rate.

The EHL disc machine has been used as a rheometer in order to predict the viscosity of oil at very high pressures since Evans and Johnson has developed the method [20]. Sutcliffe [24] investigated the rheological properties of a kerosene oil in the line-contact condition, while two kinds of paraffinic mineral oil were used by Muraki and Dong [25].

Bair commented on the discrepancy between the viscosity data from contact measurements and from conventional high pressure viscometer [26]. However, those discrepancies were mainly due to the inadequacy of the EHD equipments for the pressure-viscosity coefficient

measurement, and the concept behind the method was valid for predicting the viscosity from the rheological tests.

By using a conventional viscometer, Bair found that lubricants obey two different laws in terms of the Non-Newtonian behaviour [27]. One was a power law (shear thinning) and another was a near rate-independence law. Later on, Bair developed a high pressure viscometer and measured the viscosity of some basic hydrocarbon oils in order to investigate the pressure-viscosity coefficient [28]. This study has revealed that the viscosity of cyclic structure oils was more sensitive to the pressure than that of the paraffin oils. Naphthenic oils were also more sensitive than the aromatic oils. Among paraffinic oils, those consisting of short branch molecules had large pressure-viscosity response. Other rheological studies by Bair, on low molecular weight lubricants as well as polymers, proved to follow the same laws [29].

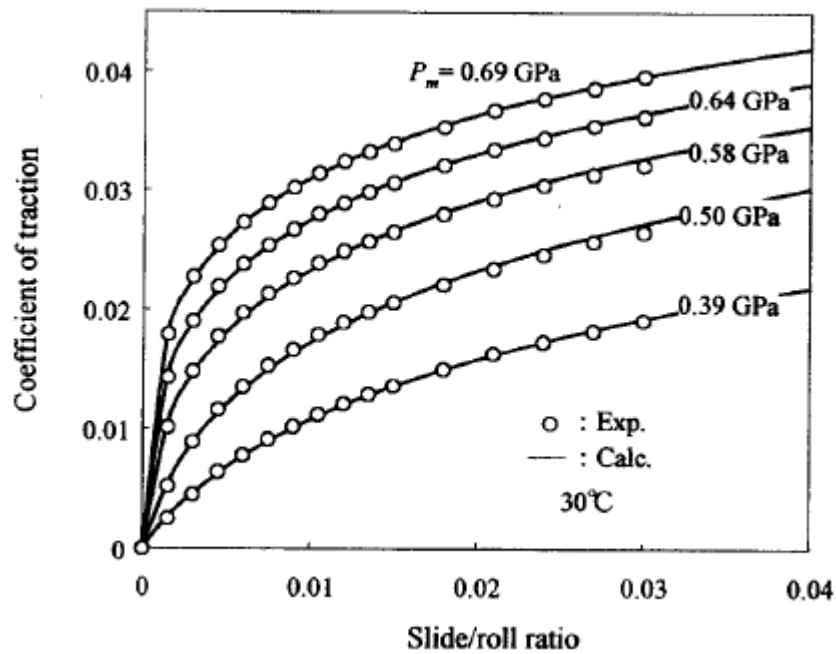


Figure 2.15 Effect of contact pressure on traction curves for SR-1 [30]

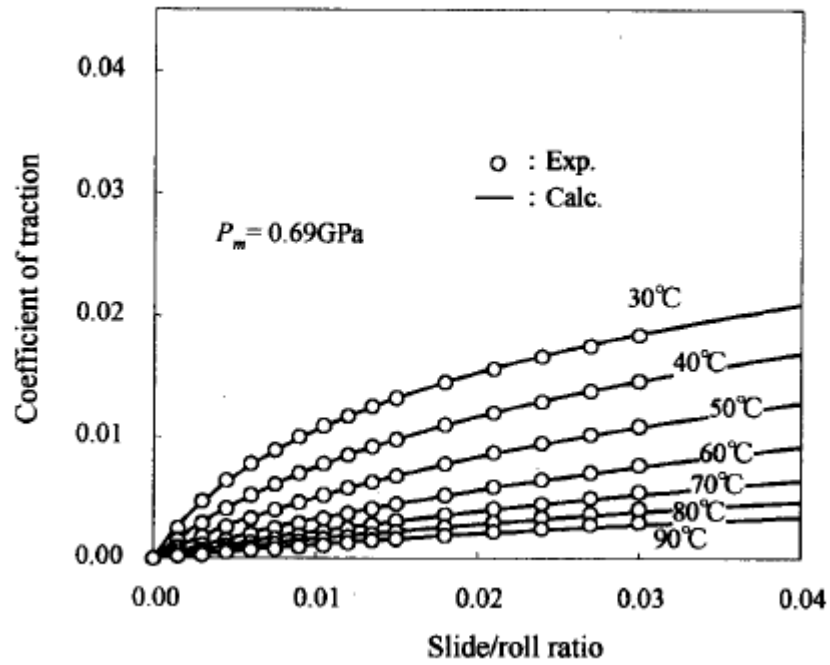


Figure 2.16 Effect of temperature on traction curves for WI-1 [30]

Investigation into the effect of pressure and temperature upon the rheological behaviour of lubricants, Murakami [30] studied the traction behaviour in EHL as functions of pressure and temperature. Figure 2.15 shows the effect of the contact pressure on the traction coefficient and the effect of temperature on the traction curve is seen in Figure 2.16. The traction coefficient increases with pressure and the slide-roll ratio whilst it decreases with increasing temperature. Overall, the behaviour of the traction curve follows its typical characteristic, however at high temperature, the traction curve approaches a linear law.

Diaconescu [31] demonstrated solid-like behaviour of EHL oil films from the fundamental theories and a simple liquid model at molecular level. A comparison between his advanced theoretical approach and published experimental results proved that the theoretical prediction was verified although only experimental results of a few oils were available.

Consequently, it was suggested that the flow of lubricating oils in the EHD condition might consist of segmental flows.

A relatively recent theoretical study of Bair [32] suggests that the film thickness under sheared conditions would be thinner than that predicted by Equation 2.34, due to shear thinning of the lubricant. He measured the film thickness at various slide-roll ratio conditions, and offered the corrected formula predicting the film thickness which takes shear thinning of oils into account.

In terms of the film thickness under shear conditions, several types of abnormal film shape were reported by Kaneta *et al* [33, 34]. These results showed the existence of a dimple in the centre of the contact, that is, the occurrence of a film depression.

The rheological behaviour of lubricants in EHD conditions has been a debated subject for many years and a number of models have been proposed by various researchers. Evans and Johnson [35] proposed four regimes, which are Newtonian, Eyring, viscoelastic and elastic-plastic depending on the response of a lubricant with pressure, temperature and shear rate. In the Newtonian regime, shear stress rises in proportion to shear rate, while in elastic-plastic regime lubricants would solidify and behave as an elastic-plastic solid due to high pressure exceeding the glass transition value. In case of Eyring and viscoelastic regimes, a lubricant behaves non-linearly because of near exponential increase of the viscosity, and the behaviour of a lubricant depends on temperature. Moore's result showed, for example, that the shear behaviour of di(2-ethylhexyl)phthalate followed the viscoelastic type at 30°C whilst the Eyring type was observed at 90°C [36].

Chapter 3

Lubricants

In this chapter, the characteristics of lubricants are presented. The behaviour of lubricating greases in EHD conditions is also evaluated.

In this section lubricant properties and characteristics relevant to this thesis will be emphasised. Lubricants commercially used today are normally made from a solvent, either a polar liquid such as water or a non-polar liquid like a mineral oil with compounding additives. A polar substance tends to be adsorbed at the metal surface, tendency of which is thought to improve the lubrication process because two metal surfaces contacting each other are covered with few layers of polar molecules. This mechanism is called boundary lubrication. Lubricants can be grouped into three categories, the liquid type, semi-solid type and solid type, from the point of view of their structure.

The lubricants are used for the main following purposes:

- (1) To reduce the friction force generated between the contacting surfaces.
- (2) To prevent the damages on the surface because of the wear, seizure and so on.
- (3) For cooling of the lubricated device.
- (4) To prevent contaminants from intruding or to exclude them from the device.
- (5) To prevent corrosion of the metal surfaces.

3.1 Lubricating Oils

Mineral oils

Lubricating oils known as mineral oils are refined from the crude oil and composed of hydrocarbons in most cases. By the composition and content of hydrocarbons, the oil is defined as paraffinic, naphthenic and aromatic. Non-hydrocarbon compounds are removed in manufacturing processes, and therefore, various additives are usually mixed in order to improve the lubrication function in commercial products. Typical chemical structures are presented in Figure 3.1.

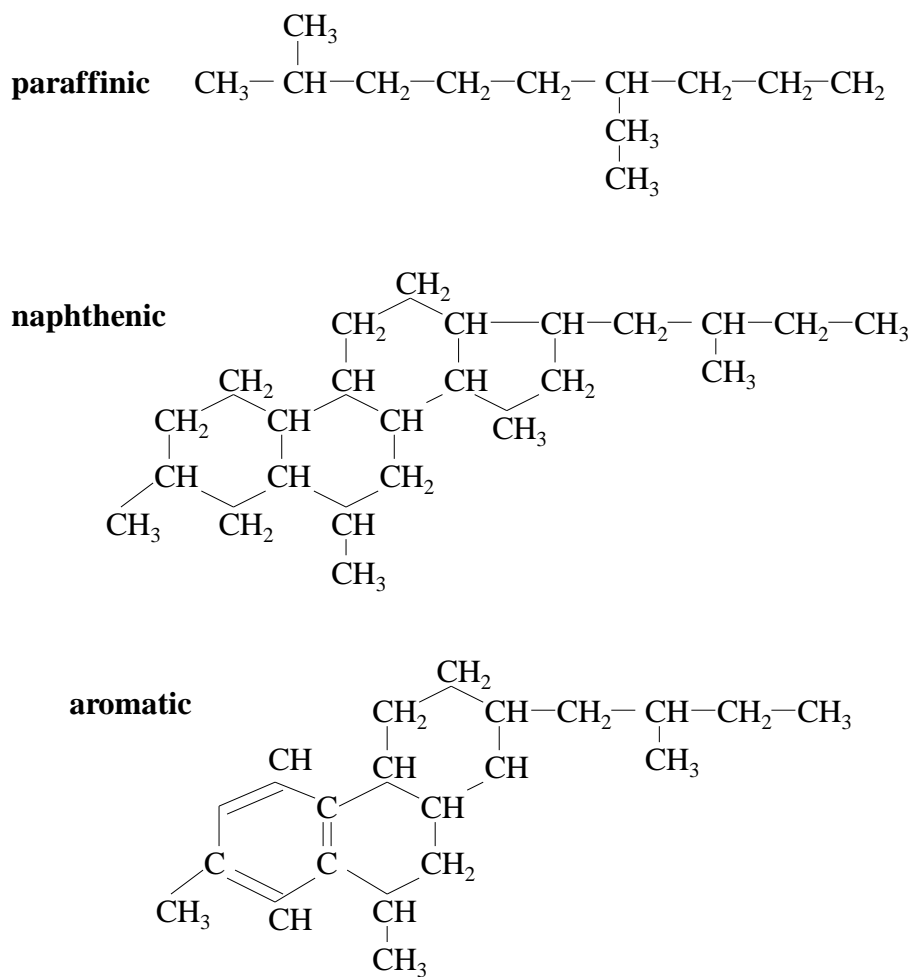


Figure 3.1 Chemical structures of hydrocarbons

Synthetic lubricants

Synthetic oils are artificially blended lubricating oils in order to gain better performance than natural oils. These oils are utilised especially for extreme high or low temperature conditions and when there is demand for anti-flammable property. Synthetic oils contain elements such as oxygen in the basic hydrocarbon structure. Common oils are represented by poly-alpha-olefin (PAO), polyolester (POE) and so on.

When the hydrocarbon chain in the molecular structure is denoted by R polar substances such as ROH, RCOOH and RNH₂ are called alcohols, fatty acids and amine respectively. The polar substances in the chemical structure, for these materials, are thought to adhere the metallic surface in the lubricating process and thereby protect the surface as if by coating it.

Use of lubricating oils

Main fields where lubricating oils are used can be divided into three, industrial, automotive and metal working.

Industrial lubricating oil

The oils are used for from bearings in mechanical devices and hydraulic systems to motors in refrigerators and windmills. Gear oils for industrial machinery are also categorised into here.

Automotive oil

Lubricants for automobile are classified into this sort. Oils used for IC engines are called engine oils, while gear oils used in cars are also categorised into this variety. For these lubricants, it is globally recognised that the viscosity of oils is distinguished by the American scale, SAE.

Metal working fluid

There are lubricating oils for machining, stamping and drawing etc. Because oils are used for deformation processing of metals, it is required to stand and perform at very high pressure, usually beyond the yield stress of metals.

3.2 Lubricating Greases

A lubricating grease is defined as “*a solid to semi-fluid product or dispersion of a thickening agent in a liquid lubricant. Other ingredients imparting special properties may also be included*” by National Lubricating Grease Institute (NLGI) [37]. Although it is difficult to predict its lubrication behaviour due to its complex, two-phase structure, nearly 90% of rolling element bearings currently in use are lubricated by grease. The following types of thickeners are most common and will be investigated in this thesis:

- (1) Polyurea thickener
- (2) Lithium stearate (LiSt) thickener
- (3) Lithum hydroxy stearate (also known 12OH-LiSt) thickener

3.2.1 Structure of greases

Either a mineral oil or a synthetic oil is usually used as a base oil for the grease manufacturing process and accounts for 80 to 90% of bulk grease which may also include anti-wear additives, extreme pressure agents and friction modifiers as well as oxidation inhibitors.

There is a consensus that the thickener fibres are developed in the micro structure of the grease and that random mesh makes the bulk grease a semi-solid nature by holding the base oil. The thickener structures will be different, depending upon the manufacturing process,

even though those greases are made with same materials and concentrations. The typical images of the grease structure (soap fibre) are shown in Figure 3.2. All of them were produced by 12OH-LiSt thickener and presented by Yamamoto *et al* [38].

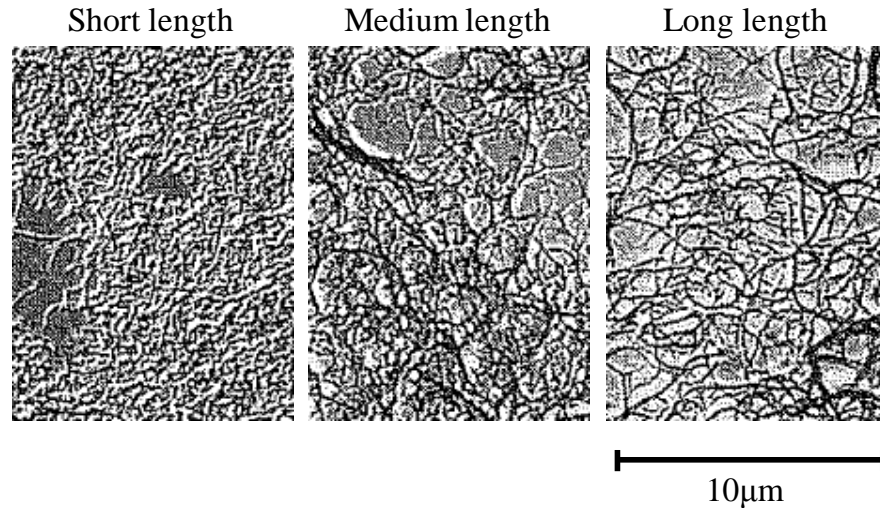


Figure 3.2 Structure of soap fibre in greases [38]

One reason why greases are widely used is because greases are packed inside the device during assembly (Design for manufacturability) and extra devices such as the lubricant storage and circulation system for oil lubricants are not needed (Simple structure). In addition, greases are generally durable to water and thereby they essentially may play the role of waterproof agent. This aspect is preferable in automotive industry, for instance, the constant velocity joints located at the underbody of a car has to be protected from rain.

3.2.2 Rheological models of greases

Unlike the behaviour of oil lubricants in EHD conditions, which is widely understood, for a grease lubricant, it is generally difficult to predict the behaviour under operation due to its dual phase composition, a liquid phase and a solid phase.

Due to its poor fluidity, a grease undergoes deformation only when the shear stress exceeds a certain point which may be an intrinsic value of the sample. Thus a grease has the yield stress τ_y in general and thereby the shear stress τ does not reach zero when the shear rate $\dot{\gamma}$ is zero. Bingham described this behaviour as seen in Equation 3.1 while Herschel-Bulkley proposed a non-linear model expressed by Equation 3.2 found in [39].

$$\tau = \tau_y + c\dot{\gamma} \quad (3.1)$$

$$\tau = \tau_y + C_1\dot{\gamma}^{C_2} \quad (3.2)$$

where c , C_1 and C_2 are constants.

Once a grease has started to flow it would need less force to shear it because the fibre connection at the molecular level might be destroyed by the first motion. This causes a reduction of the shear stress when tests are repeated or reversed. Namely, the shear behaviour of a grease is dependent on time and this kind of behaviour is called Thixotropy.

Wada *et al* [40] established the idea of core formation by investigating hydrodynamic lubrication of a Bingham material. Firstly, they derived the equivalent Reynolds equation about a core, un-sheared region inside the contact, for the case of a core floating in the film and adhering to the surface as well as the case of no core being formed. In a following paper [41], they revealed the experimental result of core formation by using a step bearing, which was proved in good agreement with the derived equations related to core formation. Finally, they applied their theory to journal bearings [42] and found that observed results of movements of a core inside bearings corresponded relatively well with the theoretical ones.

While Wada's studies were based mainly on the Bingham model, Yoo and Kim [43] analysed numerically the grease EHL film based on the Herschel-Bulkley model. It was observed that the yield stress did not affect the overall grease lubricating film. The effect of

the viscosity parameter was significant and the minimum film thickness was increased with the viscosity parameter in their calculations.

In terms of rheological models of lubricating greases, Radulescu *et al* [44] compared seven proposed models, which include the Bingham model, the Herschel-Bulkley model, Casson model [45], Papanastasiou model [46], Dorier and Tichy model [47] and others, by experimenting on two different types of greases. The experimental results obtained for Lithium and Calcium grease were fitted to above models and the un-known parameters, such as c in Equation 3.1, and the correlation coefficient were extracted for each case. Using a curve fitting method, it was concluded that Herschel-Bulkley model was the best simulating model for the grease behaviour and lithium grease showed better value in correlation coefficient, namely more stable result, than calcium grease.

3.2.3 Lubricating behaviour of greases

In an early investigation Dyson and Wilson [48] evaluated the dielectric relationship between the soap and oil in grease and explained how to calculate and extrapolate dielectric constants of lubricants at various pressures in order to measure the EHL film thickness from the electric capacitance. They compared the time dependent film thickness between several greases and corresponding base oils. They concluded that the greater the viscosity of the base oil, the rotating speed and the thickener concentration, the thicker the film thickness was formed at the initial stage of the experiment. The film thickness of the grease decreased from the thicker value than corresponding base oil's at the beginning of the experiment to approximately 40% of the film thickness of the base oil which was generally constant during the experiment. The difference in worked penetration, one of the most important bulk properties of a grease, had negligible effect on the film thickness. They also reported that at any stage during a test, the film thickness of the grease was recovered to the initial value when additional grease was supplied. This phenomenon was observed in our experiment under point EHD contact conditions while they were conducting with two rollers equipment. Another distinct feature in their study is that they attempted sudden

changes in speed during the tests and found that the film thickness was increased dramatically when the rotating speed went up but showed rapid decrease afterwards.

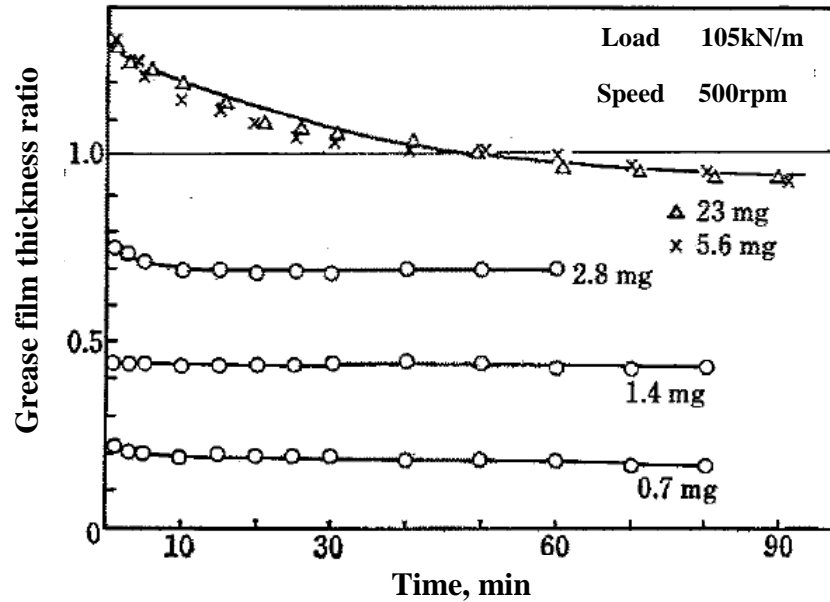


Figure 3.3 Time and amount dependence of the film thickness of the grease [49]

By using Dyson's assumption of dielectric constants of greases, Aihara *et al* [49] measured film thicknesses of greases under various conditions and compared as 'grease film thickness ratio' which is the ratio between the grease film and the fully flooded base oil film. They found that the film thickness of the grease became stable when the amount of the grease supplied to the contact region was beyond a certain value, while the film thickness was decreasing when the amount was extremely low. These results, shown in Figure 3.3 were explained by the fact that almost all greases supplied were pushed to outside of the contact.

On the other hand, Jonkisz *et al* [50] evaluated the ratio of the grease film thickness under the starvation condition to the thickness under fully flooded condition and have found that

it was about 0.5 to 0.7. In their work, it was also mentioned that the grease's yield stress had negligible effect on the film thickness.

Moreover, Wilson investigated grease films in a rolling bearing, by measuring the capacitance between the inner and outer ring [51]. He found starvation behaviour with the passage of time and insisted that, except some cases such as under heavy load, the starvation behaviour brought good aspect for the operation because thinner film contributed to decrease the friction occurring inside the bearing.

In a research on the effect of the composition of greases upon its behaviour, Cann *et al* proposed that the film thickness increased approximately linearly with soap concentration [52]. Similar relationship between the film thickness and the soap concentration was confirmed by Dalmaz *et al* [53].

Astrom [54] mentioned that a grease would not flow back to the contact after being pushed aside by the rolling motion due to the yield stress a grease possesses. However the ridges made by this motion help the base oil bled from the grease to replenish the contact. In addition to these results, Cann *et al* [55] pointed out the grease equilibrium film thickness, i.e. the film thickness under starved condition, correlated with grease's oil bleeding property. Cann, again, insisted that "*the fully flooded condition is generally undesirable as it leads to high energy losses,*" and found curious results that the film thickness under starved condition decreased with increasing thickener content and also with increasing viscosity of a base oil, which is not predicted by normal EHL theory [56].

Recent studies [57-59] have again shown that starvation of the contact occurs at a certain speed when the entrainment speed gradually increases (Figure 3.4) and that the degree of starvation increases with increasing thickener content and base oil viscosity. Also greases

with low elastic modulus would form a thick EHD film compared to a grease with high elastic modulus although the grease microstructure is not an essential factor for forming a thick lubricating film. Thus, the behaviour of the grease is generally related not to its thickener but to its base oil. On the other hand results such of those by Couronne *et al* [58] have revealed that additives such as an adherence improver seem to affect on the behaviour of greases more than the type of base oil. Yoshii and Hattori [59] compared common grease based on PEPE oil with relatively new grease based on MAC oil. They found that MAC grease obtained stable friction coefficient and therefore the potential to be an excellent grease because of high load carrying capacity.

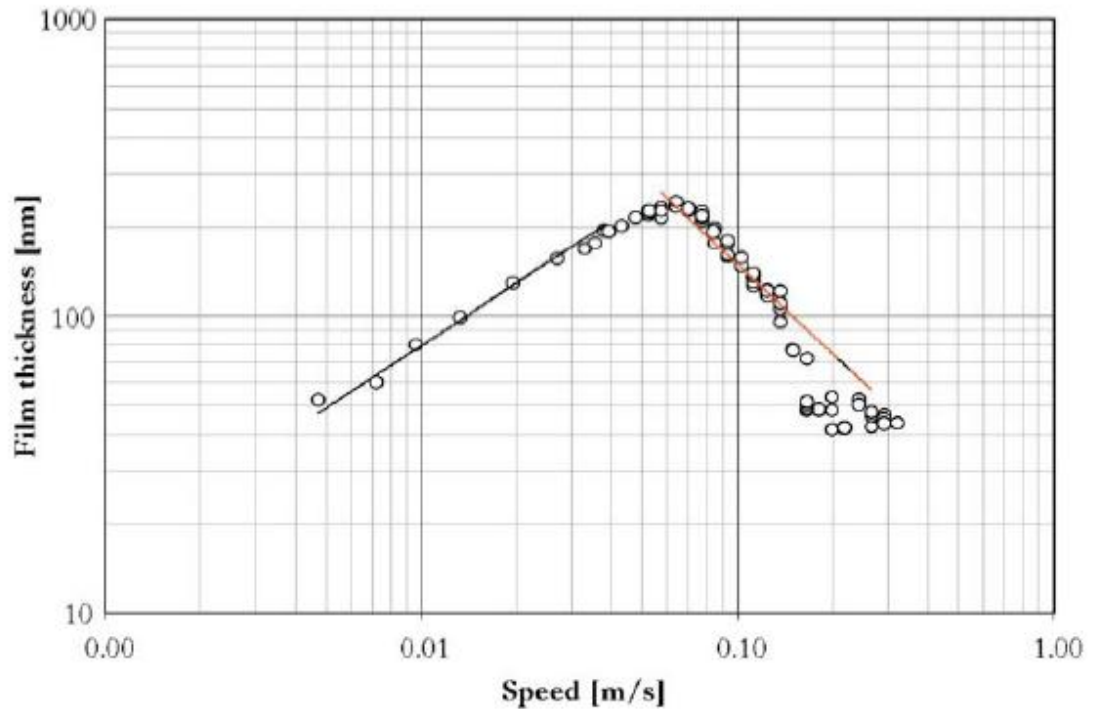


Figure 3.4 Film thickness as a function of speed for the fully flooded (black line) and starved (red line) regimes [56]

Eriksson *et al* have investigated the influence of the side slip on grease EHD contacts [60]. Similar results to their research but in pure rolling [61] were obtained, which showed that

large thickener particles kept their shape when passing through the contact under high side slip. Thus they suggested that the thickener would cover the surfaces better if a small amount of the side slip is present in the contact.

For the dielectric study of greases in EHL, Sunahara *et al* [62] investigated the relationship between the film thickness and the dielectric properties by using a disc coated with an indium tin oxide (ITO) film and found that the breakdown voltage increased with increasing film thickness, however the relationship between the breakdown position and the corresponding film thickness was not mentioned.

3.3.4 Characteristics of grease lubricants

Nowadays, it is well known that the film thickness of the grease decreases with time and its initial thickness is thicker than the film thickness of the base oil. In case of greases, oxidation and evaporation do not affect significantly on the properties of the bulk grease at low temperature whilst oxidation contributes to “*grease aging*” at high temperature [63, 64].

Lugt [63] by using electrical resistance measurements proved the occurrence of starvation in the rolling bearings operation. In the real situation, however, it is not clear how greases are operating if there is the occurrence of starvation, which implies thin film thickness. Various researchers have proposed the hypotheses that the metal-to-metal contact due to the film breakdown raised the temperature around the contact and made it easy for the grease to flow back onto the track [65-67]. Although this concept is not established sufficiently, it indicates, more or less, that the grease lubrication is associated not only with the film thickness but also with the whole condition around the contact.

Lugt [63] concluded his review over the grease lubrication that “*ultimately, knowledge on multi-phase flow, nonlinear rheology, EHL theory and chemistry need to be combined to develop predictive models for grease lubrication in rolling bearings.*”

The features of grease lubricants can be described as follows.

- (1) In continuously supplying condition, greases form thicker film than corresponding base oils.
- (2) A grease contact without replenishment becomes starved at a certain speed.
- (3) At high speed the film thickness of grease decreases with operating time in normal EHD condition (no vibration), whereas starvation is less likely to occur at very low speed.

Chapter 4

Electrical Methods in EHD Lubrication and Dielectric Applications

This chapter outlines a brief review of the use of electrical method for the study of EHD contacts. The perspective of lubricants as dielectrics is also included.

4.1 Electrical Methods in EHL

Historically, electrical methods such as voltage discharge, resistive and capacitive measurements, have preceded optical methods which are widely employed these days, for studying the EHD film formation. The main advantage of electrical methods is the fact that the test condition is formed between two bodies made out of steel, which is identical to real machine components. There are, however, some disadvantages to the electrical methods. One of them is that these methods would give only average values over the contact area and offer no indication of the local shape of the film.

Usually, electrical methods have been used to investigate lubrication phenomena for three main purposes.

- (1) To measure the thickness of the lubricant film.
- (2) To detect full-film conditions and the asperity contacts in rough surfaces.
- (3) To evaluate the performance of lubricants under the effect of an electric field.

4.1.1 Film thickness measurements

Siripongse *et al* [68, 69] carried out experiments to evaluate the film thickness in line contacts with the voltage discharge method and the film thickness in point contacts with the electrical resistance method. Both results showed full-film conditions even in the extremely large pressure condition. They also have found a variation of the breakdown voltage with film thickness following a linear relationship. It was perceived that their main obstacle was the calibration because the content and size of impurities in the oil affected significantly on the breakdown voltage dependence of the film thickness.

Using a following calibration equation, Crook [70] evaluated the film thickness formed between two parallel discs by ignoring the deformation of the contact and the variation of the dielectric constant of the oil with pressure.

$$C_D = 1.67(h_D^*)^{0.5} \quad (4.1)$$

where C_D is the capacitance between unloaded pads and h_D^* is the separation between the discs at positions just outside the pressurised region. The results calibrated by using Equation 4.1 showed that the film thickness was half the theoretical value at low loads, while exceeding it at large loads. He concluded that the variation of the viscosity with pressure and the elastic deformation of the surfaces were important for obtaining reliable results.

Archard and Kirk [71] measured both the resistance and capacitance of the contact over a wide range of loads, velocities and viscosities of the lubricant and suggested the following relation for the film thickness.

$$h \propto (\alpha\eta)^{0.57} u_s^{0.55} R'^{0.62} \quad (4.2)$$

where R' indicates the reduced radius of the contacting surfaces and u_s is the sum of two velocities.

On the other hand, Hamilton and Moore [72, 73] evaluated the oil film thickness between the piston ring and cylinder inside a combustion engine where optical methods are impracticable. The capacitance and resistance measured between the piston ring and the cylinder proved that the lubrication mechanism in the cylinder was essentially hydrodynamic.

Luo *et al* [74] also employed a capacitive method for investigating the EHD point contact, albeit they mainly focused on the gas bubbles emerging in the liquid film. They used a Cr layer which is conductive and the SiO₂ layer on a glass disc and measured the whole capacitance, theoretically determined by $1/C = 1/C_{SiO_2} + 1/C_{contact}$. In their investigation, as can be seen from the above equation, the capacitance of the rest of the EHD central region was ignored only because the central film thickness was much smaller than the film thickness outside the contact. Hudlet's calculation [75] for a sphere-plane capacitance, however, suggests that the capacitance of the EHD region accounted for at most 40% even though the regarded flat plate capacitor had only thicknesses of tens of nanometres. Thus, how much the EHD contact itself affects the total capacitance measured is another factor proposed to be evaluated in this research as it is important for understanding the behaviour of lubricants inside the contact.

4.1.2 Detection of asperity contact in mixed regime

The first notable work in this direction was done by Furey [76]. He measured the resistance of the contact and the friction force simultaneously. He stated that the rapid oscillations in the measured resistance meant that the contact was under mixed lubrication regime, and investigated the lubrication regime in a wide range of film thickness. He pointed out a value of 10^4 ohms as a threshold of fluid film lubrication, which is considered by Chu and Cameron as arbitrary [77].

Palacios [78] evaluated the occurrence of metallic contacts in a four-ball tester by correlating the surface roughness with the electric resistance results during operation.

Lord and Larson [79] explored the film formation of gear oils in mixed lubrication regime by measuring the impedance of the contact. This allowed them to obtain simultaneous output values of the resistance and capacitance of the contact. The former indicated the amount of metallic contact while the later showed the film thickness.

Guanteng *et al* correlated the electrical resistance with the lubricant film thickness and the friction force generated in a mixed lubrication regime EHD contact. They used optical interferometry to map the film thickness across the contact and directly interpreted the electrical contact resistance in terms of film thickness distribution [80]. In this study, they used both a rough ball specimen as well as a smooth one and typical results are shown in Figure 4.1. The comparison between these two sets of results confirmed the existence of metal-to-metal contact by the fluctuation in the rough ball measurement, which was outstanding compared to the other.

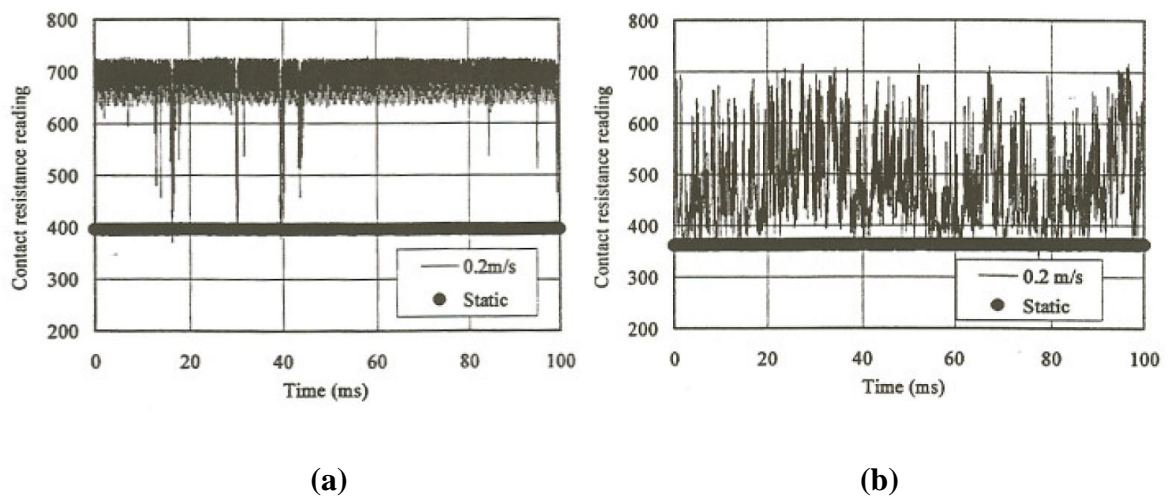


Figure 4.1 Electrical contact resistance trace for (a) smooth ball and (b) rough ball [80]

4.1.3 Effect of the electric field upon lubrication phenomena

Studies on the effect of an electric field upon a rolling element bearing have shown that the occurrence of pitting was stimulated by the passage of the electric current through the elements. Kure and Palmetshofer [81] stated that voltages exceeding 0.5V or currents more than 0.1A/mm^2 would cause damages in the rolling elements, whilst Prashad [82] suggested a value of 0.2V which might cause pitting to the contacting elements.

Yamamoto *et al* [83] found the external electric field changed film formation as well as the friction and wear pattern on the specimens by using the ball-on-disc arrangement. They also mentioned the presence of the electric field promoted the breakdown of the EHL film, while Xie *et al* [84] reported the formation of gas bubbles in the EHL film by applying the electric field.

Luo *et al* [85] have investigated the formation of ordered layers in elastohydrodynamic contacts subjected to an external electric field. They have found that film thickness and friction coefficient were related to the voltage applied. A stronger electric field will produce thicker films in pure rolling conditions, while increasing the friction coefficient under pure sliding.

4.2 Studies on Lubricants as Dielectrics

In these days, EHL films are analysed very accurately thanks to the development of the optical interferometry method. This technique, associated with high speed recording and imaging has allowed transient events to be studied and understood. It is obvious however that, in order for optical interferometry to be applied, one of the bodies must be transparent which is not the case of real machine elements. In order to avoid this, electrical methods can be used in which both contacting surfaces are metals. Electrical methods have other

limitations as it is shown in a later section of this chapter and also require detailed knowledge of the dielectric properties of the lubricants.

4.2.1 Basics of dielectrics

Materials can be divided from the point of view of their electrical conductivity into three groups, metals, semiconductors and insulators. An insulator is defined as a material that does not have free electron in its structure or a material which possesses very weak electrical conductivity. When an electric field is applied to an insulator, an electrical current does not pass through due to the absence of free electron. However, it induces an oscillatory movement to each molecule of a certain degree which is ruled by the dipole moment in the molecule structure. When studying this phenomenon, an insulator is called a dielectric.

The basic formulas and the fundamental behaviour of dielectric materials are described in many books and journals [86-88]. A perfect dielectric inside the geometry arrangement of two parallel plates is called a capacitor which, ignoring edge effects, will store the capacitance C [F] when a current is applied.

$$C = \frac{\epsilon_r \epsilon_0 A}{d} \quad (4.3)$$

where A is the area of the plates (electrodes), d is the separation and ϵ_0 is the permittivity of free space having a defined value of $(1/36\pi) \times 10^{-9}$ [Fm⁻¹]. ϵ_r is the relative permittivity also known as the dielectric constant of the material and its value is characteristic to insulating materials.

In real dielectrics, the capacitance is usually expressed as a real and imaginary part, i.e. complex capacitance, especially when alternative current (AC) is used.

$$C^* = \varepsilon^* C_0 \quad (4.4)$$

where $C_0 = \varepsilon_0 A/d$ which is geometrically constant and ε^* can be written as

$$\varepsilon^* = \varepsilon' - j\varepsilon'' \quad (4.5)$$

While the real part ε' is considered as the conventional relative permittivity, the imaginary part ε'' is a loss factor which varies strongly with variables such as temperature and pressure, compared to the real part.

The equivalent circuit of dielectrics is shown in Figure 4.2.

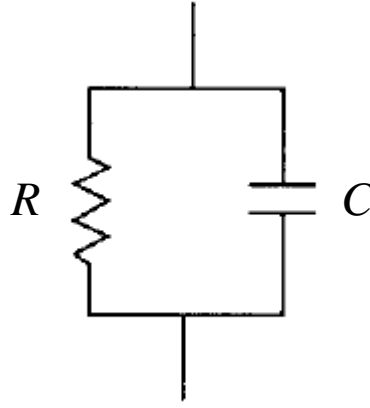


Figure 4.2 Equivalent circuit of a dielectric

The impedance Z of this circuit is given by using the angular frequency ω .

$$\frac{1}{Z} = \frac{1}{R} + j\omega C^* \quad (4.6)$$

The typical behaviour of the real and imaginary parts of a dielectric is shown in Figure 4.3. Application of an alternating electric field to a dielectric substance causes its molecules to react as a result of the interaction between the dipole moment of the substance and the external field. Each dielectric mechanism is centered around its characteristic frequency,

(these correspond to the local variation of the dielectric permittivity seen in Figure 4.3) which is the reciprocal of the characteristic time of the process. In general, dielectric mechanisms can be divided into relaxation and resonance processes. The real part of a dielectric constant decreases with frequency, however not all molecules, atoms or ions relax at the same frequency. This is because, the dielectric loss, represented by the imaginary part, increases with frequency for every relaxation process and, beyond a certain point, decreases by approaching next balanced state. Thus, the inverse of the peak frequency in the imaginary part ω_p indicates the dielectric relaxation time T_d (Equation 4.7).

$$T_d = \frac{1}{\omega_p} \quad (4.7)$$

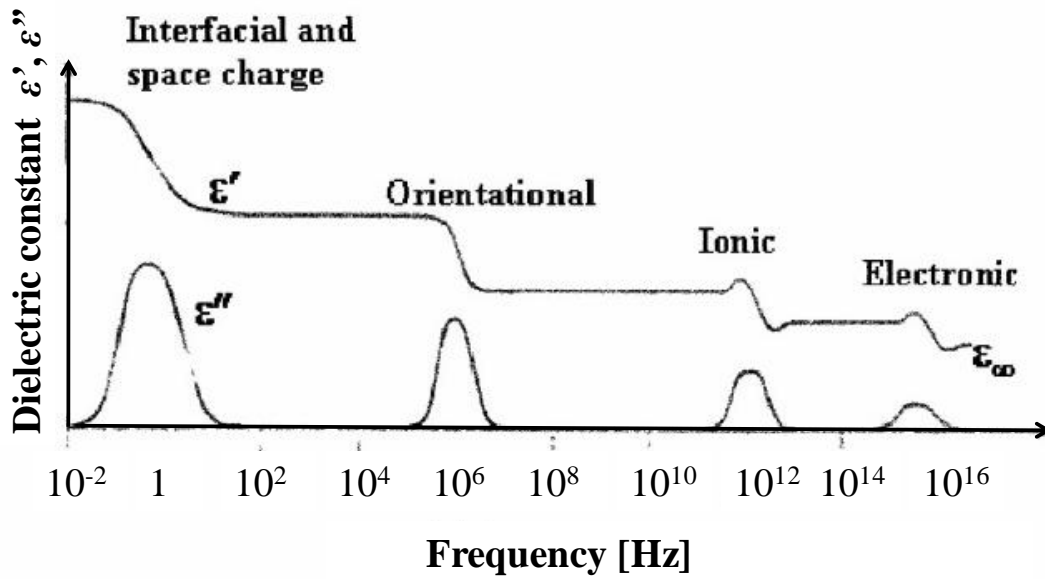


Figure 4.3 Frequency dependence of the real and imaginary parts of a dielectric constant [88]

There is a convention that the relaxation process in the lowest frequency range is called α relaxation and the following behaviour at high frequency is called β relaxation.

The ratio between imaginary and real parts of the dielectric constant is an important parameter referred as the loss tangent.

$$\tan \delta_d = \frac{\varepsilon''}{\varepsilon'} = \frac{1}{\omega RC} = \frac{\sigma_e}{\omega \varepsilon' \varepsilon_0} \quad (4.8)$$

where ω is the frequency and σ_e is the electrical conductivity of a material.

4.2.2 Dielectric studies on materials

It is one of the important methods for property analysis to see the relative permittivity because any material exhibits its own value of the relative permittivity and hence changes in this value indicate transformations of the quality or the condition within the material, such as chemical changes due to oxidation or contaminants. Regarding the specific characteristics of dielectrics, the relative permittivity generally decreases with increasing temperature. On the other hand, it is well known the dielectric constant increases with pressure.

The dielectric relaxation time, T_d , is another important property of a material, which is relevant to peaks in the behaviour of the imaginary part of permittivity shown in Figure 4.3. After Debye initially introduced the complex functional equation related to the relaxation process, Havriliak and Negami [89] expanded Debye's equation as follows:

$$\varepsilon' - j\varepsilon'' = \varepsilon_\infty - \frac{\varepsilon_0' - \varepsilon_\infty'}{[1 + (j\omega T_d)^\alpha]^\beta} \quad (0 \leq \alpha, \beta \leq 0) \quad (4.9)$$

where ε_0' is the relative permittivity at the zero frequency generally indicating the intrinsic value of materials and ε_∞' is that in the high frequency range which is equal to square of the refractive index of materials. When $\alpha = 1$ and $\beta = 1$, Equation 4.9 becomes Debye equation. For typical amorphous polymers it is reported that the behaviour can be described

by values of these constants of $\alpha = 0.8$ and $\beta = 0.5$ [89]. However, Hayakawa *et al* pointed out that those values could be affected by the length of side group from the perspective of polymer's segmental dynamics [90].

Denney *et al* [91] measured the dielectric properties of methanol and methanol-1-propanol solutions and showed that the dielectric constants of both methanol and solutions decreased with increasing temperature. Also, the results show the more weight percentage of 1-propanol it contains, the smaller value in the dielectric constant the solution has.

Shekhter *et al* [92] investigated the effect of the polarity of soaps on plastic lubricants by the changes of relative polarization resistance and relative ohmic resistance. They used five soaps, HSt, LiSt, NaSt, AlSt and PbSt, and concluded that lithium soaps had a smaller number of aggregations, a better thickening capability and a higher micellebinding energy.

Bondi *et al* [93] showed the dielectric constant and loss data of some colloidal suspensions, i.e. lubricating greases, under measuring conditions of shear. Thus one of electrodes in their equipment rotates in order not only to measure viscosity of samples but also to measure dielectric properties. Although viscosity measurements do not give clues regarding to the molecular details in samples, the electrical data can give information regarding the shape of particle aggregates. Their results revealed that the dielectric loss of Silica gels decreased by inducing shear rate and concluded this might be caused by changes in the geometry of silica particle aggregates. Another interesting behaviour found in their results was related to the relaxation time of lubricating greases which was found to become shorter when shearing was applied to the sample.

The pressure dependence of the relative permittivity was studied by Vij *et al* [94]. They measured the relative permittivity of 1-heptanol, 3-heptanol, 3-methyl-2-hexanol and 2-

methyl-2-hexanol as a function of pressure up to 3.5kbar and found that the relative permittivity increased with pressure for all cases.

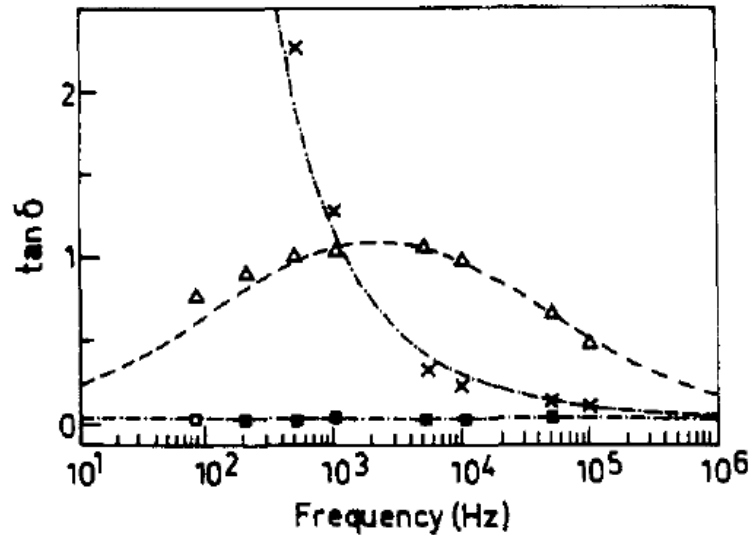


Figure 4.4 Frequency dependences of loss tangent for various solutions [95]

Aliotta *et al* [95] reported the dielectric measurements on soybean lecithin/isooctane/water gel at 30°C. Although the features of such polymer gels are complex and not analysed easily because of the two-phase aspect, they showed significant differences on the dielectric behaviour between pure isooctane, its solution with soybean lecithin and the gel based on isooctane as shown in Figure 4.4. First they measured the dielectric property of pure isooctane which is shown with squares in Figure 4.4 and is almost stable all over the frequency range. Then, the binary solution was obtained by adding lecithin into isooctane. The result of the dielectric measurements on this solution is shown with crosses in Figure 4.4. Finally, the gel was formed by adding water. The dielectric property of the lecithin gel is shown with triangles in Figure 4.4. They concluded that the solution typically indicated polar liquid features at lower frequencies and the behaviour exhibiting a peak point in the case of the polymer gel represented “*the liquid phase in the gel system.*”

Harun *et al* [96] describe the dielectric modulus as a function of the real and imaginary parts of the dielectric permittivity.

$$\begin{aligned} M' &= \frac{\varepsilon'}{\varepsilon'^2 + \varepsilon''^2} \\ M'' &= \frac{\varepsilon''}{\varepsilon'^2 + \varepsilon''^2} \end{aligned} \quad (4.10)$$

They obtained the peak angular frequency ω_p from the graph of M'' versus frequency and calculated the relaxation time T_d of PVA-PPy-FeCL₃ composite polymer films for different dopant compositions, where the relaxation time obeys a following equation.

Urakawa *et al* [97] investigated the effect of low mass compounds on the dielectric properties and viscoelastic properties in polymers. They used Polystyrene and Polyvinylethylene mixed with alkyl groups where the number of carbons is different, as an additive and they observed the relaxation behaviour mainly against temperature. According to their results, due to the large dipole moment of the low mass compounds, the dielectric behaviours of test materials are dominated by the low mass compounds, whereas the viscoelastic behaviour reflects the polymer component dynamics as well as the dissolved molecule dynamics. They also referred to the segment size of the polymer and concluded that β relaxation process, the relaxation behaviour observed at lower temperature range in their case, disappeared when the molecule size of the low mass compounds was comparable with the segment size of the polymer.

At ambient pressure and temperature, it is said that, most of the polar dielectrics show the relaxation process attributed to the dipole moment in the frequency range between 10^7 Hz to 10^9 Hz.

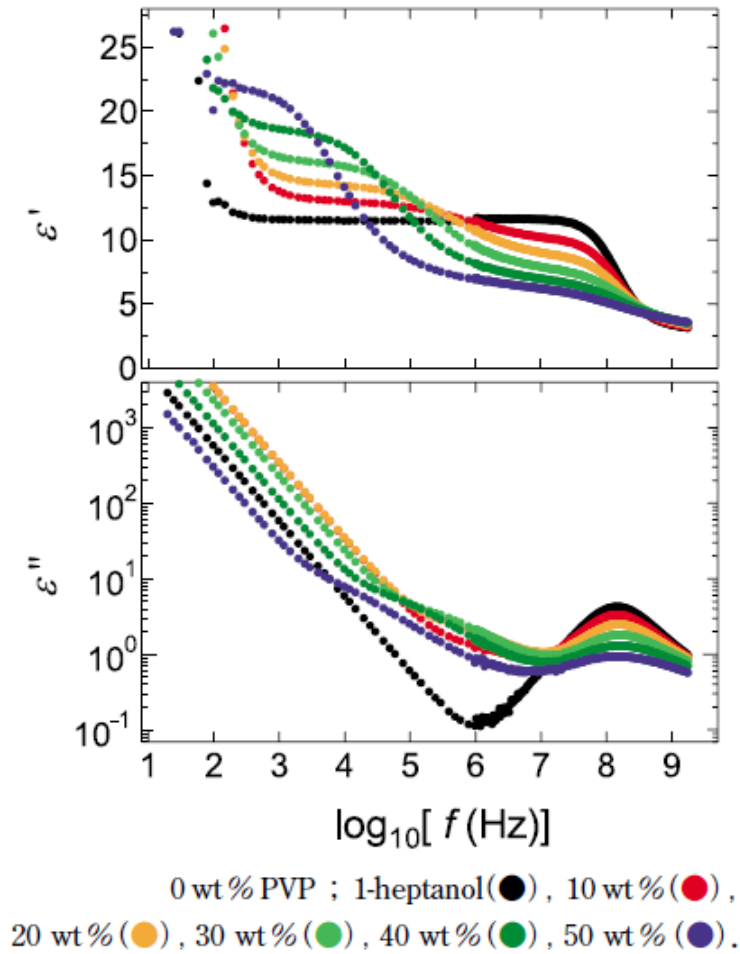


Fig. 4.5 Dielectric properties of solution PVP/1-heptanol [98]

For typical experimental results, Yagihara *et al* prepared two types of solution, polymer diluted in alcohol and in water, and investigated their dielectric properties [98]. According to their result shown in Figure 4.5, 1-heptanol, pure alcohol, showed dielectric loss peak at around 100MHz at room temperature. While the relaxation time of alcohol did not vary with the content of polymer, poly(vinyl pyrrolidone) (PVP), the relaxation process of PVP was observed in a different range with that of the alcohol. In this case, the relaxation processes of PVP were spread between 1kHz and 10MHz so that two different relaxation processes were observed in one sample. They also mentioned, on the other hand, that in the case of non-polar base oil solution only the relaxation process of additives would be

measured due to the low dipole moment in the solvent whilst the mixed solution of polar substances would show much more complicated process. Although as seen in Figure 4.5 two processes were distinguishable in the case of PVP/1-heptanol, the relaxation behaviour could overlap in some cases, where the output shape was not predictable, that is, it could indicate the shape of one mountain in one case and in some cases it could become the mountain with a dip on the top.

Adachi *et al* [99] investigated the effect not only of entanglement in the structure but also of molecular weight on the dielectric properties of lubricants and found that the dielectric relaxation time was approximately proportional to the square of molecular weight in the case of liner chain samples.

Almost all studies in the field of polymers are based on Stockmayer's theory [100], who considers that there are three types in polymers from dielectric point of view. One is that the dipole moment is parallel to the direction of the chain, which is called type A. Type B has polar groups in the side group and those groups are rigidly attached to the backbone chain. Type C also has polar groups in the side, however, under the condition that side groups including polar substances can be rotating. Figure 4.6 shows the description of these three types. In terms of the relaxation process type C is the fastest while type A is the slowest.

In other examples of the dielectric relaxation process, solutions made of water and protein indicated a fast relaxation process in the frequency range around 400GHz [101, 102]. This behaviour was attributed to the local dynamics of hydroxyl group in the solution, which is described as type C and gives the fast relaxation process.

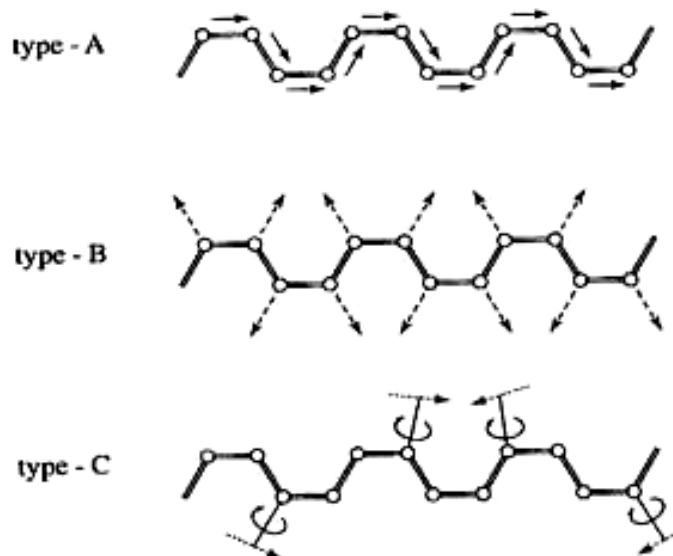


Figure 4.6 Schematic representations of dipole vectors in polymer [100]

Furthermore, Watanabe [103] points out that water above critical point, 373.95°C and 22.064MPa , reaches a state in which it cannot be distinguished as liquid nor as gas so that the electrical permittivity of water decreases dramatically due to the weakened hydrogen bond. Above this point, thus, water represents the dielectric property similar to non-polar substances.

Galvin *et al* [104] measured dielectric properties of some lubrication fluids including mineral, vegetable and synthetic oils in the conditions of pressure range up to 50000lb/in^2 and with temperature of 20°C and 100°C . They reached the conclusion that oils could be divided into two groups from the perspective of dielectrics; one is the non-mineral group and another is the mineral oil group. The dielectric constant of mineral oils was less affected by pressure and temperature than that of non-mineral oils. Thus the dielectric constant of mineral oil varies slightly with changes of pressure and temperature. Moreover, some of their results showed the dielectric constant decreased with increasing pressure. Their results are presented in Table 4.1.

Table 4.1 Dielectric constant of lubricants [104]

| Lubricant | Temperature, °C | Dielectric constant at | | | | | |
|-----------|--------------------|-------------------------|------------------------------|------------------------------|------------------------------|------------------------------|------------------------------|
| | | 0 lb/in ² | 10 000 lb/in ² | 20 000 lb/in ² | 30 000 lb/in ² | 40 000 lb/in ² | 50 000 lb/in ² |
| A | 20 | 2.29 | 2.34 | 2.38 | 2.41 | 2.42 | 2.42 |
| | 100 | 2.18 | 2.23 | 2.28 | 2.32 | 2.35 | 2.37 |
| B | 20 | 2.33 | 2.38 | 2.42 | 2.44 | 2.45 | 2.46 |
| | 100 | 2.19 | 2.25 | 2.30 | 2.33 | 2.36 | 2.39 |
| C | 20 | 2.20 | 2.25 | 2.30 | 2.33 | 2.34 | 2.36 |
| | 100 | 2.08 | 2.13 | 2.17 | 2.20 | 2.24 | 2.27 |
| D | 20 | 2.58 | 2.63 | 2.58 | 2.54 | 2.53 | 2.53 |
| | 100 | 2.41 | 2.47 | 2.52 | 2.57 | 2.60 | 2.63 |
| E | 20 | 2.49 | 2.54 | 2.59 | 2.62 | 2.64 | 2.62 |
| | 100 | 2.32 | 2.39 | 2.44 | 2.48 | 2.51 | 2.53 |
| F | 20 | 2.57 | 2.63 | 2.65 | 2.60 | 2.55 | 2.53 |
| | 100 | 2.41 | 2.48 | 2.53 | 2.58 | 2.61 | 2.62 |
| G | 20 | 5.85 | 6.17 | 6.42 | 6.61 | 6.77 | 6.91 |
| | 100 | 4.74 | 5.09 | 5.36 | 5.62 | 5.83 | 6.01 |
| H | 20 | 2.77 | 2.91 | 3.00 | 3.08 | 3.15 | 3.20 |
| | 100 | 2.49 | 2.63 | 2.74 | 2.82 | 2.89 | 2.95 |
| I | 20 | 4.71 | 4.87 | 5.02 | 5.14 | 5.23 | 5.28 |
| | 100 | 3.89 | 4.06 | 4.19 | 4.30 | 4.39 | 4.48 |
| J | 20 | 5.35 | 5.49 | 5.63 | 5.74 | 5.85 | 5.93 |
| | 100 | 4.30 | 4.51 | 4.65 | 4.77 | 4.88 | 4.99 |

| Lubricant | Description | | |
|-----------|---|---|--|
| A | High-viscosity index mineral oil (predominantly naphthenic and paraffinic) | E | Low-viscosity, low-viscosity index mineral oil (predominantly aromatic and naphthenic) |
| B | Medium-viscosity index mineral oil to OM 100 specification | F | Low-viscosity index mineral oil + methacrylate polymer |
| C | Medicinal white oil (naphthenic) | G | Ethylene oxide-propylene oxide copolymer |
| D | High-viscosity, low-viscosity index mineral oil (predominantly aromatic and naphthenic) | H | Polydimethylsilicone fluid |
| | | I | Castor oil |
| | | J | Di(2-ethylhexyl) phthalate |
| | | K | Glycerol (glycerine) |

4.2.3 Dielectric relaxation versus mechanical relaxation

It is of interest to predict mechanical properties from dielectric properties especially for lubricants in EHD conditions, as it is difficult to measure mechanical properties, such as the viscosity at pressures of a few giga pascals. On the other hand dielectric measurements are much simpler than mechanical measurements in general experimental laboratories. During the past decades several studies have been conducted in order to correlate the relaxation process at the molecular level and at the bulk material level.

Williams, Landel and Ferry [105] remarked that dielectric relaxation behaviour was the same for any temperature though the position at the peak might differ, that is, the relaxation curves were overlapped each other when one was moved by a certain distance along the frequency axis. The amount how much one curve is moved to be laid upon the other is called shift factor. They proposed the so-called WLF Equation expressing the relationship between the shift factor and temperature.

$$\log a_{\theta} = -\frac{C_1(\theta - \theta_r)}{C_2 + \theta - \theta_r} \quad (4.11)$$

where a_{θ} is the shift factor, θ is temperature, θ_r is the reference temperature and C_1 and C_2 are constants. The shift factor obtained from dielectric measurements is considered to correlate with rheological properties of materials.

Suzuki *et al* [106-108] obtained relaxation times of a sample for various temperatures by fitting measured data to Equation 4.9 and calculated shift factors for each temperature by Equation 4.11. They could successfully predict the viscosity at various temperatures from the dielectric relaxation time by a following equation.

$$a_{\theta} = \frac{\eta_{\theta_r} \rho_r}{\eta_r \theta \rho} \quad (4.12)$$

where ρ is the density and r refers to the reference state.

Subsequently they expanded their research for predicting the viscosity at high pressure as well as various temperatures. They obtained shift factors for various temperatures and pressures from fitting dielectric data to Equation 4.9 and superimposing dielectric curves. They suggested that viscosity can be predicted in various conditions by the following equation.

$$a_{\theta,p} = \frac{\eta(\theta, p)G_e(\theta_r, p_r)}{\eta(\theta_r, p_r)G_e(\theta, p)} \quad (4.13)$$

where G_e is the shear modulus and subscript r refers to the reference state. $a_{\theta,p}$ is a shift factor relating to both temperature and pressure. The predicted viscosity in various conditions of temperature and pressure from dielectric measurements was successfully matched with the value measured by standard mechanical measurements.

In a further study [109], Suzuki *et al* tried to combine mechanical and dielectric properties of greases. However, they have not yet succeeded to find the relationship in the case of greases. From the data they got which showed that the slope (rate of change) of dielectric data against temperature is different from the slope of the apparent viscosity of the grease, they concluded that the type of dielectric relaxation of greases is not the same type as the mechanical one.

Chapter 5

Experimental Methodology

In this chapter experimental methods used in this study are described. The dielectric measurements on the static condition, as well as on the dynamic condition, are described while the experimental measurements of the film thickness and the film formation are explained. It also describes the test materials.

5.1 General Introduction

The test rig employed in this study was supplied by PCS Instruments, which was designed to simulate an EHD point contact and allowed measurements of the film thickness and friction force at the operating temperature between the room temperature and 150°C and loads up to 50N. The contacting surfaces are the flat of a disc and a ball. The disc and ball are independently driven at appropriate velocities so that a desired slide-roll ratio is obtained. The friction force generated between the disc and ball is measured by strain gauges located on a thin plate which drives the ball's shaft. A picture of the rig is shown in Figure 5.1. The tests on the effect of the oscillatory motion on the EHD contact were conducted on another specialised rig within the Tribology laboratory, which was developed by another PhD research.

The PCS Instruments rig has been modified and adapted to allow the capacitance of the contact to be measured. In this case a Solartron Impedance analyser, also shown in Figure 5.1, has been employed which is able to generate signals and perform measurements in the frequency range between 10 μ Hz and 32MHz. However, in this study, the frequency range from at least 100Hz to at most 1MHz will be used in order to obtain reliable results. When connecting to the PCS test rig, resonance was observed in the range between 10MHz and 32MHz while measured points are not stabilised at low frequencies especially below 100Hz.

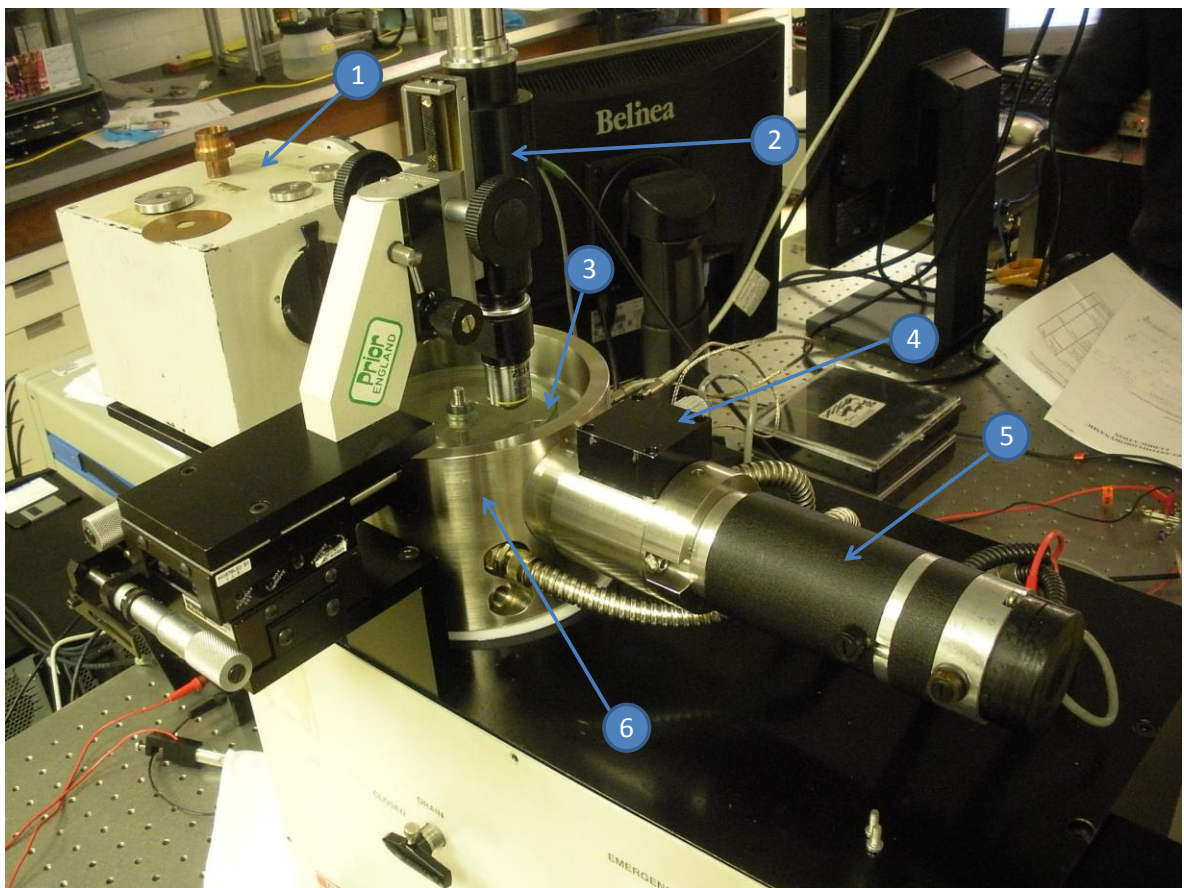


Figure 5.1 PCS Instruments test rig (1 = spectrometer, 2 = microscope, 3 = disc, 4 = friction measurement system, 5 = motor, 6 = lubricant pot)

5.2 Static Conditions

5.2.1 Description of the micrometre based measurements

Two circular plates have been set up between the jaws of a micrometre, which allows the separation of the capacitor plates to be set with one micrometre precision. A photograph of this arrangement is shown in Figure 5.2. The gap between the plates is normally set at 0.25mm and the air capacitance measured in that condition was about 12pF, though this calibration is repeated for every measurement.



Figure 5.2 Micrometre based measurement

The dielectric constant of material ϵ' and dielectric loss ϵ'' are calculated from Equation 5.1 by using measured capacitance of the material C , the capacitance of air C_{air} and measured resistance R .

$$\begin{aligned}\varepsilon' &= \frac{C}{C_{air}} \\ \varepsilon'' &= \frac{1}{\omega RC_{air}}\end{aligned}\quad (5.1)$$

In Equation (5.1) ω is the frequency of the current used in the measurement.

Although most lubricants studied in this research had too weak polarity for the relaxation phenomena to be observed in the studied frequency range, the dielectric relaxation time in some materials was calculated by fitting the measured data to Debye equation (Equation 5.2) and following the method described below [110].

$$\varepsilon' - j\varepsilon'' = \varepsilon'_\infty + \frac{\varepsilon'_0 - \varepsilon'_\infty}{1 + j\omega T_d} \quad (5.2)$$

where subscript 0 and ∞ indicate the values at zero and infinite frequency. T_d is the *dielectric relaxation time* of the material. Equation 5.2 can be expanded as follows.

$$\begin{aligned}\varepsilon' - \varepsilon'_\infty &= \frac{1}{T_d} \cdot \frac{\varepsilon''}{\omega} \\ \varepsilon'_0 - \varepsilon' &= T_d \cdot (\varepsilon''\omega)\end{aligned}\quad (5.3)$$

Thus, the dielectric relaxation time can be obtained from the linear relationship between measured permittivity of real and imaginary parts.

5.2.2 Description of the EHD rig modified for dielectric measurements

The EHD lubrication regime found in many machine elements can be simulated by a disc and ball machine, a description of which is shown in Figure 5.3. In order to reproduce the condition in real machine components the steel disc and ball are adopted to the EHD rig instead of the transparent disc for optical interferometry, the most widely used method for the EHL study. The disc and ball are insulated from shafts and other parts inside the rig so that lubricant films between them can be regarded as dielectrics.

The air capacitance between the disc and ball in static condition was measured in advance of the measurement with rotating disc and ball in order to evaluate the effect of the connection between electrodes and brushes. As shown in Figure 5.4, the significant difference could not be observed so that the effect of the connection against rotating bodies would be ignored. As an aptitude test, the pod of the rig was filled with a synthetic ester oil and the capacitance of the oil between the disc and ball was measured. Consequently, the measurement gave the result more than twice as high as values of air, which is the normal value of the dielectric constant for lubricants.

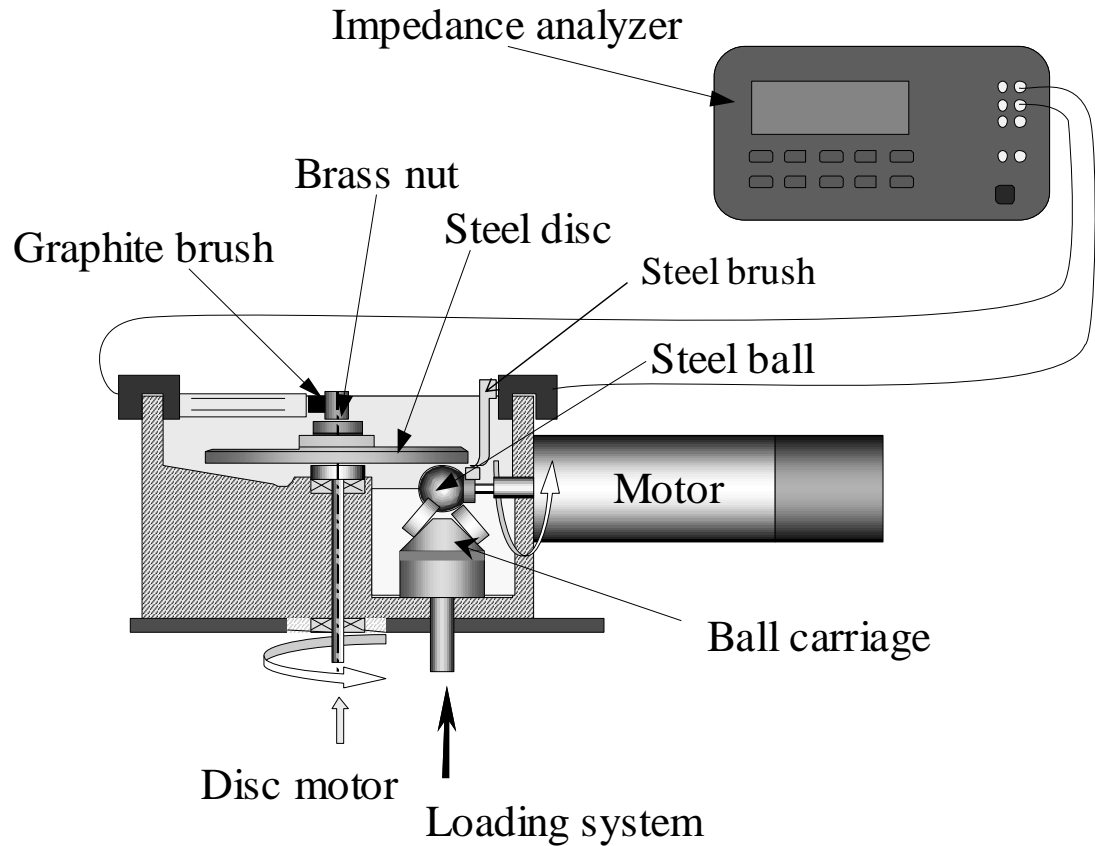


Figure 5.3 Schematic diagram of the EHD rig for dielectric measurements

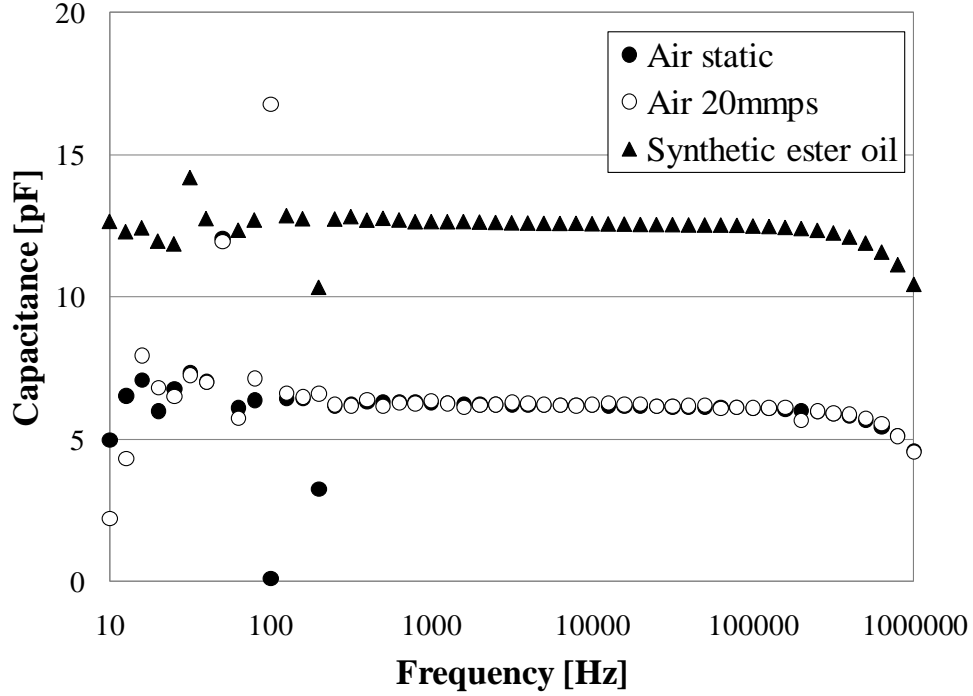


Figure 5.4 Capacitance of the rig for air and full-oil measurements

Although the capacitance of the lubricant between the disc and ball in the EHD rig is successfully measured as proved by the reasonable values obtained in Figure 5.4, it is not possible to measure the air capacitance between the disc and ball in loading conditions. In order to extract the dielectric properties of lubricants under EHD conditions, the following assumption are taken in this research.

$$C_m - C_b = \epsilon_0 \epsilon_r \frac{A}{d} \quad (5.4)$$

where C_m is a measured capacitance in operation and C_b is a background capacitance which is defined as the capacitance with the contact unloaded and at experimental speed with the rig filled with the oil. The area of the capacitor A is considered as the contact area given by Hertz theory and the separation d is replaced by either the theoretical film thickness or the film thickness measured with optical interferometry, but in identical kinematic conditions.

5.3 EHD Measurements

5.3.1 Film thickness measurements

The EHL film thickness studied in this research is experimentally obtained by three methods which are all variants of the optical interferometry technique. One method is the PCS ULTRA system, which relies upon the principle of two-beam interferometry. This is utilised for measurements with the PCS test rig as default. The second method is sometime called SLIM (Spacer Layer Imaging Method [14]) and it calibrates the RGB (Red, Green and Blue) values of the interference map of the contact with the aid of the ULTRA method. Finally the other method is a variant of the SLIM method and translated RGB values into Hue values in order for the film thickness to be obtained without being influenced by the variation of the light intensity.

5.3.1.1 Optical interferometry

The principle of optical interferometry is interference of light by division of amplitude. The fundamentals of optical interferometry are well described in Françon's book [111] and reviewed with more emphasis on experimental details by Spikes and Cann [14] and Johnston, Wayte and Spikes [112]. The application of the optical interferometry to the measurement of the film thickness of the EHD contacts was described in a sequence of studies by Cameron and Gohar [10, 113, 114]. The principle is schematically shown in Figure 5.5.

One of the contacting bodies is made of a transparent material to transmit light into the contact and the other surface should be highly reflective. In this study, the angle of incidence i and reflection i' are nearly zero. In addition, the transparent disc is coated with a semi-reflective chromium layer of few nano metres (usually 5-10 nanometres), and a silica spacer layer (100nm to 500nm thick), which allows measurements of the oil film thickness to be reliable down to few nanometres.

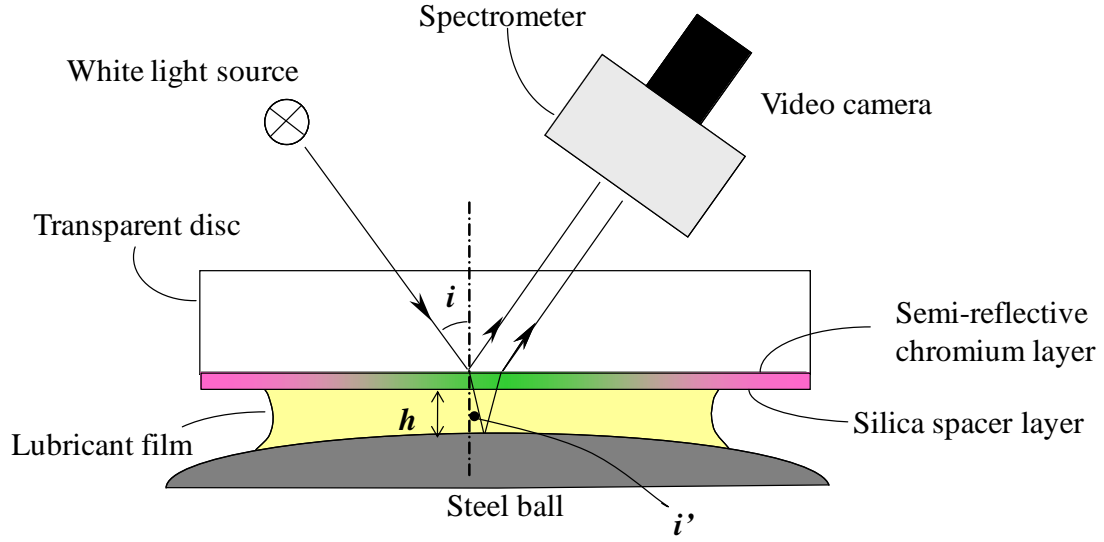


Figure 5.5 ULTRA interferometric system

The light coming from a light source is partially reflected by the surface of the semi-reflective layer on the disc (amplitude division) and partially passes through the oil and is reflected by the ball surface as seen in Figure 5.5.

In this study white light source is used for measuring a film thickness, therefore the constructive and destructive interference of light rays create a coloured image which indicate a larger or lesser constructive interference of various wavelengths. The incident light ray is divided on the semi-reflective surface and one part of the beam reaches the ball surface and is reflected back. When two parts of the beam recombine in the glass disc, there is an optical path difference δ_o between them. If the path difference between two beams (in Figure 5.5) is an integer number of wavelengths, the constructive interference will occur.

$$\delta_o = N\lambda = 2nh\cos i + \varphi \quad (N = 1, 2, 3 \dots) \quad (5.5)$$

where N is an optical order, λ is the wavelength of the light, n is the reflective index of the oil and φ is a correction factor for the net phase change which occurs at the reflecting surfaces.

Destructive interference, on the other hand, occurs when the optical path difference is a half of the wavelength, namely when expressed as a follow.

$$\delta = \left(N - \frac{1}{2} \right) \lambda = 2nh \cos i + \varphi \quad (5.6)$$

In the ULTRA method employed by the PCS EHL Ultra Thin Measurement System, the transparent disc is coated with an additional layer of silica on the contacting surface. This increases the separation between surfaces and allows measurements of films thinner than one quarter of the wavelength of light. Also specific to this rig is the presence of a spectrometer which separates the white light into individual wavelength components. This helps finding the wavelength of maximum constructive interference and thus the calculation of the film thickness according to Equation 5.5. The typical result of the film thickness against the entrainment speed measured by ULTRA is presented in Figure 5.6.

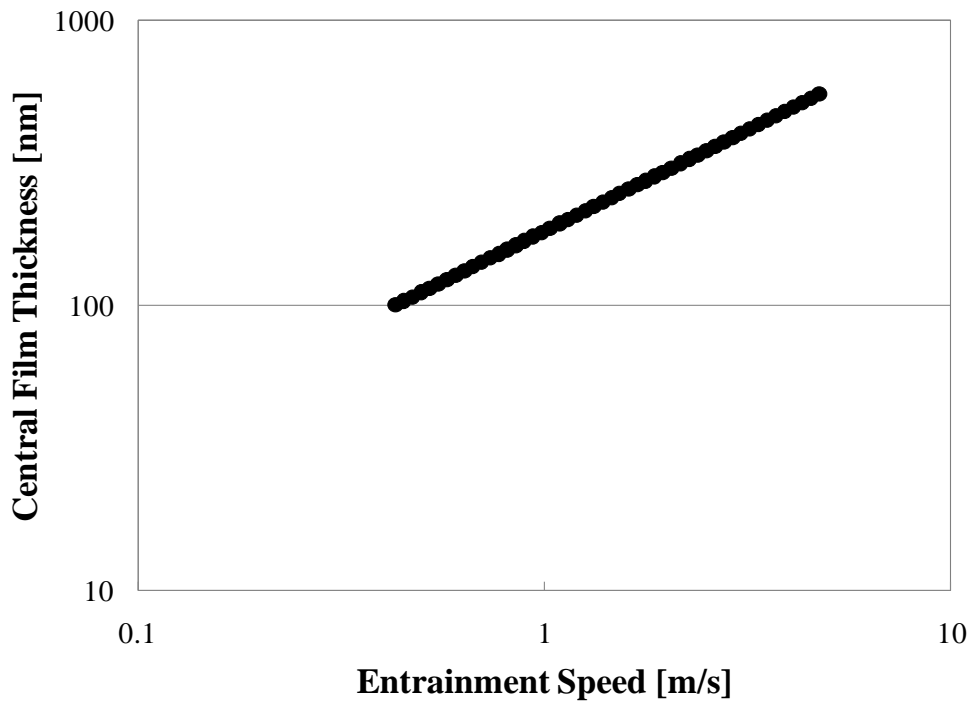


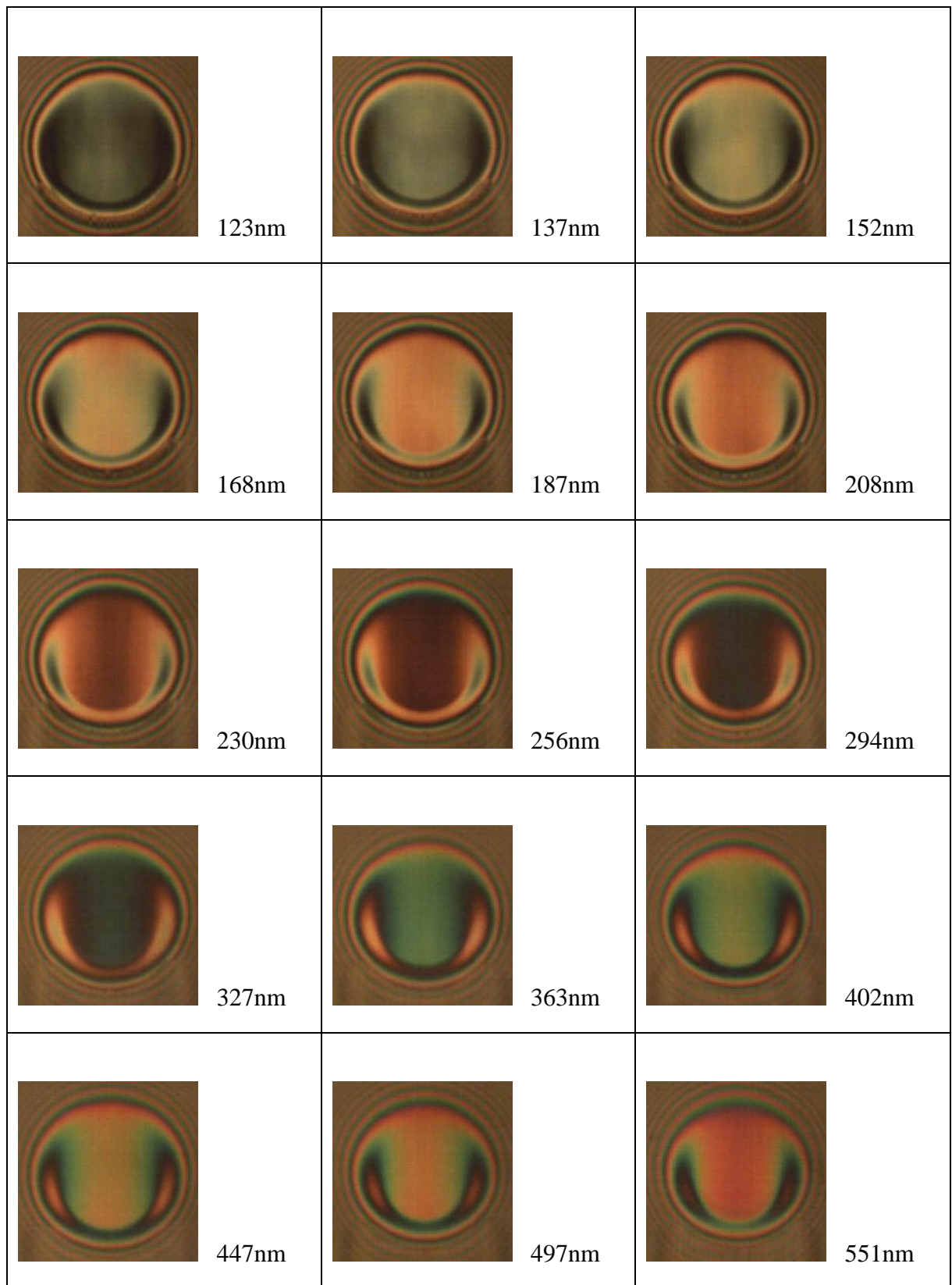
Figure 5.6 Film thickness versus entrainment speed

5.3.1.2 RGB value

As shown in Figure 5.7, the contact images captured by the CCD camera are coloured, representing a combination of all wavelengths interfered constructively in more or less extent. Because each colour represents a certain wavelength, a map of the film thickness can be extracted from these images.

In order to find the relationship between the film thickness and corresponding colour of the image, the central film thickness versus the entrainment speed has to be obtained as the first step. By using the PCS rig the measurement of the film thickness versus entrainment speed under accurately controlled conditions was carried out, which provides a straight line in a log-log representation as previously seen in Figure 5.6, because the dependence of the EHD film thickness upon the entrainment speed follows a power law.

In the next step of the calibration procedure, images of the contact are recorded at exactly the same conditions as the film thickness was measured in the previous step. As seen in Figure 5.7, the film thickness of the EHD contact is constant over most of the central area of the contact. Therefore, the RGB values for every pixel within a certain rectangle positioned in the central region were extracted from the recorded image at a certain speed, and then averaged RGB values for a corresponding entrainment speed were obtained. After obtaining the RGB versus the entrainment speed correspondence, the entrainment speed is eliminated from the two sets of the data and finally the RGB-film thickness dependence is obtained shown in Figure 5.8.

**Figure 5.7 Typical images of various film thickness**

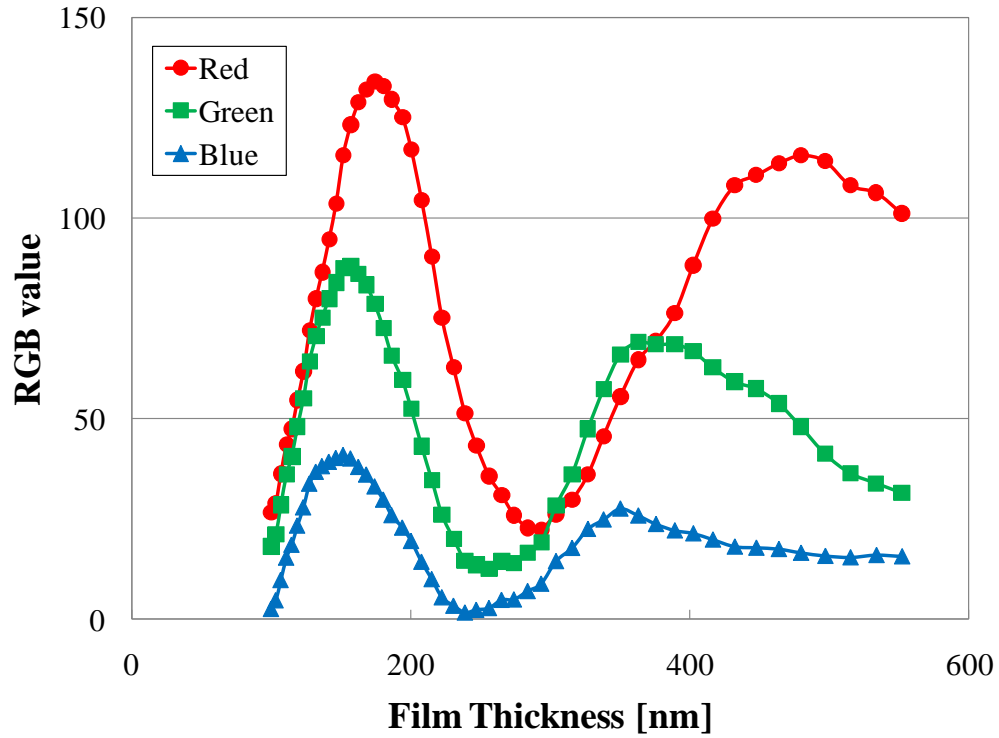


Figure 5.8 RGB value function of film thickness

5.3.1.3 Hue value

In this section, the calibration of the film thickness from Hue values is introduced. The converting formulae are not necessarily restricted to Equation 5.7 which is based on Haydn's equation [115] and used in this research. By calibrating the zero film thickness from the dry contact image in advance of each of experiments, this method would much easily remove disturbing factors, such as the difference of surrounding brightness, from results.

$$\begin{aligned}
 R, G \geq B \quad H &= \frac{G - B}{R + G - 2B} \\
 G, B \geq R \quad H &= \frac{B - R}{G + B - 2R} + 1 \\
 R, B \geq G \quad H &= \frac{R - G}{B + R - 2G} + 2
 \end{aligned} \tag{5.7}$$

where R , G , B and H are the value of red, green, blue and Hue respectively.

For the calibration, the colour details of the interference of the static contact shown in Figure 5.9 and the Hertz theory of the gap between two bodies outside the contact are used.

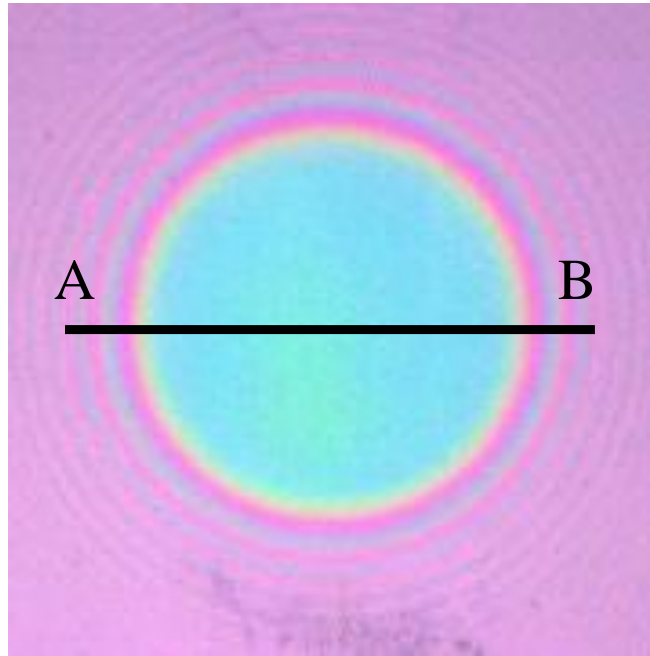


Figure 5.9 Typical interference image of a static contact

The rings of colour outside the contact are called Newton's ring and represent the different order of the interference of light. The gap outside the contact is calculated with the following formula provided by Hertz theory [1]:

$$h_H = \frac{a^2}{\pi R_b} \left(- \left(2 - \frac{x^2}{a^2} \right) \cos^{-1} \frac{a}{x} + \left(\frac{x^2}{a^2} - 1 \right)^{0.5} \right) \quad (5.8)$$

where h_H is the gap and a is the radius of the dry contact while R_b is the radius of the ball and x is the distance from the centre of the contact.

In Figure 5.10 the Hue values at the cross section AB in Figure 5.9 are described.

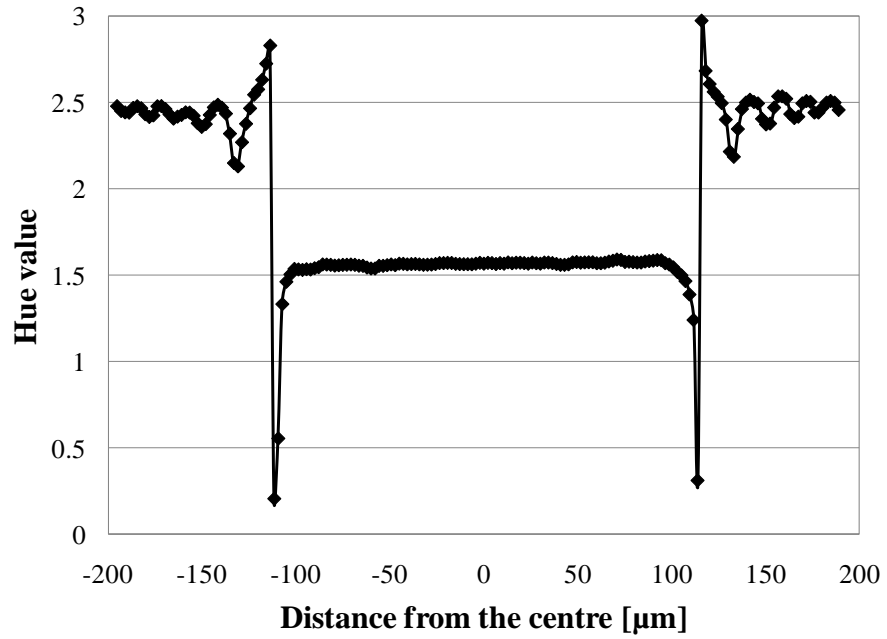


Figure 5.10 Hue values at the cross section AB in Figure 5.9

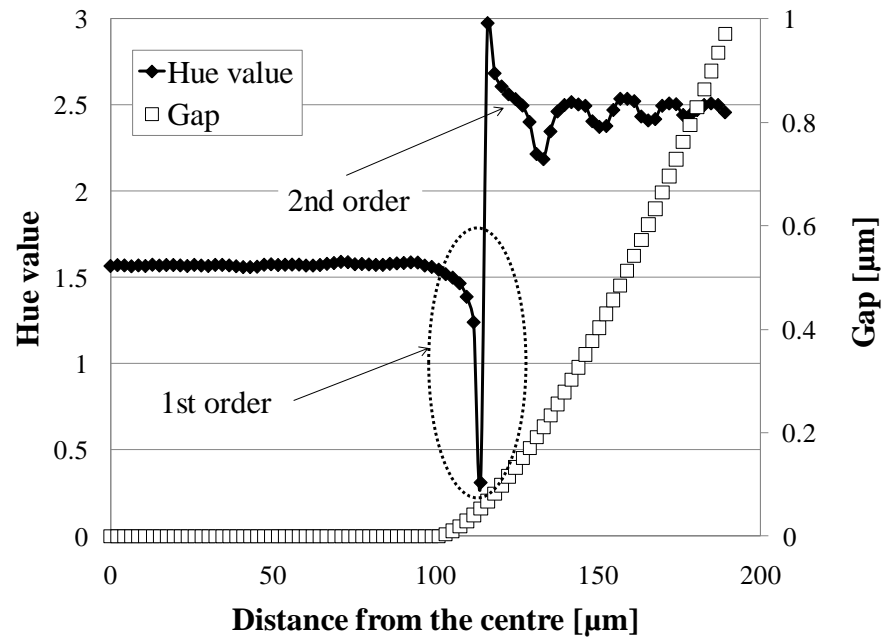


Figure 5.11 Relationship between Hue values and gap

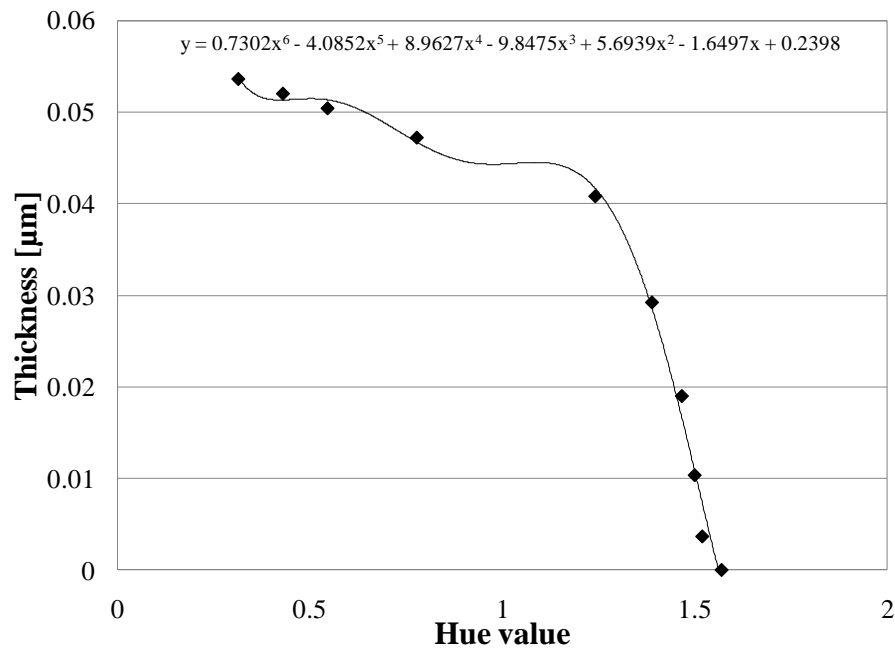


Figure 5.12 Film thickness as a function of Hue values (1st order in Figure 5.10)

As shown in Figure 5.11, the calibration curves are derived for every order by correlating the Hue values to the distance from the disc surface to the ball surface. This result is illustrated in Figure 5.12.

5.3.2 Starvation measurements

As mentioned earlier, a lubricating film will not be able to be formed in certain conditions, in particular for grease lubricants. In order to observe this behaviour in steel-steel contacts, the electrical method employed in this research has proved more useful method than others because the decrease in the film thickness due to starvation can be directly detected by measuring the capacitance and resistance of the contact. Although the steel disc and ball used in this study are super-finished, the surface roughness (Ra of the disc: 7nm, Ra of the ball: 9nm) and the direct interaction between the two bodies could be negligible for cases studied here, the electric breakdown phenomenon of the film will occur for too thin film separation.

The typical behaviour of an EHD contact lubricated by grease is shown in Figure 5.13. The voltage used in this study is 1V and the current is automatically adjusted by the software which interfaces with the Impedance Phase Shift Analyser at between 3mA and 3A. Although the pictures of the contact were taken separately by using a glass disc, the contact pressure and entrainment speed as well as test temperature were kept at the same values. In order to optimise the measurements in the EHD rig, an external 2k Ω resistor is connected in parallel to the contact, which indicates the breakdown of the film by a sudden drop in whole resistance. Each region defining a certain behaviour is defined as follows in this study.

Region A: The disc and ball are rotating without loading. In order to stabilise the conditions of a contact, the load is exerted after two minutes even though a consistent amount of the grease is spread onto the disc surface.

Region B: Fully flooded region. The inlet region of the contact is covered by enough amount of the lubricant. In this study, the duration of this regime will be discussed in later sections as “time to starvation.”

Region C: Shortage of the supply of the lubricant starts to occur. In the case of Figure 5.13, the air coming from the top left side of the inlet can be observed as a result of very small amount of the lubricant covering the surfaces. In the experimental data, this is indicated by small fluctuations of the capacitance with nearly stable resistance.

Region D: The track becomes visible in the picture which indicates that the air is present in a greater proportion in the inlet region. This is accompanied by fluctuations of both measured resistance and capacitance. Although, under such conditions, it is difficult to calculate the film thickness from the capacitance, the grease lubricating film seems to be still formed with sufficient thickness due to the lubricant attached to the surface.

Region E: In this region, the picture shows the film thickness has already been dramatically decreased while the dielectric measurement fluctuates significantly for both measured capacitance and resistance.

Region F: This region is called as “severe starvation” and it is thought a very thin film is formed to separate the two surfaces.

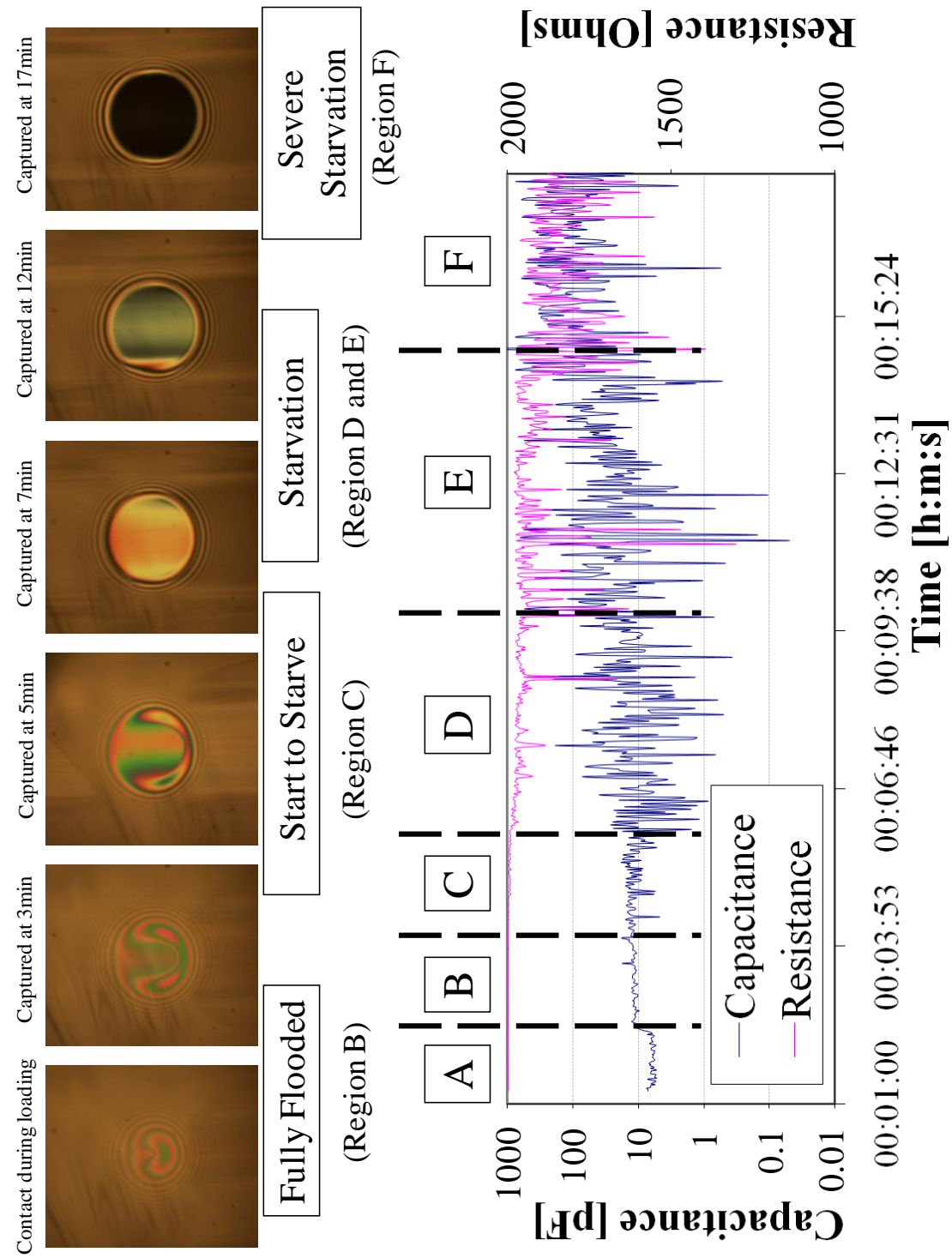


Figure 5.13 Grease film thickness decay

5.3.3 Traction measurements

PCS Traction Control System used in this study was developed especially for the EHL rig, a schematic diagram of which is shown in Figure 5.14.

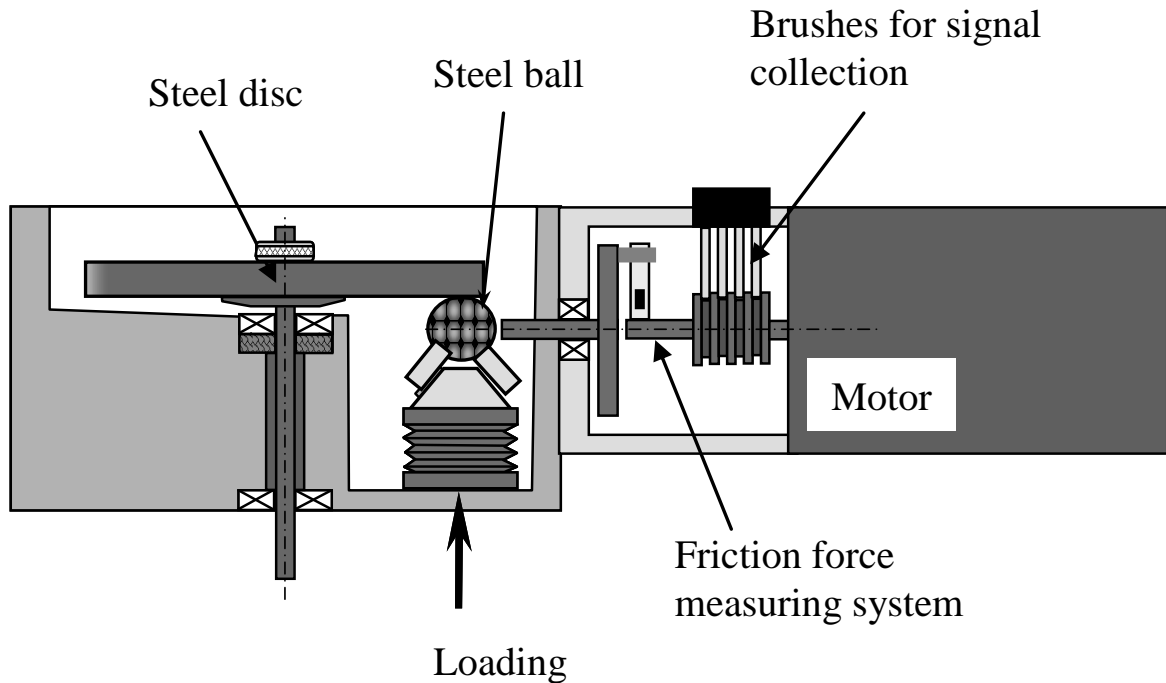


Figure 5.14 Friction force measurement on PCS Instruments test rig

As known that traction measurements are very sensitive compared to measurements of the steady state film thickness, tests were conducted three times in different days for checking the repeatability. For all traction measurements conducted here, a steel disc and ball were used, which produced the maximum contact pressure with 1.1GPa for a load of 50N, and a constant entrainment speed of 20mm/s was used. The typical traction curves obtained for SRL at 50N and 20mm/s are shown in Figure 5.15.

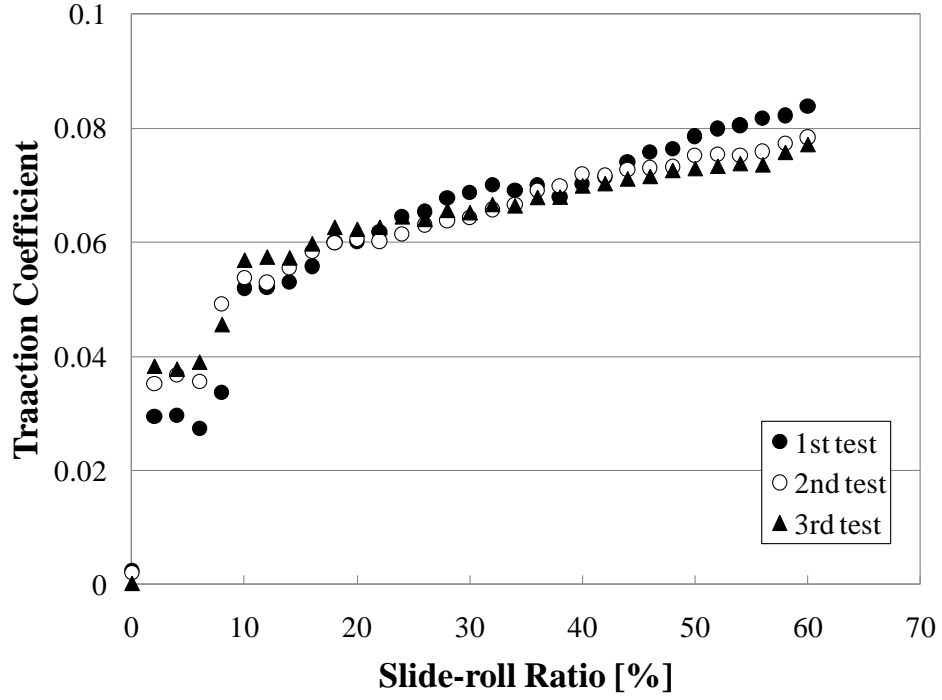


Figure 5.15 Typical traction curves

By analysing these raw data, it is found that the maximum difference was 10%. From now on, 10% error for both sides (positive and negative) is allowed for the calculation of Eyring stress from raw data and the process will be presented below.

In this section, averaged values of each ratio in Figure 5.15 are used for following steps. To obtain the shear rate $\dot{\gamma}$ and the shear stress τ , following two equations are reminded.

$$\dot{\gamma} = \frac{\Delta u}{h} \quad (5.9)$$

$$\tau = \frac{T}{A} = \mu \frac{w}{A} \quad (5.10)$$

where A is the area of the contact and calculated from Hertz theory.

Consequently, the relation between the shear rate and shear stress (Figure 5.16) is obtained from Figure 5.15.

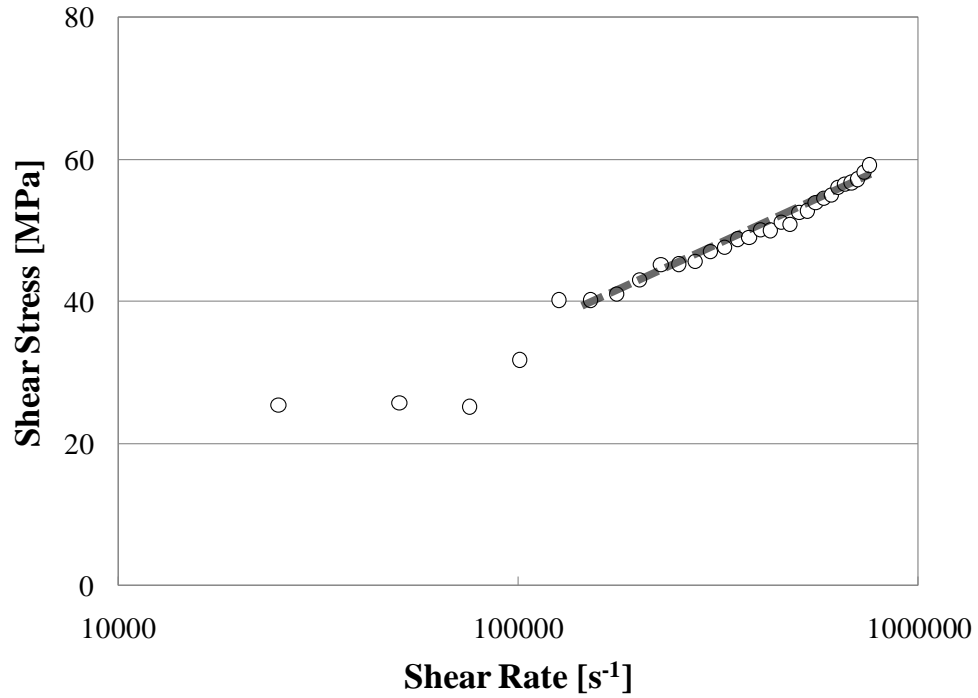


Figure 5.16 Traction curves for calculating Eyring stress and effective viscosity

To extract the reasonably reliable value of the effective viscosity η and Eyring stress τ_0 , data on the broken line in Figure 5.16 are fitted to Equation 2.46, where Eyring stress can be deduced from the linearity in logarithm scale followed by the effective viscosity.

$$\tau \cong \tau_0 \ln \dot{\gamma} + \tau_0 \ln \left(\frac{2\eta}{\tau_0} \right)$$

5.3.4 Vibration measurements

Vibrations are almost unavoidable in the operation of machine elements working with EHD contacts, such as rolling element bearings, gears or cams. For example a gearbox generates vibrations itself due to the shock loading of the engaging teeth, geometrical inaccuracies of the tooth's profile or shafts and others. At the same time vibrations are transmitted from the machinery or mechanism which incorporates the gearbox.

The effect of lateral vibrations upon the formation of the EHD film in grease lubricated contacts was studied on a purposely built rig which exists in the Tribology Laboratory. In this rig the ball and carriage are able to execute oscillatory motion in a direction perpendicular to the surface of the disc and in a direction contained in the plane of the disc, but perpendicular to the main rolling direction.

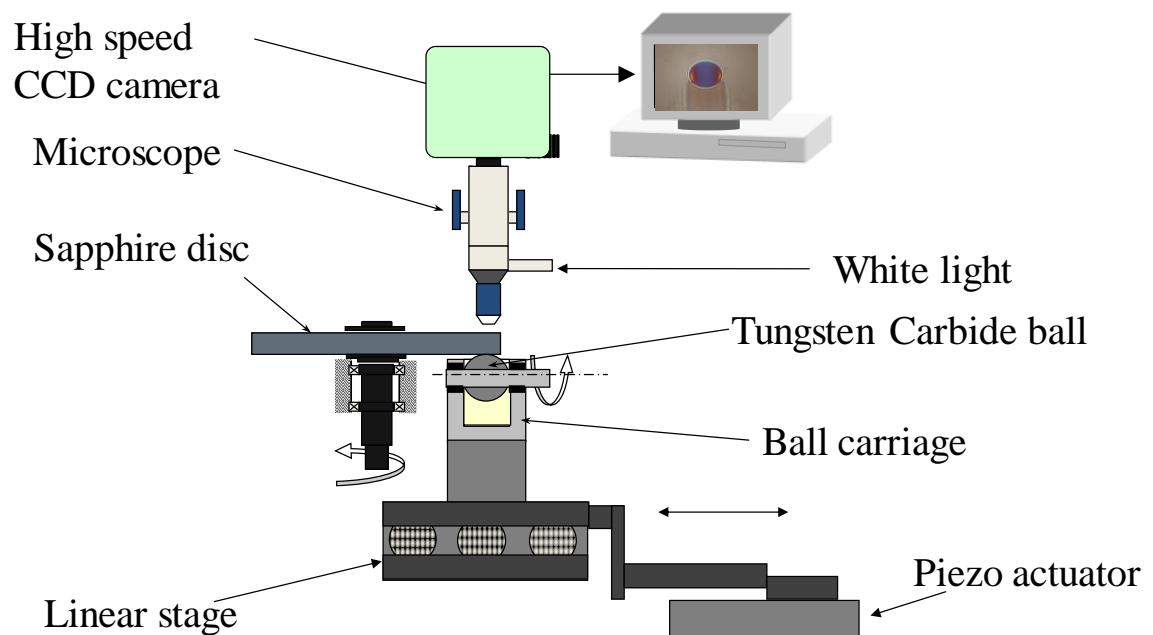


Figure 5.17 Schematic diagram of EHL vibration rig

The lateral oscillations are controlled by a piezo actuator as seen in the schematic diagram shown in Figure 5.17. For these tests, a sapphire disc and tungsten carbide ball were used and the load was kept constant at 45N which gave a Hertzian pressure of 1.8GPa. The conditions were pure rolling with a 0.5m/s entrainment speed.

Two values of the frequency of lateral motion were chosen: 10Hz and 100Hz. The stroke length of the oscillatory motion was larger than the contact diameter, which means the extremes of the stroke covered the width of the race track. Before the lateral motion was applied to the contact, the test was kept in pure rolling conditions for three to five minutes.

5.3.5 Camera equipment

In this study, a high speed CCD camera was mounted on the top of the microscope for detecting the contact image under vibrations as well as the conventional rolling condition. This camera has a resolution of 512x512 pixels and the images were captured by using provided software from the manufacturer with a 3000fps recording speed. The microscope was fitted with a x10 objective and the contact was illuminated by Schott KL1500 white light source through a liquid light guide.

5.4 Test Materials

5.4.1 Oil lubricants

In order to assess the contribution of the base oil to the behaviour of the grease, five oils were chosen and the effect of their composition upon the relationship between their tribological properties and the dielectric properties were evaluated. These oils listed in Table 5.1 were chosen because they all have the same kinematic viscosity of 68mm²/s at 40°C. These oils were supplied by Mr. Hiroyoshi Tanaka of Kyushu University, Japan.

5.4.2 Grease lubricants

Ten different types of greases were investigated in this research work and their detail compositions are listed in Table 5.2.

Grease1 to 6 are made by NSK for research purposes, which contains no additives solely to see the effect of the base oil or thickener upon the bulk properties and the behaviour of the grease. The material data was sourced from Prof. Joichi Sugimura of Kyushu University, Japan.

Stamina RL2 and RLS2 are commercially produced by Shell Global Solutions and they contain some additives. The data sheets were supplied by Mr. Howard Mead, where RL2 is a mineral oil based grease with a diurea thickener while RLS2 is a lubricating grease containing a blend of fully synthetic base fluids with a diurea thickener. However, the details of additives for both greases were not available.

SB-M and SRL greases are products of Kyodo Yushi, Japan and are also commercial greases, which means that both contain additives. These greases and the corresponding base oils were supplied by Dr. Shinya Kondo. The base oil is a synthetic hydrocarbon oil blend for SB-M, and a synthetic ester oil is used for SRL. In addition, SB-M is produced especially as a low-noise grease.

After the disc and ball were thoroughly cleaned with Analar Toluene and Iso Propyl Alcohol, in all experiments an amount of about 0.4ml of the grease was uniformly spread onto the disc surface and set into the rig ready for the test.

Table 5.1 Physical and chemical properties of oils

| Oil | Chemical structure | Kinematic viscosity | Density |
|---------------------------------|---|---|---|
| Polypropylene-glycol (PPG) diol | $\text{HO} - \left[\text{CH}_2 - \underset{\text{CH}_3}{\underset{ }{\text{CH}}} - \text{O} \right]_n - \text{H}$ | $68.0 \text{ mm}^2/\text{s}$ at 40°C $10.7 \text{ mm}^2/\text{s}$ at 100°C | 0.9890 g/cm^3 at 40°C |
| PPG monomethyle | $\text{CH}_3\text{O} - \left[\text{CH}_2 - \underset{\text{CH}_3}{\underset{ }{\text{CH}}} - \text{O} \right]_n - \text{H}$ | $68.4 \text{ mm}^2/\text{s}$ at 40°C $12.8 \text{ mm}^2/\text{s}$ at 100°C | 0.9820 g/cm^3 at 40°C |
| PPG dimethyle | $\text{CH}_3\text{O} - \left[\text{CH}_2 - \underset{\text{CH}_3}{\underset{ }{\text{CH}}} - \text{O} \right]_n - \text{CH}_3$ | $68.2 \text{ mm}^2/\text{s}$ at 40°C $14.0 \text{ mm}^2/\text{s}$ at 100°C | 0.9767 g/cm^3 at 40°C |
| Polyolester (POE) 68 | $ \begin{array}{c} \text{R} \\ \\ \text{C}=\text{O} \\ \\ \text{O} \\ \\ \text{H}-\text{C}-\text{H} \\ \quad \quad \\ \text{O} \quad \text{H} \quad \text{O} \\ \quad \quad \\ \text{R}-\text{C}-\text{O}-\text{C}-\text{C}-\text{C}-\text{O}-\text{C}-\text{R} \\ \quad \quad \\ \text{H} \quad \text{H} \quad \text{H} \\ \quad \\ \text{H}-\text{C}-\text{H} \\ \\ \text{O} \\ \\ \text{C}=\text{O} \\ \\ \text{R} \end{array} $ | $67.2 \text{ mm}^2/\text{s}$ at 40°C $12.3 \text{ mm}^2/\text{s}$ at 100°C | 0.9097 g/cm^3 at 40°C |
| Polyalphaolefin (PAO) 68 | $\text{R} - \underset{\text{CH}_2}{\underset{ }{\text{CH}}} - \left[\text{CH}_2 - \underset{\text{R}}{\underset{ }{\text{CH}}} \right]_n - \text{H}$ | $63.2 \text{ mm}^2/\text{s}$ at 40°C $9.7 \text{ mm}^2/\text{s}$ at 100°C | 0.8205 g/cm^3 at 40°C |

Table 5.2 Physical properties of studied greases

| Grease | Base oil | Base oil viscosity | Thickener (weight percentage) | Additives (contents) | Worked penetration |
|---------|---------------------------|--|-------------------------------|---|--------------------|
| Grease1 | PAO | 31mm ² /s at 40°C 5.8mm ² /s at 100°C | 12OH-LiSt (12%) | None | 236 |
| Grease2 | PAO | 66mm ² /s at 40°C 10mm ² /s at 100°C | 12OH-LiSt (12%) | None | 291 |
| Grease3 | PAO | 411mm ² /s at 40°C 41mm ² /s at 100°C | 12OH-LiSt (12%) | None | 386 |
| Grease4 | PAO | 31mm ² /s at 40°C 5.8mm ² /s at 100°C | Diurea (13.4%) | None | 280 |
| Grease5 | PAO | 19mm ² /s at 40°C 4.1mm ² /s at 100°C | LiSt (12%) | None | 336 |
| Grease6 | PAO | 411mm ² /s at 40°C 41mm ² /s at 100°C | LiSt (12%) | None | 339 |
| RL2 | HVI160S | 107mm ² /s at 40°C 12mm ² /s at 100°C | Diurea (not applicable) | Not applicable | 280 |
| RLS2 | PAD1450 | 100mm ² /s at 40°C 13mm ² /s at 100°C | Diurea (not applicable) | Not applicable | 265 - 295 |
| SB-M | Synthetic hydrocarbon oil | 45mm ² /s at 40°C 7.7mm ² /s at 100°C | Urea (10 - 20%) | Zinc compound and barium compound (10%) | 220 |
| SRL | Synthetic ester oil | 23mm ² /s at 40°C 4.7mm ² /s at 100°C | LiSt (5 - 15%) | Barium compound (5%) | 250 |

Chapter 6

Dielectric Properties of Lubricants

This chapter contains experimental results in static and EHD conditions. From the perspective of dielectrics, dielectric properties of greases are compared with those of corresponding base oils. The dielectric properties extracted from the work carried out in the EHD condition are evaluated.

6.1 Static Conditions

Non-polar substances such as PAO oils do not show the dielectric relaxation process because they do not have dipole moment. In fact it can be said that most of the lubricants studied here do not show the relaxation behaviour in the studied range of frequencies. In order to evaluate the dielectric relaxation process in static conditions, an external resistor of $2\text{k}\Omega$ was introduced and fitted in series with the micrometre capacitor, which made it possible for all samples to show the relaxation behaviour at around 1MHz. In this way the relaxation time measured may not indicate the intrinsic properties of lubricant itself, yet the difference between samples could be observed. Although a quantitative evaluation of the dielectric relaxation time was not possible, a qualitative comparison of this parameter between the studied greases and between the grease and its base oil could be performed using this artefact. On the other hand, the dielectric constant of lubricants which was evaluated by taking the average of measured points in flat region in the capacitance versus frequency curves was not influenced by the resistor.

6.1.1 Oil lubricants

In addition to grease base oils, the experiments using five different oils listed in Chapter 5 were conducted in order to understand the effect of dielectric properties not only on the viscosity but also on the rheological properties inside the EHD contact. In this section the results of those “viscosity 68” oils were compared and discussed while the results of the base oils were comparatively shown, along with those of greases in the next section. The test rig and experimental method are described in Chapter 5.

6.1.1.1 Dielectric constant

The results in Figure 6.1 show the dielectric constant of five oils at 40°C, all of which exhibit the same viscosity at that temperature.

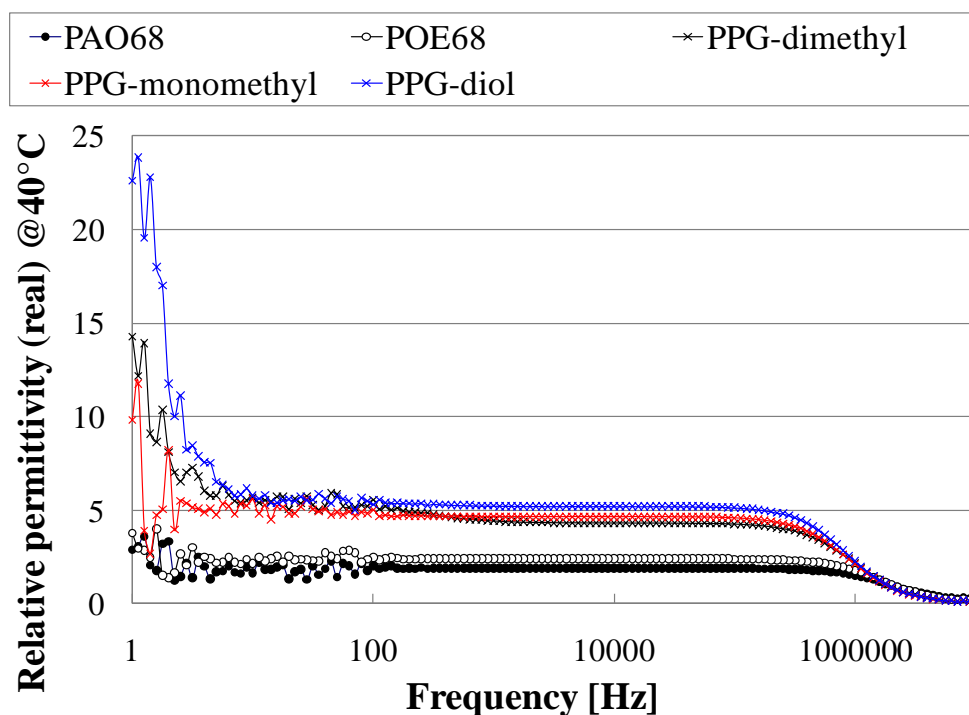


Figure 6.1 Dielectric constant of “viscosity 68” oils

From these results, the dielectric constant of each oil was calculated by taking the average between 10kHz and 1kHz. PPG-diol showed the highest permittivity which was 5.21 while the dielectric constants of PPG-monomethyl and dimethyl were 4.65 and 4.34 respectively. POE had slightly higher permittivity, 2.40, than general lubrication oils which were known to show dielectric constant of roughly between 1.7 and 2.1. For example this value was 1.89 for PAO68 used in this case.

The experimental results indicate that the dielectric properties depend much more on the molecular structure rather than the physical properties of liquids such as the viscosity. On the other hand it has to be kept in mind that many previous studies have shown that the higher viscosity an oil has, the higher permittivity it exhibits.

By combining Figure 4.5 and Table 5.1, PPG-diol and monomethyl can be classified into the type C. The experimental results of those two oils are in accordance with the fact that the type C oils indicate strong polarity due to their structural strong dipole moment. On the other hand, it is assumed that the second methyl group attached to the other edge weakens the bulk polarity in the case of PPG-dimethyl which showed the smallest permittivity among the three PPG oils. Moreover, it is found that the hydroxyl group contributes to the polarization of the molecule more than the methyl group because the dielectric strength of PPG-diol was not alleviated by attaching OH groups at both ends of the structure.

The scatter of measured points especially below 100Hz is attributed to interfacial polarization, also known as space charge polarization. This mechanism is different from the so-called dielectric polarization such as the orientational polarization attributed to the dipole moment of the molecule and the electric or atomic polarization induced by the distortions of the electrons or atoms. In the case of interfacial polarization, a large scale distortions of the electric field take place, which is caused, for example, by the accumulation of charges in the region inside the dielectric where small amount of moisture

is trapped at the surface of the electrode, or at the boundary of materials when considering more than two dielectrics, where the local conductivity changes. This phenomenon can also be induced by the inequality of the overall structure in case of polymers [76].

6.1.1.2 Dielectric relaxation behaviour

The results in Figure 6.2 show the variation of the imaginary part of the dielectric permittivity which indicates the dielectric relaxation behaviour of the studied lubricants. In this experiment the presence of the external resistor influences the behaviour relating to the energy absorption but the clear differences are observed between five different oils. The discontinuity below 1MHz it appears to be an experimental artefact and observed every time in measurements with the micrometer.

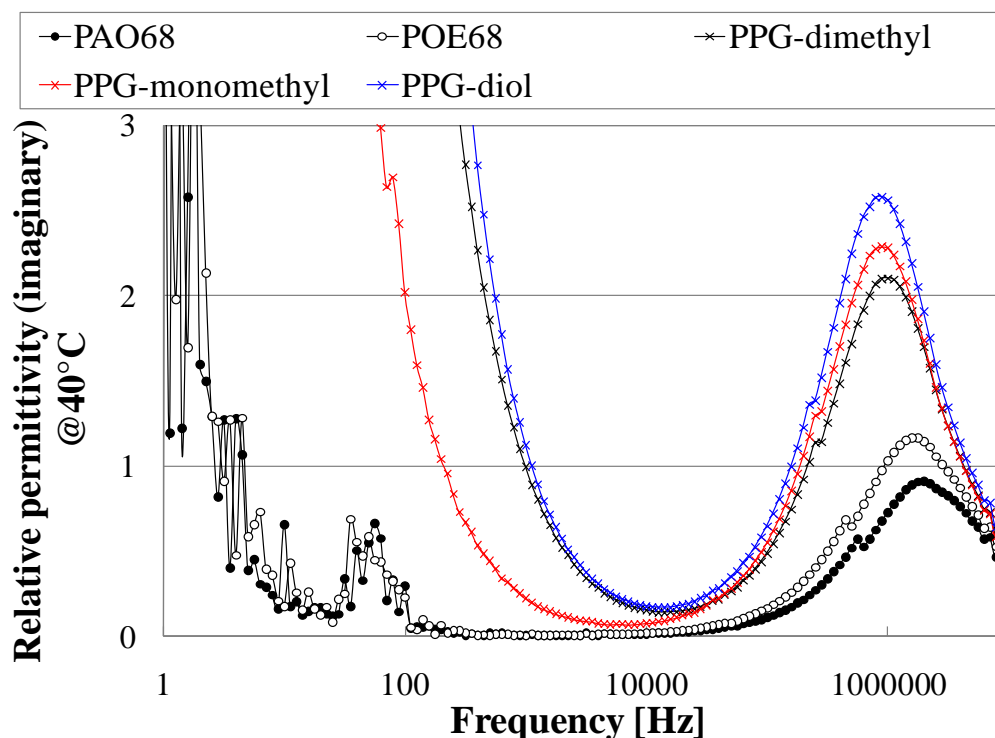


Figure 6.2 Dielectric loss of “viscosity 68” oils

The strength of the relaxation process of the oil, which can be compared by the position of the peak points, is increased with the value of its dielectric constant. It can be seen that the position of the peak is shifted towards lower frequency region though the three PPG oils have the position of the peaks at nearly the same frequency. This suggests that the relaxation time attributed to the external resistor becomes longer when the experiment is conducted with polar substances. An explanation to this phenomenon can be obtained if we refer to the dielectric as a material described as in Figure 4.2. In this case the whole resistance in the circuit will be increased when the capacitor is filled with a strong polar material, which leads to the slower relaxation (that is, peak obtained at lower frequency). On the other hand, the capacitor filled with PAO can be regarded as a perfect capacitor because the oil does not show the dipole moment, and therefore the whole circuit can be expressed as the series circuit with one capacitor and resistor. The resistance of the whole circuit is lower than that in the above case, which allows a faster relaxation process in the lubricants, compared to polar substances.

Another distinct feature of the results shown in Figure 6.2 refers to the behaviour of the polar liquids in low frequency region. This difference of the behaviour of the polar liquids from the non-polar liquids stands out even more than that the peak point shifts. From the observation of the dielectric loss in low frequency region, PPG oils can easily be distinguished as strong polar liquids. Such a strong polar material could show sharp increase with decreasing frequency in the low frequency region, below 10kHz in this case, in other words, could show good conductivity as explained earlier.

6.1.1.3 Conclusions

The strength order of the dielectric constant in terms of the type of the oil was found as follows:

Glycol > Ester > Olefin

The experimental work has shown that the dielectric properties for the liquid state are dependent much more upon the chemical properties such as the dipole moment than upon the rheological properties such as viscosity of oils. This conclusion has been drawn by preparing oils consisting of different structure but having the same viscosity and comparing their dielectric properties.

It has been proposed that PPG-diol and monomethyl are classified, from the dielectric point of view, as type C polymers, which shows polar groups at the side of the chain and therefore shows strong dipole moment due to the side group rotating freely. This has been proved by the experimental results which showed that PPG-diol and monomethyl have indicated higher dielectric constant than PPG-dimethyl.

The experimental results also show that the hydroxyl group affects strongly the polarization of the bulk molecule and the dipole moment will not be balanced or weakened when hydroxyl groups are attached to both sides of the molecular chain. On the other hand, the polarity of PPG-dimethyl becomes weak by obtaining methyl groups at both ends of the molecular chain.

6.1.2 Grease lubricants

As a starting point for the evaluation of the dielectric properties of greases, the dielectric properties of their base oils are investigated. From the perspective of dielectric behaviour, it is expected that the thickener and additives would strongly influence the dielectric properties of the bulk grease because those are usually either metallic materials or polar substances. It is difficult, however, to separately evaluate the thickener and its own dielectric properties because of the complicated manufacturing process especially for urea thickeners, although the dielectric properties of some kinds of representative thickeners are presented in Appendix 1.

The base oils for Greases 1 to 6 could not be obtained from the manufacturer of those greases, however those oils are commercially available lubricants, thus three different viscosity PAOs were obtained for the base oils of these six greases. PAO4 was supplied by Lubrizol and has kinematic viscosity of $21\text{mm}^2/\text{s}$ and $4.0\text{mm}^2/\text{s}$ at 40°C and 100°C respectively. PAO40 was supplied by Shell and shows values of the kinematic viscosity of $386\text{mm}^2/\text{s}$ and $39\text{mm}^2/\text{s}$ at 40°C and 100°C respectively, while the properties of PAO68 are listed in Chapter 5.

In this study, Grease 1 to 3, SRL, the 12OH-LiSt thickener and the ester base oil of SRL are known as “polar” materials. All experimental work was conducted at 20°C (the room temperature).

6.1.2.1 Dielectric constant

The results of the dielectric constant of the greases and corresponding base oils are shown in Figure 6.3.

For all investigated greases, the dielectric constant is higher than that of its base oil. From this point of view, the dielectric constant of a grease will depend mainly upon the property of the corresponding base oil, which may be natural behaviour because the base oil normally accounts for about 70% of the bulk grease. Thus it has been found, for at least the studied greases, that the dielectric properties of a grease are mainly determined by the corresponding base oil even though a grease contains additives.

SRL grease which consists of a polar ester oil as its base oil shows the highest permittivity among the ten studied greases, while all other greases are produced with non-polar base oils, thus showing lower dielectric permittivity.

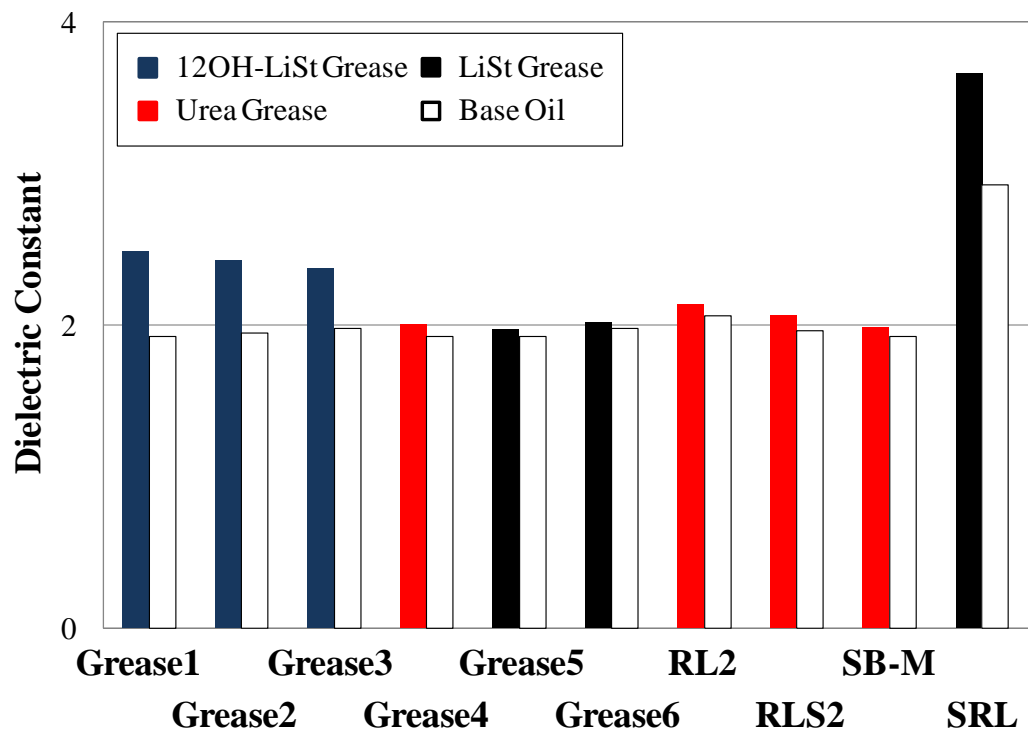


Figure 6.3 Dielectric constant of greases

When comparing LiSt greases with non-polar ingredients to urea greases, it is observed that LiSt greases tend to show smaller dielectric constant compared to other greases and the relatively higher dielectric constant of Grease6 would be attributed to its high viscosity base oil.

The results in Figure 6.3 show that by the value of their dielectric constant, greases, except SRL, can be classified according to the nature of their thickeners. Greases made from 12OH-LiSt thickener show relatively large dielectric constant while LiSt greases show smaller dielectric constant than urea greases.

In order to assess the relative contribution of the thickener to the overall dielectric properties of greases, the ratio between the dielectric constant of the grease and base oil is

introduced. The results show that this ratio depends on what kind of thickener is used. Although very polar Lithium grease, SRL, showed relatively high ratio of 1.252, the dielectric constants of Grease5 and 6 were increased only by 1.028 and 1.023 times in comparison to the permittivities of corresponding base oils. On the other hand, the ratio from 1.032 in the case of SB-M to 1.053 in the case of RLS2 was obtained for urea greases. For polar greases, the dielectric constant of Grease1 increased by 1.295 times relative to its base oil, while Grease2 and 3 indicated a ratio of 1.247 and 1.203 respectively. From these results, it can be said that the degree of polarization of the grease due to thickener would follow the order below.

12OH-LiSt > Urea > LiSt

Furthermore, the distinguishing feature observed in Figure 6.3 is that the non-polar greases made from higher viscosity oil give larger dielectric constant than those made from lower viscosity oil, which can be predicted by the fact that higher viscosity oil shows large dielectric constant than the oil indicating low viscosity. For example, Grease5 shows 1.98 of the dielectric constant while Grease6 shows 2.02. However, the same thing cannot be said about polar greases. Grease2 has a larger dielectric constant than Grease3, while Grease1 has the largest dielectric constant among 12OH-LiSt greases. An explanation for this behaviour can be found if comparing the chain lengths of the base oils' molecules. It is well known that oils which contain longer chain in its chemical structure tend to have high viscosity, and the higher viscosity the oil has the higher the relative permittivity becomes. In the case of non-polar greases, this mechanism can be applied and the dielectric constant of the bulk grease increases with its base oil's viscosity. In the case of polar greases, on the other hand, the dipole moment of the bulk structure (which includes both polarities of polar and non-polar materials) may become weak when the polar substance is located in the long molecular structure. From this perspective it could be explained why the 12OH-LiSt grease formed from the high viscosity base oil showed relatively small dielectric constant.

Finally, the value of worked penetration will have minor effects on the dielectric constant of the grease. Comparing Grease5 and Grease6, the dielectric constants of these two greases are distinctly different due to the effect of the base oil as discussed earlier, though these two greases indicate almost the same values of the worked penetration.

6.1.2.2 Dielectric relaxation behaviour

The experimental results concerning the relaxation time of the studied greases and their base oils are compared in Figure 6.4. The relaxation time of greases increased with the dielectric constant of the bulk grease and was longer than that of the corresponding base oils. This suggests that the semi-solid state of the grease makes it more difficult for the molecules to activate and respond quickly to a variable external electric field.

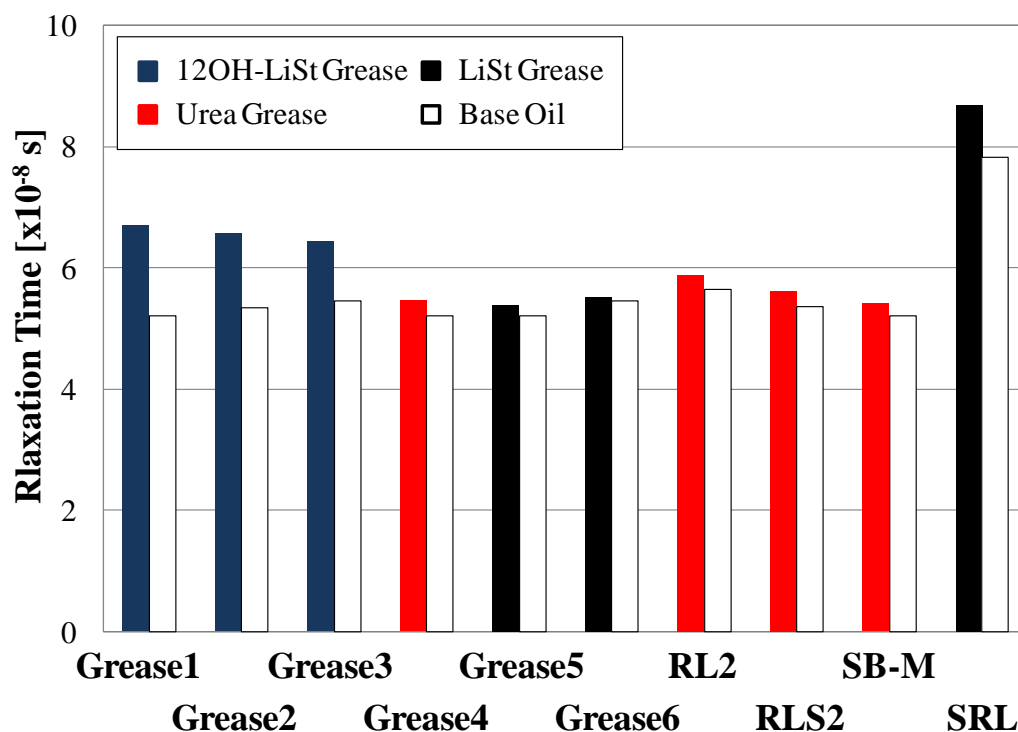


Figure 6.4 Relaxation time of greases

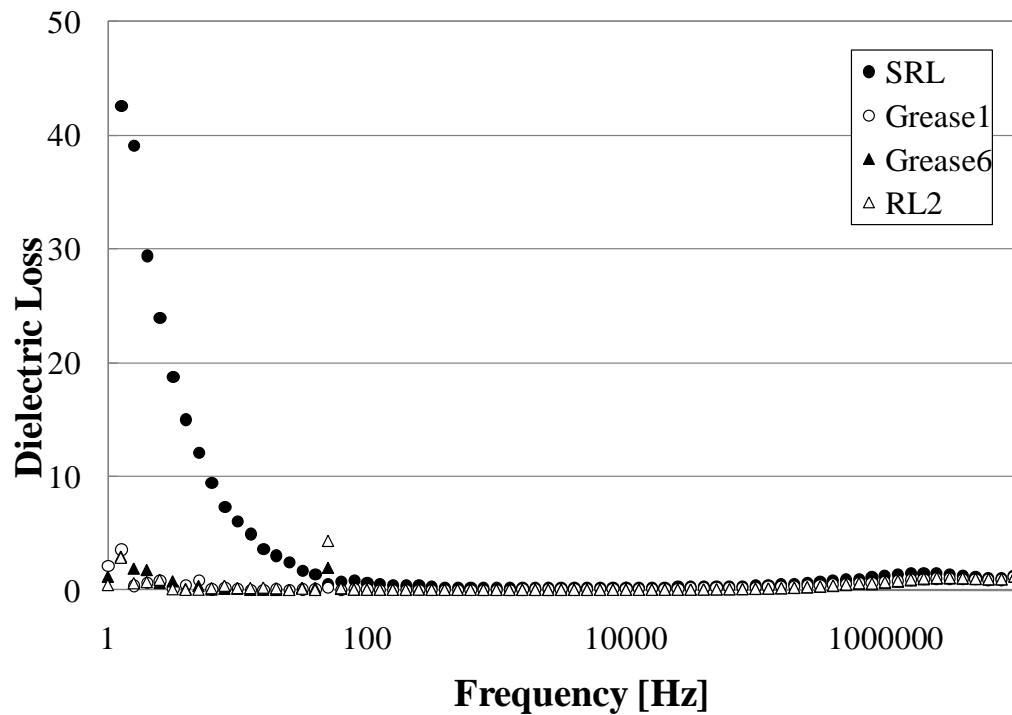


Figure 6.5 Dielectric loss of greases

Yet another distinguished behaviour has been found in the imaginary part of the dielectric constant; good conductivity was observed only in the case of SRL out of all ten greases. This behaviour is compared to that of Grease1, Grease6 and RL2 in Figure 6.5.

6.1.2.3 Conclusions

The experimental results of greases' dielectric constant and relaxation time are summed up in Figure 6.6. It has been found that the dielectric properties of greases depend strongly upon the properties of the corresponding base oil, where all greases investigated are showing higher dielectric constant and longer relaxation time than the corresponding base oils. When there is little difference between the base oils, the dielectric properties of greases will follow the rules advocated below.

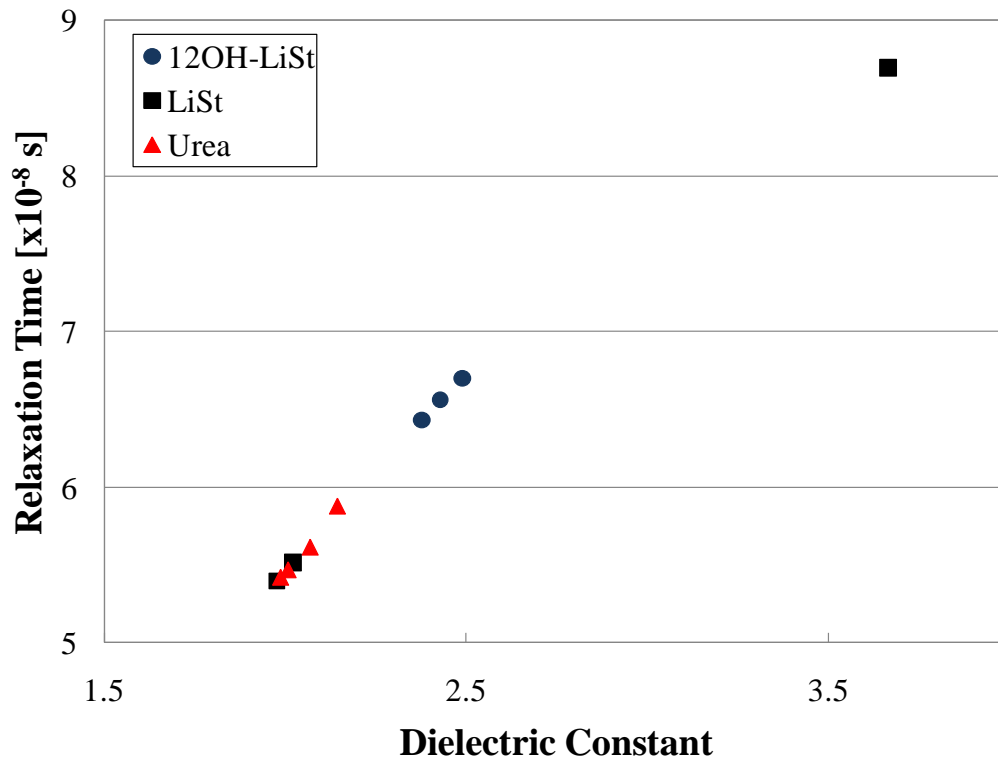


Figure 6.6 Dielectric properties of greases

Greases can be classified by its thickener type and in order of the magnitude of their dielectric constant they can be ordered as follows;

12OH-LiSt group > Urea group > LiSt group

In addition, the dielectric relaxation time of greases seems to become long with increasing dielectric constant and therefore it also depends upon the type of thickener. LiSt greases show the shortest relaxation time whilst 12OH-LiSt greases exhibit the longest relaxation time among greases investigated here, except the very polar grease SRL.

Overall results show that the effect of the worked penetration upon the dielectric properties of greases is negligible.

6.2 EHD Conditions

The dielectric measurements on EHD contacts were done with the test rig employing the steel disc and ball as described in Chapter 5. The dielectric properties under EHD conditions of the pure rolling and sliding/rolling conditions were evaluated and any change relative to the static condition was studied and presented in this section.

The experiments were conducted at room temperature and it was tried to maintain these conditions as long as possible. However, it is inevitable that the temperature of the test rig reaches higher temperature than the atmospheric one, which leads the temperature of lubricants in these tests of about 30°C in all experiments. This will be one reason why slightly smaller dielectric constants of lubricants were observed in following results compared to the ones measured in static conditions and presented in the previous section. For dynamic experiments, an external resistor was not introduced so that the whole relaxation behaviour was not observed in the studied frequency range. (The relaxation behaviour seems to be partially observed in Figure 6.8, however it has been difficult to gain sustainable data beyond the studied frequency range at the moment of writing this thesis.)

6.2.1 Dielectric properties under shear conditions

The measurement of the dielectric permittivity was firstly done with static disc and ball in the EHD rig. Subsequently, the dielectric properties under shear (pure sliding) conditions were measured by rotating only disc at 20mm/s and under unload conditions because measurements become more or less unstable if load applied.

In order to evaluate the effect of shear upon the dielectric properties, the polar ester oil which is the base oil of SRL, was chosen for these tests. The dielectric constant of the oil in static conditions and under sheared conditions is comparatively shown in Figure 6.7. The dielectric loss in the two cases is illustrated in Figure 6.8.

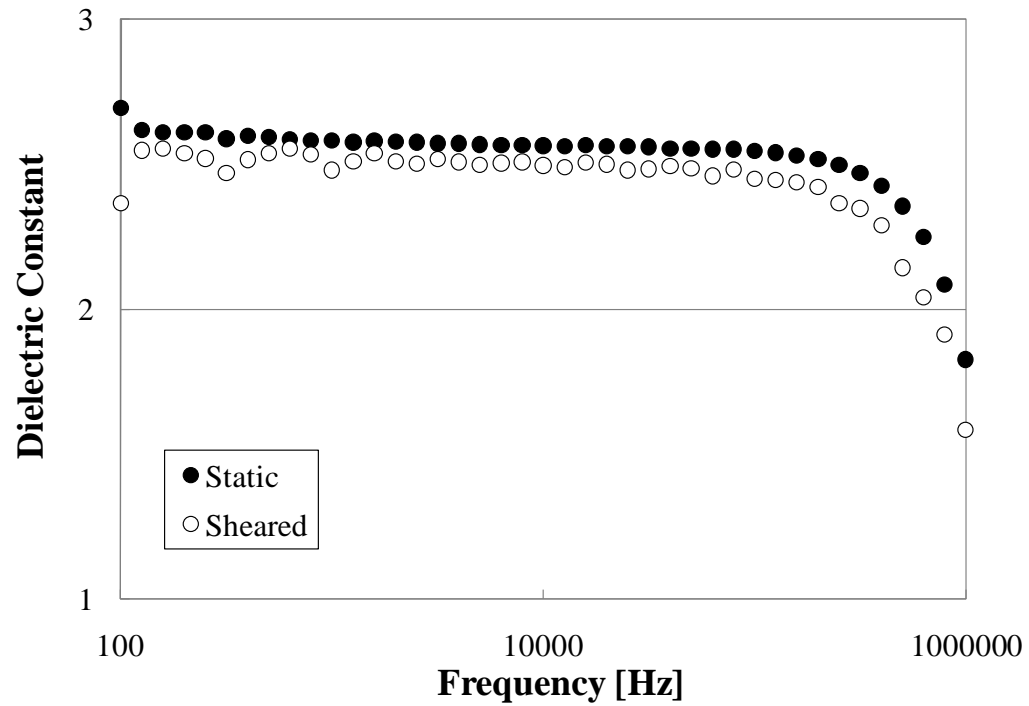


Figure 6.7 Dielectric constant of the base oil of SRL under sheared condition

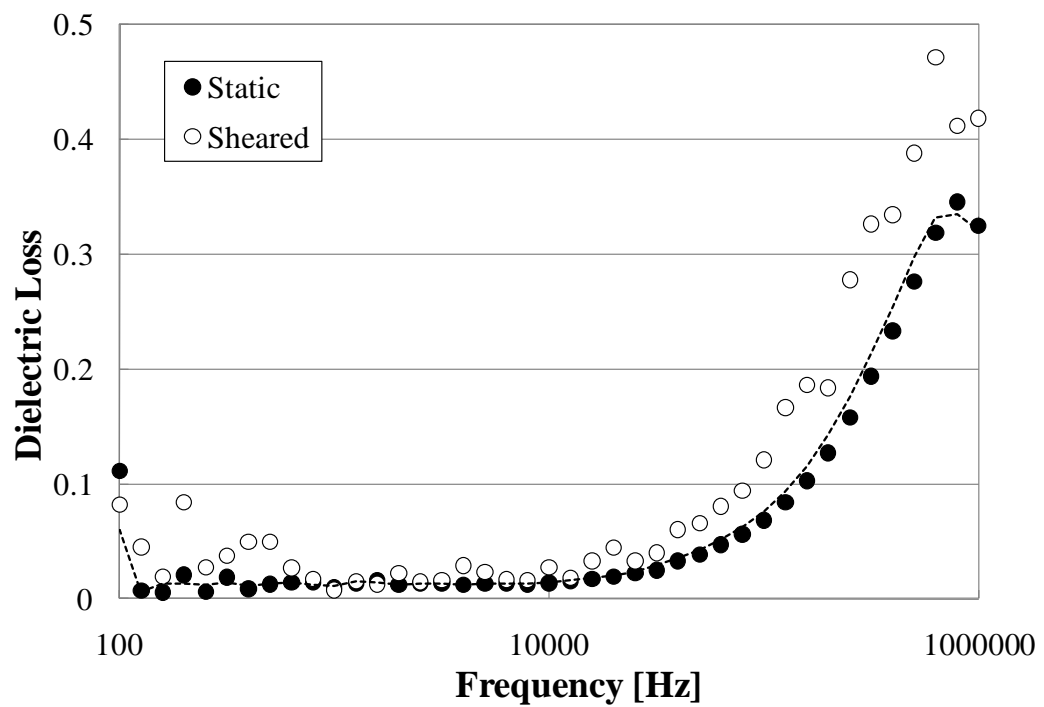


Figure 6.8 Dielectric loss of the base oil of SRL under sheared condition

It is found that the dielectric constant of the lubricant subjected to the shear was slightly smaller than that obtained in static conditions. On the other hand, the peak in the dielectric loss under sheared conditions seems to be shifted towards higher frequencies although the whole relaxation process does not appear within the studied frequency range.

There have been a very small number of theoretical studies into the effect of shear on the dielectric properties of materials, however the behaviour found in the current study was found to be well in accordance with the experimental results of Block *et al* [116].

According to them the dielectric constants of ethyl cellulose and PBLG (poly- γ -benzyl-L-glutamate) decrease and the peak of the dielectric loss is shifted to higher frequency with increasing shear rate.

6.2.2 Dielectric constant under pure rolling EHD conditions

Due to the fact that it is difficult to obtain stable film thickness in the case of grease lubricated contacts (due to starvation) the relative permittivity of oil lubricants rather than greases was evaluated under EHD conditions. The pressure in these contacts was up to 1.11GPa. An additional difficulty was the fact that, in higher loaded and slower speed conditions, the results were less stable because the gap between the ball and disc (electrodes of the capacitor) was so small that the electric breakdown through the film will sometimes occur. The broad behaviour was similar to Figure 6.7 and there were stable regions in measured capacitances around 100kHz in most of cases, which allowed the evaluation of the dielectric constant of the lubricant films for each case. However, the relaxation process could not be observed. Thus in this section only the behaviour of the dielectric constant under high pressures will be discussed.

The measurements were conducted under pure rolling conditions at 0.3m/s with increasing load in steps of 2N from the start value of 10N. The results of the base oil of SRL are shown in Figure 6.9.

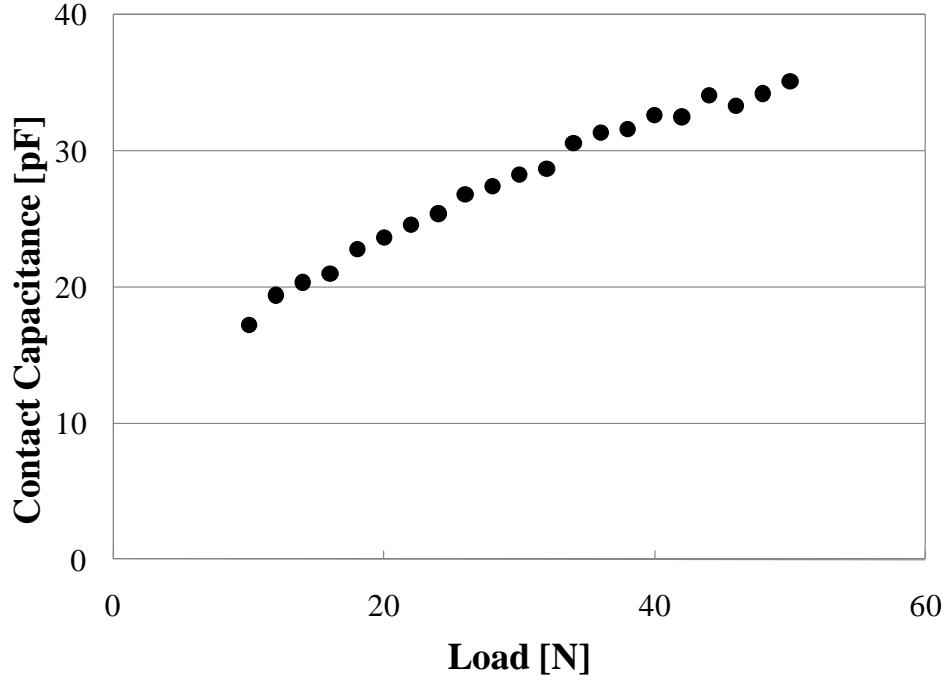


Figure 6.9 EHD contact capacitance of the base oil of SRL at 0.3m/s

The technique of determining the dielectric constant of the lubricant film inside the EHD contact has been described in Chapter 5. The film thickness herein was treated to be uniform across the contact for any load and the value of the film thickness measured at the same speed and 20N with glass disc by using ULTRA, shown in Figure 6.10 with the broad speed range, was used for calculations. As indicated by broken lines in Figure 6.10, the value of 82nm at 0.3m/s was measured, while the area of the contact for each load was calculated by Hertz theory described as Equation 2.1.

$$A = \pi a^2 = \pi \left(\frac{3wR_A}{E'} \right)^{2/3} \quad (6.1)$$

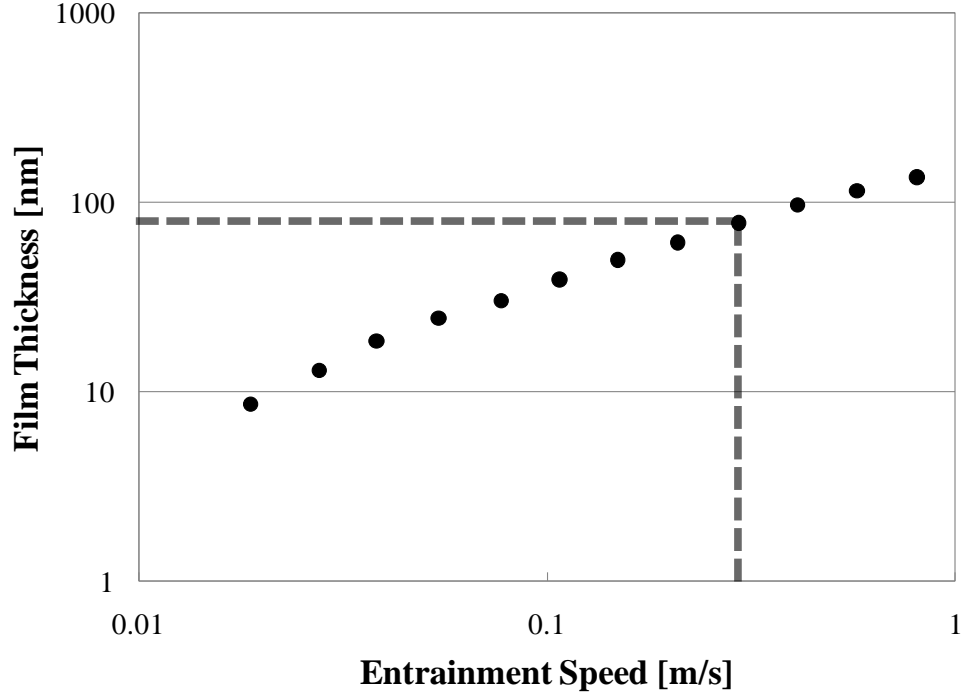


Figure 6.10 ULTRA film thickness measurement for base oil of SRL

Thence, the dielectric constant inside the EHD contact was extracted from measured contact capacitance C_c by using Equation 5.4.

$$C_c = \varepsilon_0 \varepsilon_r \frac{A}{d} \quad \therefore \varepsilon_r = \frac{C_c d}{\varepsilon_0 A} \quad (6.2)$$

where A is obtained from Equation 6.1 and d is regarded as 82nm.

As shown in Figure 6.9, the measured capacitance increased with pressure, which will be attributed mainly to the increase of the contact area diameter. When extracting the relative permittivity from this result, it has been found that this parameter decreases with increasing pressure as shown in Figure 6.11.

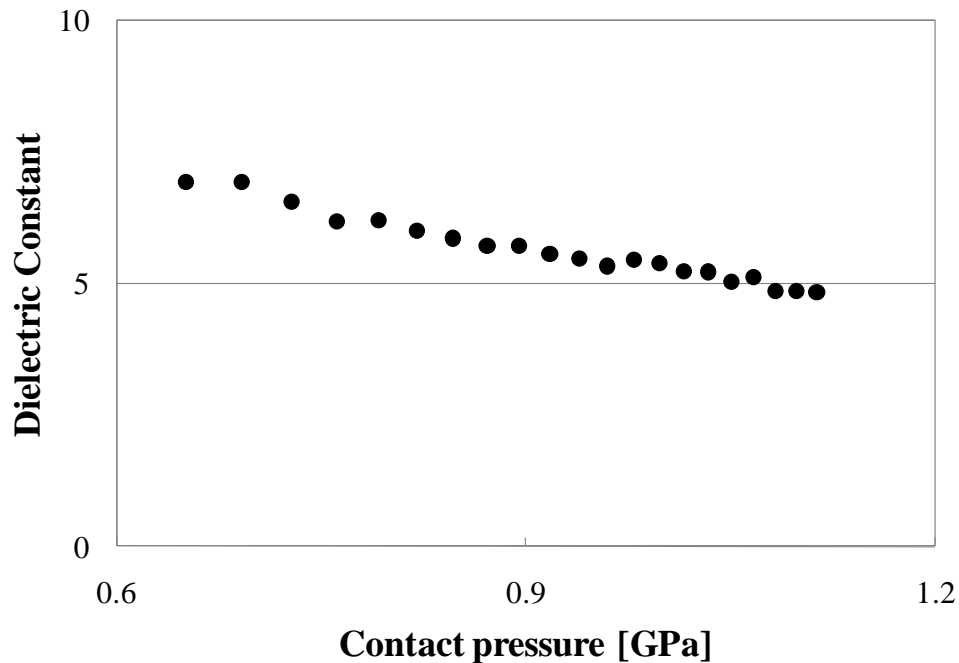


Figure 6.11 Dielectric constant of the base oil of SRL in the EHD condition

Although those results still indicate higher values than the dielectric constant at atmospheric pressure, this trend is not predicted by other experimental results where the dielectric constant increases with pressure [94, 106-108]. It is to be noted though that in those studies the pressure does not reach values as high as 1 GPa which is used in this research. Also those results were reported for other liquids, not necessarily lubricating oils. In fact there are few studies reporting the decrease of the relative permittivity with increasing pressure. Hirst and Moore [117] used the relative permittivity of the lubricant for their line contact film thickness calculations, where the relative permittivity was separately measured in the static condition showing a decreasing behaviour against increasing pressure.

In order to clarify this somehow unexpected behaviour (Figure 6.11), it has to be taken into consideration that changes in film thickness with pressure was ignored as the influence of load on the film thickness is experimentally and theoretically known to be small. Thinner

film leads to slightly smaller values in the dielectric constant when calculating it from the measured capacitance in the EHD condition (Equation 6.2). Thus, this would not change the overall tendency where the dielectric constant decreases with increasing pressure though it would lead to a value closer to that corresponding to atmospheric condition.

It has been found that, due to imperfections of the rig, the pressure on the contact and therefore its dimensions vary. It is evident that proportionally this variation must be larger at low loads than at large loads. It is therefore thought that in this case the film thickness would not be constant both over the contact area and over time in comparison with the high pressure case as illustrated in Figure 6.12.

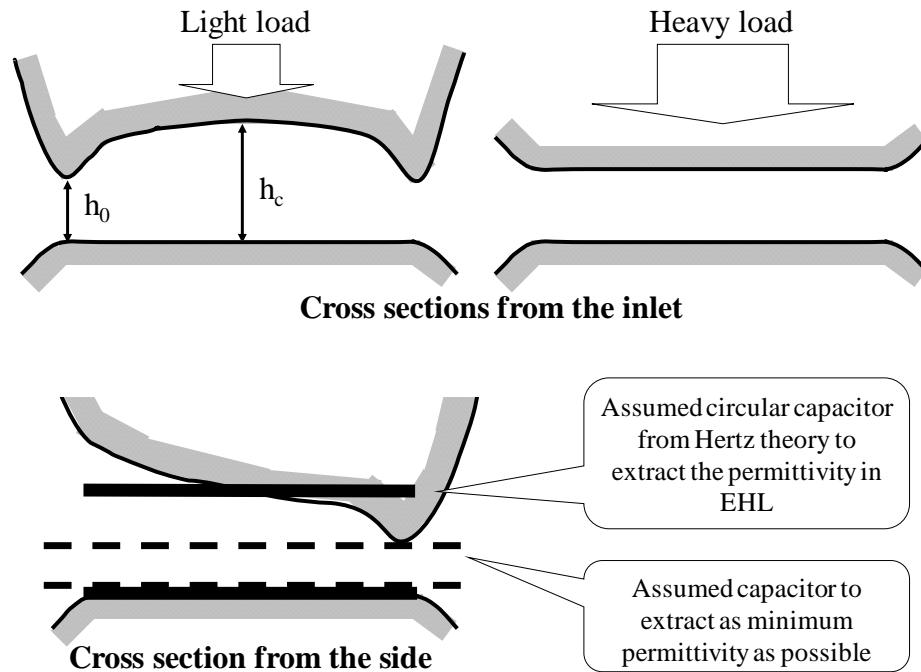


Figure 6.12 Schematic diagram of the EHD contact and assumed capacitor

Thus, in order to evaluate the errors in the calculation of the dielectric permittivity (the minimum value of the dielectric constant) the minimum film thickness, which is equal to

66nm, was used instead of the value of 82nm which was measured with ULTRA and used for the results in Figure 6.11. Moreover, a 10% error (attributed to varying in the contact diameter) has been allowed for the calculation of the dielectric constant. The new evaluated values are illustrated as the error bars in Figure 6.13.

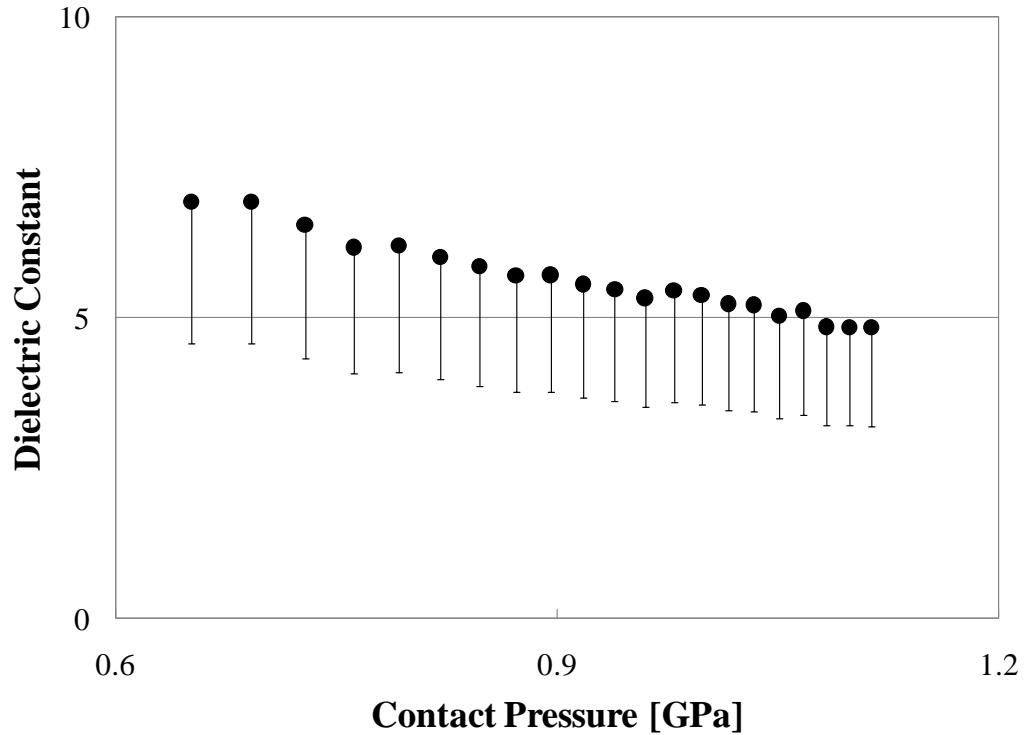


Figure 6.13 Dielectric constant of the base oil of SRL with error bars

From the perspective of the error analysis, all measured points would be obtained within a certain range and it would be possible to say that the dielectric constant shows a constant value in EHD condition though the value is higher than the value at atmospheric pressure. However, the trend of decrease in the dielectric constant with increasing pressure is still observable, which was not predicted before the experiments were conducted.

Nonetheless, this unexpected behaviour would be possible to happen especially in extreme conditions such those found in EHD contacts and might be explained by considering the concept of entropy. Fröhlich [118] proposed a relationship between entropy, dielectric constant and temperature, which is given by Equation 6.3.

$$s = s_0(\theta) + \frac{\partial \epsilon'}{\partial \theta} \frac{E^2}{8\pi} \quad (6.3)$$

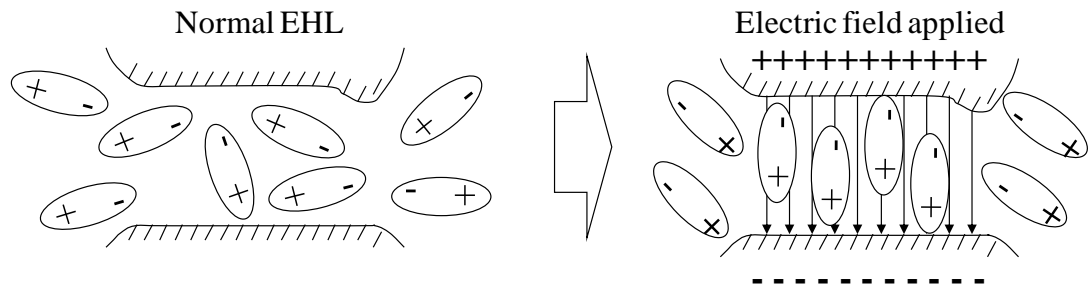
where s , $s_0(\theta)$ and E indicate entropy, the entropy under no electric field and electric field respectively. According to Equation 6.3 and the fact that entropy is regarded as indicating a degree of disorder of molecules, entropy will decrease by the application of an electric field when $\partial \epsilon' / \partial \theta < 0$, which means that molecules are aligned by the applied electric field. At present it is not known how the effect of pressure on entropy is expressed, however, it can be predicted that a similar relationship may hold, in which the term $\partial \epsilon' / \partial \theta$ is replaced by $-\partial \epsilon' / \partial p$. This can be justified by the fact that there is a physical similarity between decreasing temperature and increasing pressure in terms of decreasing the free volume in the liquid.

From this point of view, decreasing dielectric constant with increasing pressure indicates that the entropy increases with the application of the electric field.

It is therefore hypothesised that, in the EHD conditions, the electric field disorganises the alignment of molecules, which is possible to happen only when molecules are initially aligned. Thus this experimental work suggests that molecules are forced to be somehow aligned in the inlet region and consequently are ordered inside the EHD contact. Figure 6.14 represents a schematic diagram of the concept relating to entropy and the electric field, where the left hand side drawings represent the conditions before the electric field is applied while both right hand side ones represent the conditions after and during the electric

field has been applied. The shape of the molecules was just illustrated for easy understanding and the brief diagrams do not reflect the real molecular movements or alignment inside the EHD contact. It is of course considered what forces the molecules to be aligned are the viscous forces due to the flow and thereby the real alignment of the molecules would be along the direction of flow.

$$\frac{\partial \varepsilon'}{\partial p} > 0 \quad \therefore s : \text{decreases (with applying an electric field)}$$



$$\frac{\partial \varepsilon'}{\partial p} < 0 \quad \therefore s : \text{increases (with applying an electric field)}$$

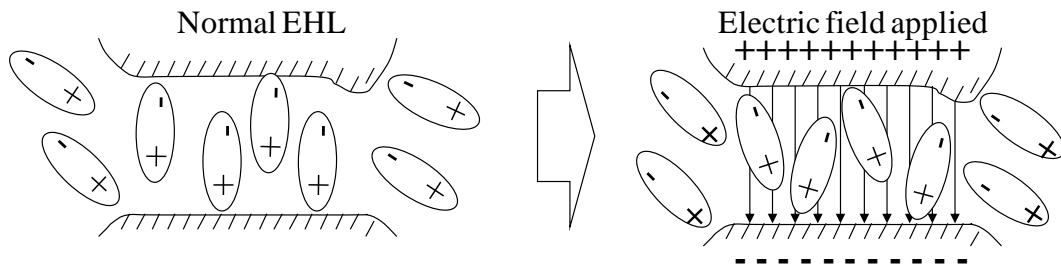


Figure 6.14 Molecular behaviour inside the EHD contact

6.2.3 Dielectric constant under sliding rolling EHD conditions

From the assumption achieved in the above section, it is expected that the rate of change in the permittivity-pressure curve, $\partial \varepsilon' / \partial p$, obtained in sliding conditions will be moderate compared to pure rolling conditions such as one in Figure 6.11, since molecules under

sheared conditions are thought to be aligned much more and this fact contributes to reduce the chaotic movement of molecules induced by the applied electric field.

While the experimental and evaluation procedure were same as in the above case, the mineral oil HVI 160S, the base oil of RL2, was examined under both pure rolling and slide-roll ratio conditions ($SRR = 100\%$). Figure 6.15 shows the measured contact capacitance as a function of the load applied to the contact.

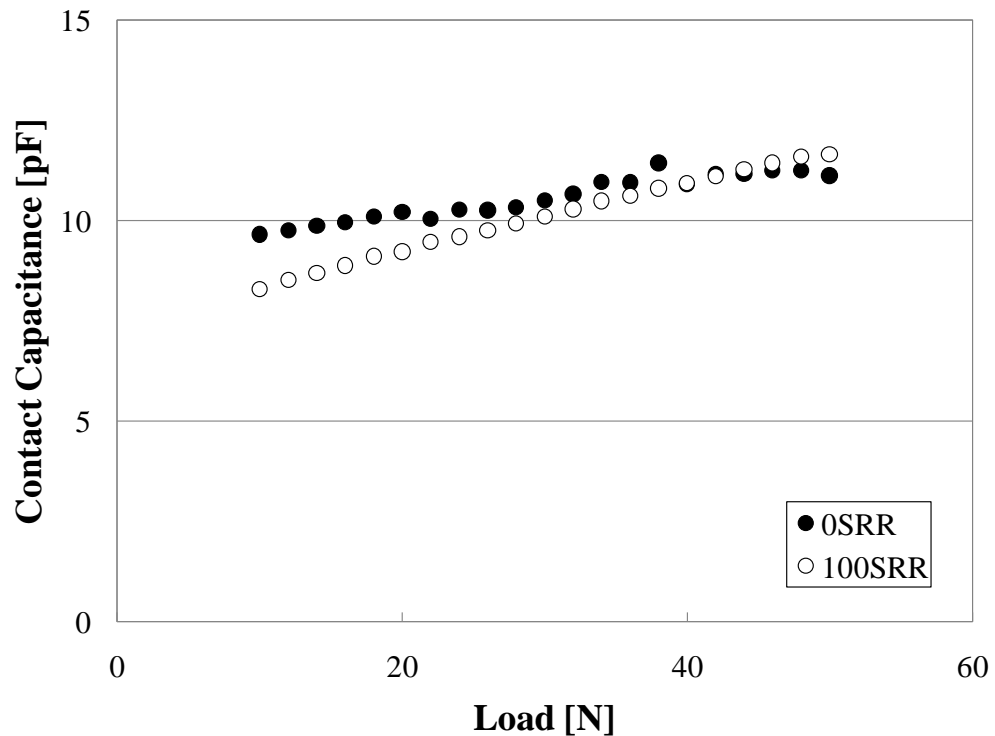


Figure 6.15 EHD contact capacitance of HVI 160S

Measured capacitances for each case have been converted to the dielectric constant of the lubricant in EHD conditions by utilising a film thickness of 240nm extracted from ULTRA measurements and Hertz contact theory. Figure 6.16 represents the dielectric constant in the EHD condition as a function of pressure.

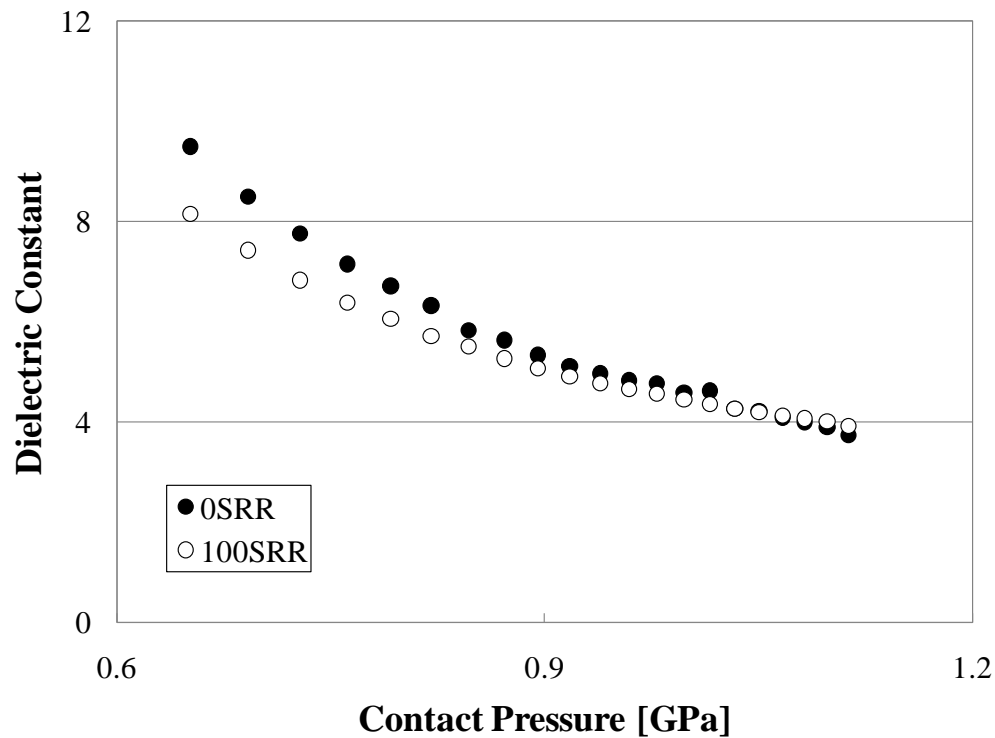


Figure 6.16 Dielectric constant of HVI 160S in the EHD condition

As shown in Figure 6.16, the overall value of the dielectric constant, under sheared conditions, indicates a lower value than in pure rolling and a moderate trend of decreasing with pressure. According to the analysis in the previous section this means the degree of entropy changes will be smaller compared to pure rolling conditions thus the disorganisation of molecules is less likely to be induced in this case. Consequently, this fact is in accordance with the hypothesis that molecules' alignment under shear will be much stronger and therefore will be affected to a lesser extent by an external electric field than the molecules under pure rolling conditions.

6.2.4 Conclusions

It is confirmed that the shear behaviour induces changes in the dielectric properties by using the EHD rig without loading. The dielectric constant decreased slightly and the relaxation peak seemed to be shifted to higher frequencies under sheared conditions.

Under loading, on the other hand, the dielectric constant of lubricants did not increase with pressure as it was expected based on other studies. This behaviour could be explained by the concept of entropy, concept of which was confirmed by the behaviour of the EHD films in pure rolling and sliding/rolling conditions. Hence, it is concluded that these experiments prove the alignment of molecules in EHD contacts.

Chapter 7

Observation of Rheological Behaviour of Lubricants

This chapter describes the experimental results of rheological properties of lubricants. The greases were tested under a variety of conditions and evaluated compared to their base oils.

7.1 Traction Curves

The EHD traction measurements were conducted for all samples of greases and corresponding base oils at the entrainment speed of 20mm/s. The temperature was maintained at 30°C and experiments were conducted between 0% *SRR* and 60% *SRR*. The load was increased from 10N to 50N in 10N steps. In each test the measurement of the traction coefficient was carried out twice. After a first test the rig was left to run for five minutes in pure rolling conditions with loading and after that the test was run again in order to check whether starvation occurs due to the grease pushed to the sides of the track.

Figure 7.1 shows a typical result of traction curves in the grease EHL films, which is taken in the case of SRL at 10N. According to these results, significant difference between two measurements was not observed and this can be said for all greases. On the other hand, SRL gave the smallest thickness among ten greases and changes in film thickness with time shown in Figure 7.2 were also investigated.

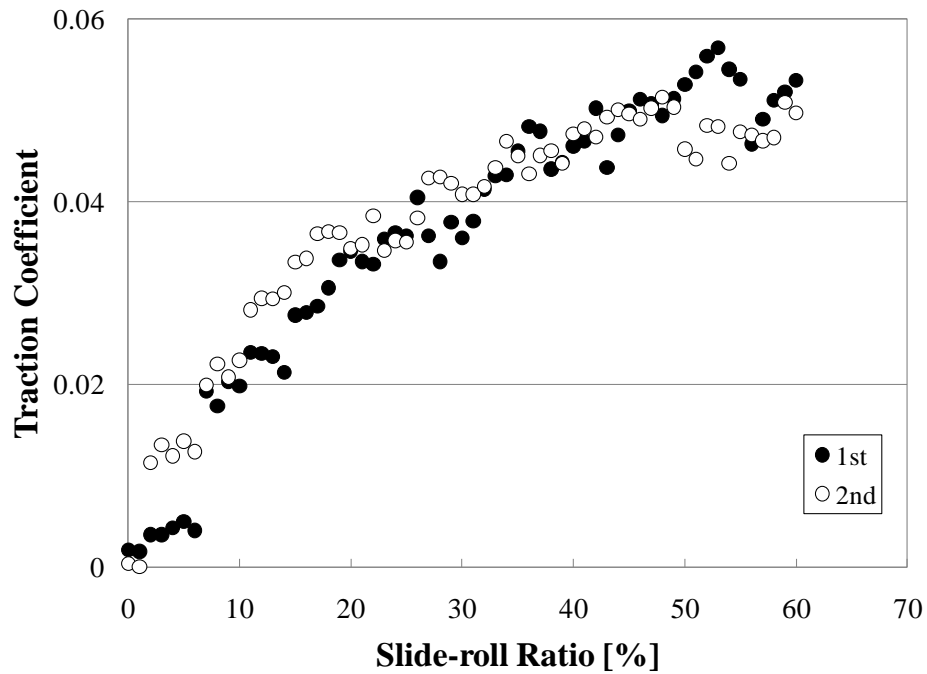


Figure 7.1 Traction curves of SRL at 10N and 20mm/s

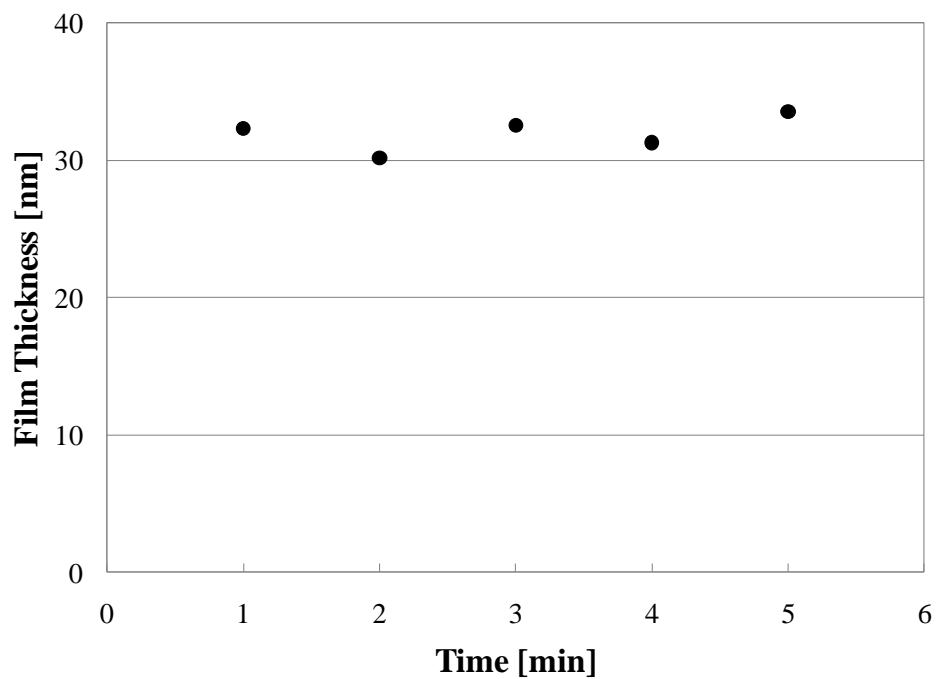


Figure 7.2 SRL film thickness changes with time at 20mm/s

Although this measurement was done at 20N with glass disc for five minutes, starvation was not observed and the average film thickness of 32nm was obtained from this result. Therefore, it can be concluded that the starvation did not occur at least during these experiments so that intrinsic aspects of the grease behaviour in the EHD condition were able to be investigated and compared. From now on, for simplicity the results are shown as the average of two measured points. Finally, the traction curves obtained were subsequently used, in an analysis similar to that done by Evans and Johnson [20], to extract the viscosity η , usually stated as the effective viscosity, and the Eyring stress τ_0 of the lubricants tested.

7.1.1 12OH-LiSt greases

7.1.1.1 Grease and corresponding base oil

The traction curves of Grease1 to 3 accompanied by those of their corresponding base oils are illustrated in Figure 7.3 to 7.5, respectively.

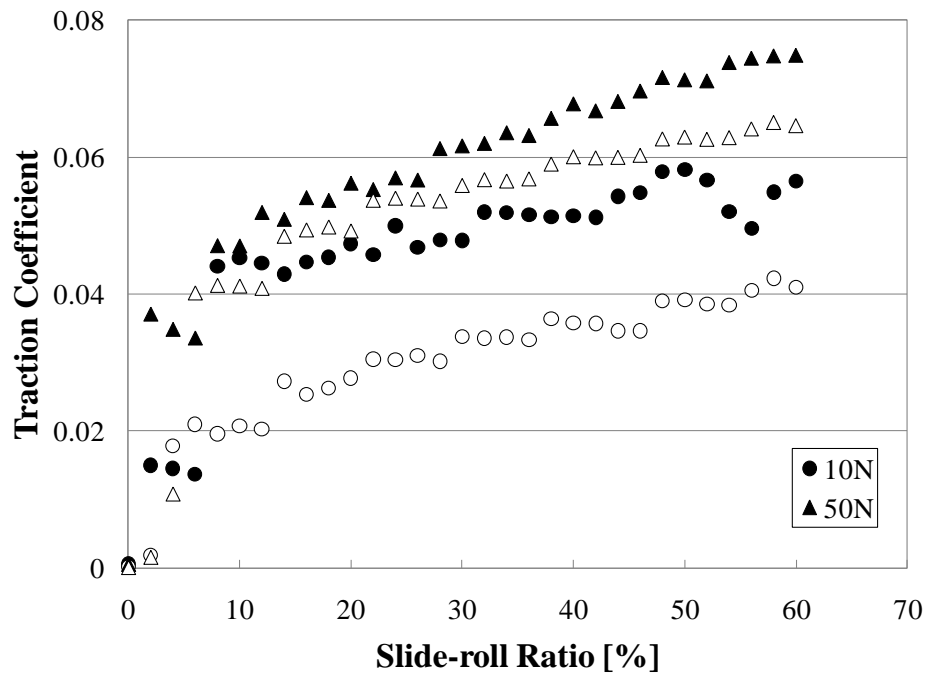


Figure 7.3 Traction curves of Grease1 (black points) and PAO4 (white points)

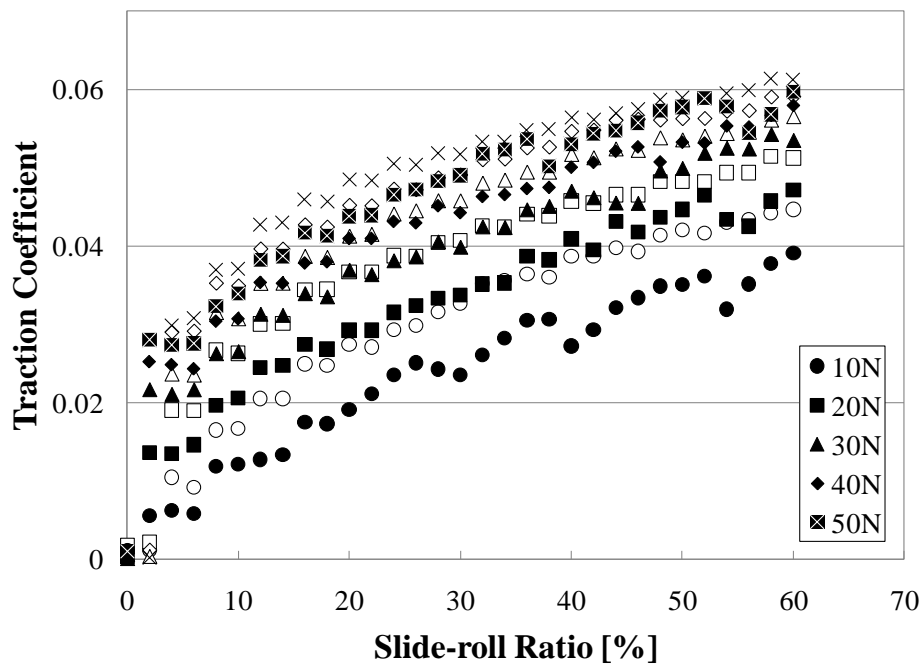


Figure 7.4 Traction curves of Grease2 (black points) and PAO68 (white points)

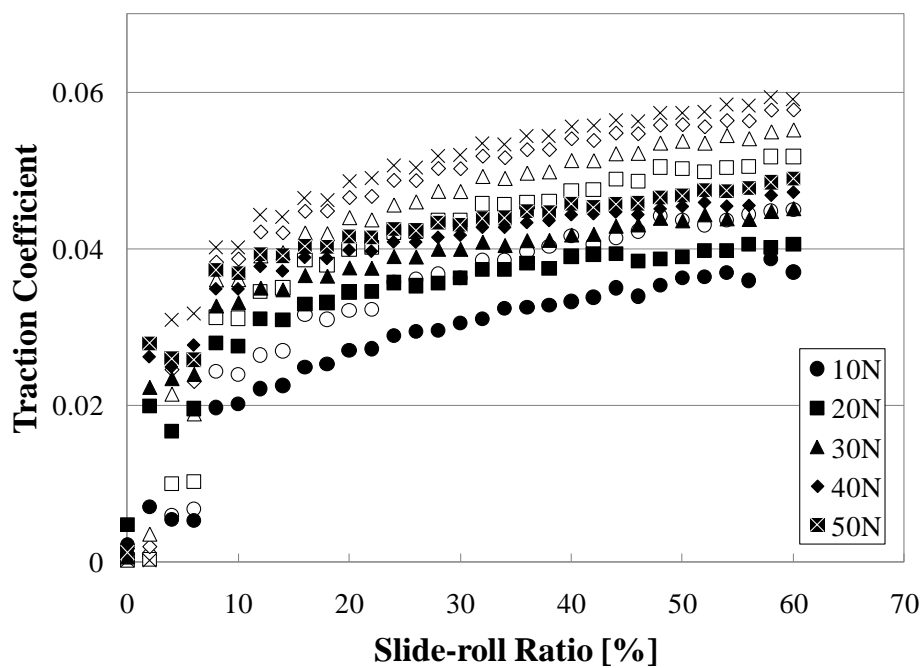


Figure 7.5 Traction curves of Grease3 (black points) and PAO40 (white points)

Due to the lack of availability of the grease, the experiments for Grease1 were conducted only at 10N and 50N.

It has been found that polar greases, Grease2 and 3, showed overall lower traction coefficient than the corresponding base oils in the same condition of speed and load. The difference between the grease and the oil, however, became smaller for heavier loads, though there are constant differences in the case Grease3.

7.1.1.2 Effect of base oil and correlation to dielectric properties

In this case, only the results at 50N will be used to compare between the behaviour of different greases since it can be considered the most severe loaded cases reflect the desirable properties in the EHD condition such as durability against starvation.

The shear rate was calculated from the sliding speed in the contact and the film thickness separately measured by ULTRA with a glass disc at 20N (Equation 2.41 and 5.9). On the other hand, the shear stress was obtained by using Equation 5.10, where the area of the contact was same for all materials in this kind of study.

$$\dot{\gamma} = \frac{\Delta u}{h} = SRR \times \frac{\bar{u}}{h} \quad (7.1)$$

$$\tau = \frac{T}{A} = \mu \frac{w}{A} \quad (7.2)$$

Consequently, the slide-roll ratio SRR and traction coefficient μ at 50N in Figure 7.3 to 7.5 are transformed into the shear rate and shear stress and shown in Figure 7.6. The film thickness used in order to extract the shear rate is presented in Appendix 2 for all lubricants studied in this chapter.

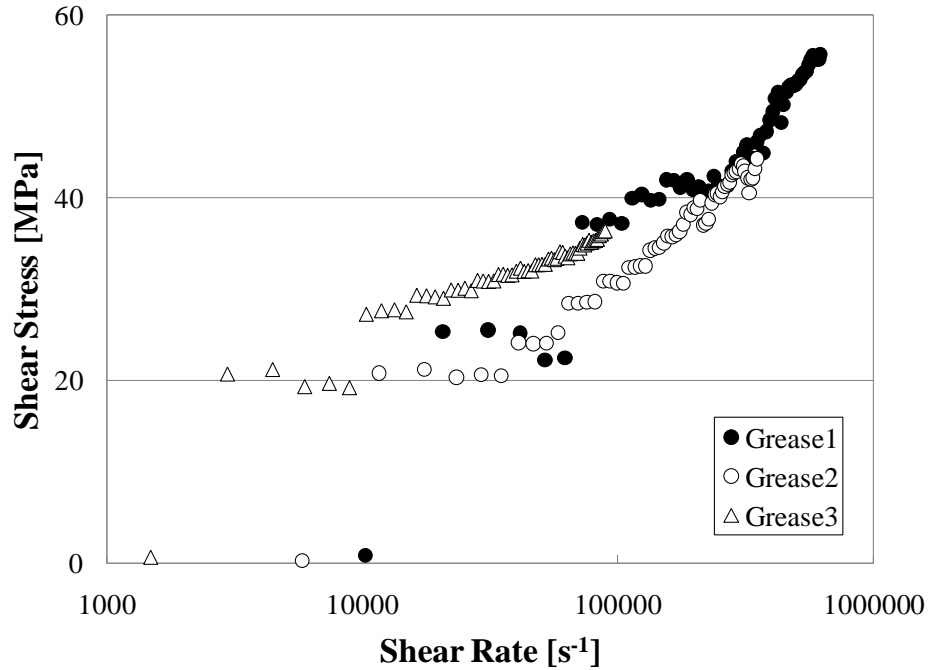


Figure 7.6 Traction curves of 12OH-LiSt greases

Figure 7.6 shows the shear stress function of the shear rate for the polar thickener (12OH-LiSt) greases, Grease1, 2 and 3. It can be seen that the shear stress of Grease3 increases at a slower rate and has lower values, at high shear rate, compared with other greases of the same type. This graph would suggest that Grease1 has the largest shear stress and Grease3 has the smallest shear stress at high shear rate range. Thus, considering the effect of the base oil upon the shear behaviour of 12OH-LiSt greases, it can be concluded that increasing viscosity of the base oil results in a decrease of the shear stress in EHD conditions.

It can be noted on the other hand, that the dielectric results for these greases showed that Grease1 has the largest permittivity, 2.49, while the dielectric constant of Grease2 and 3 are 2.43 and 2.38 respectively. Thus, it is found that polar grease lubricants show the tendency that the stronger the polarity the grease possesses the higher the shear stress it experiences in the EHD operation.

7.1.2 LiSt greases

7.1.2.1 Grease and corresponding base oil

Figure 7.7, 7.8 and 7.9 show the comparison of the traction behaviour of lithium stearate greases, Grease5, Grease6 and SRL, and their base oils.

As presented in the graphs below, the behaviour of NSK greases is similar to that of the base oil at 50N. However, SRL shows a different behaviour indicating relatively higher traction coefficients compared to the corresponding base oil for all ranges of the load.

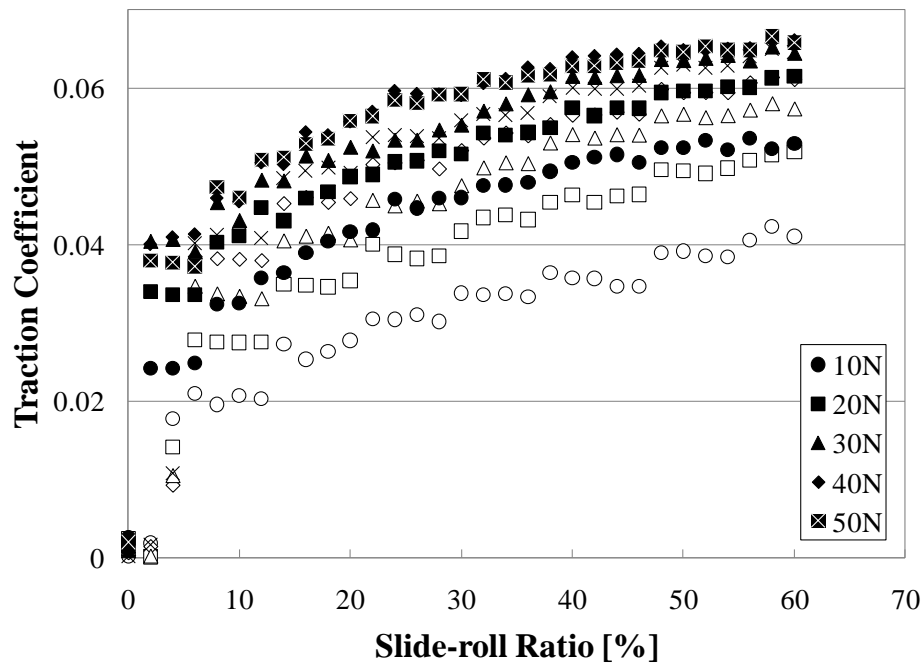


Figure 7.7 Traction curves of Grease5 (black points) and PAO4 (white points)

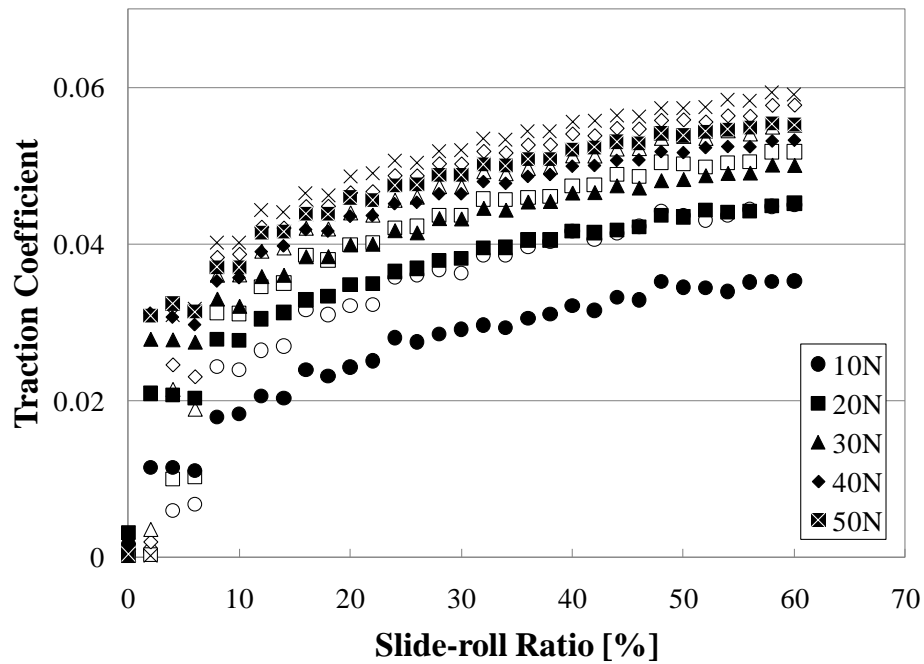


Figure 7.8 Traction curves of Grease6 (black points) and PAO40 (white points)

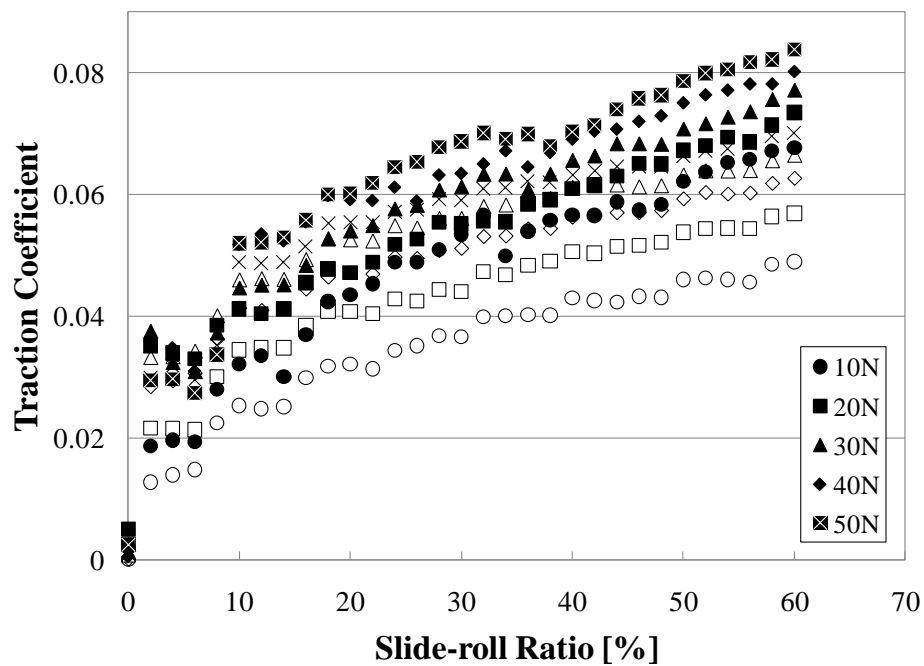


Figure 7.9 Traction curves of SRL (black points) and its base oil (white points)

7.1.2.2 Effect of base oil and correlation to dielectric properties

The traction curves of LiSt greases are compared in Figure 7.10.

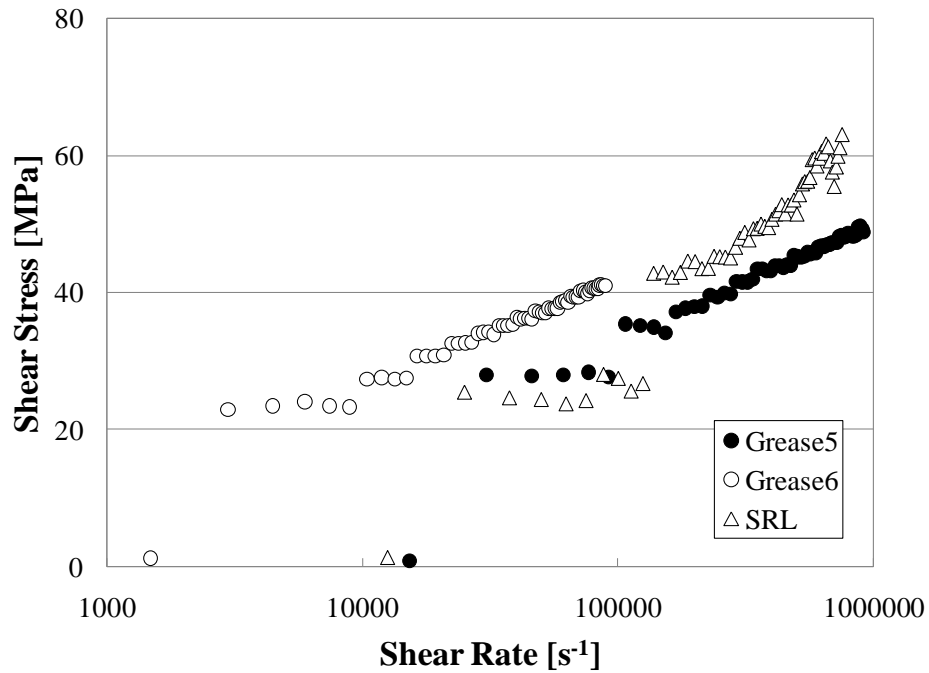


Figure 7.10 Traction curves of LiSt greases

Because Grease6 formed a relatively thick EHL film compared to counterparts due to the large viscosity of its corresponding base oil, the experimental results of Grease6 were placed in a different range of the shear rate. However, the trend obviously shows that Grease6 may experience higher shear stress than Grease5 at high shear rate. Consequently, the similar trend to that found in the case of 12OH-LiSt greases is also observed in this case, in relation to the dielectric investigation whose results are shown in Figure 6.3. In other words greases which exhibit large dielectric constant in static measurements show high shear stress in dynamic measurements.

Although the base oil of SRL which also includes additives is different from others, it seems to be appropriate to conclude that the shear stress in LiSt greases increases with the viscosity of the base oil.

7.1.3 Urea greases

7.1.3.1 Grease and corresponding base oil

The results of traction curves for urea greases are shown in Figure 7.11 to 7.14 together with the results of the corresponding base oils.

In all cases for urea greases, the traction force (and by extension traction coefficient) generated in the grease film tends to be larger than that observed in the base oil alone. This trend can be explained by the fact that the grease is less likely to slip at the boundary between the lubricant and the bounding surface due to grease's low fluidity and good ability to adhere.

The result of urea greases presented here is totally different from the results obtained from NSK greases, except Grease5 and incomplete results of Grease1, where lower shear stress was observed in the case of greases. Thus the urea grease shows bigger shear stress than the base oil. The discrepancy of these results will be attributed partly to the characteristics of low fluidity and good ability to adhere, features of which may be accelerated by urea thickeners more than by other types of the thickener, and partly to the fact that NSK greases are not compared to their genuine base oils.

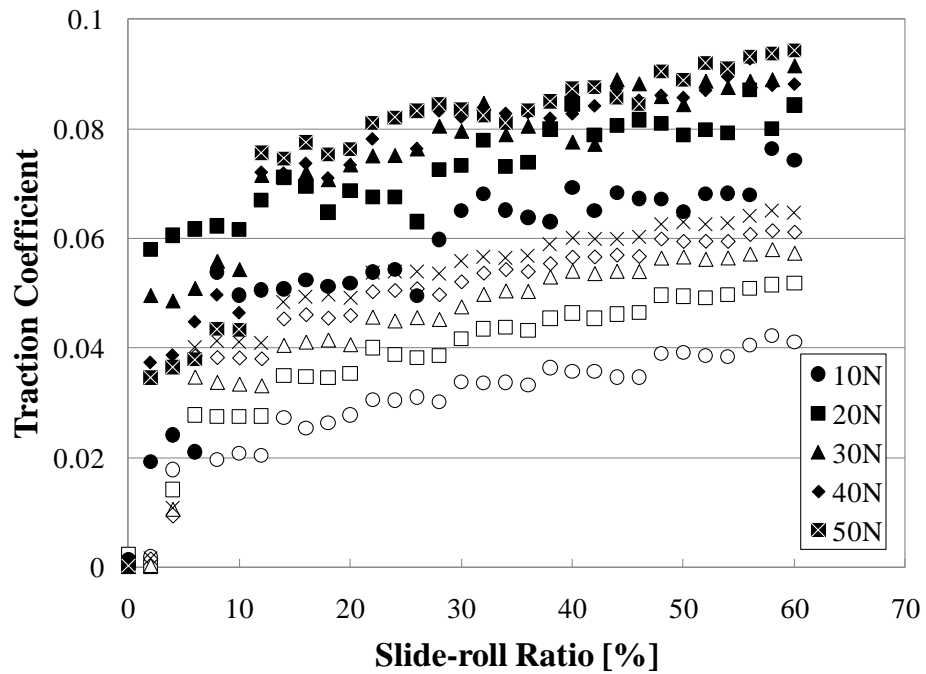


Figure 7.11 Traction curves of Grease4 (black points) and PAO4 (white points)

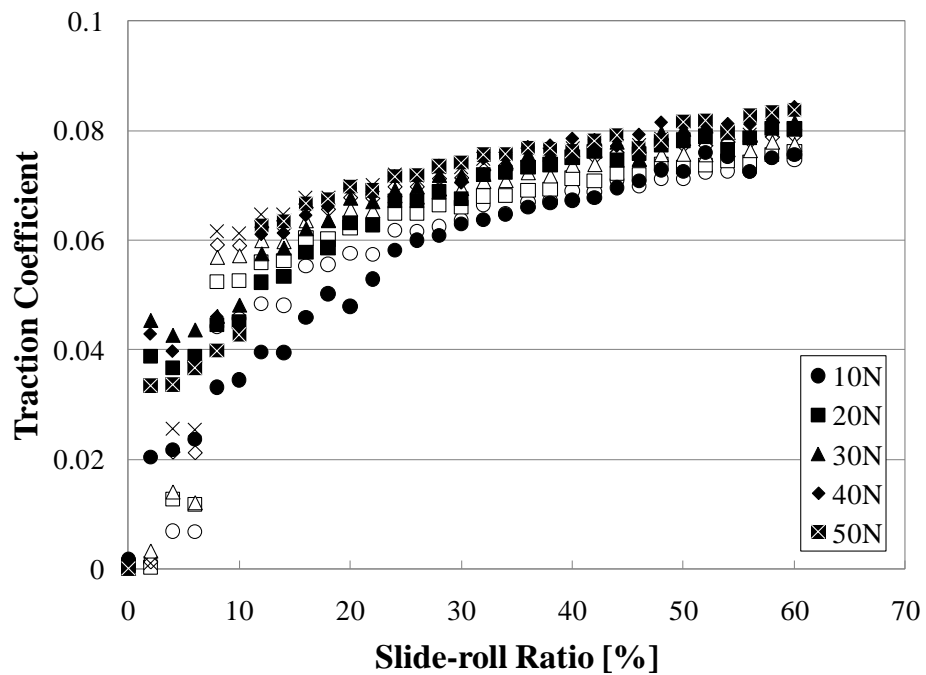


Figure 7.12 Traction curves of RL2 (black points) and its base oil (white points)

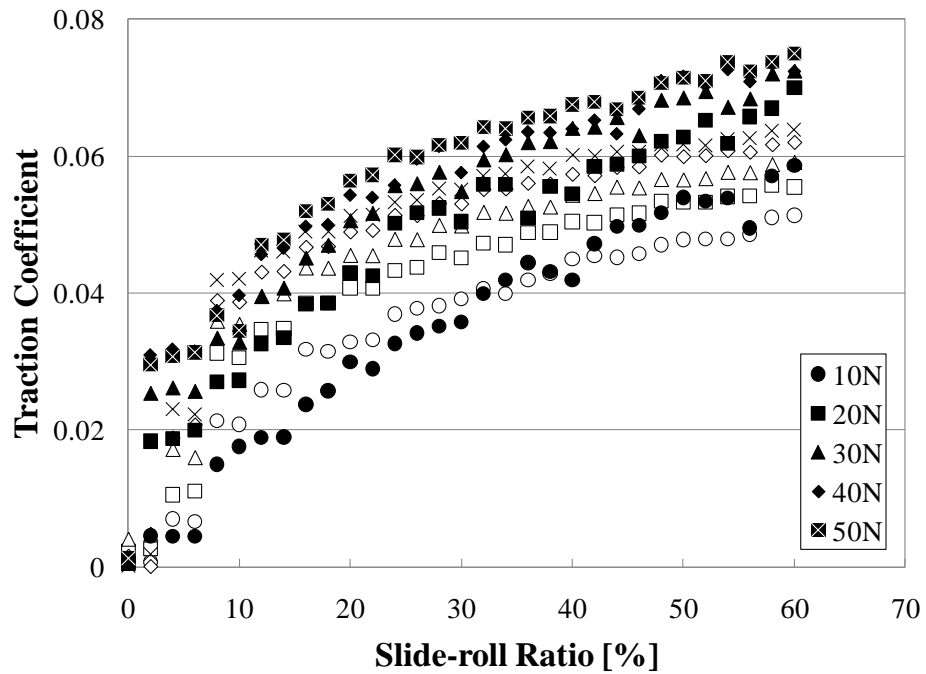


Figure 7.13 Traction curves of RLS2 (black points) and its base oil (white points)

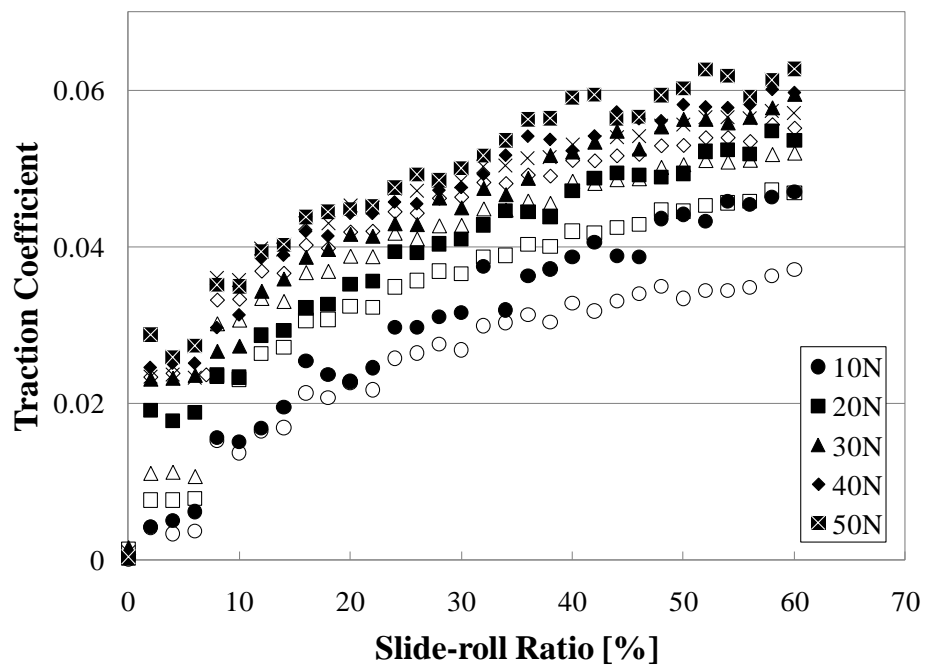


Figure 7.14 Traction curves of SB-M (black points) and its base oil (white points)

7.1.3.2 Correlation to dielectric properties

The comparison between urea greases regarding to their rheological properties is shown in Figure 7.15.

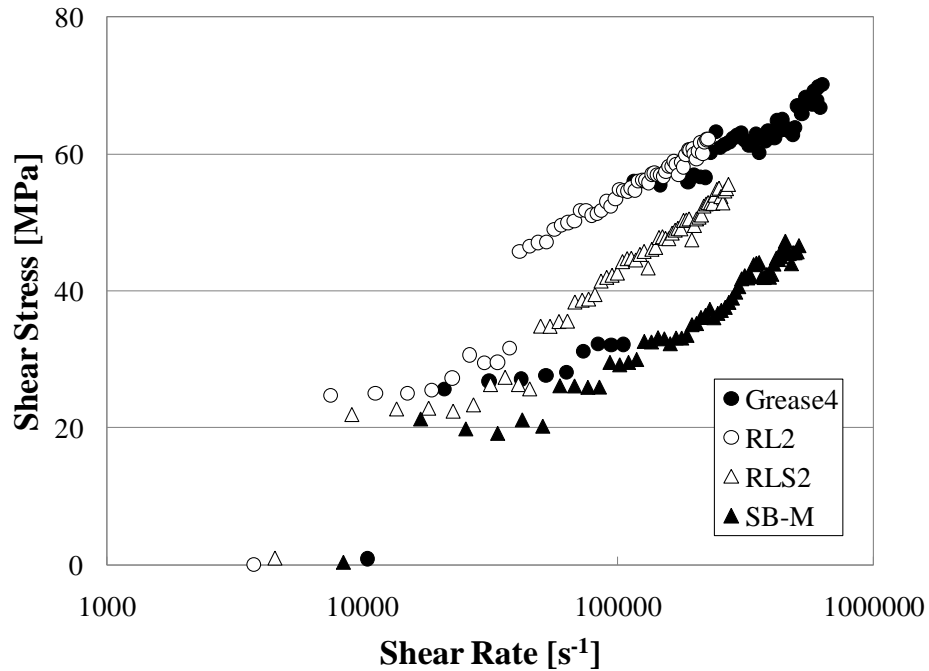


Figure 7.15 Traction curves of urea greases

The results show a similar trend of all other types of greases in terms of the shear stress. RL2 and RLS2 show sharper increase in the shear stress than Grease4 and therefore they are predicted to experience larger shear stress at high shear rate though Grease4 has shown larger values than other greases. On the other hand, SB-M whose dielectric constant was measured as the lowest among urea greases shows the lowest shear stress level.

In investigating the effect of the base oil, these four greases show not only different viscosities of the base oil but also different types of the corresponding oils as well as

different types of additives. Thus, it is difficult to clarify the effect of the base oil upon the urea greases studied in this research.

However, it can be concluded that there is a correlation between the dielectric properties and rheological properties of greases and the traction behaviour, such that the shear stress in the EHD condition, could, at a first approximation, be predicted by their dielectric properties.

7.1.4 “Viscosity 68” oils

In order to clarify the relationship between the dielectric and tribological properties of lubricants, oils with similar rheological properties prepared in Chapter 6 were also tested in this section of the research. The experiments were conducted at 40°C, which leads to the same rheological conditions for all oils, in other words almost the same film thickness in operations, and hence the film thickness for the calculation of the shear rate could be assumed to be the same. Figure 7.16 may therefore indicate a more direct correlation of dielectric properties to the traction behaviour in the EHD condition, by avoiding the concern about viscosity’s effect on traction.

Overall, an expectation that polar oils show relatively large shear stress is conformed in these results, except for the ester oil which is known to indicate low shear stress. Although the three PPG oils show similar values to each other and it is difficult to see the differences, those very polar oils show large traction coefficient of 0.09 at high slide-roll ratio. In addition, the differences between PPG-monomethyl and dimethyl can also be analysed from the results in Figure 7.16 and it is found that the PPG-monomethyl which has higher dielectric constant shows slightly larger traction coefficient than PPG-dimethyl.

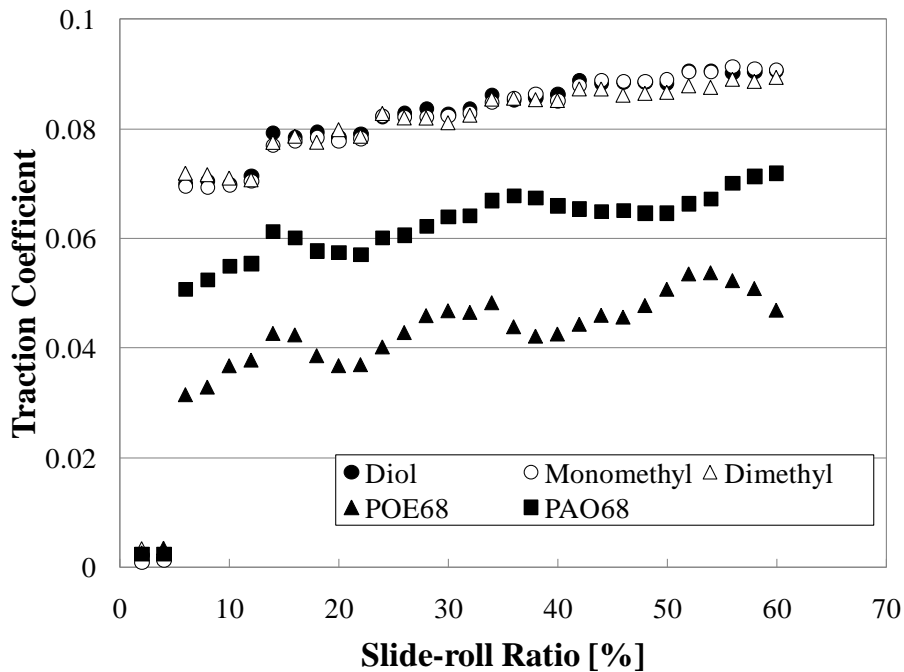


Figure 7.16 Traction curves of “viscosity 68” oils

It can be concluded that polar oils experience high shear stress in the EHD measurements and the value of the traction coefficient can be in general correlated with the strength of their dielectric constant.

7.1.5 Conclusions

EHD traction measurements, coupled with dielectric spectroscopy studies, have been carried out for a number of ten greases with various compositions and properties and for their corresponding base oils. The results of all greases are illustrated in one graph, Figure 7.17, leading to the following conclusions which have been drawn from this study.

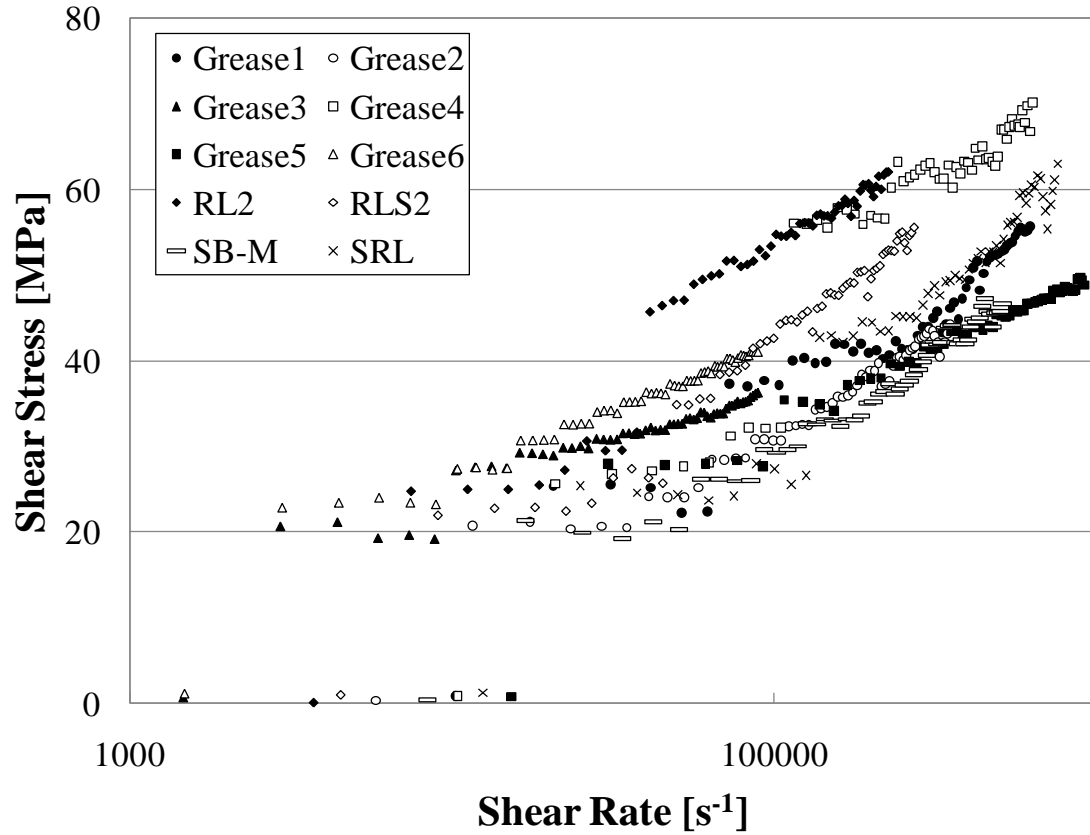


Figure 7.17 Traction curves of investigated greases

From the traction results for all greases it can be concluded that urea greases tend to exhibit relatively high shear stress in their operation. An exception to this rule is SB-M, which shows relatively low shear stress. This grease, which is produced especially as low-noise grease, also has the smallest dielectric permittivity among urea greases.

In terms of the traction coefficient, greases show slightly higher values than corresponding base oils in EHD operations, which may suggest that greases transmit more traction force than oils.

It has been also found that greases with higher dielectric constant show larger shear stress when compared to other greases containing the same type of the thickener. This would suggest that a correlation between the dielectric and tribological properties in the EHD conditions exists. It may therefore be possible for the shear behaviour of the lubricant in EHD contacts to be predicted by dielectric measurements.

The effect of the structure of the fibre in greases on frictional characteristics was studied by Yamamoto *et al* [38] and the images of typical grease structure are illustrated in Figure 7.18. They concluded that the traction characteristics of greases were governed mainly by the structure of the grease, and that the longer fibre a grease consisted of, the lower friction coefficient the grease showed. From the dielectric point of view, namely concerning the movement of molecules under an electric field, a short-fibre grease will show faster relaxation process and therefore higher dielectric constant. In this aspect, the results obtained in the present study are well in accordance with their results though their research was based on the comparison not of the shear stress but of the traction coefficient. This trend has also been confirmed by testing oils prepared with same viscosities but with different dielectric properties. Thus it can be concluded that the stronger the polarity a lubricant has, the larger the shear stress the lubricant exhibits in EHD conditions.

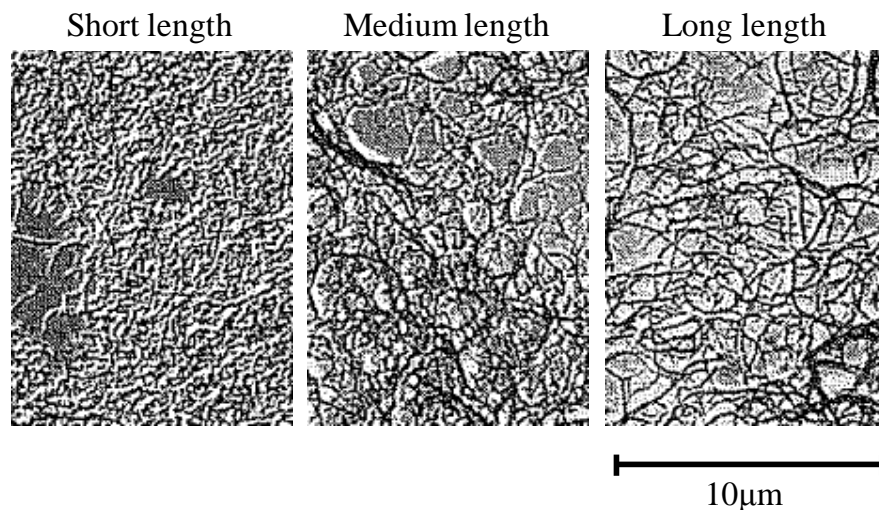


Figure 7.18 Structure of soap fibre in greases [38]

7.2 Eyring Stress

The Eyring stress is not directly measured, but it is calculated as explained in Chapter 5. For example, the result of SRL (Figure 7.9) is reproduced in Figure 7.19 with only grease points.

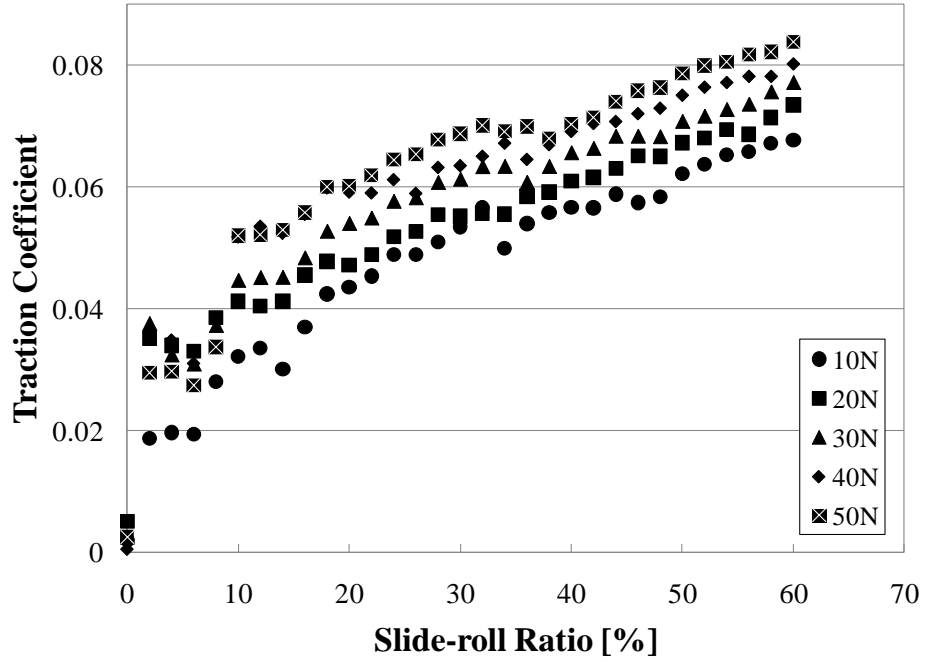


Figure 7.19 Traction curves of SRL

From this result, traction curves between the shear rate and shear stress (Figure 7.20) is obtained by using Equation 7.1 and 7.2. By deducing the trendline in the range of high shear rate for each curve (normally with least square method) and the comparison with following equation (Equation 2.46), Eyring stress τ_0 and the effective viscosity η for each pressure can be obtained.

$$\tau \cong \tau_0 \ln \dot{\gamma} + \tau_0 \ln \left(\frac{2\eta}{\tau_0} \right)$$

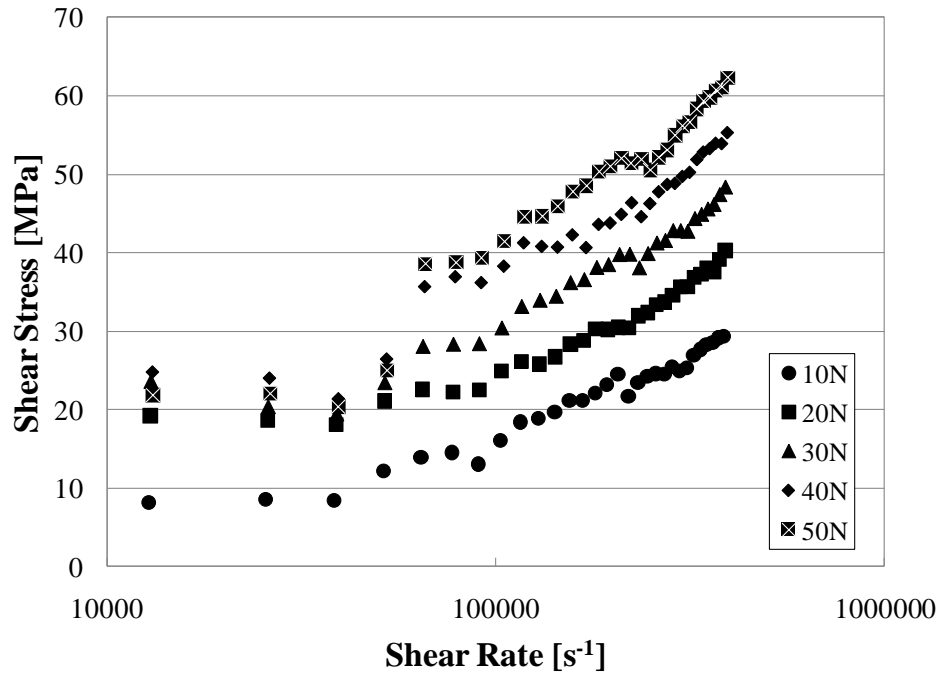


Figure 7.20 Traction curves of SRL for Eyring stress and effective viscosity

Thus it is very sensitive to the accuracy of the traction coefficient and film thickness measurements. For this reason the tests have been repeated and the average values together with error bars have been shown in following figures. It is clear that the Eyring stress of greases, in most cases presented here, is larger than that of the base oil even when taking a 10% error (Chapter 5) in the calculations into consideration.

7.2.1 12OH-LiSt greases

In Figure 7.21 the results of calculated Eyring stress of both Grease1 and PAO4 are shown. Figure 7.22 shows the results of Grease2 and PAO68, while Figure 7.23 includes the results of Grease3 and PAO40. As mentioned earlier, it is emphasised that these oils are not genuine base oils of the examined greases.

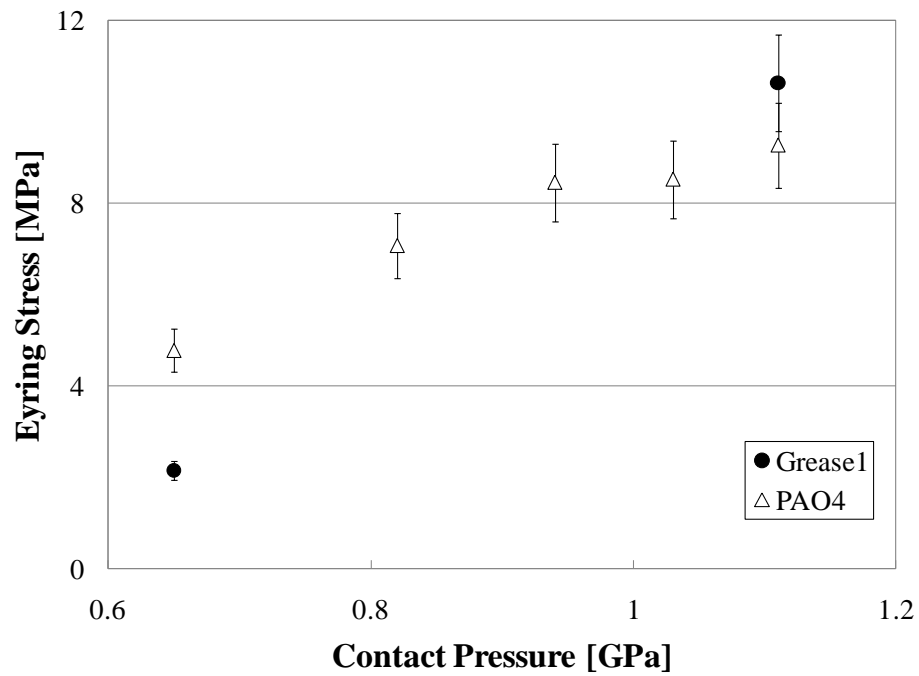


Figure 7.21 Eyring stress of Grease1 and PAO4

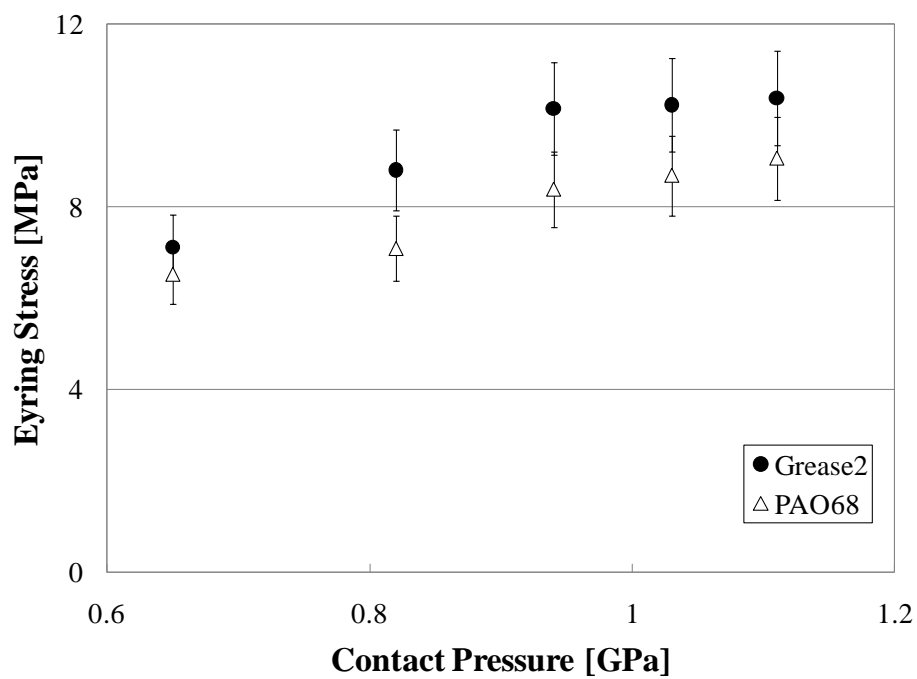


Figure 7.22 Eyring stress of Grease2 and PAO68

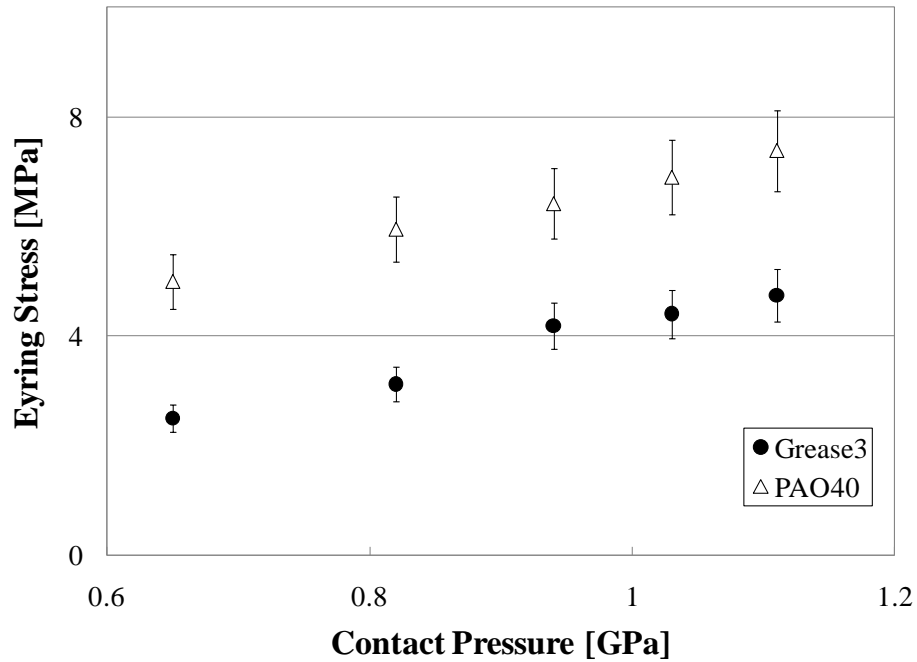


Figure 7.23 Eyring stress of Grease3 and PAO40

The Eyring stress of 12OH-LiSt greases tends to increase with decreasing viscosity of the base oil, and also being influenced by the nature of lubricants. The Eyring stress indicates the stress above which the fluid does not obey the Newtonian law of proportionality between shear stress and shear rate. From this point of view, the Eyring stress of the grease will ascribe not only to the viscosity of the base oil but also to the worked penetration, one of the bulk properties of the grease. Consequently the result shows that the Eyring stress of 12OH-LiSt greases decreases with increasing value of worked penetration.

7.2.2 LiSt greases

The Eyring stresses of Grease5 and PAO4 are compared in Figure 7.24 while the results of Grease6 and PAO40 in Figure 7.25. Figure 7.26 shows the relationship between the Eyring stress of SRL grease and its base oil.

In terms of the hypothesis that the Eyring stress of the grease becomes larger than that of the corresponding base oil, two of four major discrepancies among all ten greases were observed in this case (if ignoring Grease1 or considering only the case of 50N in Grease1). As for Grease3 and 4, Grease5 and 6 showed relatively small Eyring stress compared to their base oils as shown in Figure 7.24 and 7.25 respectively. Although these two greases have very different viscosity of their base oils, they show similar values of the worked penetration which are comparatively high values of 336 from Grease5 and 339 from Grease6. This looks to be in accordance with the previous results which implied that relatively small Eyring stress is obtained for large worked penetration greases.

When investigating the effect of the base oil, that is comparing Grease5 with Grease6, the tendency of increasing Eyring stress with decreasing viscosity of the base oil of the grease was also observed in LiSt greases.

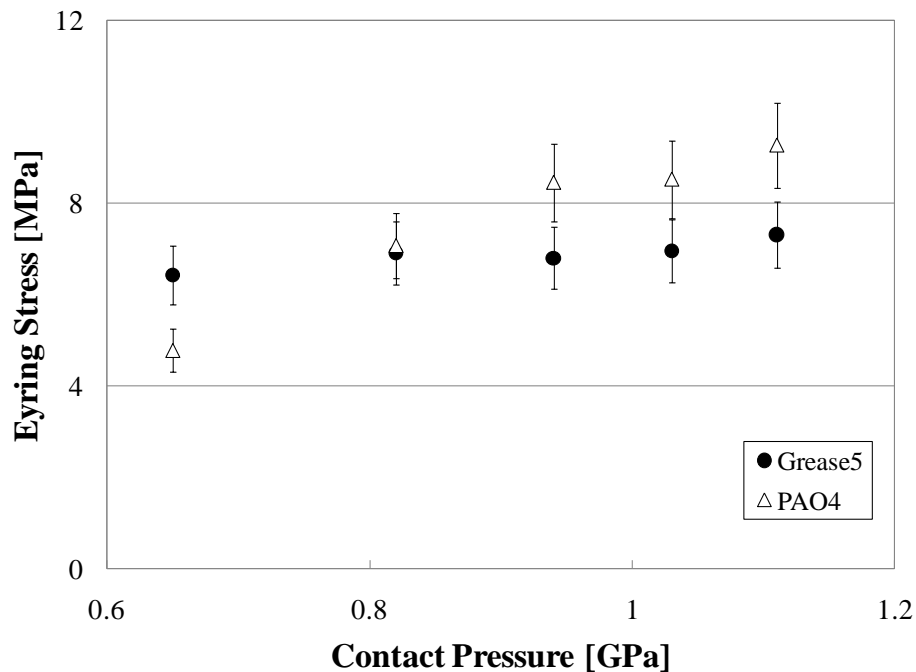


Figure 7.24 Eyring stress of Grease5 and PAO4

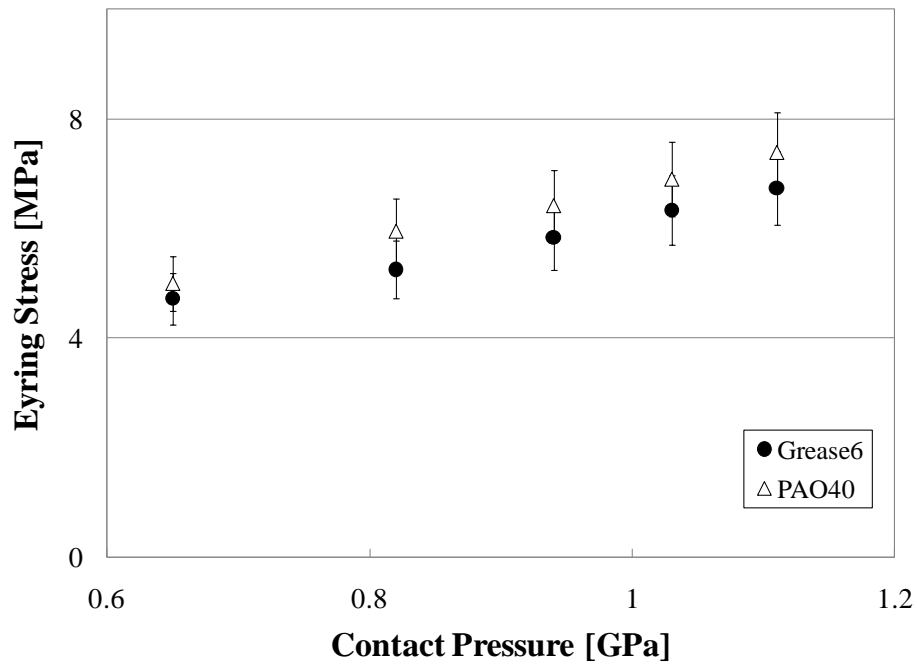


Figure 7.25 Eyring stress of Grease6 and PAO40

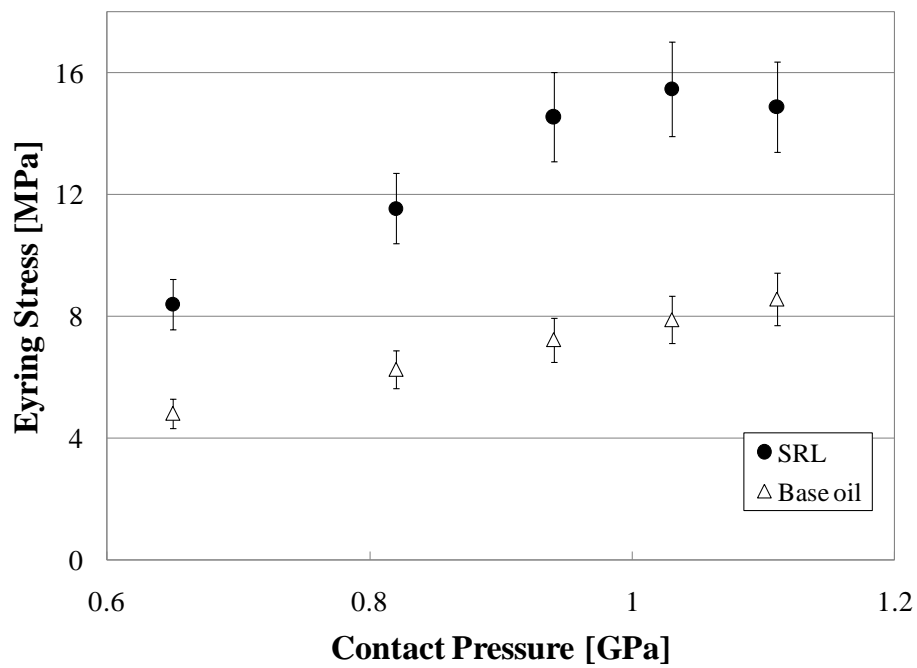


Figure 7.26 Eyring stress of SRL and its base oil

7.2.3 Urea greases

The results for urea greases are shown in following figures in the order of Grease4, RL2, RLS2, and SB-M. It is mentioned again that the oil compared to Grease4 is not the genuine base oil but with the same chemical structure and similar viscosity.

For all urea greases, it was observed that the grease showed larger Eyring stress than the oil did though the values in the case of Grease4 were close and the Eyring stress of the grease at 50N dropped slightly down to the value of the oil.

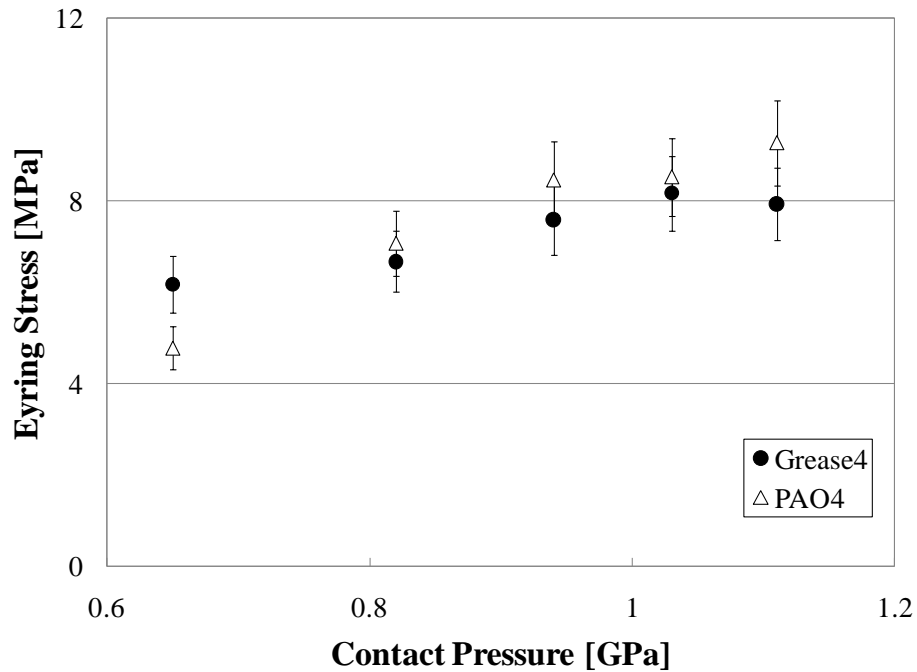


Figure 7.27 Eyring stress of Grease4 and PAO4

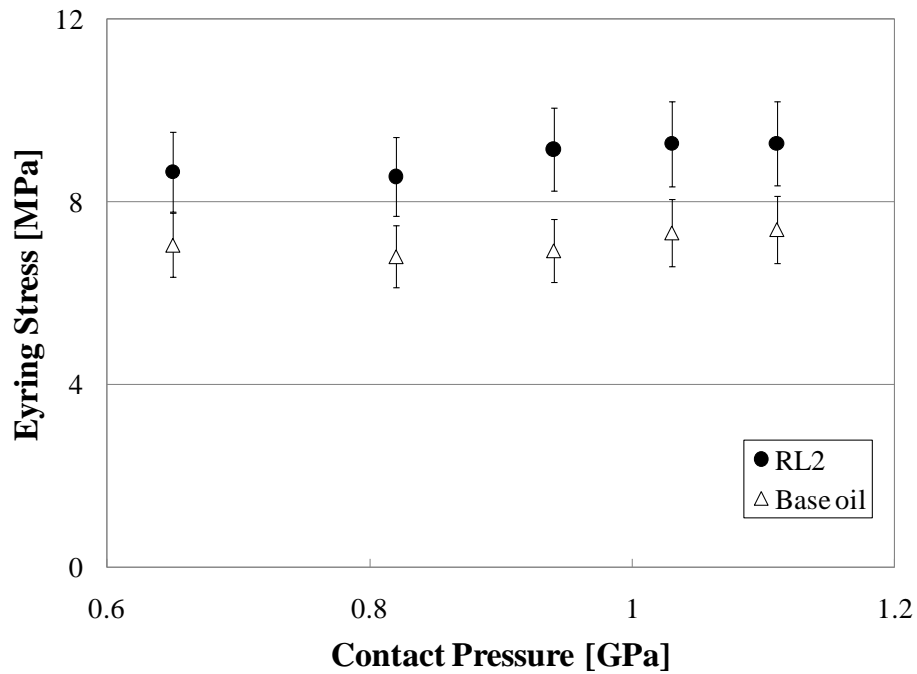


Figure 7.28 Eyring stress of RL2 and its base oil

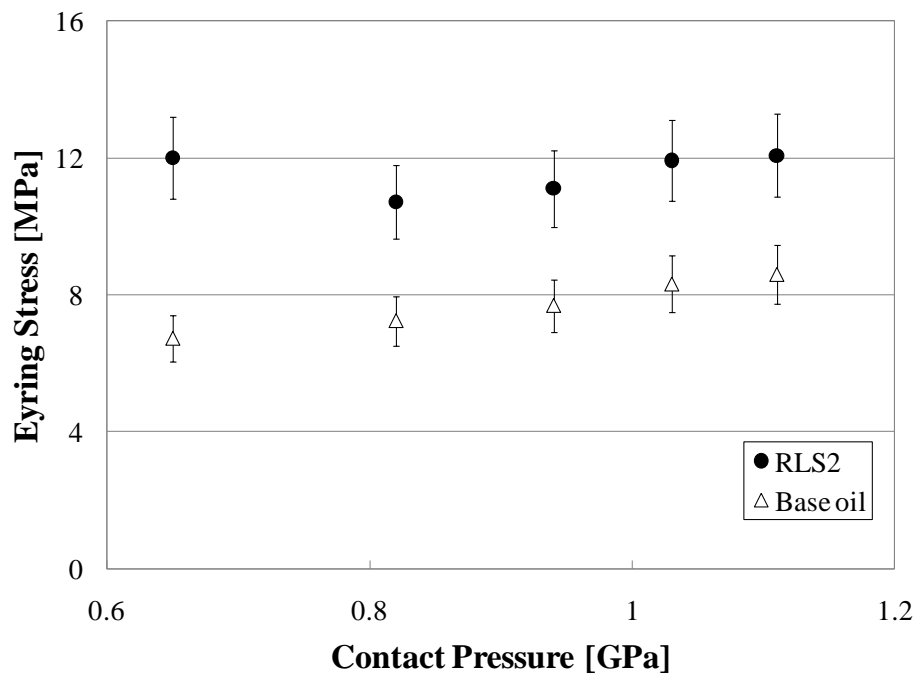


Figure 7.29 Eyring stress of RLS2 and its base oil

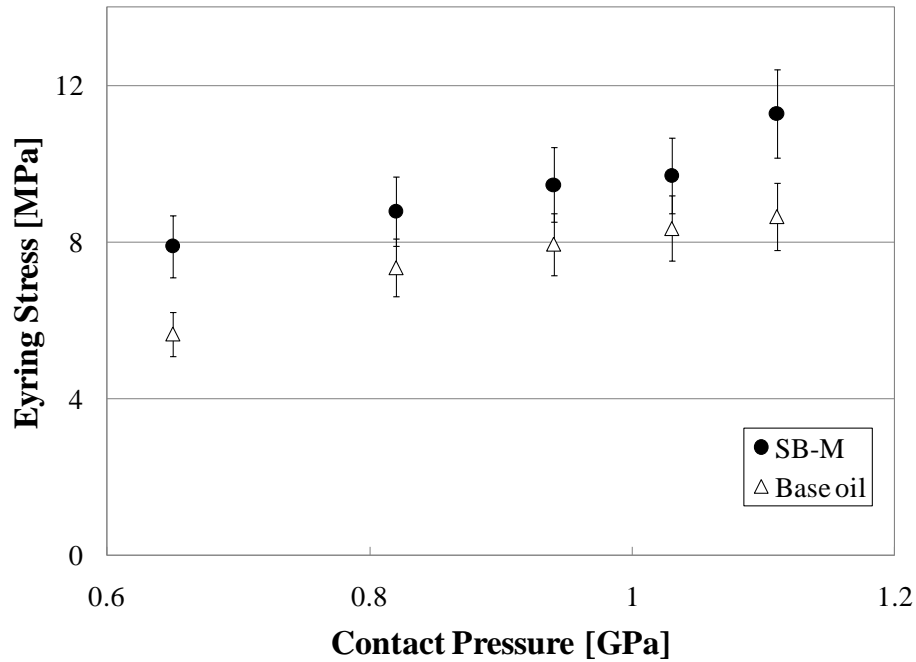


Figure 7.30 Eyring stress of SB-M and its base oil

7.2.4 Conclusions

The relationship between the Eyring stress of greases and base oils is investigated in this section. In cases of Grease3, 5 and 6, the Eyring stress of greases is smaller than that of oils, whilst it can be seen Grease4 showed almost the same Eyring stress as the oil. In other cases greases showed larger Eyring stress than corresponding base oils.

In the former cases (greases showing smaller Eyring stress), it has to be emphasised that those oils investigated are not the genuine base oils so it may be possible that, if compared to genuine corresponding base oils, those greases might also show larger Eyring stress than the base oils. Also it should be taken into account that those greases are very soft as their worked penetration indicates. Indeed, Grease3, 5 and 6 show relatively high worked penetration and all of them showed lower Eyring stress when compared to the base oils.

From this point of view, it can be concluded that the Eyring stress of greases will be influenced not only by their base oil's viscosity but also by their worked penetration.

In the latter cases, all of those greases contain additives which may influence the trend that greases show larger Eyring stress than the corresponding base oils. Nevertheless, the amount of additives is relatively small and therefore it would be negligible in these experiments.

As an example, a comparison of the central film thickness for SRL and the base oil is shown in Figure 7.31. For the low speeds region, where the traction coefficient tests have been conducted, the grease has a film thickness about four times larger than that of the base oil. It is not clear, at this point, whether the larger value of the Eyring stress for these greases is a genuine effect or an experimental artefact, however the fact that this tendency appeared every time the test was repeated and that the tests for all greases are done in identical conditions suggest indeed that, for all greases tested in this study, their Eyring stresses generally have larger values than their base oils.

To sum up, it can be concluded that the Eyring stress of the grease will be larger than that of the corresponding base oil, but it will also be sensitive to the intrinsic properties of the grease. Hence, the Eyring stress of the grease indicating high value of the worked penetration possibly experiences lower value than the corresponding base oil. However it is almost certain that the Eyring stress of the grease will increase with decreasing viscosity of its base oil when compared to same thickener type greases.

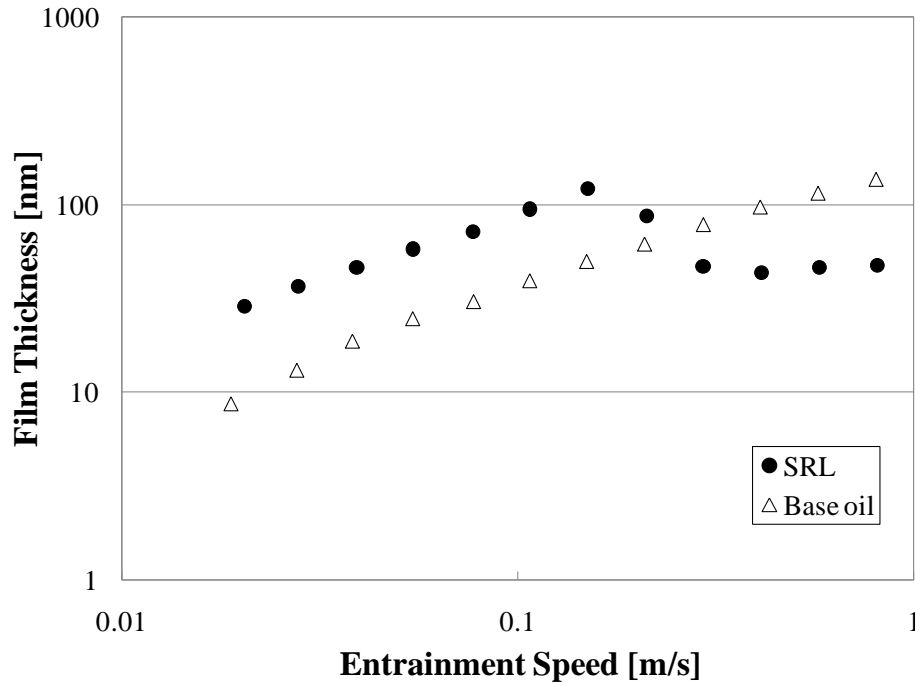


Figure 7.31 Film thickness measurements of SRL and its base oil at 30°C

7.3 Effective Viscosity

After determining the Eyring stress, the effective viscosity is derived by applying one of the rheological models to the behaviour of lubricants under real operation conditions. In this study the effective viscosity is calculated from the results of EHD traction measurements and would reflect the properties of the lubricants closer to real situations than properties measured by a conventional rheometer. The calculating process was almost same as Eyring stress and mentioned in previous section together with it.

7.3.1 12OH-LiSt greases

The results for 12OH-LiSt greases are shown in Figure 7.32 to 7.34. As seen in these figures, the values of the effective viscosity of the grease tend to increase with pressure at similar rates to the base oils.

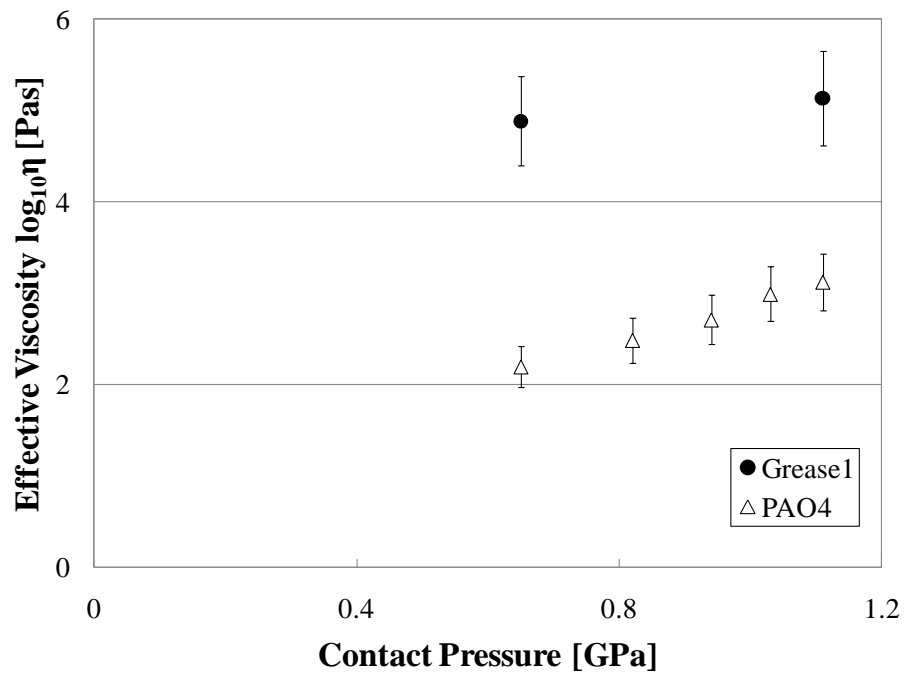


Figure 7.32 Effective viscosity of Grease1 and PAO4

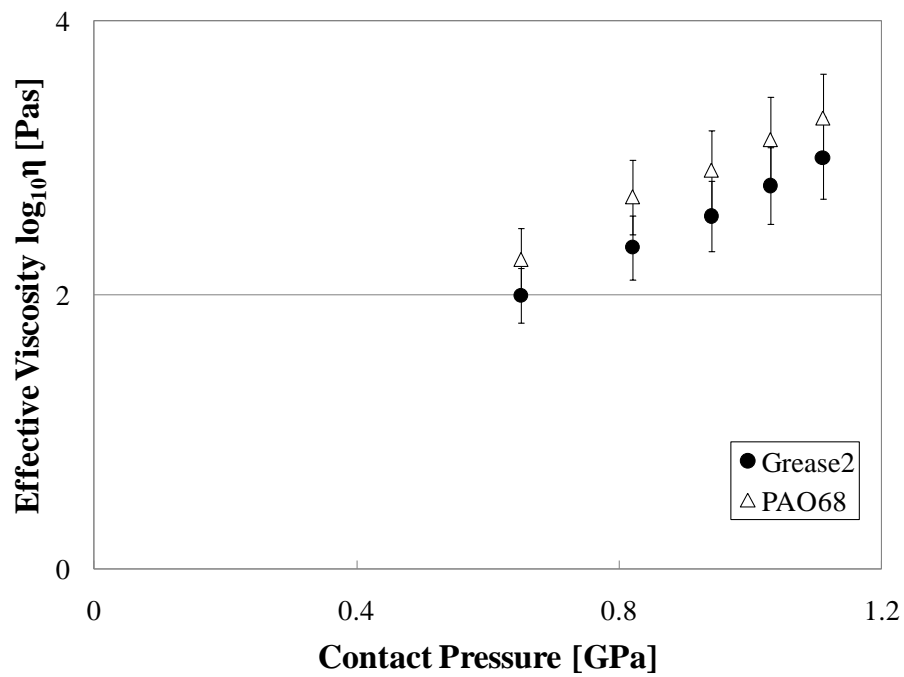


Figure 7.33 Effective viscosity of Grease2 and PAO68

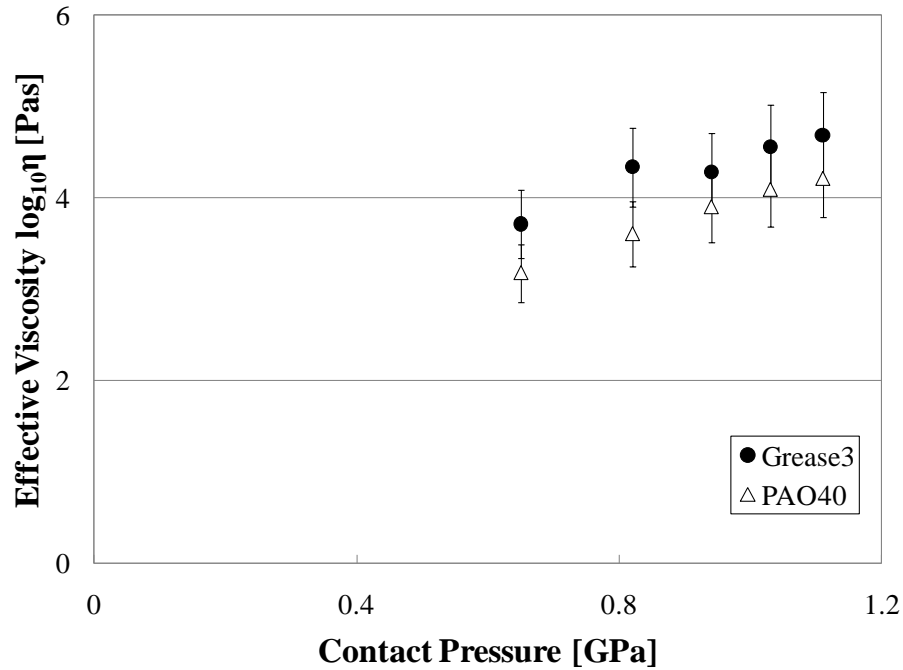


Figure 7.34 Effective viscosity of Grease3 and PAO40

It is also observed that Grease2 gives smaller values of the calculated viscosity than the oil while other two greases shows larger viscosity compared to their base oils.

In order to evaluate the effect of the base oil upon the effective viscosity of the grease, Grease2 was compared to Grease3 and it was found that the effective viscosity of the grease increased with the viscosity of the base oil, which would be expected because the base oil accounted for the main consistence of the bulk grease.

7.3.2 LiSt greases

The results of LiSt greases are presented in this section. Figure 7.35 shows the effective viscosity of Grease5 and PAO4. At low pressure, relatively small values of viscosity were obtained from the grease. On the other hand, the effective viscosity of this grease rapidly

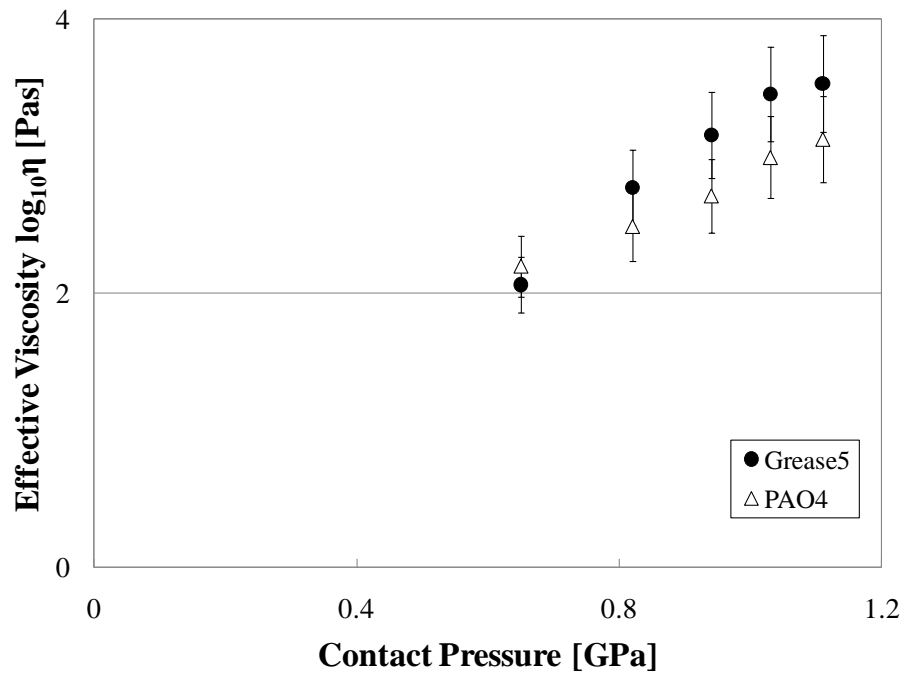


Figure 7.35 Effective viscosity of Grease5 and PAO4

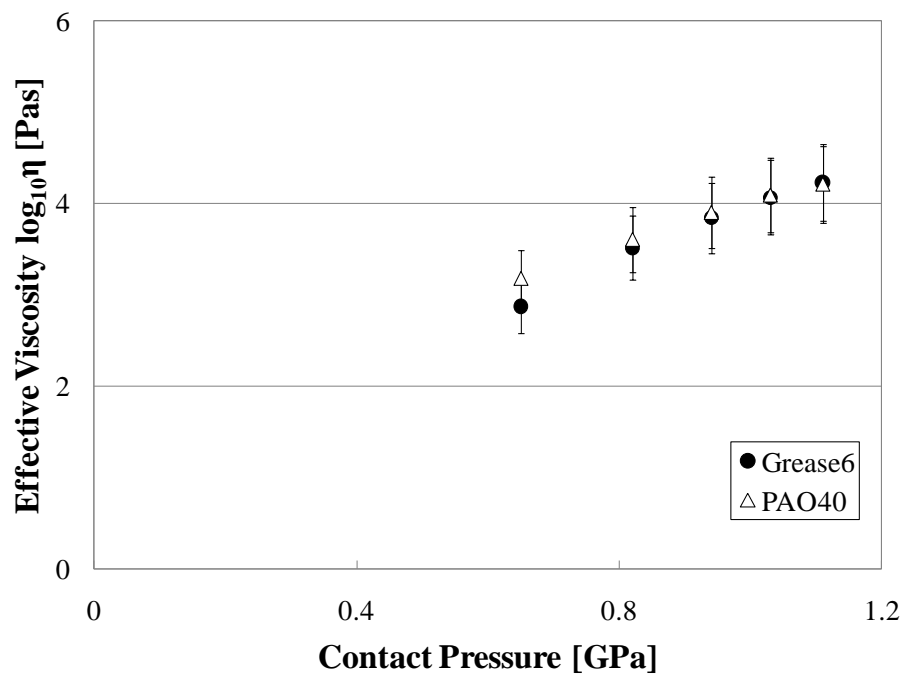


Figure 7.36 Effective viscosity of Grease6 and PAO40

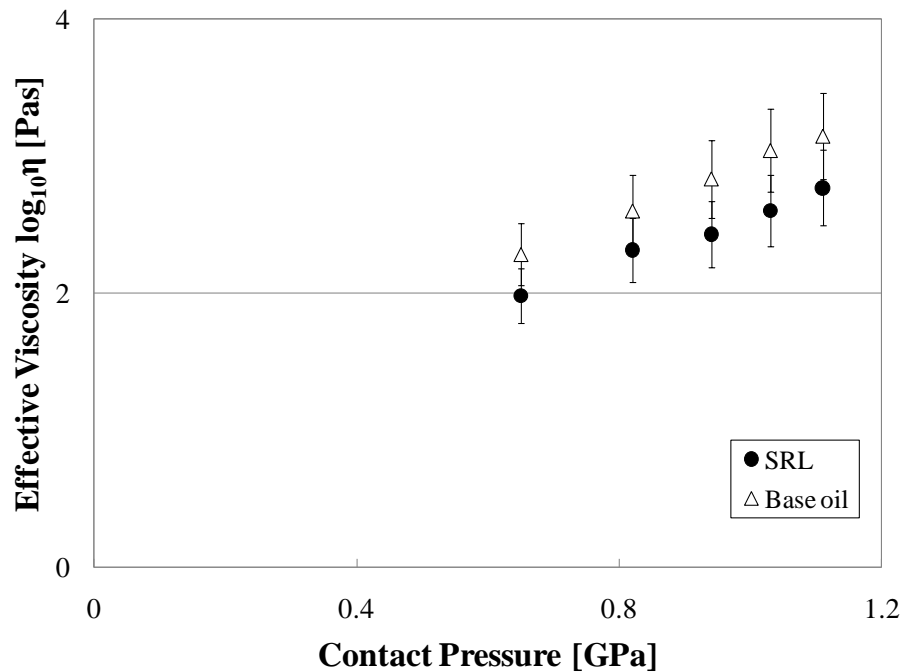


Figure 7.37 Effective viscosity of SRL and its base oil

increased compared to PAO4 and, at high pressure, the values of the grease became larger than those of the oil.

Figure 7.36 shows the results for Grease6 and PAO40 whilst Figure 7.37 shows the behaviour of the effective viscosity of SRL grease. In both cases these values are compared to those of the genuine base oils of the corresponding grease. From these results, it may be seen that these greases showed similar behaviour of the effective viscosity to their base oil, in EHD conditions.

The effect of the viscosity of the base oil has also been evaluated for LiSt thickener greases by comparing Grease5 and Grease6, and the same result as the case of 12OH-LiSt greases has been obtained, which is that the higher viscosity base oil gives the higher effective viscosity of the bulk grease.

7.3.3 Urea greases

Grease4 showed a steep increase in the effective viscosity compared to the base oil and overall provided larger viscosity than the oil. However, all other urea greases exhibited similar behaviour to their base oils in terms of the increase of the viscosity with pressure. Both RL2 and RLS2 showed a smaller effective viscosity compared to their base oils but identical rate of increase with pressure to the oils. Similar absolute values for the viscosity of the grease and the oil were obtained for SB-M.

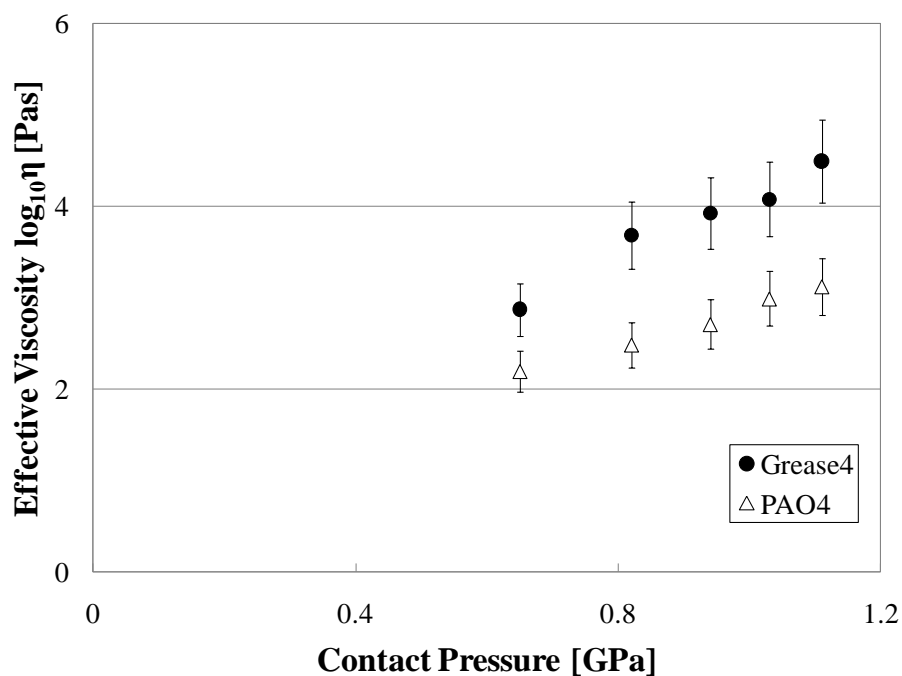


Figure 7.38 Effective viscosity of Grease4 and PAO4

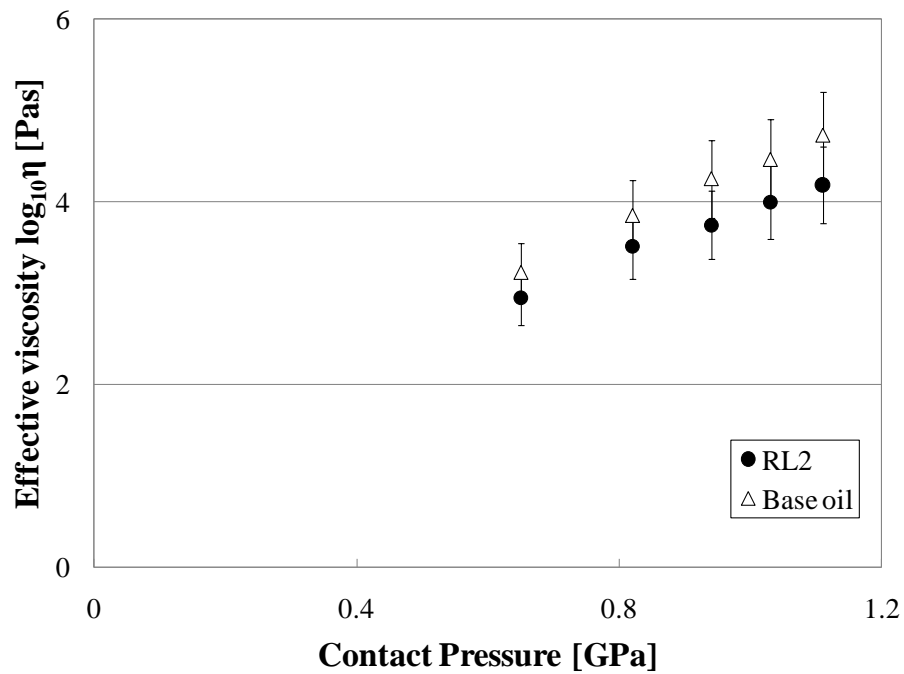


Figure 7.39 Effective viscosity of RL2 and its base oil

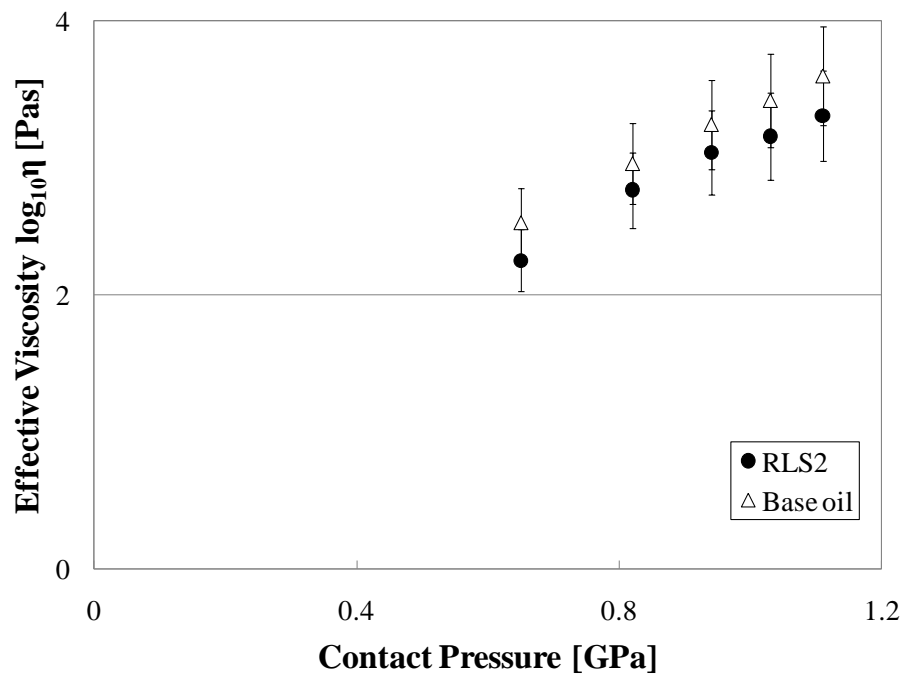


Figure 7.40 Effective viscosity of RLS2 and its base oil

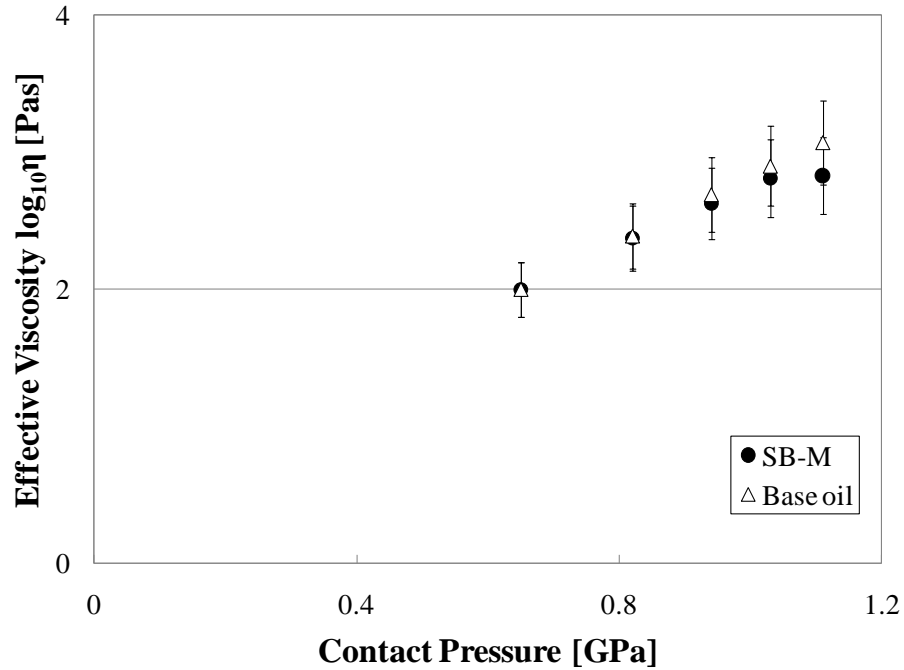


Figure 7.41 Effective viscosity of SB-M and its base oil

7.3.4 Conclusions

The experimental results revealed that the logarithm of the effective viscosity of greases varies linearly with pressure and the rate of change is similar to the base oils. Thus, generally speaking, the effective viscosity of the grease in EHD conditions is similar to that of the corresponding base oil in terms of both the behaviour and value (all greases except for Grease1 and 4 showed similar viscosity to the corresponding oils within a permissible range).

Regarding to the effect of the base oil, it has been found that for all kinds of greases, the higher viscosity the base oil has the higher effective viscosity the grease shows. This is unlike the cases of the dielectric constant of the grease whose trend depends upon the type of thickener. This fact has been confirmed by comparing the same type thickener greases, that is comparing Grease2 to Grease3 and Grease5 to Grease6.

Grease3 and 6 have been selected to evaluate the effect of the thickener since they have the same base oil but different thickener. The result reveals that the grease consisting of 12OH-LiSt thickener shows higher effective viscosity inside the EHD condition.

Higher the viscosity of the grease, as observed in some cases, implies that the grease exhibits higher resistance to flow and this is predictable when considering its semi-solid feature. However, this is more likely the behaviour characteristic to static conditions or in the measurements using a proper rheometer and it would not be applied to the EHD condition, as is the experimental case above. Indeed, the behaviour of the viscosity of the grease in EHD condition varies and it is difficult to analyse the correlation between the grease and the base oil. Nevertheless, it can be concluded, when looking at only RL2, RLS2, SB-M and SRL whose base oils are genuine, that the effective viscosity of the grease depends mainly on the properties of the corresponding base oil and behaves like the base oil does in the EHD conditions. Consequently, these results strengthen the belief that in EHD conditions the base oil plays an important role in the behaviour of grease lubricants.

7.4 Mechanical Relaxation

The mechanical relaxation time, T_m , is calculated by Equation 7.3 from the viscosity data obtained in the preceding section. The relaxation times of the grease and base oil are comparatively presented here. The shear (elastic) modulus of the material which is needed for calculating the mechanical relaxation time is not measured but only assumed according to Equation 7.4. This is because the experimental equipment was not accurate enough at very small slide-roll ratio range (percentages of the order of one tenth) where the shear modulus could be obtained from the linear part of the traction curve. Nevertheless, the comparison of the values from the equation with the experimental results was known to be very satisfactory according to Evan and Johnson [20].

$$T_m = \eta / G_e \quad (7.3)$$

$$\tau_c = G_e / 45 \quad (7.4)$$

where τ_c is the limiting shear stress and G_e is the shear modulus.

In the traction measurements the maximum pressure was limited to 1.1GPa and it was not certain if the limiting shear stress was obtained. This means that the limiting shear stress for calculating the shear modulus was taken as the value at 50N and 60% *SRR* and a 20% error was allowed in the upper direction of the shear stress. Thus the minimum values represented by the error bar in following figures were calculated by using 1.2 times of the measured shear stress value, while the relaxation time was calculated by using the measured value at 50N and 60% *SRR* as the limiting shear stress.

7.4.1 12OH-LiSt greases

The greases in 12OH-LiSt thickener group are presented in from Figure 7.42 to Figure 7.44.

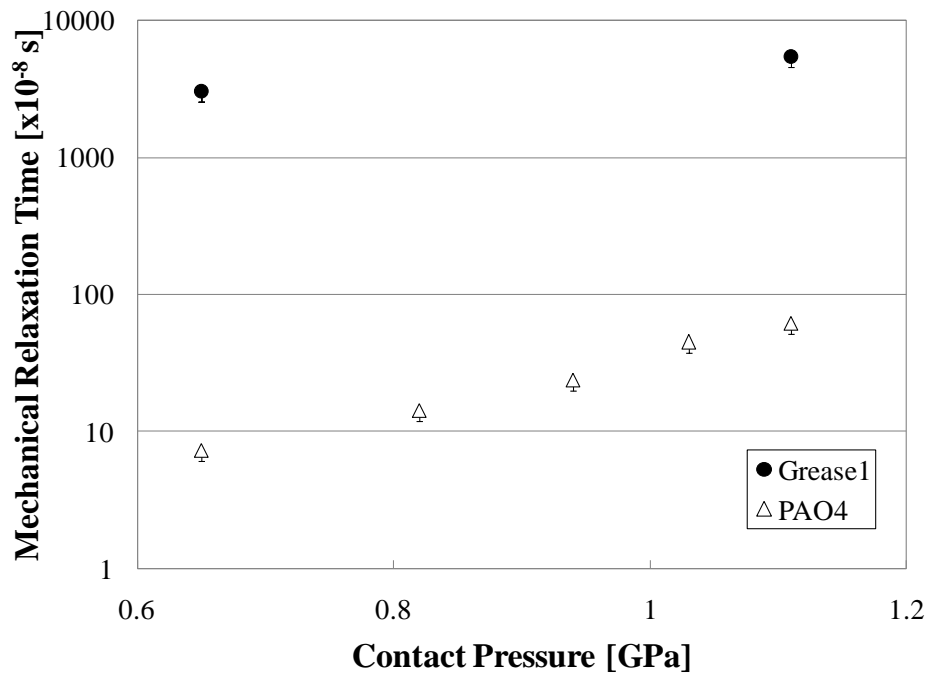


Figure 7.42 Mechanical relaxation time of Grease1 and PAO4

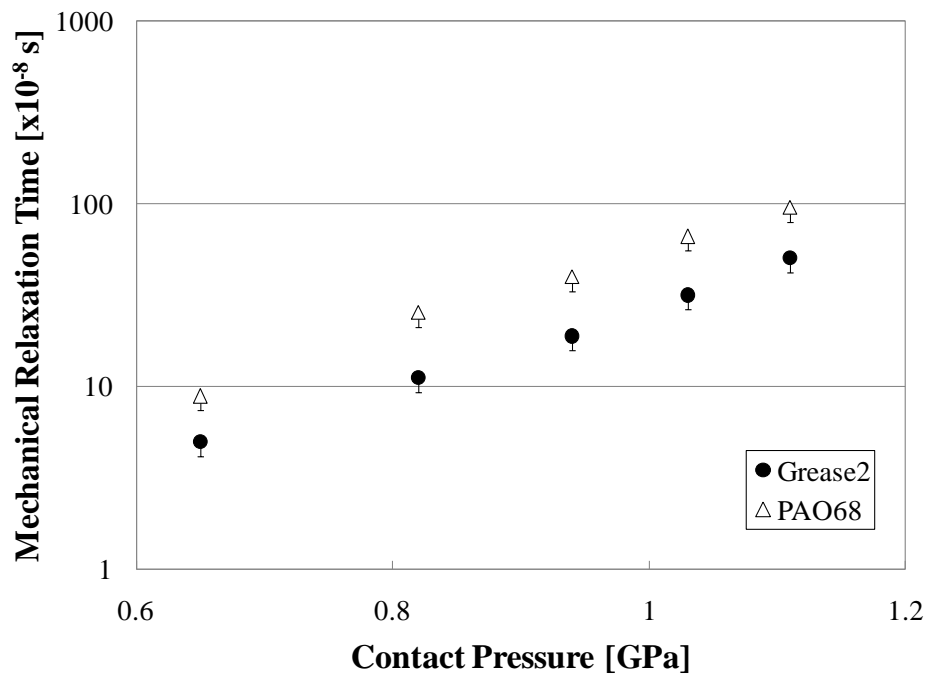


Figure 7.43 Mechanical relaxation time of Grease2 and PAO68

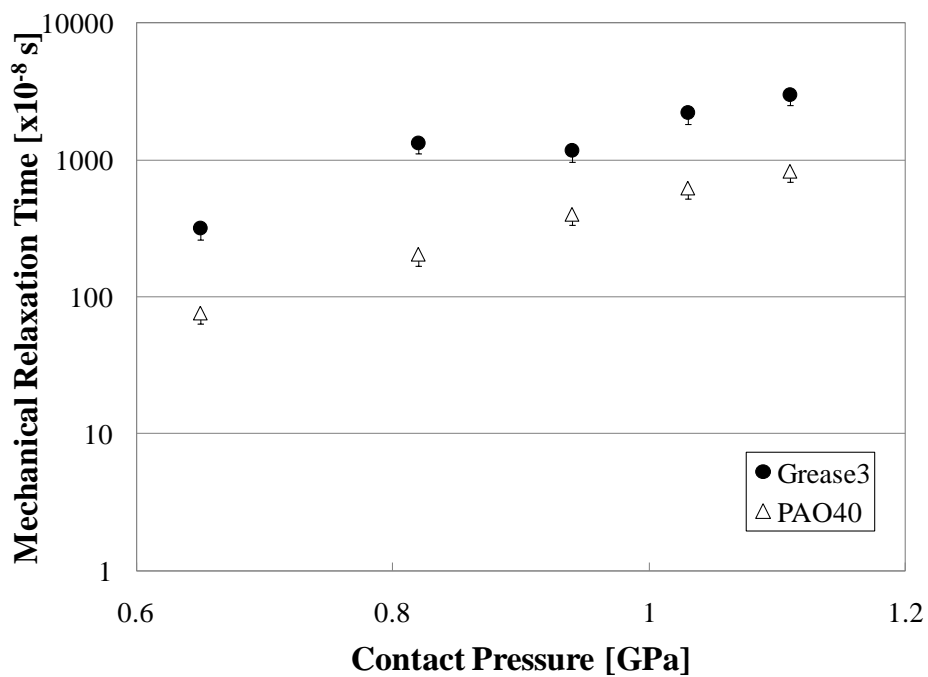


Figure 7.44 Mechanical relaxation time of Grease3 and PAO40

Over the whole pressure range, Grease1 and 3 show longer relaxation time than the base oil, while the mechanical relaxation time of Grease2 is shorter compared to the oil. However, almost the same tendency toward the increase of the mechanical relaxation time with pressure is observed for all greases and corresponding oils.

7.4.2 LiSt greases

In this section, the group of LiSt thickener greases is presented. Figure 7.45 represents the mechanical relaxation time of Grease5 compared to that of PAO4. In this result, there is a similarity between the grease and oil particularly at low pressure, where the grease shows even shorter relaxation time however the rate of increase with pressure is larger for the grease than for the oil, which means that at a pressure over 0.8GPa the grease relaxation time overcomes that of the oil. At high pressure range, the slope of the relaxation time versus pressure for the grease decreases and becomes comparable to that of the oil.

Figure 7.46 represents the result obtained for Grease6 and its corresponding base oil. Although Grease6 has faster relaxation process at low pressure, as Grease5 showed, the overall behaviour is very similar to that of the base oil and the discrepancy between the grease and oil is also very small in this case.

The last experimental result in LiSt greases is that of a very polar grease SRL and its corresponding base oil. These results are presented in Figure 7.47. As the greases presented earlier, SRL shows very similar trend to its corresponding base oil, and, in this case, the mechanical relaxation process in the grease becomes faster.

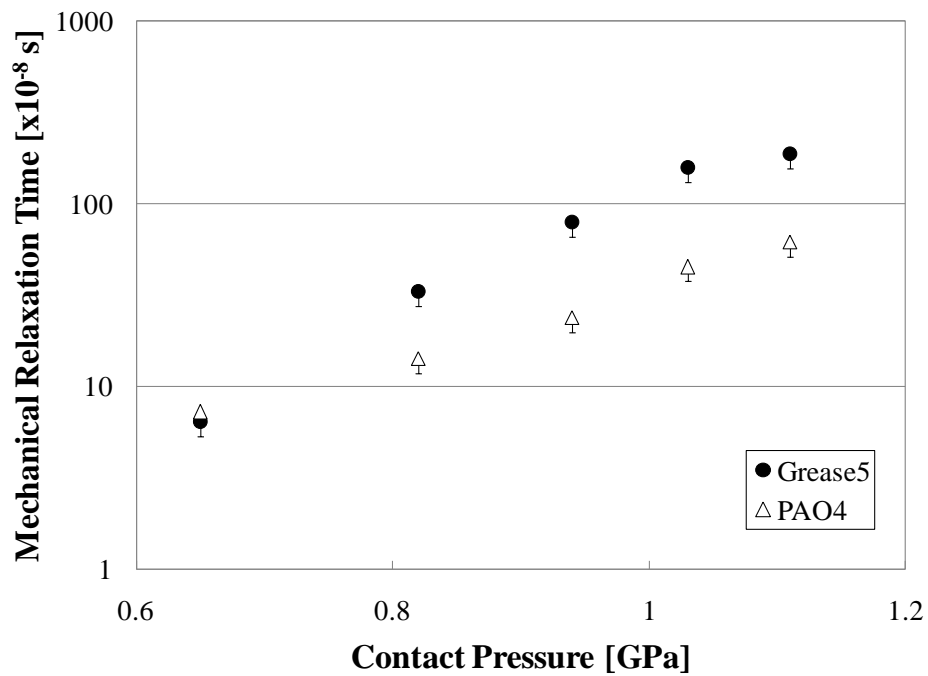


Figure 7.45 Mechanical relaxation time of Grease5 and PAO4

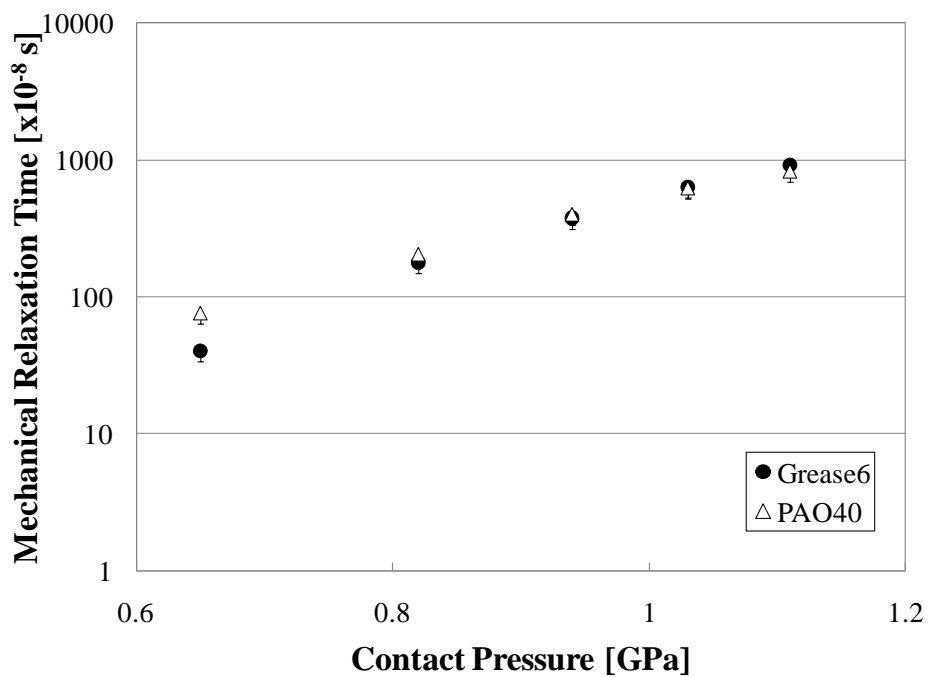


Figure 7.46 Mechanical relaxation time of Grease6 and PAO40

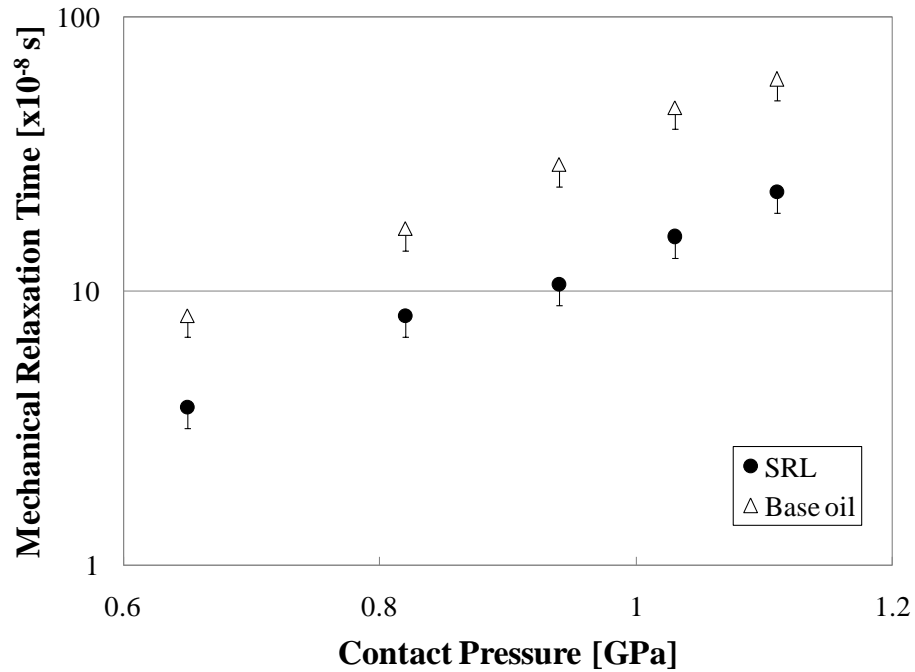


Figure 7.47 Mechanical relaxation time of SRL and its base oil

7.4.3 Urea greases

Figures from Figure 7.48 to Figure 7.51 include the comparison of the mechanical relaxation time between urea greases and their corresponding base oils. Figure 4.48 shows the result of Grease4, while Figure 4.49 shows the result of RL2, supplied by the same manufacturer as RLS2 whose results are presented in Figure 4.50. Finally the result of SB-M and its corresponding base oil is shown in Figure 4.51.

For urea greases, only Grease4 indicates overall slower relaxation process, over the pressure range, than the oil.

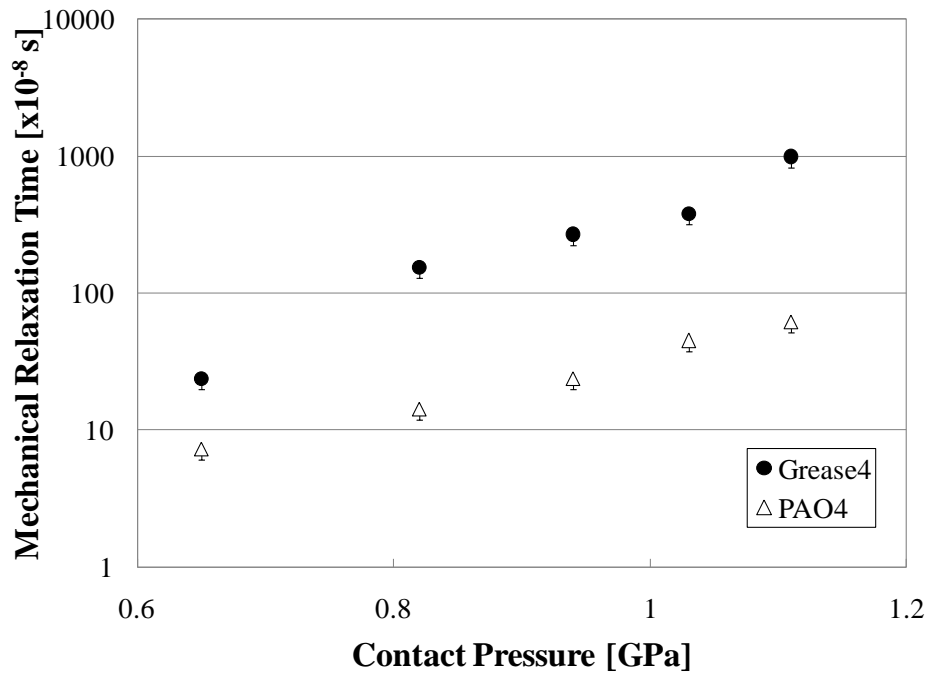


Figure 7.48 Mechanical relaxation time of Grease4 and PAO4

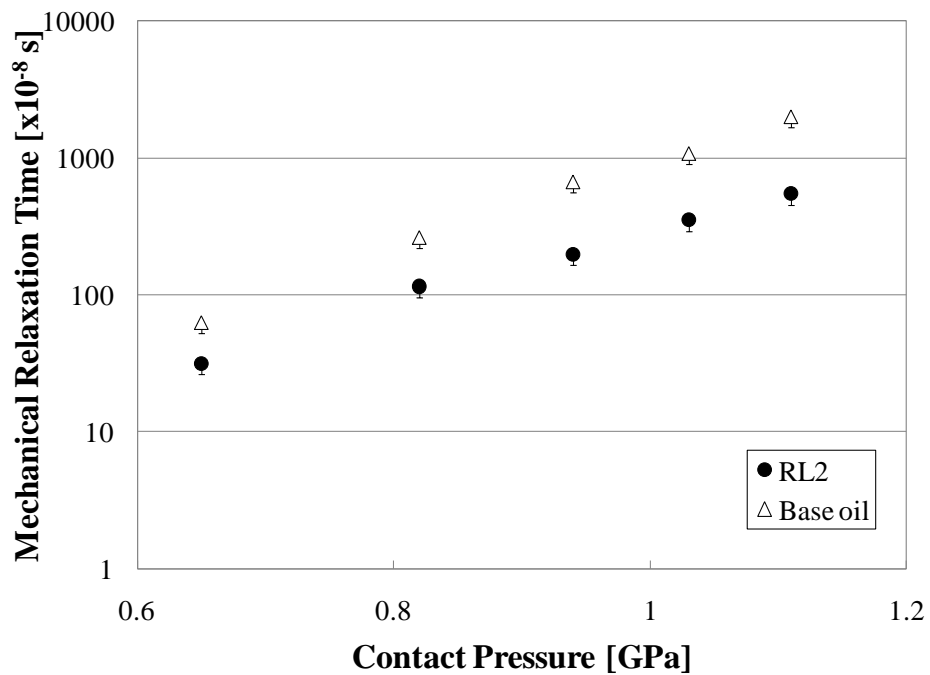


Figure 7.49 Mechanical relaxation time of RL2 and its base oil

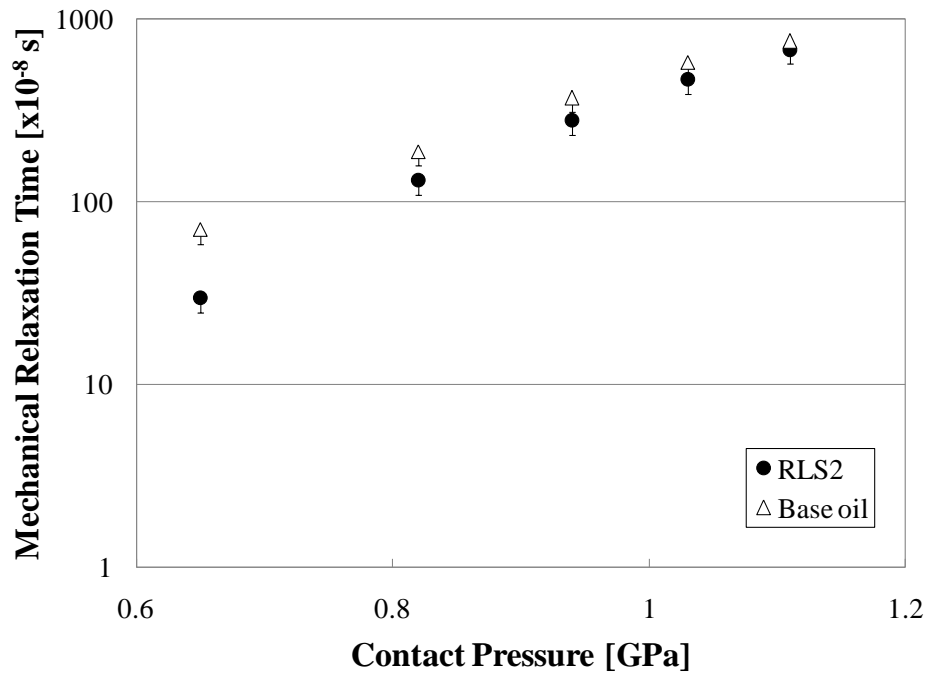


Figure 7.50 Mechanical relaxation time of RLS2 and its base oil

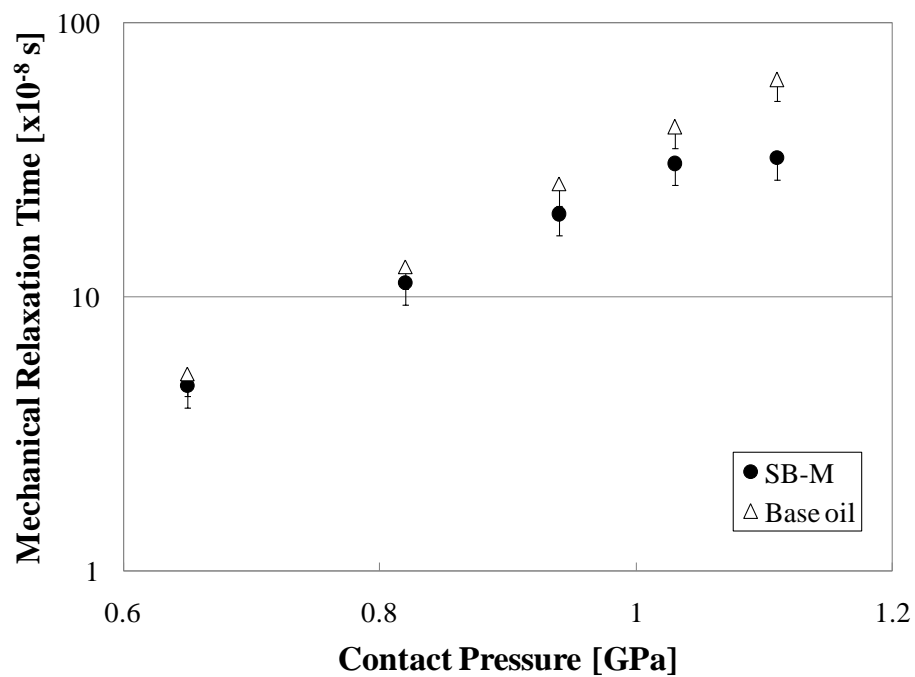


Figure 7.51 Mechanical relaxation time of SB-M and its base oil

7.4.4 Comparison between mechanical and dielectric relaxation

A comparison between the mechanical relaxation and the dielectric relaxation has revealed that an opposite behaviour to the dielectric measurements was observed. Whilst the dielectric relaxation time became longer by transforming the physical state of the grease from the liquid to semisolid as shown in Figure 6.4, the mechanical relaxation time of the grease was found to be shorter than that of the corresponding base oil. Only four out of ten greases were exceptions and all of them were compared to the oils which were not their genuine base oils.

7.4.5 Conclusions

Overall speaking the experimental results have revealed that in EHD conditions greases exhibit faster mechanical relaxation process than the oils, which is particularly true at the lowest pressure measurements, where there are only three exceptional cases for Grease1, 3 and 4 out of ten samples. This observation is supported by the results obtained in the previous section, which showed that the grease would possess similar effective viscosity to the oil under EHD conditions. Thus this behaviour may be due largely to the relatively higher shear stress of the grease film observed at 50N and 60% *SRR* than the oil.

When compared to their genuine base oil, i.e. in the cases of RL2, RLS2, SB-M and SRL, the behaviour of the grease will depend mainly on the corresponding base oil and they show the same rate of change in their mechanical relaxation behaviour against pressure as does the oil. This would imply that there is a mechanically certain similar mode between the structure of the grease and the corresponding base oil, or that the base oil plays main roles at least in the grease EHD lubrication as generally known these days [63].

When it comes to the comparison between the mechanical relaxation and the dielectric relaxation, however, the opposite behaviour was observed. Whilst the dielectric relaxation

time became slower by forming the state of the grease from the liquid state for all cases, the mechanical relaxation time of the grease was concluded to be faster than that of the corresponding base oil. This would be due partly to the relatively high shear stress observed in the case of greases. These results, on the other hand, may be supported by the observation by Kotake *et al* who pointed out that the dependence of the dielectric behaviour of the grease on temperature was different from the dependence of the apparent viscosity of the grease on temperature and also different from the dependence of the base oil's viscosity on temperature [109].

The obvious trends of the effect of the viscosity of the base oil upon the mechanical relaxation time of the grease were observed in the case of both 12OH-LiSt greases (Grease2 and Grease3) and LiSt greases (Grease5 and Grease6). It has been found that the relaxation time of the grease became shorter with decreasing base oil's viscosity. Although it is difficult to make this evaluation for the urea grease group, this trend can be obtained when comparing RL2 or RLS2 with SB-M which shows significantly smaller viscosity of the base oil compared to them. Thus it could be concluded, in general, that the mechanical relaxation time of the grease depends upon the base oil and it increases with viscosity of the base oil.

Finally, a comparison between greases is illustrated in Figure 7.52.

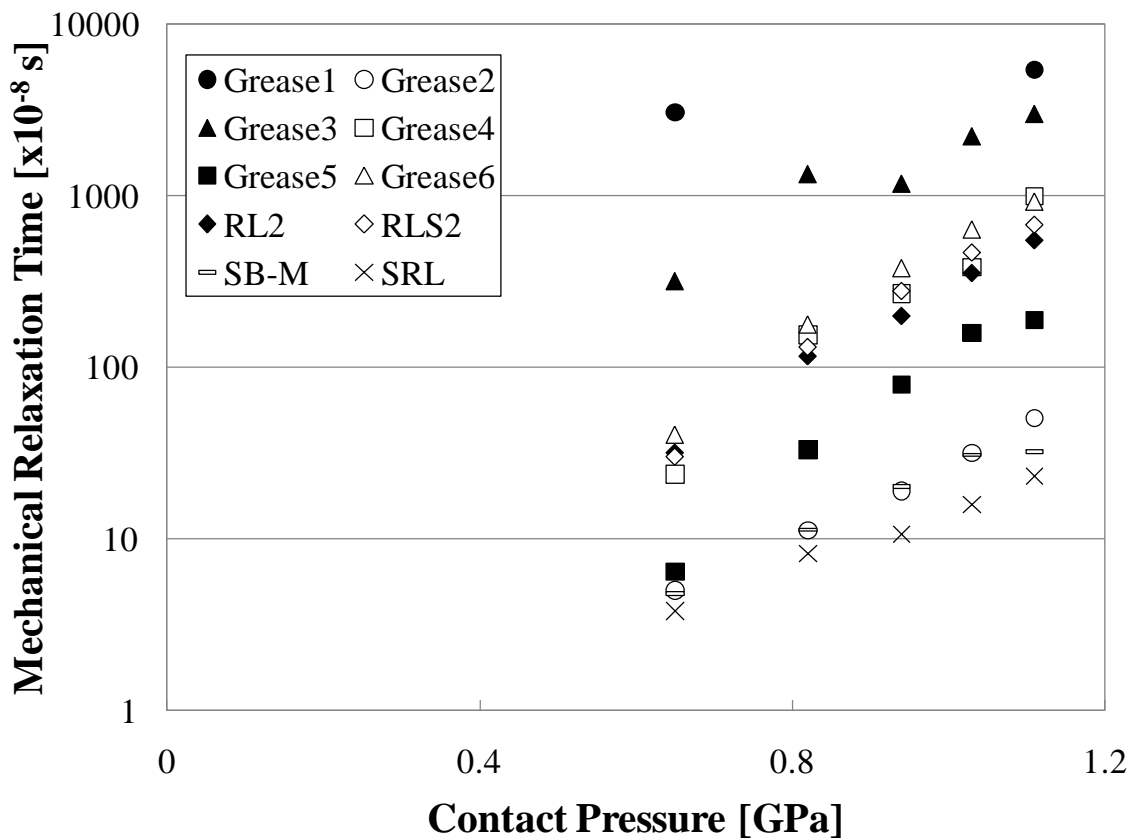


Figure 7.52 Mechanical relaxation time of greases

It has been found that, as shown in Figure 7.52, the dependence of the mechanical relaxation time of the grease on pressure tends not to depend on the type of the thickener nor the corresponding base oil and the worked penetration, because all greases show similar gradient.

Chapter 8

Observation of EHD Film Formation

This chapter describes the experimental results of the EHL behaviour of the greases including starvation, film decay and cavitation.

The EHL film of various greases was investigated in order to assess the starvation behaviour in operation. Firstly, the measurement of the electric parameters of the EHL film (capacitance and resistance) was performed for a relative long operation time of up to 30min, while the time and the sliding distance to the occurrence of starvation (“sliding distance to starvation” was calculated just by integrating the operating speed during “time to starvation” defined in Chapter 5) in EHD conditions were measured. Secondly lateral oscillations were imposed onto the contact in order to simulate real situations, where vibrations are likely to occur and eventually perturb the normal formation of the EHD film. Finally, the grease film thickness under sheared conditions was observed in order to assess whether shear has any effect upon starvation in EHD films.

8.1 Starvation Behaviour by Electrical Method

The experimental apparatus and method were explained in Chapter 5. In this part of the study, RL2, RLS2, SB-M and SRL greases were tested while the measurements were repeated at least three times for each testing condition. Due probably to its consistency, however, the formation of a continuous grease film was not always possible and sometimes the contact became starved from the beginning of the operation. This means that the experimental results shown in here are not reproduced with excellent accuracy and do not

include such cases in which it was not able to measure the time until the contact became starved. This is because, in some cases there are less than three measured points presented in the following figures. Nevertheless, a particular tendency could be observed when all results were put together in a broad scale graph.

As an example, results of different grease cases are shown in Figure 8.1 and measured period was reminded. In following sections, this measured time was presented followed by the sliding distance, integrating speed during this time, for each grease.

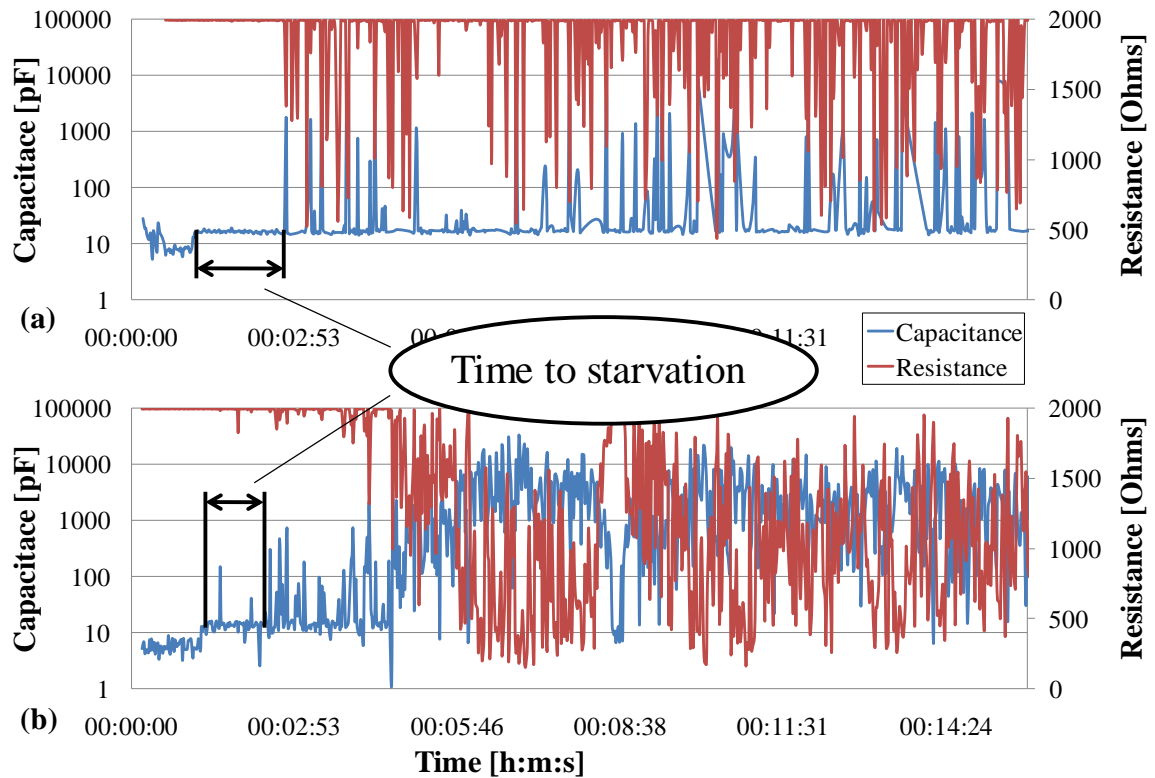


Figure 8.1 Comparison of grease film decay; (a) RL2 at 107mm/s and 10N, (b) RLS2 at 810mm/s and 10N

8.1.1 Results of RL2

Figure 8.2 shows the time to starvation for each operating condition. These results suggest that at heavy load and low operating speed, i.e. under thin film thickness conditions, the starvation is more likely to occur. Thus for the 30N and 50N measurements which showed relatively short time to starvation at low speed, some measured points of those cases were discarded in this figure. However, overall behaviour in RL2 could be evaluated, in terms of the time to starvation. The duration of the fully flooded film linearly diminished with increasing entrainment speed in a logarithmic scale, and it appears to be independent of the load exerted onto the contact. The red square represents the observed trend of data.

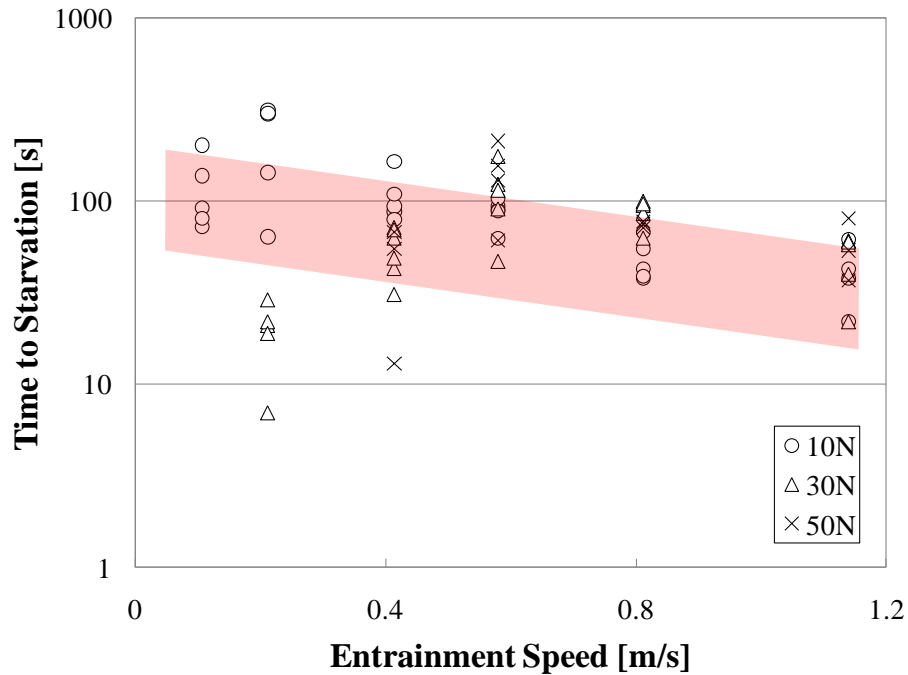


Figure 8.2 RL2 time to starvation

These results were subsequently converted into a relationship between the sliding distance to starvation and the value of PV (pressure multiplied by speed). In a study by Cann *et al* [119] the degree of starvation was shown to deteriorate with increasing entrainment speed

and widening track width, which implied that the SD (*starvation degree*) parameter, expressed by Equation 8.1, would increase with increasing load. Therefore the value of PV was considered to play an important role in terms of the starvation behaviour and it was expected that the degree of starvation would be more likely to deteriorate with the value of PV than the entrainment speed itself.

$$SD \propto \eta u a_t \quad (8.1)$$

where η is the viscosity of the lubricant, u is the velocity and a_t is the track width.

However, as shown in Figure 8.3, the sliding distance to the occurrence of starvation seems to be prolonged with increasing PV value and only to become invariable in the high PV value range.

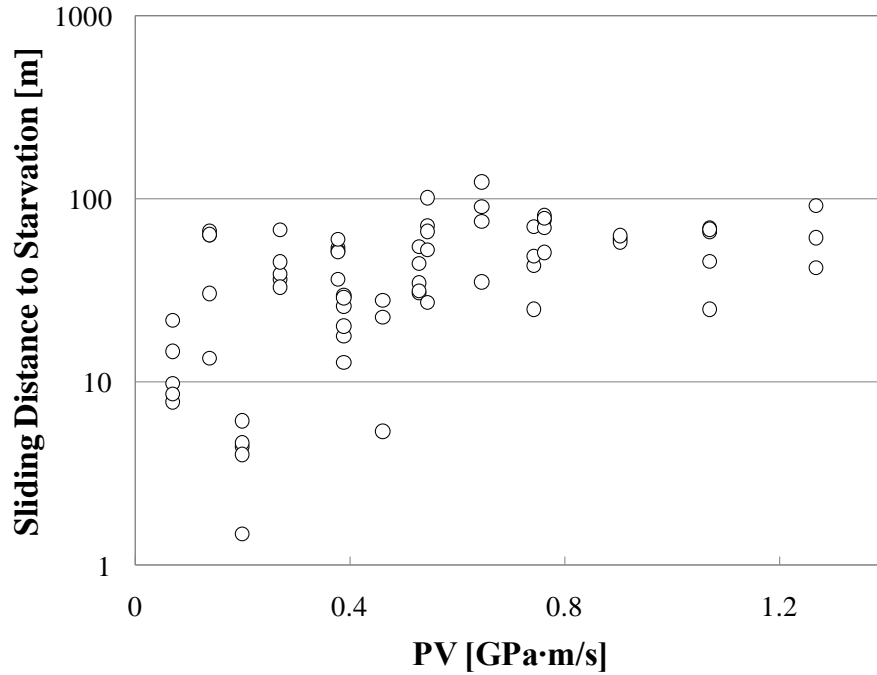


Figure 8.3 RL2 sliding distance to starvation

Thus when trying to predict the occurrence of starvation in the contacts lubricated by RL2 grease, it can be assumed that starvation would start to occur at the same time from the beginning of the EHD operation at any load. While the duration of the fully flooded condition decreases with increasing entrainment speed, the distance to the starvation increases over the low PV range and eventually becomes invariable at high speed and high pressure.

8.1.2 Results of RLS2

Figures 8.4 and 8.5 show the starvation behaviour of RLS2 grease. As found in the previous case, the time duration until starvation occurs is presented first, whereas the calculated distance of the fully flooded condition is presented against PV value in the latter figure.

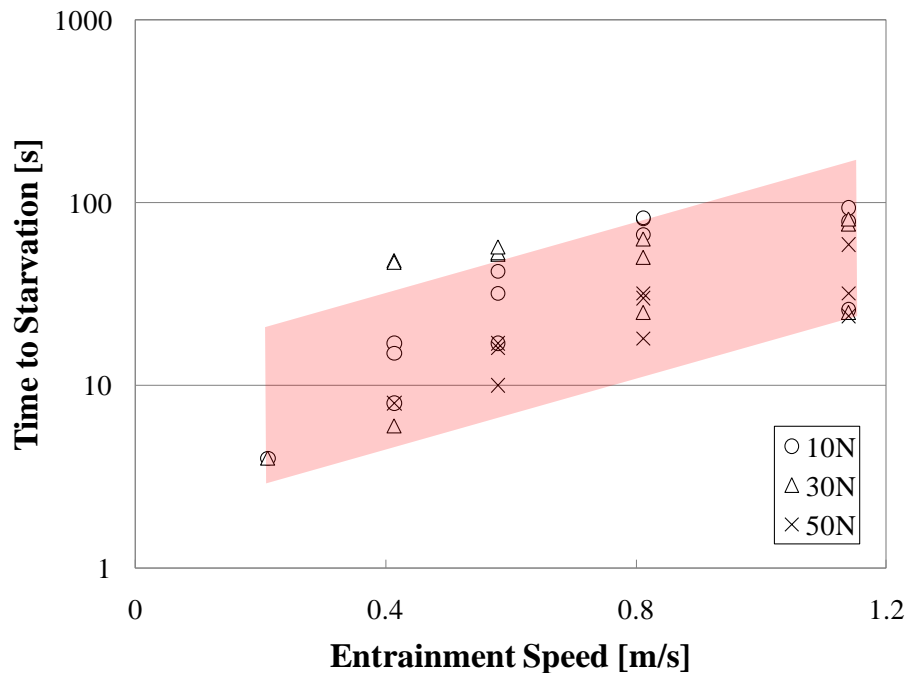


Figure 8.4 RLS2 time to starvation

The results of the experiments with RLS2 grease showed the different behaviour with RL2 in terms of the time to starvation. The time, that is the duration of fully flooded film, prolonged almost exponentially with increasing entrainment speed. Consequently, the sliding distance was more likely to be extended rather than constant in RL2 with increasing the PV value, as observed in Figure 8.5.

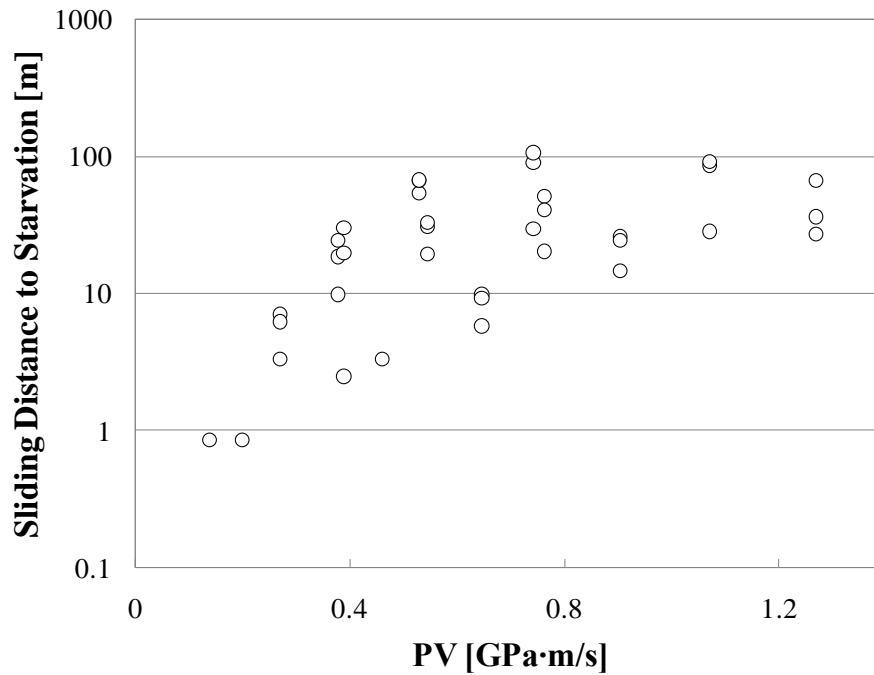


Figure 8.5 RLS2 sliding distance to starvation

8.1.3 Results of SB-M

Figures 8.6 and 8.7 show the starvation behaviour in SB-M grease lubricating films. The relationship between the measured time until the contact starved and the operating speed can be found in Figure 8.6, whereas the operating length with fully flooded condition was plotted against PV value in Figure 8.7.

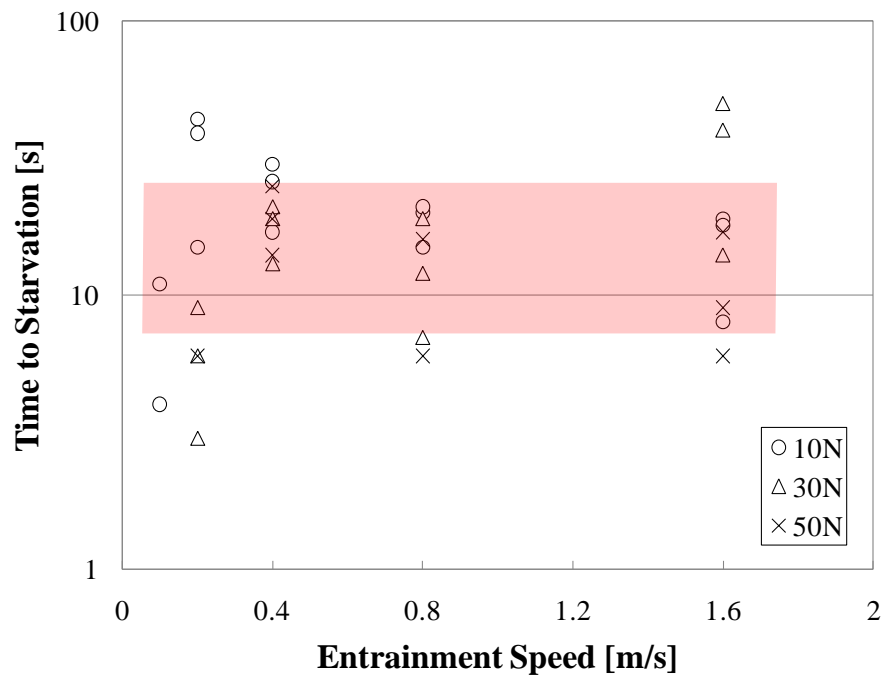


Figure 8.6 SB-M time to starvation

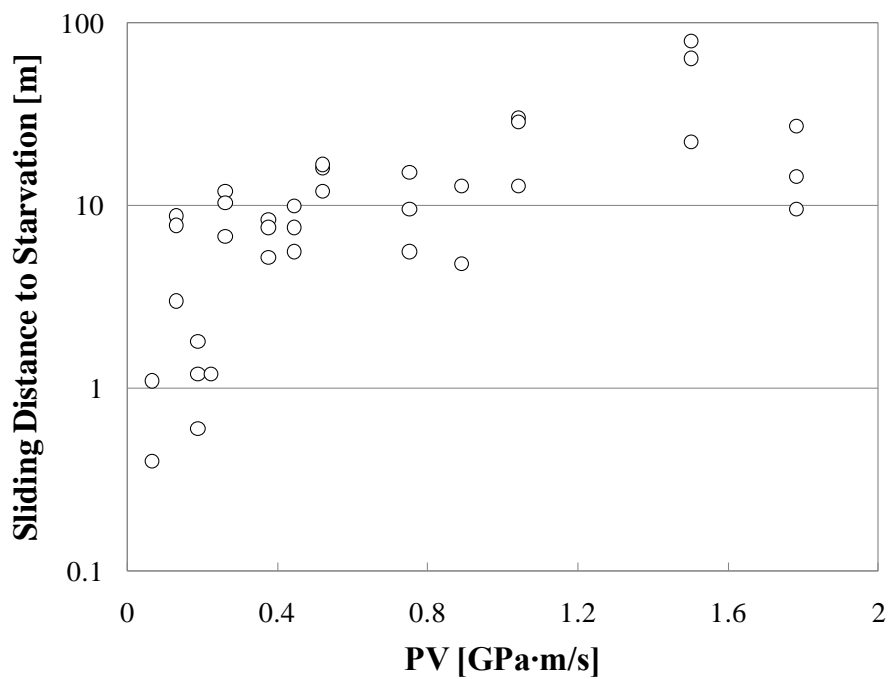


Figure 8.7 SB-M sliding distance to starvation

In terms of time duration, SB-M will allow a certain period before the lubricated contact becomes starved, which is also proved to be independent upon the entrainment speed. However, in terms of the distance to starvation, this seems to increase moderately with increasing PV value in SB-M and may not be constant as observed in RL2.

8.1.4 Results of SRL

The final results on the study of the starvation behaviour by using the electrical method are those for SRL grease and are shown in Figures 8.8 and 8.9. From the results in Figure 8.8, it can be concluded that SRL shows a strong tendency that the EHL film, in terms of the duration of fully flooded condition, is improved with increasing pressure and speed. Although starvation was quickly observed at low speeds with high load condition, the time to starvation in the case of this grease would show similar behaviour to SB-M. Thus it is rather independent of the entrainment speed.

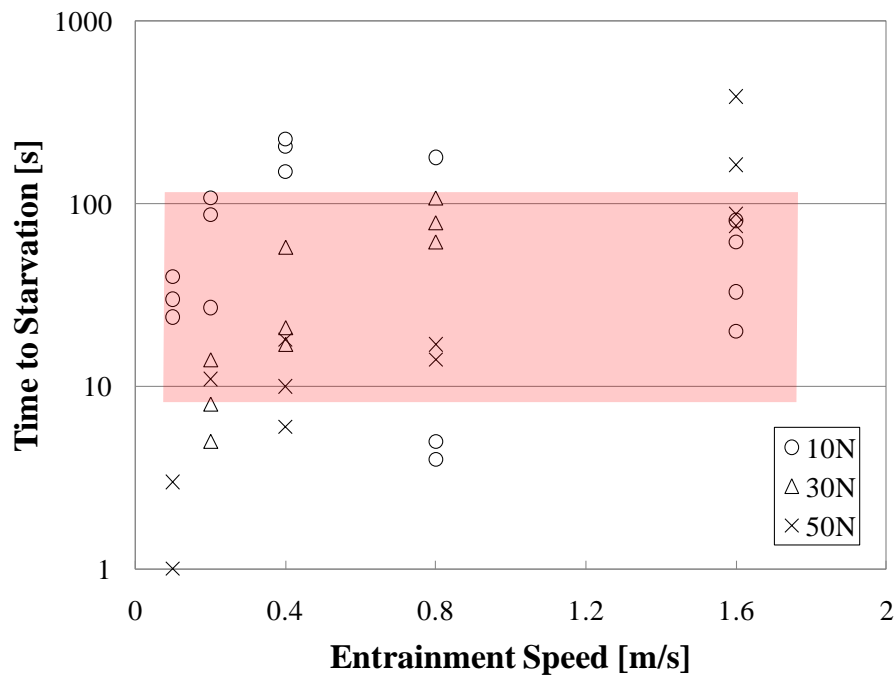


Figure 8.8 SRL time to starvation

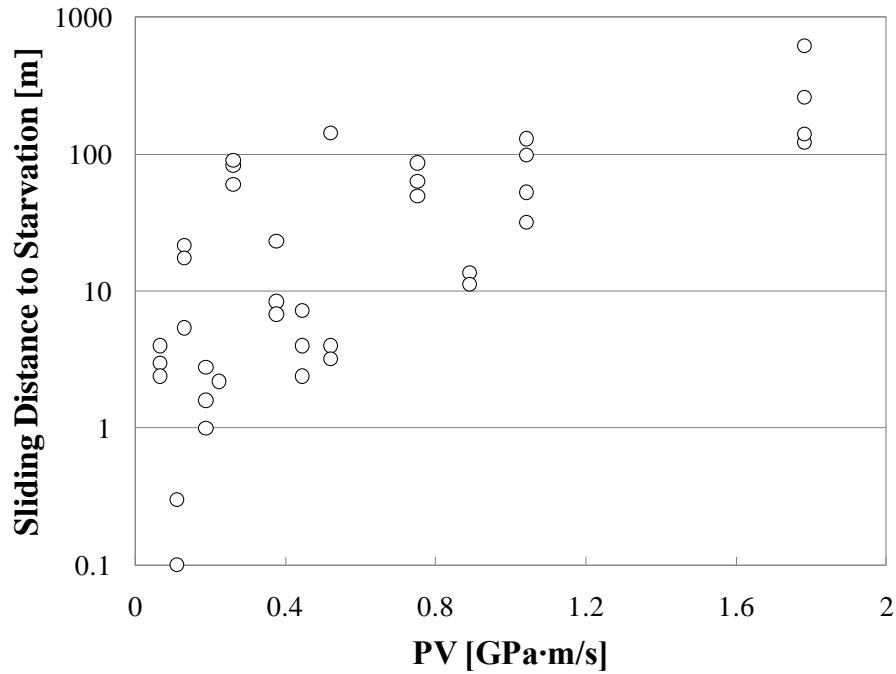


Figure 8.9 SRL sliding distance to starvation

From the overall results, by measuring the distance to starvation while the grease film is fully formed, the starvation is less likely to occur at high PV value. Especially in the case of RLS2, both time and sliding distance to starvation became longer at high speed and heavy load. The sliding distance to starvation also dramatically prolonged in this case. Thus it has been found that the degree of starvation would not be necessarily increased by increasing speed for all greases investigated.

8.1.5 Conclusions

The starvation behaviour in the grease EHL film has been investigated for four greases. Although it is well known that the degree of starvation increases with speed, that fact is based on the experimental results conducted by accelerating the contacting bodies step by step from low speed where the starvation is rarely observed, and is possibly affected by the time-dependent behaviour of the grease film.

In other studies such as presented in Figure 3.4, it was suggested that in high speed regime longer experimental time has been passed and this influences the grease film thickness more or less. Furthermore, there are very few reports concerning a quantitative analysis of the time to starvation (within author's knowledge no published paper comparing the time or duration to starvation). In this study, the occurrence of starvation was defined by measuring the resistance and capacitance of the contact. The lubricating film at a certain speed was formed by loading the contact after the aimed operating speed was reached in order to obtain the pure time-dependent behaviour of the grease at a certain speed.

The experimental results revealed that the starvation behaviour depends on the grease type. In terms of the time to starvation, SB-M and SRL showed a constant behaviour against the entrainment speed. On the one hand, RL2 grease film was more likely to tolerate starvation at low speed so that the measured time became shorter with increasing speed, whilst RLS2 film showed a longer period until the occurrence of starvation at high speed.

From the overall results, the contact pressure would not affect the starvation behaviour of the grease film. This is proved by the fact that the measurements at 10N, the lowest load in this study, have not necessarily indicated the longest period of operating with fully flooded lubricating film.

It has been also concluded that the high speed operation does not necessarily have a bad affect on the grease films. For example at 1.15m/s RLS2 will operate with fully flooded EHL film for much longer time compared to the operation at 0.1m/s.

8.2 Effects of Lateral Oscillations on EHD Film Formation

Although vibrations are inevitable in real machines operation, it is difficult to predict the behaviour caused by such movement. It is nevertheless assumed that vibrations will affect grease lubricating films more than oil films because the vibrating movement may influence the fluidity of the grease. In this study, only lateral motion has been applied onto the contact region between a sapphire disc and tungsten carbide ball, and the behaviour of the grease film has been examined to assess the effect not only of the type of the grease but also of the lateral motion speed, namely the frequency of oscillation. During the tests, the contact load and main rolling speed remained constant at 45N and 0.5m/s respectively, with pure rolling conditions. The length of the stroke of the lateral motion was about 564 μ m for 100Hz and 335 μ m for 10Hz, and the evaluation of the film thickness was done by the RGB method described in Chapter 5.

8.2.1 Grease film thickness decay and recovery

The experiments were conducted under lateral oscillations with 100Hz for seven greases, Grease2, Grease4, Grease5, RL2, RLS2, SB-M and SRL. The lateral motion was exerted after 5minutes running in steady state conditions. The pictures for the evaluation of the film thickness were generally taken at every one minute from the beginning of the test. In terms of evaluating the result of the film thickness under the lateral motion, the picture captured at the centre position of the stroke was used as a reference value.

Figures 8.10 represents the typical behaviour of the grease lubricated contact under the lateral oscillatory motion. It has to be noted that in some cases starvation occurred just after the contact was loaded.

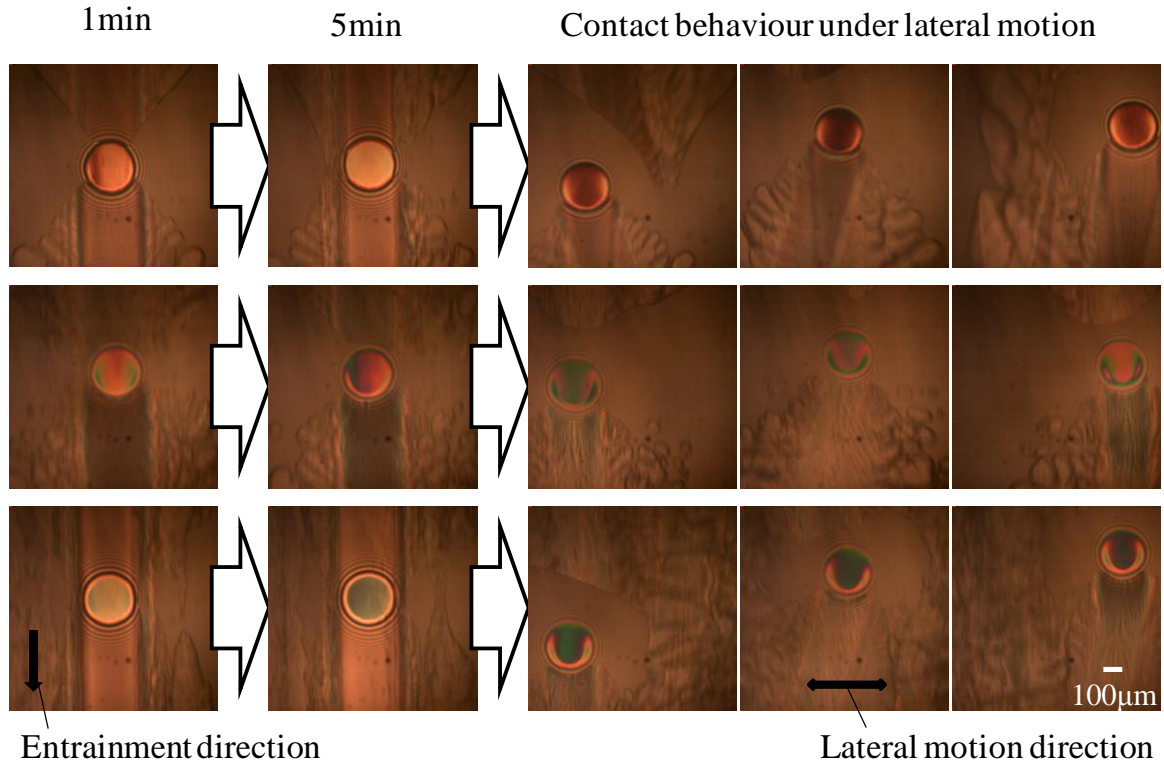


Figure 8.10 Grease film thickness decay and recovery under lateral oscillations; pictures in top row = Grease5, pictures in middle row = RLS2 and pictures in bottom row = SB-M

As shown in Figure 8.10, the film thickness has recovered by the application of lateral oscillations to the contact even after the contact was starved in normal rolling condition.

The test was conducted for ten minutes (five minutes for the steady state condition and five minutes for the vibrating condition) and for all cases the inlet of the oscillating contact was fully flooded with the lubricant and starvation was never observed again. The changes in the film thickness for each of the studied greases are illustrated in following figures. The broken line indicates the film thickness theoretically calculated in the case of the base oil.

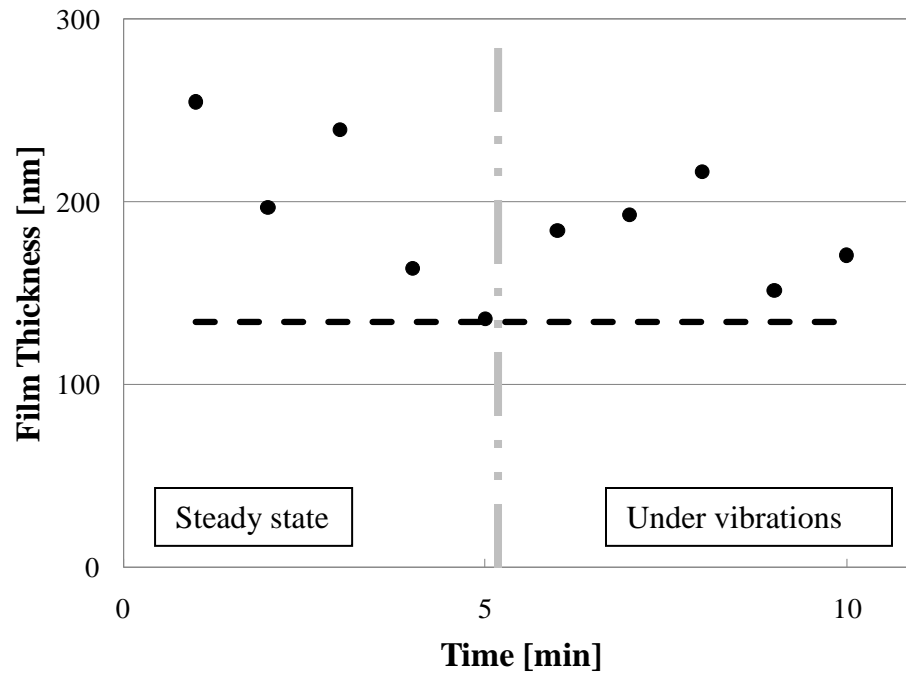


Figure 8.11 Grease2 film thickness decay and recovery (broken line: film thickness of the base oil)

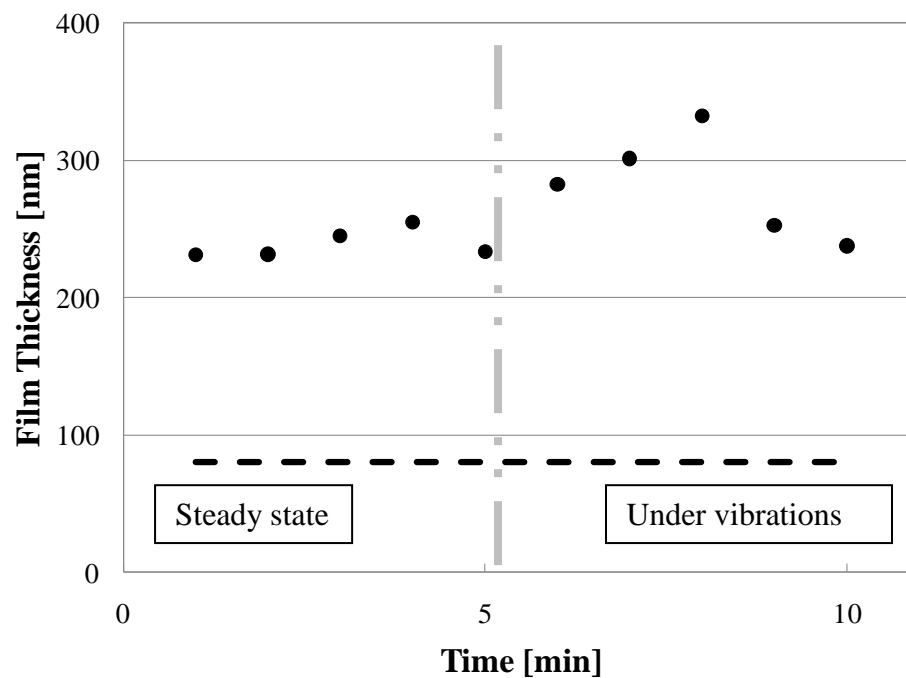


Figure 8.12 Grease4 film thickness decay and recovery (broken line: film thickness of the base oil)

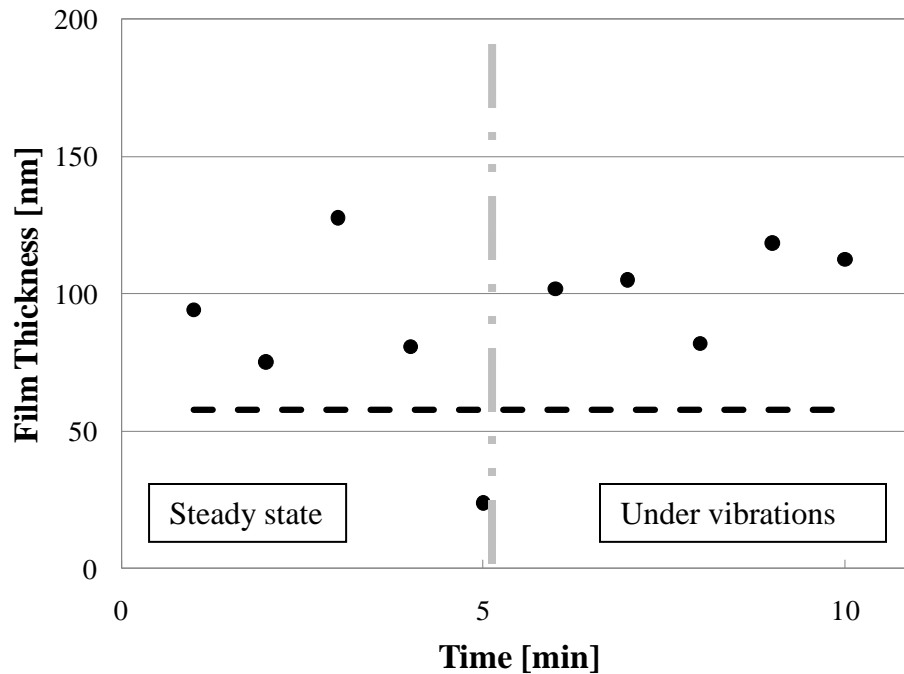


Figure 8.13 Grease5 film thickness decay and recovery (broken line: film thickness of the base oil)

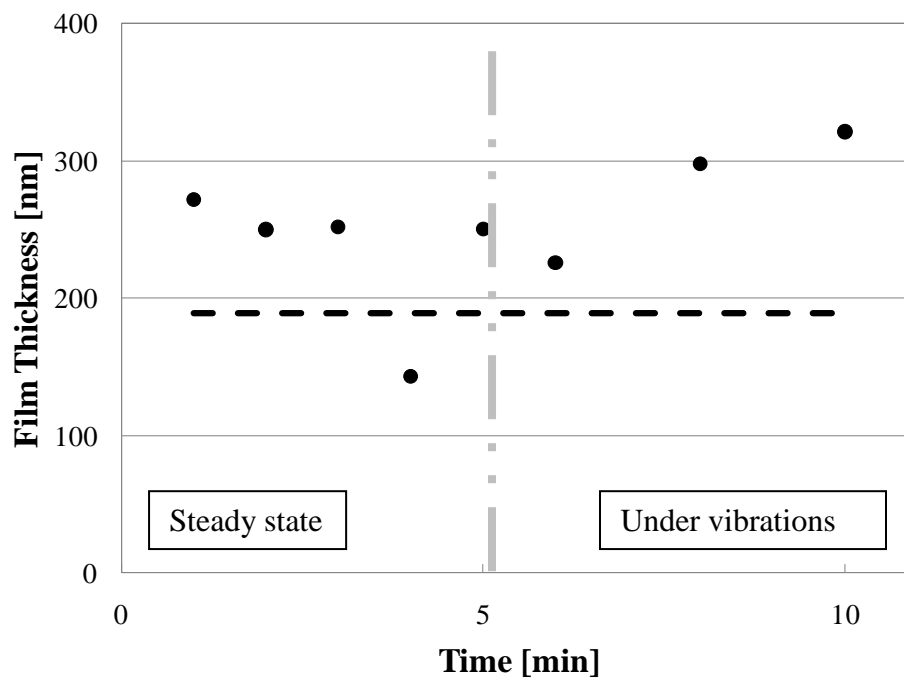


Figure 8.14 RL2 film thickness decay and recovery (broken line: film thickness of the base oil)

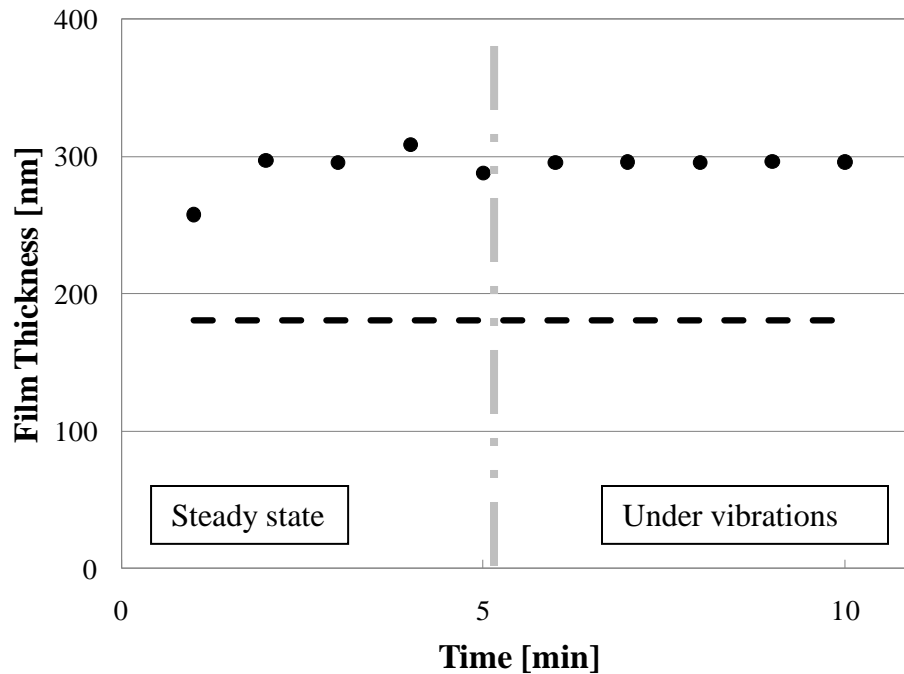


Figure 8.15 RLS2 film thickness decay and recovery (broken line: film thickness of the base oil)

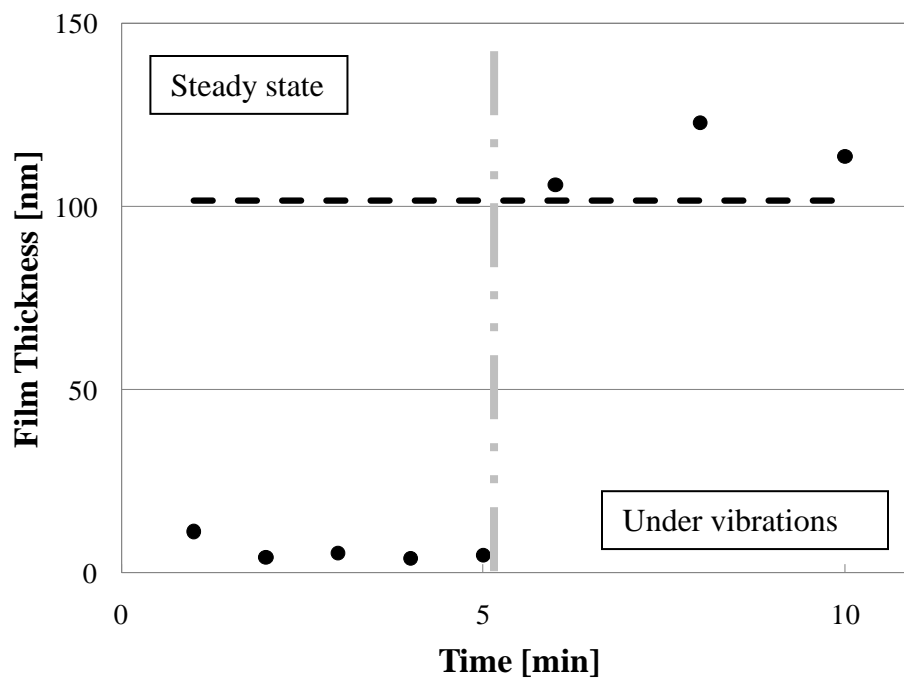


Figure 8.16 SB-M film thickness decay and recovery (broken line: film thickness of the base oil)

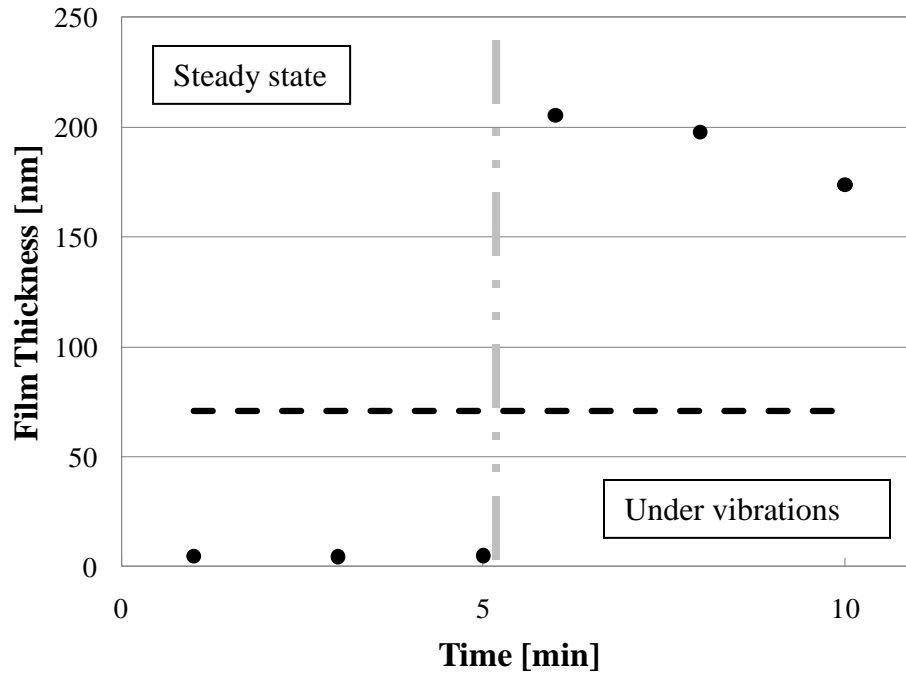


Figure 8.17 SRL film thickness decay and recovery (broken line: film thickness of the base oil)

RL2 and RLS2 showed very good film forming ability, which is partly due to their high viscous base oils, and the starvation was not observed at all in these experimental conditions. Therefore, the film thickness in the case of RL2 and RLS2 did not change much after the lateral vibration was applied. However, the overall results showed the trend of recovery in the film thickness up to the level above the thickness of the corresponding base oil by applying an external oscillatory motion.

Also starvation was not observed under vibrating conditions. This suggests that, in the real machine components lubricated by the grease this sort of mechanism ensures fully flooded conditions. Thus starvation will be less likely to occur due to the presence of vibrations despite predictions by many authors [63].

8.2.2 Grease film thickness changes during the vibration cycle

Further experiments relating to vibrations were conducted at the vibrating frequency of 10Hz by using the SB-M grease. In these tests, the stroke length was shorter than in the case of 100Hz that is about 335 μ m. Although 250 images were captured for one cycle (full cycle movement is shown in Figure 8.18), one image out of every ten images was analysed so that the film thickness was obtained at 25 different points for one stroke. The experimental procedure was the same as in the previous case, but the running duration of the test was extended to 15 minutes. Figure 8.19 illustrates the changes in the film thickness during one cycle of the lateral motion. The out-bound corresponds to the behaviour of the contact from No.1 to No.12 in Figure 8.18 and the return-bound means the process between No.13 and No.25.

The overall film was formed with sufficient thickness like in the result of 100Hz during the motion and starvation was not observed even after 15 minutes running. It was found however, that the film thickness dropped at a certain point along the stroke path, as shown in Figure 8.19. This low-film point always occurred at the centre of the stroke, where very small amount of lubricant was stored after the first five minutes of pure rolling conditions. Indeed starvation of the contact was observed before the lateral motion was applied. This is the reason why the relatively thin film was observed around the centre of the stroke, although the lateral speed was maximum there. Nevertheless it was clearly showed that the lateral motion helped the grease pushed away from the rolling track to be brought back onto the track and to flood the inlet region of the contact.

As shown in Figure 8.19, at least for 15 minutes, the overall film thickness was constantly formed and no decreasing tendency in the film thickness with time passage was observed, though the absolute values observed around the track centre were thinner than the fully flooded film of the corresponding base oil.



Figure 8.18 Typical behaviour of an EHD contact in lateral vibrations

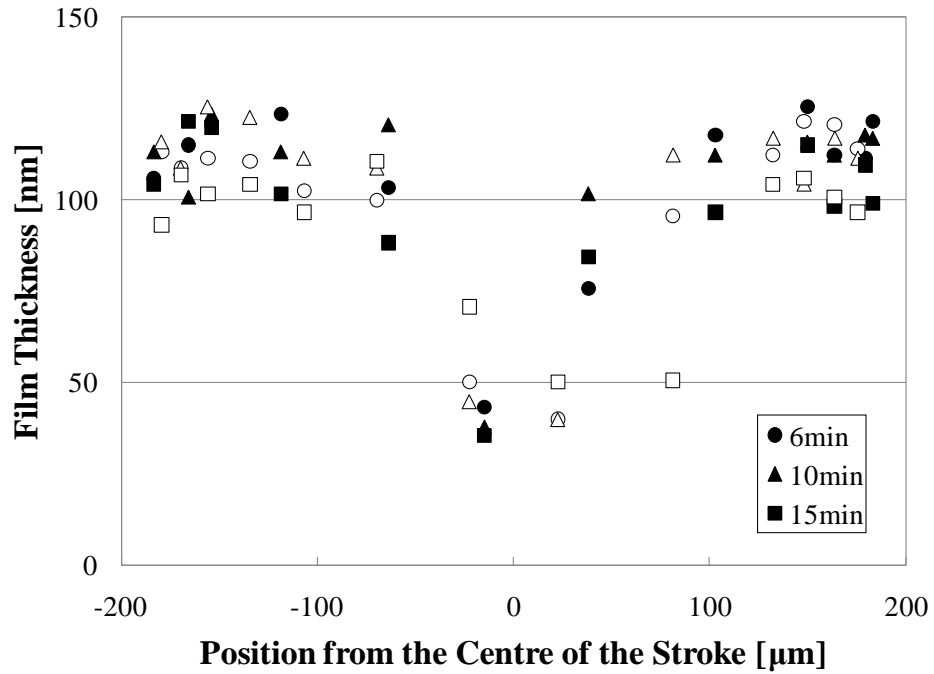


Figure 8.19 SB-M film thickness changes during one lateral cycle at 10Hz (black points = out-bound from the left side of the stroke, white points = return-bound)

For each of the 25 pictures captured over 15 minutes, meanwhile, the amount of the grease replenishing the inlet region was evaluated by the inlet distance for fully flooded conditions as illustrated in Figure 8.20. This distance corresponds to the S value advanced by Wedeven *et al* [17].

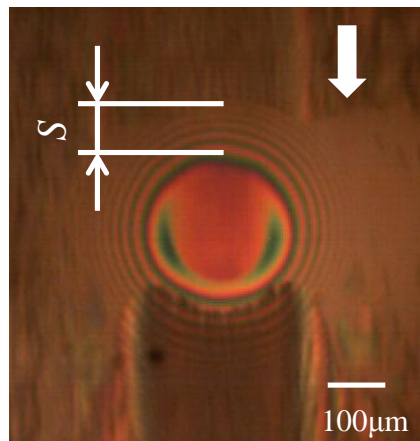


Figure 8.20 Definition of the S value (arrow indicates the direction of main speed)

Figure 8.21 shows the changes in the S value across the whole cycle over 15 minutes period, accompanied by the corresponding central film thickness.

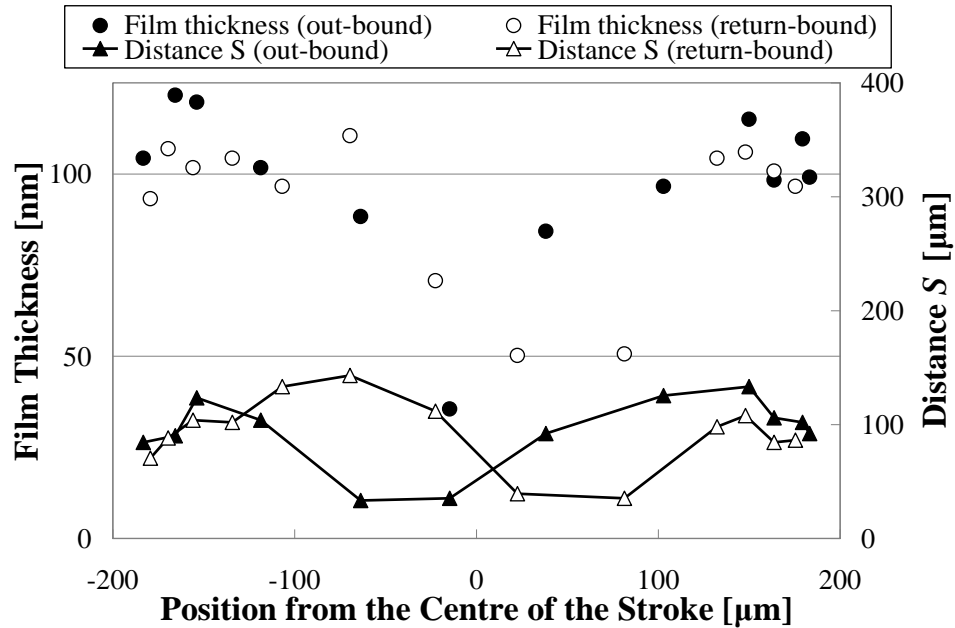


Figure 8.21 SB-M relationship between film thickness and distance S

It has been found that in the central position where the value of the film thickness dropped, the distance S was also measured as a small value, and the overall behaviour of the S value corresponded to the film thickness changes.

The boundary of starvation was calculated for each measured points based on Wedeven's theory and illustrated as white triangle points in Figure 8.22. According to Wedeven, only four points, two for the out-bound and two for the return-bound, were starved whilst 11 points were calculated as thinner film thickness than the base oil, the value of which was 101nm.

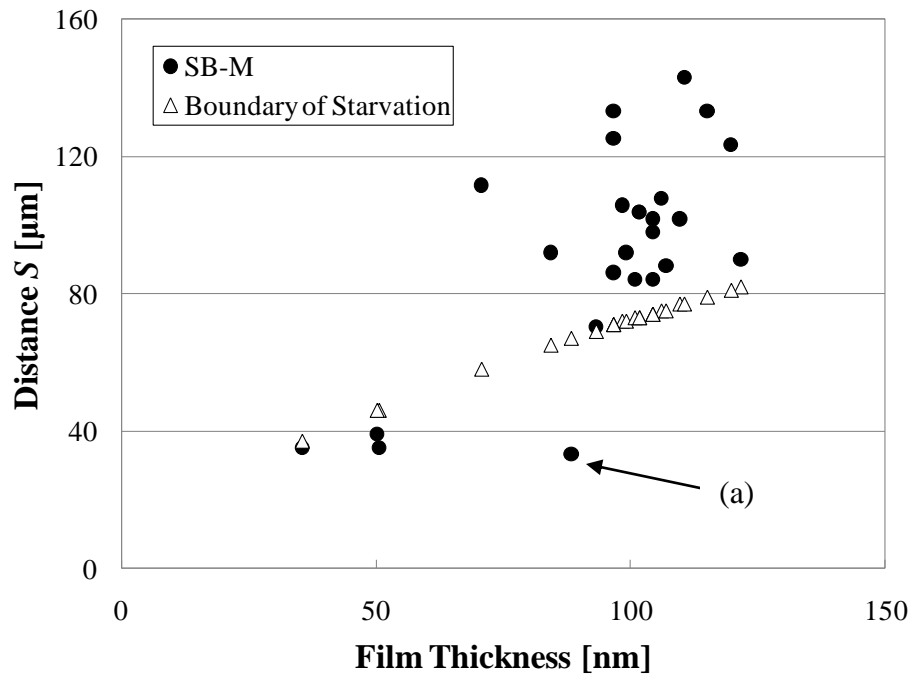


Figure 8.22 SB-M measured S values and theoretical values for each film

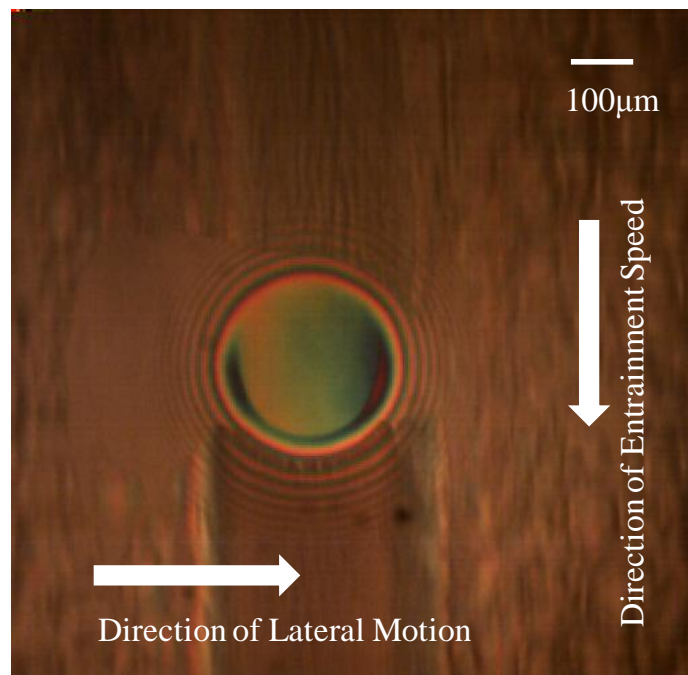


Figure 8.23 SB-M EHD contact under lateral vibrations at the point of (a)

As an example, the interferogram of the contact indicated by (a) in Figure 8.22 is shown in Figure 8.23. As seen in the picture, the grease lubricating film will not be determined only by the condition of the inlet of the contact, because the adequate film was observed under the far below condition of the S value against the traditional assumption. This adequate film might be formed by the contribution of the stored grease in the left side of the contact.

Thus, when the S values are evaluated along the associated direction of both speeds, namely the distance S diagonally taken in Figure 8.23, it will show sufficient large value. However, at this moment, it is not clear which direction for the estimation of the S value can be taken as the overall shape of the contact is not changed by the lateral motion. In addition, as the case of RLS2 shown in Figure 8.10, the film thickness after 5 minutes in the pure rolling condition was measured as 288nm surpassing the oil film thickness by almost 60% whereas the S value in the inlet region was measured as 24 μm , which is clearly far below the level assumed by Wedeven's theory. Consequently, it has been concluded that the grease lubricating EHL films may not be determined by a certain distance in the inlet unlike the oil case since the adequate film thickness has been observed under poor conditions in terms of the S value.

For more insight into this aspect of the grease lubrication, the film thickness for various positions of the contact along the stroke path for SB-M at 10Hz and 100Hz, over six minutes running, were compared in Figure 8.24. As shown in this figure the film thickness did not drop much around the centre of the initial rolling track at 100Hz and the overall film was formed with the thickness of roughly between 100nm and 150nm in comparison with 101nm for the base oil. At 100Hz, the film in the out-bound motion was constantly thicker than that in the return motion. However, it is thought that this is a temporary tendency partly because of the nature of the grease and partly because of vibrations making the contact condition a bit unstable.

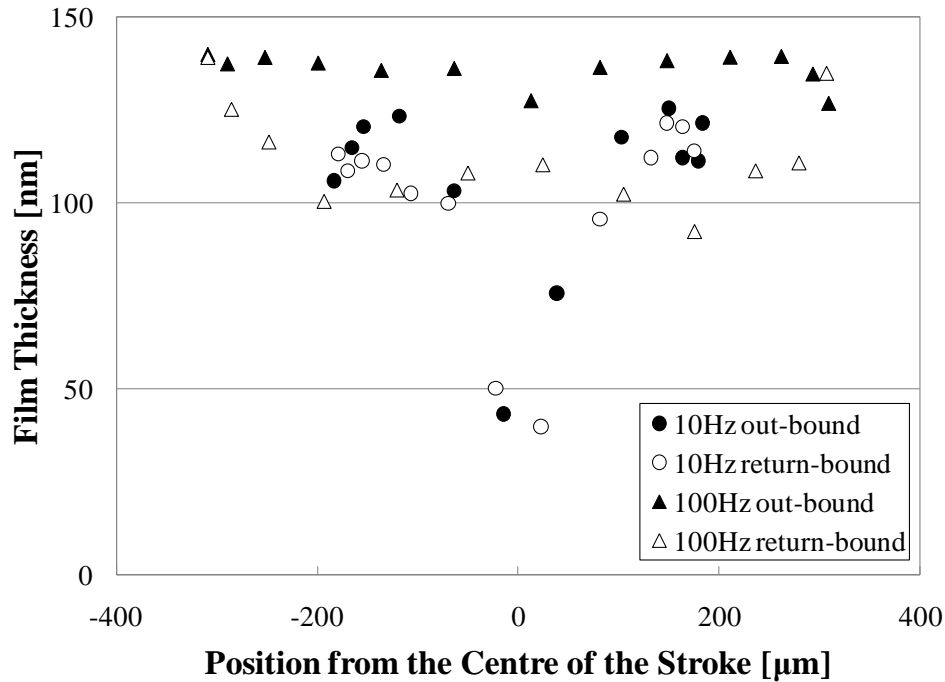


Figure 8.24 SB-M film thickness changes under lateral motion

From the overall results it would be mentioned that the vibration speed does not influence so much upon the grease film since the film thickness at both 10Hz and 100Hz has been obtained in the same range. This is probably because the lateral speed is relatively low in comparison to the main rolling speed. On the other hand, the reason why a drop around the centre track was not observed at 100Hz vibrations is thought to be due to the vibration speed. It is thought that the faster motion in the lateral direction provides the thicker film as the entrainment speed does in the normal case, though it was concluded earlier that this cannot be said at least for this grease. Another reason will be that the faster motion supplies more grease into the inlet region and also churns the grease around the contact, which leads to thicker and more constant thickness.

Although it has been found that in a certain condition the film thickness decreases even under vibrations, this would be the rare case in the real operation and such rolling truck would be rarely formed because the contact experiences vibrations in many directions.

8.2.3 Conclusions

It has been found that lateral vibrations alleviate the starvation problem by bringing the grease from outside the track back into the contact region even after the contact became starved in normal rolling conditions. Under certain conditions, this behaviour may not be enough to recover the film thickness to the lubricating levels of the base oil, however, this is the case only around the position where the amount of the grease is initially very low, and may not have significant influence on the overall operation. In fact, a sufficiently thick film was observed outside that narrow region of the lateral motion stroke.

In both 10Hz and 100Hz cases, it has been found that the film thickness under lateral vibrations does not decrease after at least 10minutes of running. Also it has been found that the vibration speed does not influence so much upon the grease film since the film thickness at both 10Hz and 100Hz has been obtained in the same range which is roughly between 100nm and 150nm.

Moreover, the investigation based on the traditional assumption for starved conditions in oil lubricants has revealed that in the case of grease lubricants not only the condition of the inlet but also the condition around the contact would need to be considered for elucidating the lubricating grease behaviour. This is because adequate film thickness has been observed in spite of the lack of the necessary amount of the lubricant in the inlet region.

According to the experimental results and the fact that vibrations in various directions are almost always present in the real world, it is thought that a certain level of film thickness will remain in grease lubricated contacts, ensuring full film conditions in machine elements such as rolling bearings.

8.3 Film Thickness under Shear Conditions

In addition to vibrations, the speed difference generated in rotating bodies is also inevitable for real operations. Thus the grease behaviour under sheared conditions was also investigated so as to assess the nature of the grease lubricant inside the EHD contact. The film was formed in conditions of 0% and 100% slide-roll ratios at an entrainment speed of 0.1m/s. The film thickness was observed by using a chromium and silica coated glass disc which was loaded by the steel ball at 10N. The coloured pictures of the contact were captured at the same time for all measurements and the film thickness was calculated by the Hue value method described in Chapter 5.

8.3.1 Results and discussions

The results for RL2, RLS2, SB-M and SRL are shown in following figures. In the experiment with SB-M, due to severe starvation observed, the experiments were suspended at five minutes in order to avoid damaging the disc surface.

Overall results shows that the film thickness tends to remain thicker in pure rolling conditions and this is obvious in the case of RLS2, where the film thickness with 100% slide-roll ratio rapidly decreased from the beginning of the test while the film thickness formed in pure rolling conditions was thicker than the reference thickness of the corresponding base oil.

This is partly due to the difference in speeds between the ball and disc. As revealed in section 8.1, the grease will indicate less durability against starvation at low speed, though it has been concluded that RL2 will show a constant behaviour. In the arrangement of the rig the speed of the ball slows down when the slide-roll ratio is set. This made the contact condition be more similar to the low speed range rather than the high speed range where the durability against starvation was prolonged according to previous results.

Another factor may be the heat generation which is induced by the shearing motion. Thermally affected greases might be more easily removed from the track.

In pure rolling measurements, RL2 and RLS2 formed a constant film which was thicker than that of the base oil for the experimental period. On the other hand, the film thickness of SB-M and SRL tended to decrease rapidly from the beginning of experiments. Although those two greases formed thicker films than the corresponding base oils at very early stage of experiments, it would be suggested that the higher viscosity base oil may be preferred in order to maintain a grease lubricating film with a sufficient thickness over an extended period of time.

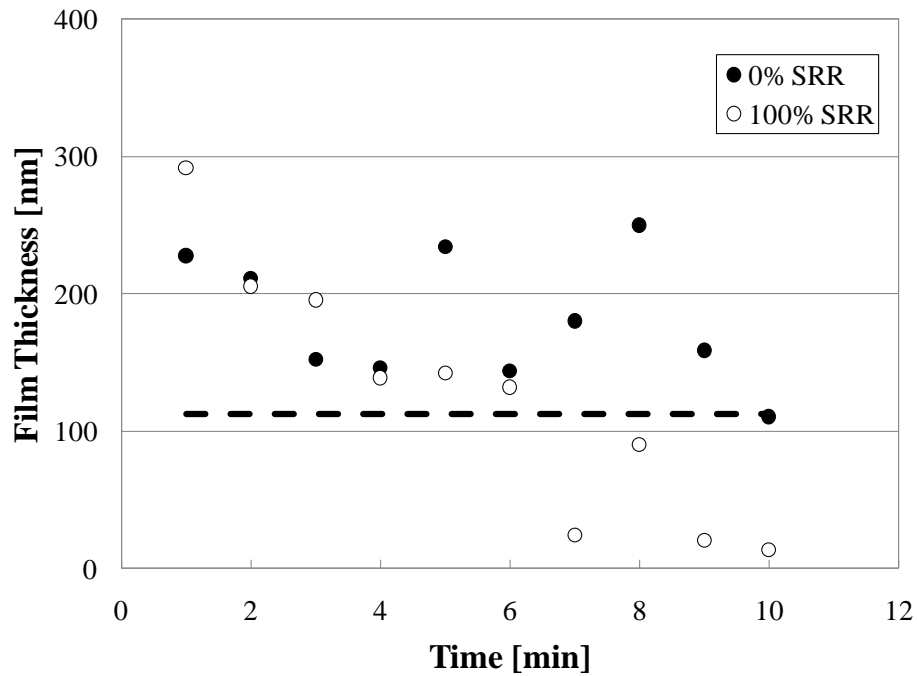


Figure 8.25 RL2 film thickness decay under shear (broken line: film thickness of the base oil)

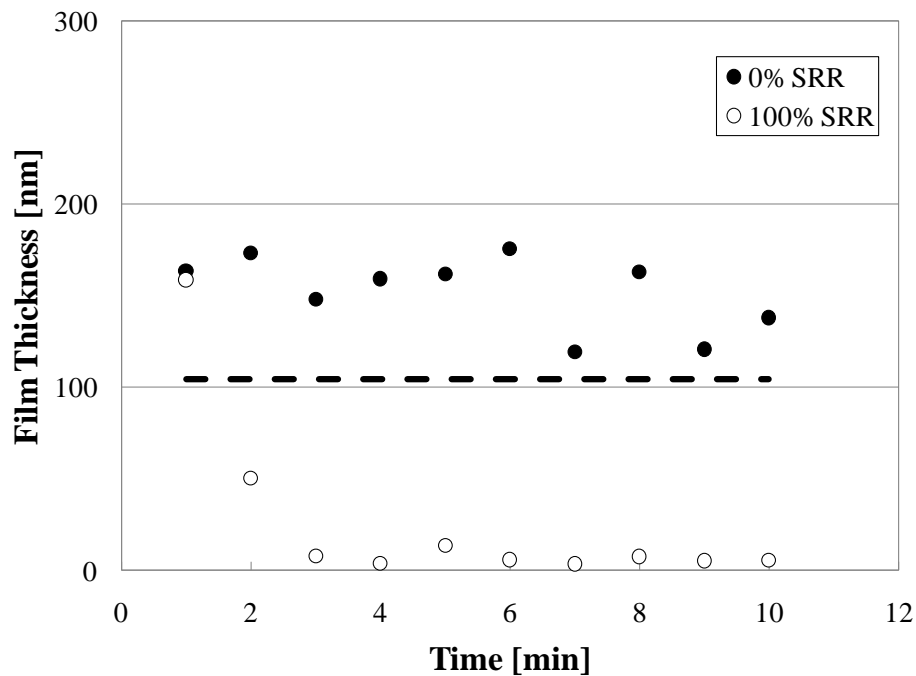


Figure 8.26 RLS2 film thickness decay under shear (broken line: film thickness of the base oil)

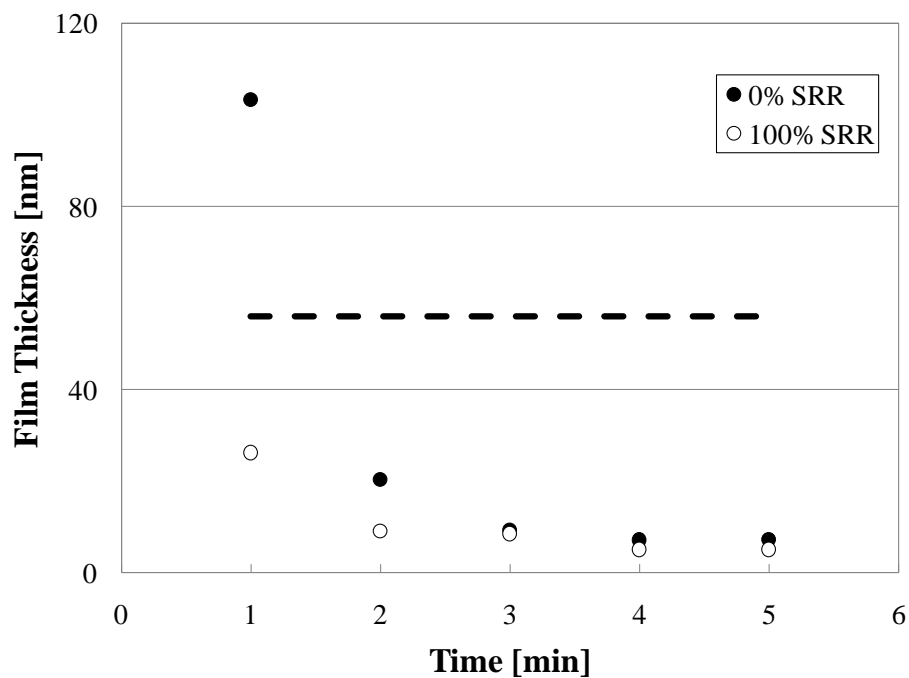


Figure 8.27 SB-M film thickness decay under shear (broken line: film thickness of the base oil)

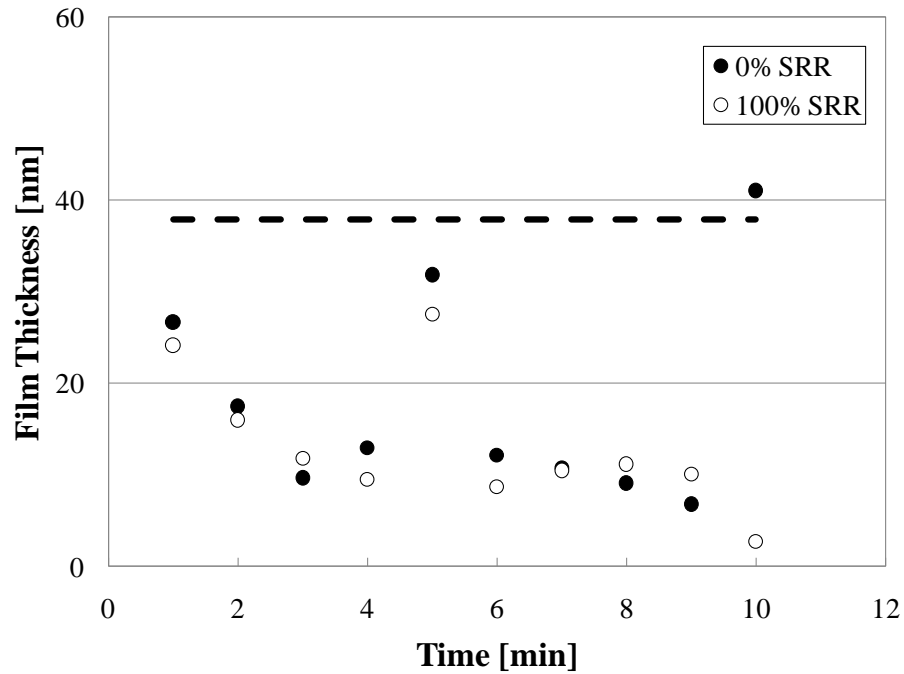


Figure 8.28 SRL film thickness decay under shear (broken line: film thickness of the base oil)

8.3.2 Conclusions

The experiments in which shear was applied to the grease films have revealed that the grease film will be more likely to become starved in sheared conditions than in pure rolling conditions. One of the reasons for this behaviour will be that the slower motion of one of the contacting bodies has a strong influence upon the lubricant circulation and leads to the lesser durability against the starvation as observed in section 8.1.

The results in this section would also suggest that higher viscosity base oils may be able to maintain a sufficiently thick lubricant film over longer periods of time.

8.4 Cavitation Phenomena in Grease EHL Films

8.4.1 Introduction

Cavitation is one aspect of the lubrication of the EHD contact which is very little studied and can be linked to the starvation behaviour of the contact. Using the optical interferometry technique, the relation between the lubricating grease composition and operating parameters on one hand and the cavity length on the other hand has been evaluated in this section.

Nishikawa *et al* [120] studied the cavitation phenomena in EHD contacts in relation to reciprocated systems and showed that short stroke length of the motion could lead to severe starvation though this was the case of oil lubricated contact. Leonard *et al* [121] carried out an experimental and theoretical analysis of the cavity and fretting wear in a point grease lubricated contact by observing the gaseous cavity whose length extended with speed.

The cavitation phenomenon can be related to starvation, or rather to the amount of lubricant available in the inlet of the contact, not only in reciprocated motion systems but also in normal, namely unidirectional, motion case. As observed by Dowson and Taylor [122] in rotating systems, the inlet and cavity boundaries cannot be separately considered, since the film thickness in the inlet region would be determined by the cavity in the divergent region in the outlet of the contact. This is evidently true in the case of rolling element bearings where the exit of one element is the inlet for the next.

8.4.2 Experimental procedure

The length of the cavity has been defined as the distance from the exit edge of the contact to the trailing edge of the cavity, as illustrated in Figure 8.29. Five greases were studied in order to evaluate the effect of the thickener as well as the viscosity. The base oils for all of

these greases were PAO with various viscosities. All tests were carried out at room temperature and in the condition of pure sliding. Initially the ball was slowly loaded onto the disc surface where the grease was uniformly spread and the static contact was made. Subsequently, the disc started rotating and was accelerated until the aimed speed was achieved. In this way the cavitation phenomena in the range of speeds between zero and the final nominal value were observed.

The majority of the tests was conducted by using a glass disc and a 19.5mm diameter steel ball at 45N, however tests where the ball was replaced by a glass lens of a radius of curvature equal to 10.38mm were also performed. Distinct differences between these two conditions, as far as the cavitation phenomenon was concerned, were not observed.

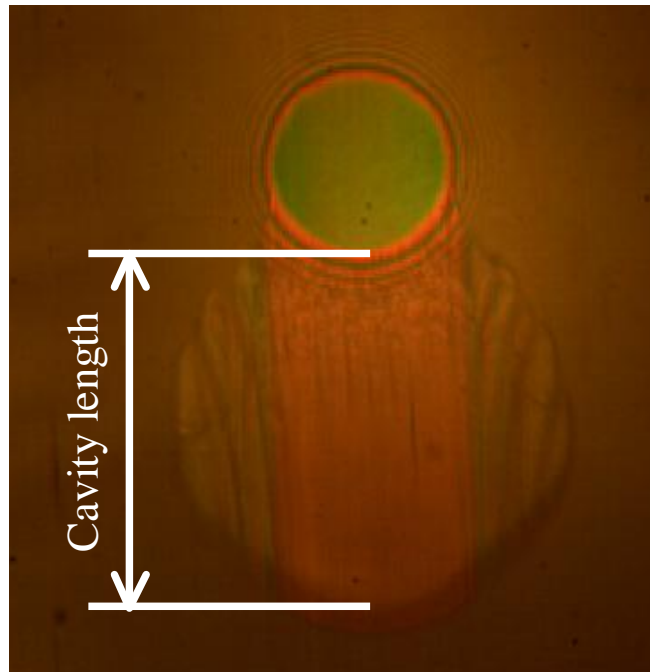


Figure 8.29 Definition of the cavity length

8.4.3 Results and discussions

As a mechanism of the formation of the cavity, bubbles of gases are formed at the exit of the contact when the disc starts rotating. At the same time the grease layer trapped between the disc and ball moves away from the contact along the entrainment direction. As the speed and the distance of the travel of the disc increase, the cavity region enlarges until reaching a certain equilibrium dimension.

First, Grease1 and 4 were selected in order to evaluate the effect of the thickener because these two greases were manufactured with the same base oil. Figure 8.30 shows the cavity length of Grease1 and 4 as well as their base oil as a function of time.

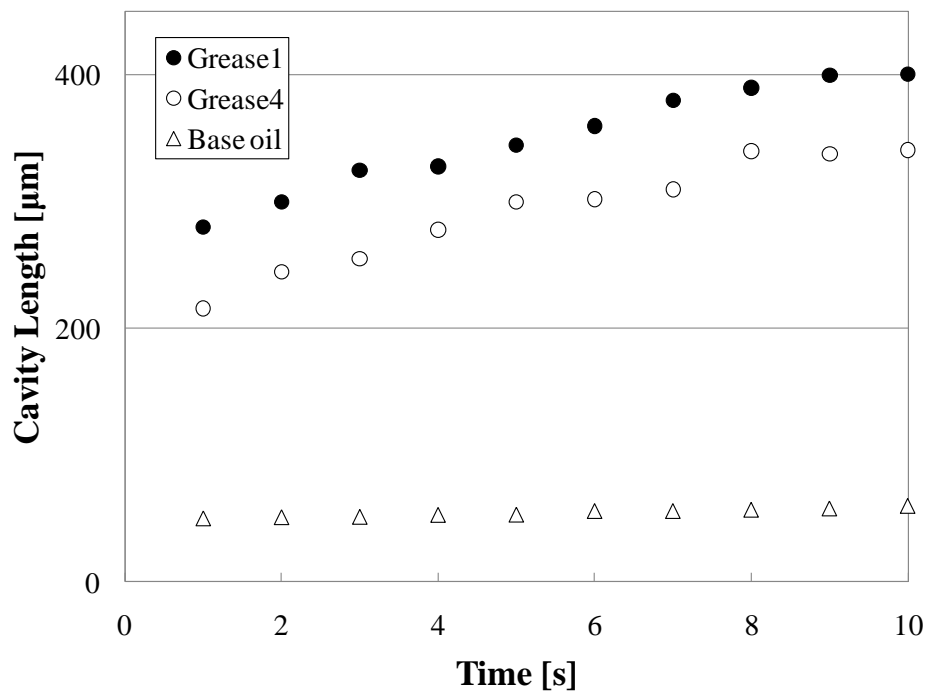


Figure 8.30 Changes of cavity length with time

The disc was moving at a constant speed of 5mm/s. As shown in this figure, the cavity length of the oil ceased to grow soon after the start of the test, while the cavity length of the grease rapidly increased at the early stage of the test until eventually reached an equilibrium value. Greases showed significantly longer cavity length as much as six times that of the base oil. This suggests that the semi-solid consistence of the grease contributes to the entrapment of cavity gases which are released at sub-ambient pressures at the exit of the contact thus leading to the longer cavity region. Also a greater amount of gases is assumed to be initially dissolved in the bulk grease (due probably to their manufacturing process) and this contributes to extending the cavity length compared to the oil. Although Grease1 constantly showed larger cavity length than Grease4, it can be concluded that, in general, the type of the thickener may not influence the cavity length as strong as other factors.

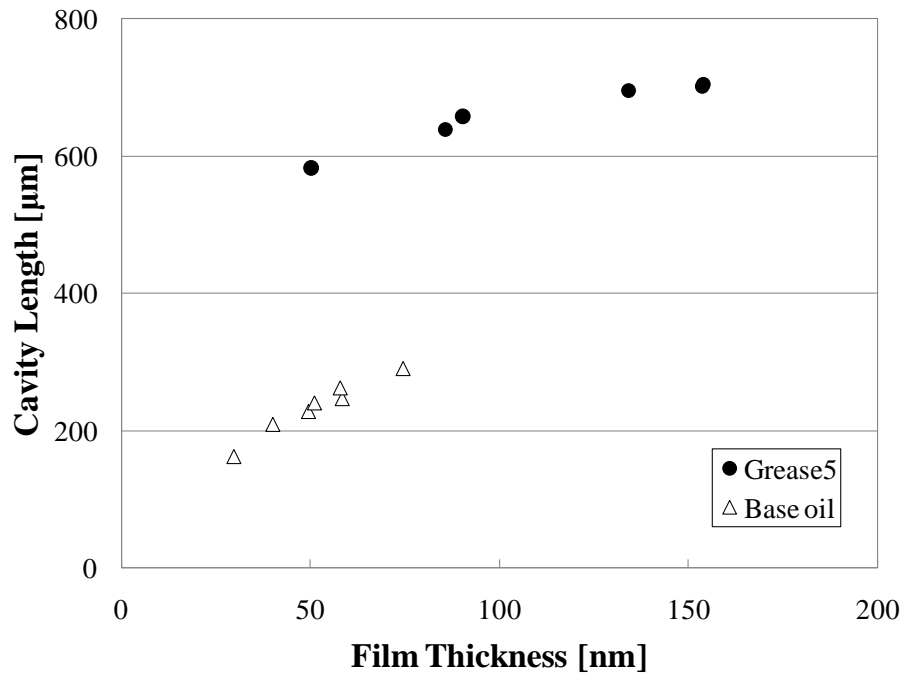


Figure 8.31 Cavity length as a function of film thickness

Figure 8.31 shows the correlation between the cavity length and film thickness for Grease5 and the corresponding base oil. Stadler and co-workers [123] have shown that the cavity

length would be related to the film thickness by a power law. Results obtained here revealed that the cavity length of the base oil varied approximately with a power 0.6 of the central film thickness, while for the grease this exponent became 0.17. Stadler *et al* suggested that a PAO lubricant would have a value of 0.4 for this exponent. Thus, although it has been found that the cavity length of the grease is increasing with central film thickness, i.e. speed, the rate of change of the cavity length in the grease lubrication is considerably lower than that in the oil lubrication.

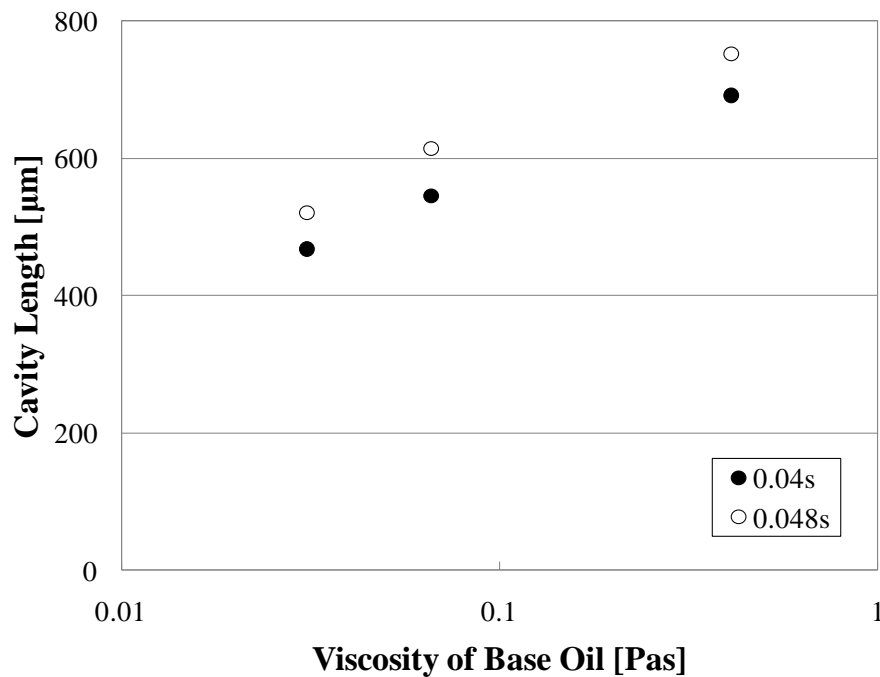


Figure 8.32 Effect of viscosity of the base oil upon the cavity length

Finally, the cavity length of 12OH-LiSt greases was investigated in order to evaluate the effect of the viscosity of the base oil upon the cavity length. Figure 8.32 shows the cavity length of the grease at 0.04s and 0.048s after the disc started rotating as a function of the logarithm of the viscosity of the base oil. As expected because of the increased central film thickness, the cavity length of the grease increased with increasing viscosity of the

corresponding base oil. This dependence is very similar to the dependence of the grease film thickness versus the viscosity of its corresponding base oil reported by Cann *et al* [52].

The effect of the viscosity upon the cavity length can be qualitatively modeled by treating the grease as a rheological material with a viscosity depending on the shear rate.

$$\eta = C_1 + C_2 \dot{\gamma}^N \quad (8.2)$$

where C_1 , C_2 and N are constants which determine the behaviour of the fluid. When C_1 and C_2 are not zero and N is equal to -1, Equation 8.2 corresponds to a Bingham plastic material. According to Sakurai *et al* [124], a normal grease is characterized by $C_1 = 10$, $C_2 = 10$ and $N = -0.8$, while for oils C_2 is zero to express the independent viscosity upon shear rate. Consequently, the constant C_1 can be assumed as the viscosity of the base oil of the grease. On the other hand, the pressure distribution at the exit region of the contact is evaluated by numerical integration of the pressure represented by the following equation. Details of the calculation are shown in Appendix 3.

$$p = 6C_1 u \left(\int_{x_1}^{x_2} \frac{1}{h^2} dx - h_m \int_{x_1}^{x_2} \frac{1}{h^3} dx \right) + 6C_2 u^{1+N} \left(\int_{x_1}^{x_2} \frac{1}{h^{2+N}} dx - h_m \int_{x_1}^{x_2} \frac{1}{h^{3+N}} dx \right)$$

$$h_m = \frac{C_1 \int_{x_1}^{x_2} \frac{1}{h^2} dx + C_2 u^N \int_{x_1}^{x_2} \frac{1}{h^{2+N}} dx}{C_1 \int_{x_1}^{x_2} \frac{1}{h^3} dx + C_2 u^N \int_{x_1}^{x_2} \frac{1}{h^{3+N}} dx} \quad (8.3)$$

where h is the separation between the solid surfaces, x_1 and x_2 are the coordinates along the entrainment direction and u is the speed of the disc.

In this investigation, x_l is the exit of the contact and x_2 is regarded as the point far from the contact. The general solution of Equation 8.3 can be found in Figure 8.33.

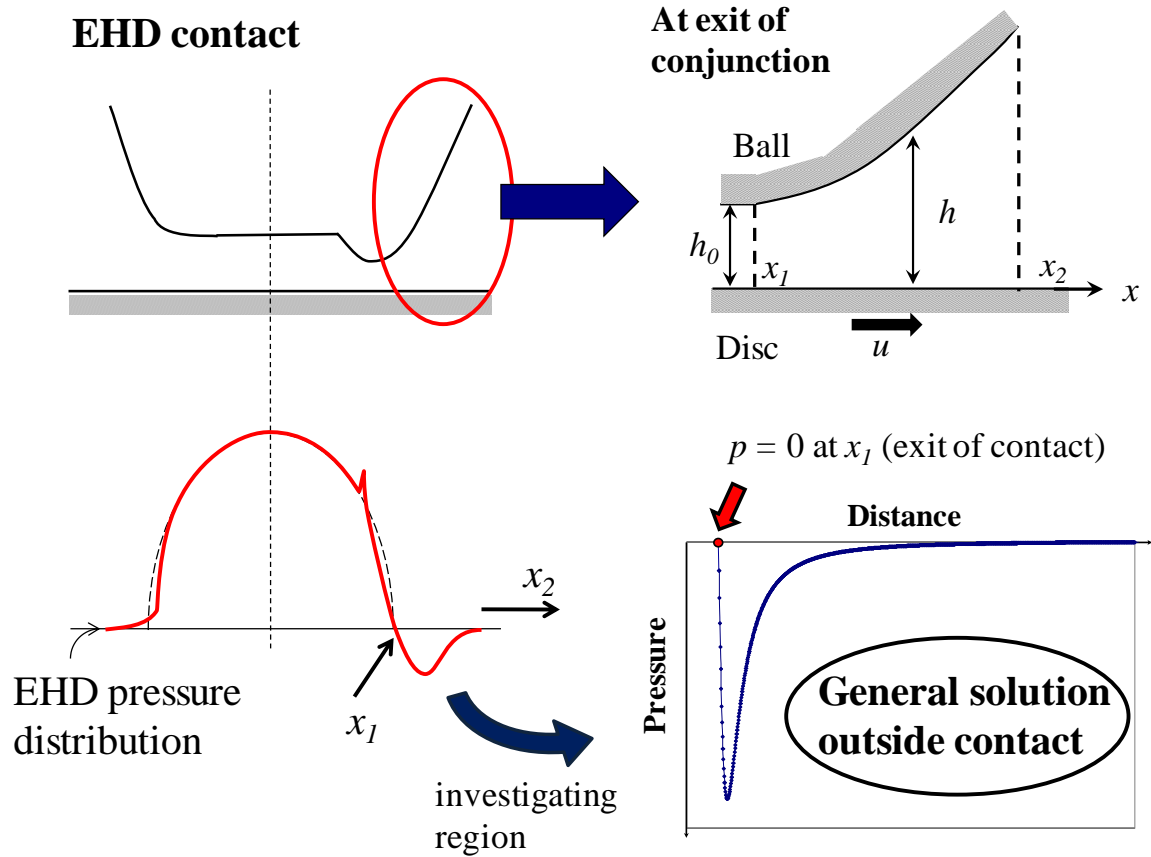


Figure 8.33 Investigating region and the general solution of Equation 8.3

For a value of N of -0.8 , the pressure curves as a function of the distance, for two oils identical to the base oils of Grease3 and 5 and four hypothetical greases, are shown as Figure 8.34. The points where the pressure curves cross the line equal to -0.1MPa can be considered as the boundary of the cavity region. Although, as mentioned earlier, this is a qualitative analysis and at this moment there is no claim that those values quantitatively represent the relation between greases and base oils, the values obtained for base oils indeed indicate similar values to the measured cavity length. Also, the grease formed by a relatively lower viscosity base oil shows larger cavity region than the high viscosity oil thanks to the shear-dependant term. This is in accordance with the experimental findings. Therefore, it would be possible to evaluate the rheological model of grease lubricants by measuring the cavity length of the EHD contact.

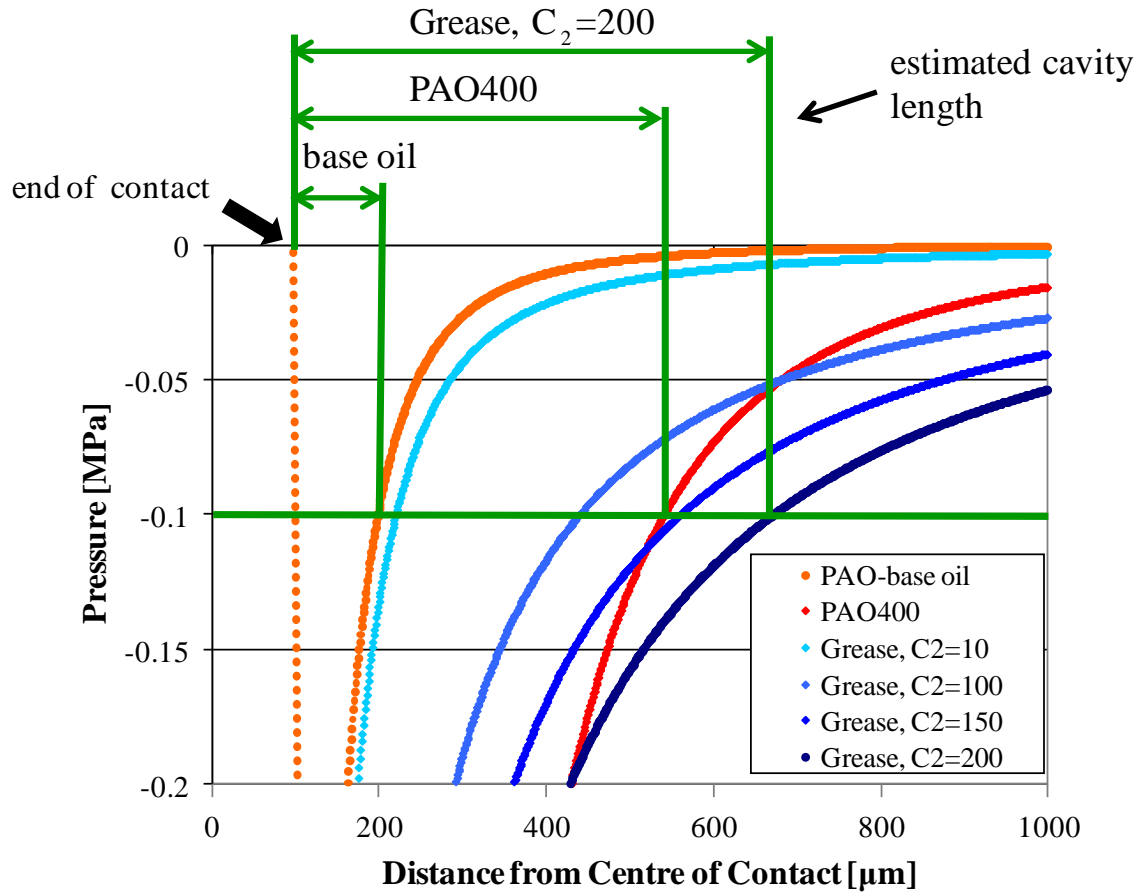


Figure 8.34 Effect of viscosity upon the cavity length in the rheological model

8.4.4 Conclusions

The cavitation phenomenon in EHD grease lubricated contacts has been studied and it has been found that the cavity length of the oil remains constant with time whilst that of the grease increases up to an equilibrium value. It has also been found that the grease forms much longer cavity region than its corresponding base oil. This is partly because the grease generally forms thicker films in the EHD condition and partly because of the shear-dependant nature of the grease.

It has been found that the type of the thickener has only a marginal effect upon the cavity length, while a strong correlation between the viscosity of the base oil and the cavity length of the grease contact has been identified.

Based on a simple rheological model, it was theoretically explained that the cavity length of the grease was longer than that of the oil. On this basis the rheological model of the grease could be predicted by measuring the cavity length in the EHD operation.

Chapter 9

Conclusions and Future Work

In this chapter conclusions of the study are presented and suggestions for future work are proposed.

9.1 Test Rig

During the course of this study an electrical method was successfully developed and deployed to an existing EHD test rig in order to simulate essential aspects of the lubrication of machine elements, that is, lubricants under metal-to-metal contact condition.

In parallel with an electrical method the standard technique of optical interferometry was also used for measuring the lubricant's film thickness and for observing the starvation behaviour especially in grease lubricated contacts as well as the cavitation behaviour of the EHD contacts.

9.2 Study of Dielectric Properties of Lubricants

The dielectric properties of lubricants under static conditions were measured by using a capacitor built on a modified micrometre. For a number of greases, i.e. RL2, RLS2, SB-M and SRL, the corresponding base oils were also evaluated whereas the base oils for the other greases investigated in this study were replaced by PAOs of similar viscosity. In addition to greases and corresponding base oils, five lubricants were also prepared in order to evaluate the correlation between their dielectric and mechanical properties. The

investigation into the dielectric properties of a number of lubricating oils on one hand and of grease lubricants and their base oils on the other hand, can be summarise in the following conclusions.

- (1) The dielectric constant of greases is larger than that of their base oil and the dielectric relaxation time of greases is longer than that of the oil.
- (2) Dielectric properties of greases are strongly influenced by their base oil for the greases investigated in this study except for SRL, the only grease consisting of a polar base oil, which showed distinct properties. However, the conclusion drawn from the overall results is that the dielectric properties of greases can be classified by the type of the thickener present in their composition. 12OH-LiSt thickener greases show high dielectric constant and slow relaxation process. On the other hand, LiSt greases tend to show smaller dielectric constant and faster relaxation process when compared to Di-urea thickener greases and of course 12OH-LiSt greases.
- (3) A significant opposite behaviour has been found between the polar thickener greases and the non-polar thickener greases. For LiSt greases and probably for urea greases as well, the dielectric constant of the grease is increased with viscosity of the corresponding base oil, which should be normal behaviour in liquids in terms of the dielectric behaviour. However, for polar thickener greases, it has been revealed that the dielectric constant decreases with increasing viscosity of the base oil. It is suggested here that this is because of the mixed structure of greases; a more viscous structure of molecules, usually longer molecular chains, restricts the movement of a polar substance.
- (4) Experiments on oils of similar viscosity oils (called here “viscosity 68 oils”), it has been concluded that the dielectric properties of lubricants depend strongly on their chemical structure and weakly on their viscosity.

9.3 Dielectric Studies in EHD Conditions

The dielectric spectroscopy technique was used for evaluating the lubricant properties inside the EHD contacts in both pure rolling and sliding conditions. Firstly, it has been revealed that the dielectric constant is slightly lower than the value corresponding to static conditions. There is a tendency observed that a lubricant shows a faster relaxation process under sliding conditions compared to under pure rolling conditions. It has also been shown that the dielectric constant of lubricants in EHD contacts tends to decrease with increasing pressure.

A hypothesis based on the concept of entropy has been advanced here and supported by the results obtained in both sliding and non-sliding conditions. Consequently the idea that molecules are normally aligned inside the EHD contact has therefore been experimentally proved.

Thus it has been concluded that the molecules would be ordered in the inlet of the EHD contact region and regularly aligned molecules form the EHL film.

9.4 Traction Measurements

EHD traction measurements have led to the conclusion that a very polar lubricant, which shows a distinct behaviour in the conductivity term like PPG oils and SRL grease, will exhibit relatively high traction coefficient or shear stress in EHD conditions. It was also found that the higher the dielectric constant a grease showed the higher the shear stress a grease featured when compared with other greases with the same type of thickener.

The effect of the thickener upon the traction behaviour of greases in EHD contacts has been evaluated and it has been found that urea greases tend to experience high shear stress compared to other types of greases.

The effect of the base oil upon the Eyring stress in grease lubricating films has also been evaluated and it has been concluded that the Eyring stress of the grease will increase with decreasing viscosity of its base oil when compared to same thickener type greases.

When compared to the corresponding base oil greases showed slightly higher traction coefficient, which would suggest that in general grease lubricated contacts transmit larger shear forces than oil lubricated contacts. In terms of the Eyring stress, the overall conclusion is that the Eyring stress of greases is larger than that of the corresponding base oils, and also the Eyring stress of the greases decreases with increasing worked penetration value. This can be explained by the fact that the Eyring stress indicates the stress above which the material no longer obeys Newtonian law and that greases may tolerate higher level of stress due to their semi-solid state.

Measurements of the effective viscosity of greases have revealed that the effective viscosity of greases exponentially increases with pressure like a liquid lubricant, but the rate of this increase is moderate because the grease already exhibits relatively higher viscosity at low pressure (even at atmospheric pressure). The overall results, from the perspective of the effective viscosity in EHL operating conditions, is that the base oil plays a major role in the grease EHD lubrication since the similar characteristics have been obtained for greases and corresponding base oils except at very low pressure conditions.

The effect of the thickener upon the effective viscosity is also evaluated by comparing two types of greases, that is 12OH-LiSt and LiSt. The conclusion of this part of the study is that 12OH-LiSt thickener forms greases with larger effective viscosity than LiSt thickener.

The mechanical relaxation of greases and their base oils has also been investigated leading to the main conclusion that, particularly at low pressure, the grease shows shorter relaxation time than the corresponding base oil. On the other hand the rate of change of the relaxation time with pressure was found similar in the grease and base oil. This would imply that similar mechanisms govern the behaviour of the grease and oil lubricants in EHD conditions, or that the base oil plays the main role in the EHD condition as is generally accepted these days. However, this is not the case for the dielectric relaxation behaviour, which has shown opposite behaviour. Thus while the mechanical relaxation time was shorter for greases than that for the base oils, the dielectric relaxation time was found longer than that of the corresponding base oils. This fact might suggest that the mechanical relaxation behaviour against pressure would be different from the dielectric behaviour against pressure in terms of the grease as pointed out by other authors.

Another worth mentioning finding is that the mechanical relaxation time of the grease depends upon the base oil and it increases with viscosity of the base oil.

Finally all greases show very similar behaviour and it has been concluded that the dependence of the mechanical relaxation time of the grease upon pressure tends not to depend on the type of the thickener nor the corresponding base oil and indeed the worked penetration.

9.5 Study of the Starvation Behaviour

The developed electrical method has been applied to the study of the starvation of grease lubricated contacts. This part of the study has revealed that the starvation behaviour depends on the type and characteristics of the grease. For example, RL2 shows good durability against starvation in low speed operation while RLS2 tends to be less prone to starvation in relatively high speed operation. When analysing the phenomenon in terms of the sliding distance to starvation it has been concluded that starvation is not necessarily likely to occur at high speed and heavy load does not necessarily lead to starvation.

The conclusions of the study into the effect of lateral vibrations upon the lubrication of grease lubricated contacts show that these have a beneficial effect on the EHD film, thus even if the contact was initially starved, sufficiently thick film was reformed when the oscillatory motion has been applied and fully flooded condition has been ensured for the rest of experimental period. These results and the fact that in real conditions vibrations are inevitable will suggest that the starvation may not happen in machine elements working with elastohydrodynamic contacts. Moreover, the investigation based on the traditional assumption for the starved condition in oil lubricants has revealed that, in the case of grease lubricants, not only the condition of the inlet but also the condition around the contact would be needed for elucidating the lubricating grease behaviour. This is suggested by the fact that adequate film thickness has been observed in spite of the lack of the necessary amount of the grease in the inlet region, from the traditional point of view.

9.6 Study of the Cavitation Behaviour

This part of the study has revealed that grease lubricants show a length of the cavity region greater than their base oils. This is due partly to the fact that greases give thicker film thickness compared to the base oils, and partly to the fact that oils are more likely to be pulled back towards the contact because of higher surface tension. A strong correlation

between the viscosity of the base oil and the cavity length of the grease has also been found, while the type of the thickener has been proved to have only a marginal effect upon the cavity length. A simple rheological model for the cavitation behaviour was proposed, which suggests that it would be possible to predict the rheological properties of the grease by measuring the cavity length in an EHD contact.

9.7 Suggestions for Future Work

The work described in this thesis has covered an investigation into the dielectric properties of lubricants and rheological properties of grease lubricants in EHD contacts, as well as the film forming behaviour of grease lubricants in these conditions. The film formation behaviour and the starvation behaviour under pure rolling conditions, sliding conditions and lateral vibrations were evaluated as well as the cavitation behaviour. Suggestions for future work are presented as below.

9.7.1 Dielectric properties of lubricants

The investigation into the dielectric properties of base oil lubricants highlighted the significant influence of the base oil upon the dielectric properties of the bulk grease. This work could be extended to cover the grease consisting of the polar base oil and polar thickener. Based on the results of this thesis it may be assumed that such grease will exhibit a far larger dielectric constant than greases investigated in this thesis. Also, it is predicted from this study's result that such high polar grease will show very high shear stress and high traction coefficient in sheared conditions.

It would also be of interest to evaluate the dielectric relaxation time in various operating conditions of the EHD contact. In order to do so, the arrangement of the electric method should be amended. It is considered that lubricants tend to show their relaxation processes

between 10MHz and 100MHz. Thus the measuring point range should be extended by resolving the resonance problem.

9.7.2 Starvation behaviour under lateral oscillations

The experimental work in this study indicated that the lateral motion helped the grease to be brought back into the contact region and created conditions for a full film to be re-formed over the contact. It was also found, on the other hand, that the sliding motion had a bad influence upon the grease lubricating film. Therefore it would be of particular interest in conducting the lateral vibrations test with a various range of slide-roll ratios and in determining at what point the vibrating behaviour loses its effectiveness in preventing starvation against sliding.

An interesting topic for further investigation would be to change a number of working parameters such as vibration frequency, stroke length and nominal rolling speed.

Another suggestion for future work would be to mount the microscope apart from the foundation of the rig. Because of vibrations, especially at high frequencies, the image captured was difficult to be focused. In this study, recording was repeated until a good image was captured, however especially for grease lubricants because the contact conditions vary with time, this procedure should be avoided and further modification to the rig would be needed.

9.7.3 Study of the cavitation behaviour

The experimental results were well matched by the calculations derived from a simple rheological model and Reynolds equation. Although at a certain condition the observed values were likely to follow this calculation, most parts of this study were qualitative only.

Thus it would be interesting to analyse if changing operating parameters such as load would give a better insight into a quantitative behaviour of greases in order to determine their rheological properties. Also it is of importance to consider the cavity width and the shape and size of bubbles around the cavity. Finally, incorporating surface tension into more sophisticated rheological models of the grease would probably help evaluate more realistically the rheological properties of grease lubricants.

References

- [1] D. E. Jones and G. A. Schott (Editors), "Miscellaneous Papers by Heinrich Hertz", Macmillan, 1896.
- [2] G. Stachowiak and A. W. Batchelor, "Engineering Tribology", Elsevier Inc., 2005.
- [3] Y. Wijnant, "Contact Dynamics in the Field of Elastohydrodynamic Lubrication", PhD-thesis, University of Twente, 1998.
- [4] R. Gohar, "Elastohydrodynamics", Ellis Horwood, 1988.
- [5] A. Cameron, "Basic Lubrication Theory 3rd edition", Ellis Horwood, 1981.
- [6] D. Dowson and G. R. Higginson, "A Numerical Solution to the Elasto-hydrodynamic Problem", Journal Mechanical Engineering Science, 1, 6-15, 1959.
- [7] B. J. Hamrock and D. Dowson, "Ball Bearing Lubrication: Elastohydrodynamics of Elliptical Contacts", John Wiley & Sons Inc., 1981.
- [8] A.N. Grubin and I.E. Vinogradova, "Fundamentals of the Hydrodynamic Theory of Lubrication of Heavily Loaded Cylindrical Surfaces", Central Scientific Research Institute for Technology and Mechanical Engineering, Book No. 30, DSIR London Translation No. 337, 1949.
- [9] K. L. Johnson, "Contact Mechanics", Cambridge University Press, 1985.
- [10] A. Cameron and R. Gohar, "Theoretical and Experimental Studies of the Oil Film in Lubricated Point Contact", Proceedings of the Royal Society, Series A, 291, 520-536, 1966.
- [11] J. Luo, S. Wen and P. Huang, "Thin Film Lubrication Part I: Study on the Transition between EHL and Thin Film Lubrication Using a Relative Optical Interference Intensity Technique", Wear, 194, 107-115, 1996.
- [12] H. A. Spikes, V. Anghel and R. Glovnea, "Measurement of the Rheology of Lubricant Films within Elastohydrodynamic Contacts", Tribology Letters, 17, 593-605, 2004.
- [13] J. H. Choo, H. A. Spikes, M. Ratoi, R. Glovnea and A. Forrest, "Friction Reduction in Low-load Hydrodynamic Lubrication with a Hydrophobic Surface", Tribology International, 40, 154-159, 2007.
- [14] H. A. Spikes and P. M. Cann, "The Development and Application of the Spacer Layer Imaging Method for Measuring Lubricant Film Thickness", Proceedings of the Institution of Mechanical Engineers, Part J, 215, 261-277, 2001.

-
- [15] J. Molimard, M. Querry, P. Vergne, I. Krupka and M. Hartl, "Calculation of Pressure Distribution in EHD Point Contacts from Experimentally Determinated Film Thickness", *Tribology International*, 38, 391-401, 2005.
- [16] G. D. Archard, F. C. Gair and W. Hirst, "The Elasto-Hydrodynamic Lubrication of Rollers", *Proceedings of the Royal Society of London, Series A*, 262, 51-72, 1961.
- [17] L. D. Wedeven, D. Evans and A. Cameron, "Optical Analysis of Ball Bearing Starvation", *NASA Technical Paper*, 1970.
- [18] K. L. Johnson and J. L. Tevaarwerk, "Shear Behaviour of Elastohydrodynamic Oil Films", *Proceedings of the Royal Society of London, Series A*, 356, 215-236, 1977.
- [19] G. Dalmaz (Editors), "Transient Processes in Tribology", Elsevier, 2004.
- [20] C. R. Evans and K. L. Johnson, "The Rheological Properties of Elastohydrodynamic Lubricants", *Proceedings of the Institution of Mechanical Engineers, Part C*, 200, 303-312, 1986.
- [21] W. Hirst and A. J. Moore, "Elastohydrodynamic Lubrication at High Pressures. II. Non-Newtonian Behaviour", *Proceedings of the Royal Society of London, Series A*, 365, 537-565, 1979.
- [22] R. T. Lee and B. J. Hamrock, "A Circular Non-Newtonian Fluid Model: Part I-Used in Elastohydrodynamic Lubrication", *Journal of Tribology*, 112, 486-495, 1990.
- [23] A. Z. Szeri, "Fluid Film Lubrication Theory & Design", Cambridge University Press, 1998.
- [24] M. P. F. Sutcliffe, "Measurements of Rheological Properties of a Kerosene Metal-Rolling Lubricant", *Proceedings of the Institution of Mechanical Engineers, Part B*, 205, 215-219, 1991.
- [25] M. Muraki and D. Dong, "Derivation of Basic Rheological Parameters from Experimental Traction Curves", *Proceedings of the Institution of Mechanical Engineers, Part J*, 213, 53-61, 1999.
- [26] S. Bair, "On the Concentrated Contact as a Viscometer", *Proceedings of the Institution of Mechanical Engineers, Part J*, 214, 515-521, 2000.
- [27] S. Bair, "Measurements of Real Non-Newtonian Response for Liquid Lubricants under Moderate Pressures", *Proceedings of the Institution of Mechanical Engineers, Part J*, 215, 223-233, 2001.
- [28] S. Bair, "The High Pressure Rheology of Some Simple Model Hydrocarbons", *Proceedings of the Institution of Mechanical Engineers, Part J*, 216, 139-149, 2002.

- [29] S. Bair, "The Shear Rheology of Thin Compressed Liquid Films", *Proceedings of the Institution of Mechanical Engineers, Part J*, 216, 1-17, 2002.
- [30] M. Muraki, "Viscosity-Pressure-Temperature Characteristics of High Viscosity Index Mineral Base Oils and Their EHL Traction", *The Japan Society of Mechanical Engineers*, 69, 2482-2488, 2003 (in Japanese).
- [31] E. Diaconescu, "Solidlike Behaviour of EHD Oil Films", *European Economic Community*, 1993.
- [32] S. Bair, "Shear Thinning Correction for Rolling/sliding Elastohydrodynamic Film Thickness", *Proceedings of the Institution of Mechanical Engineers, Part J*, 219, 69-74, 2005.
- [33] M. Kaneta, H. Nishikawa, K. Kameishi, T. Sakai and N. Ohno, "Effects of Elastic Moduli of Contact Surfaces in Elastohydrodynamic Lubrication", *Journal of Tribology*, 114, 75-80, 1992.
- [34] M. Kaneta, H. Nishikawa, T. Kanada and K. Matsuda, "Abnormal Phenomena Appearing in EHL Contacts", *Journal of Tribology*, 118, 886-892, 1996.
- [35] C. R. Evans and K. L. Johnson, "Regimes of Traction in Elastohydrodynamic Lubrication", *Proceedings of the Institution of Mechanical Engineers, Part C*, 200, 313-324, 1986.
- [36] A. J. Moore, "The Behaviour of Lubricants in Elastohydrodynamic Contacts", *Proceedings of the Institution of Mechanical Engineers, Part J*, 211, 91-106, 1997.
- [37] NLGI, "Lubricating Grease Guide, 2nd ed.", NLGI, 1987.
- [38] Y. Yamamoto, S. Gondo and T. Kita, "Effect of Soap Fiber Structure of Lithium 12-Hydroxystearate Greases on Frictional Characteristics under Boundary Lubricating Condition", *Tribologist*, 42, 462-469, 1996 (in Japanese).
- [37] K. Yagi and P. Vergne, "Film Thickness Changes in EHD Sliding Contacts Lubricated by a Fatty Alcohol", *Tribology Online*, 1, 5-8, 2006.
- [38] P. Yang and M. Kaneta, "Multi-dimple Phenomena in TEHL Point Contacts", *Science in China, Series B*, 45, 127-134, 2002.
- [39] O. Pinkus and B. Sternlicht, "Theory of Hydrodynamic Lubrication", McGraw-Hill, 1961.
- [40] S. Wada, H. Hayashi and K. Haga, "Behavior of a Bingham Solid in Hydrodynamic Lubrication (Part 1, General Theory)", *Bulletin of the JSME*, 16, 422-431, 1973.

-
- [41] S. Wada, H. Hayashi and K. Haga, "Behavior of a Bingham Solid in Hydrodynamic Lubrication (Part 2, Application to Step Bearing)", *Bulletin of the JSME*, 16, 432-440, 1973.
- [42] S. Wada, H. Hayashi and K. Haga, "Behavior of a Bingham Solid in Hydrodynamic Lubrication (Part 3, Application to Journal Bearing)", *Bulletin of the JSME*, 17, 1182-1191, 1974.
- [43] J. G. Yoo and K. W. Kim, "Numerical Analysis of Grease Thermal Elastohydrodynamic Lubrication Problems Using the Herschel-Bulkley model", *Tribology International*, 30, 401-408, 1997.
- [44] A. V. Radulescu and I. Radulescu, "Rheological Models for Lithium and Calcium Greases", *Mechanika*, 3, 67-70 2006.
- [45] R. Czarny and H. Mose, "Some Aspects of Lubricating Grease Flow", *Proceedings of 3rd International Tribology Congress EUROTRIB' 81*, 68-85, 1981.
- [46] C. Papanastasiou, "Flows of Materials with Yield", *Journal of Rheology*, 31, 385-404, 1987.
- [47] C. Dorier and J. Tichy, "Behavior of a Bingham-like Viscous Fluid in Lubrication Flows", *Journal of Non-Newtonian Fluid Mechanics*, 45, 291-310, 1992.
- [48] A. Dyson and A. R. Wilson, "Film Thicknesses in Elastohydrodynamic Lubrication of Rollers by Greases", *Proceedings of the Institution of Mechanical Engineers*, 184, 1-11, 1969.
- [49] S. Aihara and D. Dowson, "An Experimental Study of Grease Film Thickness under Elasto-Hydrodynamic Conditions (Part 2) –Mechanism of Grease Film Formation-", *Junkatsu*, 25, 379-386, 1980 (in Japanese).
- [50] W. Jonkisz and H. Krzeminski-Freda, "The Properties of Elastohydrodynamic Grease Films", *Wear*, 77, 277-285, 1982.
- [51] A. R. Wilson, "The Relative Thickness of Grease and Oil Films in Rolling Bearings", *Proceedings of the Institution of Mechanical Engineers*, 193, 185-192, 1979.
- [52] P. M. Cann, B. P. Williamson, R. C. Coy and H. A. Spikes, "The Behaviour of Greases in Elastohydrodynamic Contacts", *Journal of Physics D: Applied Physics*, 25, 1992.
- [53] G. Dalmaz and R. Nantua, "An Evaluation of Grease Behavior in Rolling Bearing Contacts", *Lubrication Engineering*, 43, 905-915, 1987.
- [54] H. Astrom, J. O. Ostensen and E. Hoglund, "Lubricating Grease Replenishment in an Elastohydrodynamic Point," *Journal of Tribology*, 115, 501-506, 1993.

-
- [55] P. M. E. Cann, A. A. Lubrecht and F. Chevalier, "Track Depletion and Replenishment in a Grease Lubricated Point Contact: A Quantitative Analysis", Proceedings of 23rd Leeds-Lyon Symposium, Elastohydrodynamics '96, 405-413, 1997.
- [56] P. M. Cann, "Starved Grease Lubrication of Rolling," Tribology Transactions, 42, 867-873, 1999.
- [57] J. Miettinen, P. Andersson and V. Wikström, "Analysis of Grease Lubrication of Rolling Bearings Using Acoustic Emission Measurement", Journal of Engineering Tribology, 215, 2001.
- [58] I. Couronné, D. Mazuyer, P. Vergne, N. Truong-Dinh and D. Girodin, "Effects of Grease Composition and Structure on Film Thickness in Rolling Contact", Tribology Transaction 46, 31-36, 2003.
- [59] Y. Yoshii and H. Hattori, "Sliding Friction Characteristics of MAC Greases under Vacuum Condition", Tribology Online, 1, 14-18, 2006.
- [60] P. Eriksson, V. Wikström and R. Larsson, "Grease Soap Particles Passing through an Elastohydrodynamic Contact under Side Slip Conditions", Proceedings of the Institution of Mechanical Engineers, Part J, 214, 317-325, 2000.
- [61] P. Eriksson, V. Wikström and R. Larsson, "Grease Passing through an Elastohydrodynamic Contact under Pure Rolling Conditions", Proceedings of the Institution of Mechanical Engineers, Part J, 214, 309-316, 2000.
- [62] K. Sunahara, S. Yamashita and M. Yamamoto, "Development of Grease Film Breakdown Observing Device", Tribology Online, 3, 40-43, 2008.
- [63] P. M. Lugt, "A Review on Grease Lubrication in Rolling Bearing", Tribology Transaction, 52, 470-480, 2009.
- [64] H. Ito, H. Koizumi and M. Naka, "Grease Life Equations for Sealed Ball Bearings", Proceedings of the International Tribology Conference, 1995.
- [65] R. Mas and A. Magnin, "Rheological and Physical Studies of Lubricating Greases Before and After Use in Bearings", Journal of Tribology, 118, 681-686, 1996.
- [66] P. M. Cann and A. A. Lubrecht, "An Analysis of the Mechanisms of Grease Lubrication in Rolling Element Bearings", Lubrication Science, 11, 227-245, 1999.
- [67] P. M. Lugt, S. Velickov and J. H. Tripp, "On the Chaotic Behavior of Grease Lubrication in Rolling Bearings", Tribology Transactions, 52, 581-590, 2009.
- [68] C. Siripongse, P. R. Rogers and A. Cameron, A., "Discharge through Oil Films", Engineering, 186, 146-147, 1958.

-
- [69] C. Siripongse and A. Cameron, "Lubrication of the Four Ball Machine", *Engineering*, 186, 147-149, 1958.
- [70] A. W. Crook, "Lubrication of Rollers", *Proceedings of the Royal Society of London, Series A*, 250, 387-409, 1958.
- [71] J. F. Archard and M. T. Kirk, "Lubrication at Point Contacts", *Proceedings of the Royal Society of London, Series A*, 261, 532-550, 1961.
- [72] G. M. Hamilton and S. L. Moore, "Measurement of the Oil Film Thickness between the Piston Rings and Liner of a Small Diesel Engine", *Proceedings of the Institution of Mechanical Engineers*, 188, 253-261, 1974.
- [73] G. M. Hamilton and S. L. Moore, "Comparison between Measured and Calculated Thickness of the Oil-film Lubricating Piston Rings", *Proceedings of the Institution of Mechanical Engineers*, 188, 262-268, 1974.
- [74] J. Luo, Y. He and M. Zhong, "Gas Bubble Phenomenon in Nanoscale Liquid Film under External Electric Field", *Applied Physics Letters*, 89, 013104-013106, 2006.
- [75] S. Hudlet, M. S. Jean, C. Guthmann and J. Berger, "Evaluation of the Capacitive Force between an Atomic Force Microscopy Tip and a Metallic Surface", *European Physical Journal B*, 2, 5-10, 1998.
- [76] M. J. Furey, "Surface Roughness Effect on Metallic Contact and Friction", *ASLE Transaction*, 4, 1-11, 1961.
- [77] P. S. Y. Chu and A. Cameron, "Flow of Electrical Current through Lubricated Contacts", *ASLE Transaction*, 10, 226-234, 1967.
- [78] J. M. Palacios, "Elastohydrodynamic Films in Mixed Lubrication: an Experimental Investigation", *Wear*, 89, 203-213, 1983.
- [79] J. Lord and R. Larsson, "Film Forming Capability in Rough Surface EHL Investigated Using Contact Resistance", *Tribology International*, 41, 831-838, 2008.
- [80] G. Guangteng, A. Olver and H. Spikes, "Contact Resistance Measurements in Mixed Lubrication", *The Advancing Frontier of Engineering Tribology*, 64-71, 1999.
- [81] G. Kure and W. Palmetshofer, "Electrically-insulated Bearings", *SKF Evolution online*, 3, 96, 1996.
- [82] H. Prashad, "Diagnosis of Rolling-element Bearings Failure by Localized Electrical Current between Track Surfaces of Races and Rolling-elements", *Journal of Tribology*, 124, 468-473, 2002.

- [83] Y. Yamamoto, B. Ono and A. Ura, "Effect of Applied Voltage in Friction and Wear Characteristics in Mixed Lubrication", *Lubrication Science*, 8-2, 199-207, 1996.
- [84] G. X. Xie, J. B. Luo, S. H. Liu, D. Guo, G. Li and C. H. Zhang, "Effect of Liquid Properties on the Growth and Motion Characteristics of Micro-bubbles Induced by Electric Fields in Confined Liquid Films" *Journal of Physics D: Applied Physics*, 42, 115502-115514, 2009.
- [85] J. B. Luo, M. W. Shen and S. Z. Wen, "Tribological Properties of Nanoliquid Film under an External Electric Field," *Journal of Applied Physics*, 96, 6733-6738, 2004.
- [86] V.V. Daniel, "Dielectric Relaxation", Academic Press, 1967.
- [87] P. J. Harrop, "Dielectrics", Butterworths, 1972.
- [88] G. G. Raju, "Dielectric in Electric Eields", CRC Press, 2003.
- [89] S. Havriliak and S. Negami, "A complex plane representation of dielectric and mechanical relaxation process in some polymers", *Polymer*, 8, 161-210, 1967.
- [90] T. Hayakawa and K. Adachi, "Dielectric Relaxation of Poly(n-butyl acrylate)", *Polymer Journal*, 32, 845-848, 2000.
- [91] D. J. Denney and R. H. Cole, "Dielectric Properties of Methanol and Methanol-1-Propanol Solutions", *The Journal of Chemical Physics*, 23, 1767-1772, 1955.
- [92] Yu. N. Shekhter, I. G. Fuks, L. N. Teterina, V. V. Sinitsyn and E. L. Ponomareva, "Effect of Polarity of Soaps and Micellar Binding Energy on the Structure and Properties of Plastic Lubricants", *Chemistry and Technology of Fuels and Oils*, 6, 912-915, 1970.
- [93] A. Bondi and C. J. Penther, "Some Electrical Properties of Colloidal Suspensions in Oils", *The Journal of Physical Chemistry*, 57, 72-79, 1953.
- [94] J. K. Vij, W. G. Scaife and J. H. Calderwood, "The Pressure and Temperature Dependence of the Static Permittivity and Density of Heptanol Isomers", *Journal of Physics D: Applied Physics*, 11, 545-559, 1978.
- [95] F. Aliotta, M. E. Fontanella, G. Galli, M. Lanza, P. Migliardo and G. Salvato, "Low-Frequency Dielectric Investigations in Polymer-like Lecithin Gels", *Journal of Physical Chemistry*, 97, 733-736, 1993.
- [96] M. H. Harun, E. Saion, A. Kassim, E. Mahmud, M. Y. Hussain and I. S. Mustafa, "Dielectric Properties of Poly (vinyl alcohol)/Polypyrrole Composite Polymer Films", *Journal for the Advancement of Science & Arts*, 1, 9-16, 2009.

- [97] O. Urakawa, S. Nobukawa, T. Shikata and T. Inoue, "Dynamics of Low Mass Molecules Dissolved in Polymers", *Nihon Reorogi Gakkaishi*, 38, 41-46, 2010 (in Japanese).
- [98] S. Yagihara, N. Shinyashiki and R. Kita, "How do Water Molecules Behave in Polymers?", *The Society of Polymer Science*, 58, 65-69, 2009 (in Japanese).
- [99] K. Adachi, and T. Kotaka, "Dielectric Normal Mode Process in Semidilute and Concentrated Solutions of Poly(2,6-dichloro-1,4-phenylene oxide)", *Polymer Journal*, 18, 315-322, 1986.
- [100] W. H. Stockmayer, "Dielectric dispersion in solutions of flexible polymers", *Pure Applied Chemistry*, 15, 539-554, 1967.
- [101] R. Buchner, J. Barthel and J. Stauber, "The Dielectric Relaxation of Water between 0 ° C and 35 ° C", *Chemical Physics Letters*, 306, 57-63, 1999.
- [102] T. Fukasawa, T. Sato, J. Watanabe, Y. Hama, W. Kunz and R. Buchner, "Relation between Dielectric and Low-Frequency Raman Spectra of Hydrogen-Bond Liquids", *Physical Review Letters*, 95, 197802-197805, 2005.
- [103] T. Watanabe, "Electrical Properties of Rocks: A Review", *Journal of Geography*, 114, 837-861, 2005 (in Japanese).
- [104] G. D. Galvin, H. Naylor and A. R. Wilson, "The Effect of Pressure and Temperature on Some Properties of Fluids of Importance in Elastohydrodynamic", *Proceedings of the Institution of Mechanical Engineers*, 178, 283-308, 1963.
- [105] M. L. Williams, R. F. Landel and J. D. Ferry, "The Temperature Dependence of Relaxation Mechanism in Amorphous Polymers and Other Glass-forming Liquids", *Journal of the American Chemical Society*, 77, 3701-3707, 1955.
- [106] M. Masuko and A. Suzuki, "Effects of Temperature and Pressure on Dielectric Relaxation of Lubricating Oils and Relation with Viscosity Change", *Tribologist*, 42, 455-466, 1997.
- [107] M. Masuko and A. Suzuki, "Prediction of Lubricating Oil Viscosity at High Pressure from the Dielectric Relaxation Measurements", *Tribologist*, 42, 467-475, 1997.
- [108] A. Suzuki, M. Masuko and T. Nikkuni, "High-pressure Viscosity Prediction of Di(2-ethylhexyl) phthalate and Tricresyl Phosphate Binary Mixture Using Dielectric Relaxation Data", *Tribology International*, 33, 107-113, 2000.
- [109] S. Kotake, A. Suzuki, M. Masuko and Y. Fujinami, "Dielectric Relaxation Measurement of Lithium Soap Greases", *Japanese Society of Tribologists*, 2009 (in Japanese).

-
- [110] N. Maeno, "The Dielectric Dispersion of KCL Ice. III. The Dielectric Dispersion of High-Concentration Ice", *Low Temperature Science, Series A*, 29, 1-10, 1971 (in Japanese).
- [111] M. Françon, "Optical Interferometry", Academic Press, 1966.
- [112] G. J. Jonhston, R. Wayte and H. A. Spikes, "The Measurement and Study of Very Thin Lubricant Films in Concentrated Contacts", *Tribology Transactions*, 34, 187-194, 1991.
- [113] R. Gohar and A. Cameron, "Optical Measurement of Oil Film Thickness Under Elastohydrodynamic Lubrication", *Nature*, 200, 458-459, 1963.
- [114] R. Gohar and A. Cameron, "The Mapping of Elastohydrodynamic Contacts", *ASME Transactions*, 10, 215-225, 1967.
- [115] R. Haydn, G. W. Dalke, J. Henkel and J. E. Bare, "Application of the HIS Color Transform to the Processing of Multisensor Data and Image Enhancement", *Proceedings of the International Symposium on Remote Sensing of Arid and Semi-arid Lands*, 599-616, 1982.
- [116] H. Block, W. D. Ions, G. Powell, R. P. Singh and S. M. Walker, "The Dielectric Behaviour of Solutions of Some Rigid Polymers under Shear", *Proceedings of the Royal Society of London, Series A*, 352, 153-167, 1976.
- [117] W. Hirst and A. J. Moore, "The Elastohydrodynamic Behaviour of Polyphenyl Ether", *Proceedings of the Royal Society of London, Series A*, 344, 403-426, 1975.
- [118] H. Fröhlich, "Theory of Dielectrics Dielectric Constant and Dielectric Loss", Oxford at the Clarendon Press, 1958.
- [119] P. M. E. Cann, B. Damiens and A. A. Lubrecht, "The Transition between Fully Flooded and Starved Regimes in EHL", *Tribology International*, 37, 859-864, 2004.
- [120] H. Nishikawa, Kohtaroh Handa and Motohiro Kaneta, "Behavior of EHL Films in Reciprocating Motion", *The Japan Society of Mechanical Engineers, Series C*, 38, 558-567, 1995.
- [121] B. Leonard, F. Sadeghi and R. Cipra, "Gaseous Cavitation and Wear in Lubricated Fretting Contacts", *Tribology Transactions*, 51, 351-360, 2008.
- [122] D. Dowson and C. M. Taylor, "Cavitation in Bearings", *Annual Review of Fluid Mechanics*, 11, 35-66, 1979.

- [123] K. Stadler, N. Izumi, T. Morita, J. Sugimura and B. Piccigallo, “Estimation of Cavity Length in EHL elastohydrodynamic contacts”, *Journal of Tribology*, 130, 315021-315029, 2008.
- [124] T. Sakurai, M. Hoshino, M. Tokashiki and M. Fujita, “Grease for Lubrication and Synthetic Lubricant”, *Saiwai-syobou*, 1983 (in Japanese).

Appendix 1

Dielectric Properties of Thickeners





Measurements based on the dielectric spectroscopy were carried out on thickeners. Five thickeners which are indeed used for manufacturing the commercial greases were prepared, which is cooperated by Mr Tanaka at Kyushu University and listed in Table A1.1.

In measuring the dielectric properties of thickeners, materials, a picture of which is displayed in Figure A1.1, were broken into as small pieces as possible and the capacitor were filled with powder of a thickener without connecting to an external resistor. By this means, the sample under the measurement may include air spaces and the measured values cannot be considered as 100% intrinsic properties of the material. This is because, these results are presented in appendix.



Figure A1.1 Powder of thickener

Table A1.1 Details of thickeners

| Thickener | Manufacturer | Structure |
|---|------------------|---|
| Lithium 12-hydroxy stearate (12OH-LiSt) | Kyodo Yushi | $\text{LiC}_{18}\text{H}_{35}\text{O}_3$  |
| Lithium hydroxyl stearate (OH-LiSt) | Kyodo Yushi | $\text{LiC}_{18}\text{H}_{35}\text{O}_3$  |
| Lithium stearate (LiSt) | Kyodo Yushi | $\text{LiC}_{18}\text{H}_{35}\text{O}_2$  |
| Stearic acid (St) | Kyodo Yushi | $\text{C}_{18}\text{H}_{36}\text{O}_2$ |
| Stearic acid (St) | Kishida Chemical |  |

A1.1 Dielectric Constant

Figure A1.2 shows the behaviour in the dielectric constant of thickeners. While lithium hydroxy stearate shows relatively high values and decreasing tendency with frequency in dielectric constant, which is features of a polar material, other soaps do not show the characteristics of polar materials, which becomes more obvious in the next section, A1.2.

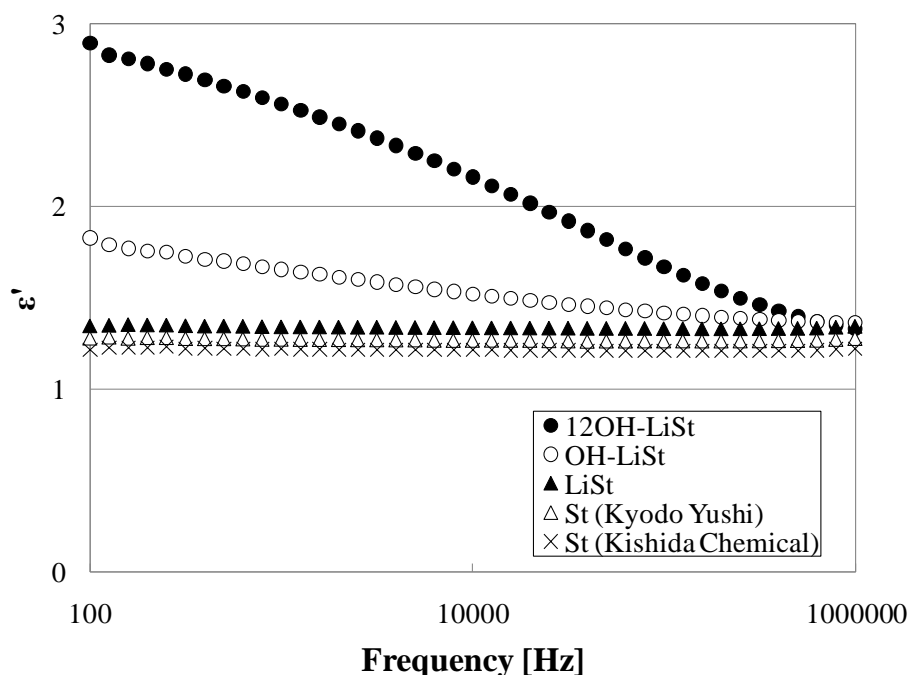


Figure A1.2 Dielectric constant of thickeners

Both stearic acid shows almost same dielectric constant, while Lithium stearate shows slightly higher values than Stearic acid. Thus this suggests lithium may have stronger effect on the bulk polarity than OH bond when considering only local structure, namely in this case only the edge of the chain.

A1.2 Dielectric Relaxation Process

Figure A1.3 shows the behaviour in the dielectric relaxation process of thickeners. In addition to the relaxation peak above 1MHz, probably around 10MHz for all thickeners, 12OH-LiSt and OH-LiSt show the relaxation process between 100Hz and 1MHz.

Comparing these two relaxation behaviour, 12OH-LiSt shows faster and stronger relaxation process than OH-LiSt. Although both 12OH-LiSt and OH-LiSt can take the form of type C according to the Stockmayer's theory [91], it has revealed that a hydroxyl group on the side gives faster process than that on the edge of the chain.

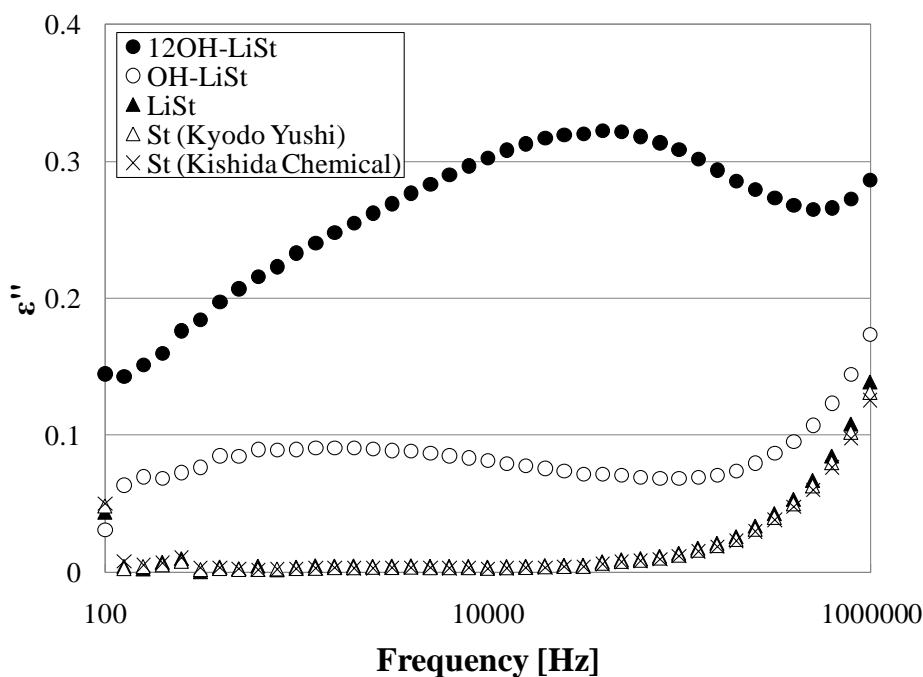


Figure A1.3 Dielectric loss of thickeners

Appendix 2

Film Thickness Used for Rheological Observation

The film thickness measured by ULTRA at 20mm/s and 20N with glass disc is shown for all investigated lubricants.

Table A2.1 Film thickness at 20mm/s and 20N for all lubricants

| Grease | Film Thickness [nm] | Base Oil's Value [nm] |
|---------------|----------------------------|------------------------------|
| Grease1 | 59.0 | 19.4 |
| Grease2 | 73.2 | 34.8 |
| Grease3 | 152 | 136 |
| Grease4 | 34.1 | 19.4 |
| Grease5 | 28.9 | 19.4 |
| Grease6 | 140 | 136 |
| RL2 | 72.3 | 54.6 |
| RLS2 | 58.0 | 44.6 |
| SRL | 31.0 | 8.6 |
| SB-M | 44.8 | 40.6 |

Appendix 3

Pressure Distribution for the Cavitation Phenomena

Consider the geometry of the ball and disc behind the exit constricted region (Figure A3.1).

Denoting the separation between the surfaces by h , this can be expressed by using Equation 5.8.

$$h = h_c + \frac{a^2}{\pi R} \left(- \left(2 - \frac{x^2}{a^2} \right) \cos^{-1} \frac{a}{x} + \left(\frac{x^2}{a^2} - 1 \right)^{0.5} \right) \quad (\text{A3.1})$$

where h_c is the separation between surfaces at the centre of the contact. It is obvious that the shear rate, defined as $\dot{\gamma} = \Delta u / h$, is not constant in this region and, according to Equation A3.1, it follows that the viscosity of the grease, described as Equation 8.2, also varies with the position from the contact, which can be expressed by the following equation:

$$\eta = C_1 + C_2 \left(\frac{\Delta u}{h} \right)^N \quad (\text{A3.2})$$

The 2D Reynolds equation is:

$$\frac{dp}{dx} = 6\eta \bar{u} \frac{h - h_m}{h^3} \quad (\text{A3.3})$$

where \bar{u} is equal to the speed of the disc in this study (pure sliding) and h_m is the lubricant film thickness at the point of maximum pressure where $\frac{dp}{dx} = 0$; η is a function of h and therefore implicit of x .

Substituting Equation A3.1 and A3.2 into Equation A3.3 yields the following equation for the pressure.

$$p = 6C_1\bar{u}\left(\int_{x_1}^{x_2} \frac{1}{h^2} dx - h_m \int_{x_1}^{x_2} \frac{1}{h^3} dx\right) + 6C_2\bar{u}^{1+N}\left(\int_{x_1}^{x_2} \frac{1}{h^{2+N}} dx - h_m \int_{x_1}^{x_2} \frac{1}{h^{3+N}} dx\right) + C_3 \quad (\text{A3.4})$$

where C_3 is a constant of integration. The boundary condition, which is $p = 0$ for $x = x_1, x_2$, yields:

$$C_3 = 0 \text{ and } h_m = \frac{C_1 \int_{x_1}^{x_2} \frac{1}{h(x)^2} dx + C_2 \bar{u}^N \int_{x_1}^{x_2} \frac{1}{h(x)^{2+N}} dx}{C_1 \int_{x_1}^{x_2} \frac{1}{h(x)^3} dx + C_2 \bar{u}^N \int_{x_1}^{x_2} \frac{1}{h(x)^{3+N}} dx} \quad (\text{A3.5})$$

It follows that the pressure distribution is:

$$p(x) = 6C_1\bar{u}\left(\int_{x_1}^{x_2} \frac{1}{h^2} dx - h_m \int_{x_1}^{x_2} \frac{1}{h^3} dx\right) + 6C_2\bar{u}^{1+N}\left(\int_{x_1}^{x_2} \frac{1}{h^{2+N}} dx - h_m \int_{x_1}^{x_2} \frac{1}{h^{3+N}} dx\right) \quad (\text{A3.6})$$

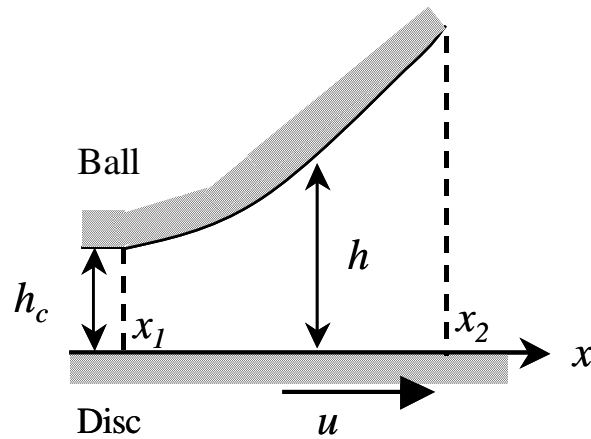


Figure A3.1 Exit of conjunction